Geotechnical Journal - Special Issue on Ground Improvement

Sri Lankan Geotechnical Society
C/o National Building Research Organisation
99/1, Jawatta Road, Colombo – 05
Sri Lanka.

EDITED BY :

Prof. Buddhima Indraratna
Prof. Athula Kulathilaka
Mr. Sinniah K. Navaratnarajah

PAPERS REVIEWED BY:

……

……

……

ISSN – 1391 – 6149

PREFACE

This Special Issue of *the Geotechnical Journal of the Sri Lankan Geotechnical Society* on Ground Improvement is the result of keen discussion among various experts, for highlighting the key geotechnical issues encompassing modern ground improvement techniques for infrastructure development. This special issue includes 9 papers from around the globe, including numerical and analytical methods, design parameters, field and laboratory testing, and case studies.

The issue begins with the paper by Balasubramaniam*et al*. titled "Interpretation and analysis of test embankments in soft clays with and without ground improvement."The paper presents the interpretation of fully-instrumented test embankments and their role in the development of appropriate ground improvement techniques for highways and airfields on soft clay deposits illustrated through well-documented case studies from Southeast Asia and Queensland, Australia.

The paper "The application of vertical drains and vacuum preloading for improving soft ground" by Rujikiatkamjorn and Indraratna introduces recent advancement in soft soil improvement using prefabricated vertical drains (PVDs) and vacuum preloading. This paper also presents an overview of the theoretical and practical developments and salient findings of soft ground improvement via PVD and vacuum preloading, with applications to selected case studies in Australia, Thailand, and China.

The article on the "Use of shock mats for mitigating degradation of railroad ballast" by Indraratna*et al*. proposes the use of artificial inclusion such as rubber shock mats with the aim of reducing particle breakage and ballast deformation as a cost-effective option for improving ballasted rail track foundation. This paper presents a state-of-the-art review of laboratory studies and numerical modelling, illustrating the benefits of Under Sleeper Pads (USP) and Under Ballast Mats (UBM) in railway practice.

A number of published geotechnical case histories involving ground improvement for mitigating liquefaction induced geotechnical hazards, originating from the Lower Mainland of British Columbia, Canada, have been reviewed by Wijewickreme in his paper, "Ground improvement to mitigate earthquake-induced soil liquefaction hazards." Current approaches for predicting earthquake-induced ground deformations and the appropriate selection of ground improvement methods and their applicability are highlighted.

In their paper on "Performance of highway embankments constructed over Sri Lankan peaty soils" with special reference to the Southern Expressway in Sri Lanka, Karunawardena and Toki performed detailed laboratory and field investigations before and after ground improvement. The paper highlights salient aspects of field instrumentation and monitoring program during and after embankment construction.

In the paper on "Design and performance of bridge approaches constructed using geogrid-reinforced piled embankment method", Karunawardena and Wedikkarage present a case history of the design and performance of geogrid- reinforced piled embankments constructed at bridge approaches in the Southern Expressway project in Sri Lanka. It provides details of the design methodology, numerical analysis and construction together with field data.

The paper by Baral*et al*. on "Practice of reinforced embankment on hard foundation - a case study of Phitsanulok, Thailand" demonstrates the application of a Mechanically Stabilized Earth Wall (MSEW)

embankment through numerical simulation. The paper elucidates the performance of a full-scale reinforced test embankment designed and constructed by Department of Highways (DOH) on relatively stiff clay foundation.

"Subgrade soil stabilization using native vegetation" by Pallewattha *et al*. explains the capability of increasing the matric suction of the soil subgrade underneath the substructure via root water uptake, in conjunction with evapo-transpiration by tree canopy. The paper demonstrates that tree roots are capable of providing significant mechanical reinforcement plus additional cohesion by generating osmotic suction.

The paper by Kodikara and Islam on "An Analysis of Compacted Pavement Subgrade Behaviour Due to Climatic Effects" presents a comprehensive description of the behaviour of pavement subgrade subjected to climatic effects. The current design approaches are reviewed in view of fresh interpretations based on a newly developed conceptual framework.

Our invitation to be Guest Editors of this Special Issue by the Sri Lankan Geotechnical Society is gratefully appreciated. The 9articlesincluded in this Special Issue cover an array of ground improvement techniques from theory to practice. We gratefully acknowledge the efforts of all Authors who accepted our invitation to submit high quality articles in a timely manner. All papers have been peer-reviewed to maintain high standards, and we acknowledge the efforts by all Reviewers. We also appreciate the support given by several PhD candidates at University of Wollongong, Australia during this task, especially Darshana Perera and Muditha Pallewattha.

It is hoped that this Special Issue on Ground Improvement would be of immense benefit to both researchers and practitioners alike.

Prof. Buddhima Indraratna

Prof. Athula Kulathilaka

Mr. Sinniah K. Navaratnarajah

GEOTECHNICAL JOURNAL
SPECIAL ISSUE ON GROUND IMPROVEMENT

CONTENTS

Geotechnical Journal Vol. 6 No. 1 2014

INTERPRETATION AND ANALYSIS OF TEST EMBANKMENTS IN SOFT CLAYS WITH AND WITHOUT GROUND IMPROVEMENT

A. S. Balasubramaniam1, B. Indraratna[2], D.T. Bergado[3], C. Rujikiatkamjorn[4]

1 Adjunct Professor, School of Engineering, Griffith University Gold Coast Campus, QLD 9726, Australia
(Ph: +61-7-55528590; Fax: +61-7-55528065; email: a.bala@griffith.edu.au)
2Professor of Civil Engineering, School of Mining and Environmental Engineering, Research Director of Centre for Geomechanics and Railway Engineering, University of Wollongong, Wollongong City, Australia
3Professor, School of Civil Engineering, Asian Institute of Technology, Bangkok, Thailand
(Ph: +66 2 524 5512, Fax: +66 2 524 6050 email: bergado@ait.ac.th)
4Associate Professor, Centre for Geomechanics and Railway Engineering, University of Wollongong, Wollongong City, Australia

ABSTRACT: In this paper the interpretation of fully instrumented test embankments and their role in the development of appropriate ground improvement techniques for highways, motorways and airfields on soft clay deposits is illustrated through well documented case studies in Bangkok, Thailand, the Muar Flat site in Kuala Lumpur, and in Southeast Queensland. With the Bangkok Plain and sand backfills, the performance of embankments with different patterns of vertical drains was evaluated over a period of 25 years. Aspects such as the recharging effects due to the drains, inadequate measures in maintaining the vacuum during vacuum applications and possible hydraulic connections with large diameter drains are discussed. With the Muar test embankments, the role of fill strength in residual soil embankment and the field deformation analysis in separating consolidation settlement from immediate settlement and creep settlements is presented. Novel interpretations of settlement from pore pressure dissipation, secondary settlement from field measurements, and the decay of the lateral deformation rate overtime were also made.

1 INTRODUCTION

To evaluate geotechnical parameters traditional laboratory tests are performed. But when the quality of undisturbed samples taken from boreholes or block samples is in doubt, in situ tests are performed. These in-situ tests can be small scale such as vane tests, cone penetration tests, pressure meter tests, and dilatometers tests. Large scale field tests are also carried out in parallel and these tests are fully instrumented. Over the last 32 years the first author has been involved in interpreting the test data from several embankments in Thailand, Malaysia, and in Southeast Queensland. This paper touches on some of the lessons learnt from these studies and how they have improved our understanding of soft clay behaviour and ground improvement schemes when studied via at least embankment. The cases in Thailand and the Muar site in Malaysia will be emphasised and these experiences will be presented in chronological order rather than country wise. The concept of large scale field test stemmed from knowing that our single element laboratory scale tests could not cover all the features that we encounter in sedimentary soils with layers that vary in thickness and properties. Not only that, small scale field tests can occasionally misrepresent large scale behaviour that covers a much larger loaded area. From this experience began the concept of building test embankments.

A typical soil profile in the Bangkok Plain is shown in Fig.1. Eide (1977) reported the results of a test section on the Bangkok-Siracha highway that were measured in 1966, and where ground along the route was considered to be very soft. Sand drains 0.2 m in diameter were installed in a triangular pattern 2 m apart by the displacement method. These sand drains increased the rate of settlement but not by much; indeed the most negative aspect quoted by Eide (1977) was that even though the sand drains accelerated consolidation over the first 18 months, at the end of this period the rate of settlement was still as much as 0.03 m per month, which was considered to be high. Possibly because the factor of safety was low, a substantial part of the total settlement was due to continuous undrained creep without volumetric strain, when the stress states when close to failure. Furthermore, Cox (1967) in his research report at AIT concluded that the design and construction of road embankments over the soft deltaic clays in South East Asia was a very complex engineering problem because the pore pressure response and settlement characteristics corresponded to lightly over-consolidated states rather than normally consolidated states.

Dr. ZaChiehMoh and his colleagues were pioneers in the study of the test embankment at the Second International Airport site in Bangkok as early as 1970. Full scale test embankments were built at Nong Ngo Hao by Moh et al (1973) to study the in-situ behaviour. Embankment I was built rapidly to failure, and indeed it failed at only 3.4 m. Embankment II was in two sections - one where the height varied from 0.5 m to 2.9 m and the other with 2.9 m of constant height. The behaviour of these embankments was studied closely by several Masters and Doctoral students at AIT.

The next major study was associated with the Royal Thai Navy Dockyard in Pomprachul, Thailand, where work had commenced in 1975. The test site is situated at the mouth of the Chao Phraya River in Samut Prakarn province, approximately 20 km south of the Bangkok city. The embankment was built in two stages, each being 90 m long by 33 m wide by 2.35 m high and consisting of three sections; a section without drains, a section with drains 2.5 m apart, and a section with drains 1.5 m apart (as shown in Fig. 2a and Fig. 2b). The profile of the soil is in Fig. 2c. The sand drains consisted of small diameter (0.05m) sand wicks and were installed to a depth of 17 m by the displacement method. These sand wicks were constructed on site by pouring sand inside a permeable membrane. First a 75 mm internal diameter steel tube closed at one end was driven into the ground and then a sand wick was lowered into the casing and the casing was subsequently withdrawn.166 piezometers were installed below the test fill area and outside of it, and then surface and sub-surface settlement points were installed to monitor settlement along the centre line and edges of the test embankment. Three hydrostatic profile gauges were installed, one along each central cross-section of a test section. Also, eleven magnetic movement plates were used to monitor lateral displacement along the gauge. Three inclinometer casings were installed along the centre line of each test section.

At the airport site in Nong NguHao, the most extensive sand drain studies on test embankments were performed in 1983 (see Moh and Woo, 1987) as part of the ground improvement scheme for the runway pavement and other sections of the taxiways and landside roads. Sand drains with a minimum diameter 0.26 m were installed by water jetting to a depth of 14.5 m. The test program included

three test areas, one with surcharge fill, one with vacuum loading, and one with ground water lowering. Test Section 1 was 40 m x 40 m in plan and sand drains were installed in a triangular pattern, 2 m

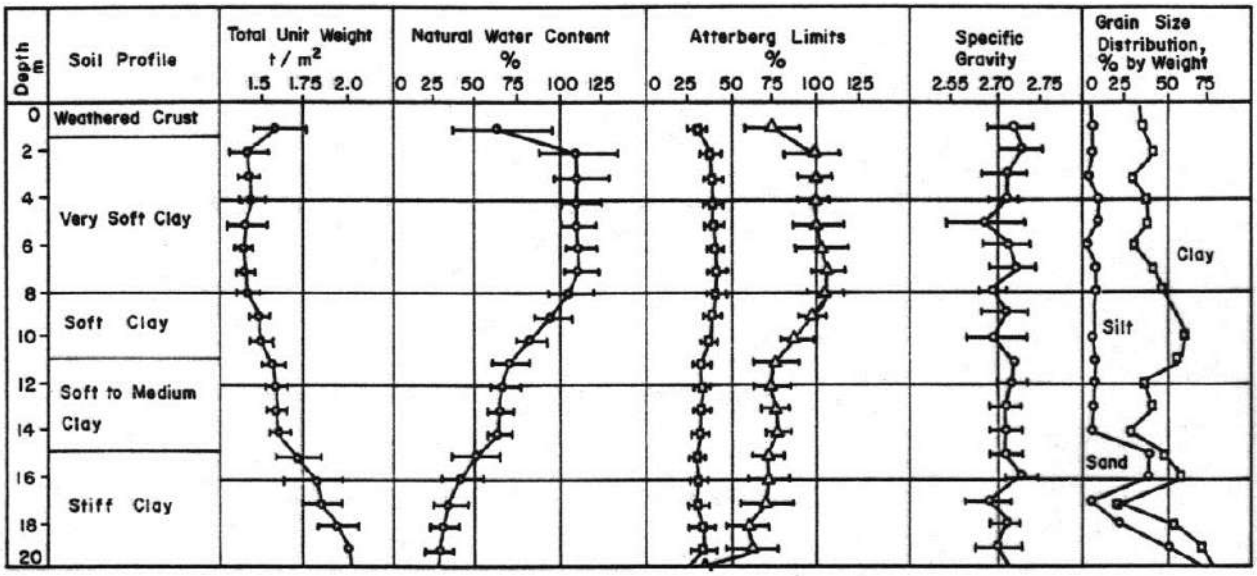

Fig. 1 Typical soil profile in the Bangkok Plain (Balasubramaniam et al. 2005)

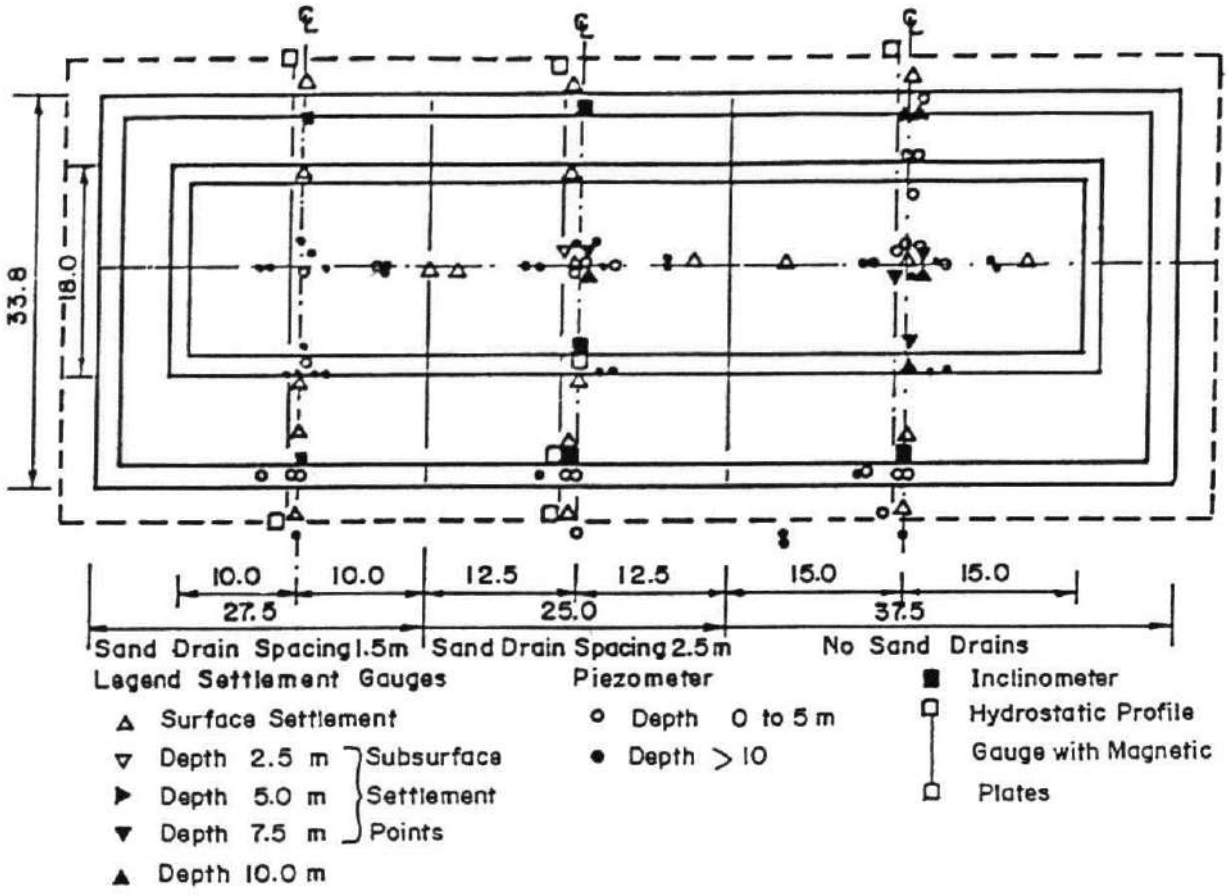

Fig. 2a Plan of test embankment at RTN Dockyard site (Balasubramaniam et al. 2005)

apart. The vacuum load was unsuccessful because several leaks so the section was covered with a plastic shield. Test Section 3 was similar to the Test in Section 1, except that the drain spacing was increased to 2.4 m because of a similar problem in Section 1 where the loading was unsuccessful. Test Section 2 was slightly larger than test Section 1 and a pre-loading of 60 kN/m2 was applied in three stages. While difficulties were encountered in maintaining the vacuum load and the ground water lowering, the embankment surcharge proved to be a more reliable technique than vacuum loading in accelerating consolidation with sand drains.

Since most of the North-South Expressway from Bukit KayuHitam at the Malaysian-Thai border to Johor Baru at the southern most location passes through soft clay deposits, fourteen soil improvement

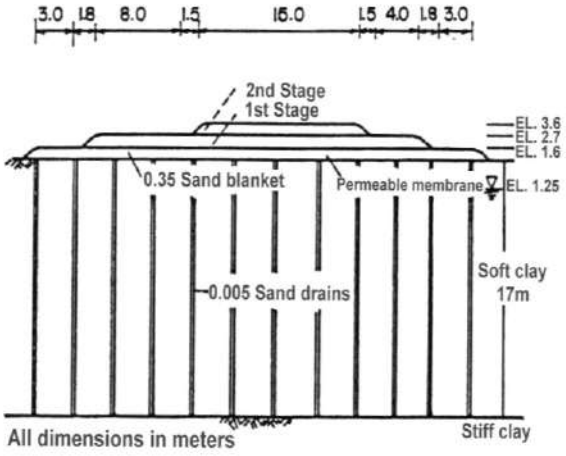

Fig. 2b: Elevation of test embankment at RTN Dockyard site (Balasubramaniam et al. 2005)

schemes were designed and constructed at the Muar flat sites. These embankments were instrumented to measure the settlement, lateral movement, and pore pressure. Details of these embankments are illustrated in Fig. 3. Several of these embankments are studied by the first author and his colleagues at AIT, along with a number of Masters Students doing their research. The embankment was built with residual soil and used as the embankment in a prediction symposium in Malaysia, while reference will be made to the work by Balachandran (1990), Ratnayake (1991), Loganathan (1992) and Sivaneswaran (1993). The work of Balachandran (1990) extends the prediction made by the first author on the embankment built to failure, while Ratnayake (1991) analysed the embankment with vertical drains. Loganthan (1991) used the field deformation analysis to separate the immediate settlement from consolidation settlement during the loading stage and to separate consolidation settlement and creep settlement during the performance stage. This technique was different from the Asaoka technique used to estimate consolidation settlement, especially under one dimensional consolidation. When high embankments were built, creep was a major factor and made it difficult to estimate the so-called residual settlements during the maintenance period in most road works and other projects. The work of Sivaneswaran (1993) illustrates how powerful the normalised settlement and normalised lateral deformation tools are in studying ground response under different schemes of ground improvement.

The above experiences and the lessons learnt led to a rather cautious approach, with the final studies being carried out (for a two year period from 1994 to 1995) for the construction of the runway and other structures at the Second Bangkok International Airport (SBIA) site. In this study it was concluded that pre-fabricated vertical drains (PVD) and surcharge was the most suitable ground improvement technique.

2 VERTICAL DRAIN STUDIES IN BANGKOK SIRACHA HIGHWAY (1967)

The potential use of surcharge and vertical drains as a ground improvement technique was explored as early as 1966 (Eide, 1977) for its application in the approach to bridges. A test section on the Bangkok-Siracha Highway was built and tested with 0.20 m diameter sand drains that varied in depths from 4 to 13 m. During construction the soft clay failed at five locations so the 2.2 m high embankment was furnished with 8 m wide berms to ensure stability. From the observed settlement of the test embankment, Eide (1977) concluded that the drained embankment section settled most to start with, but after one year the rate of settlement was almost the same, approximately 0.0025 m per month on both the drained and undrained sections. The practical conclusion reached by Eide (1977), was that this type of drain and spacing would not serve the purpose in bridge approaches. However, Eide (1977) agreed that these results might have been affected by other factors such as slip failure, are moulding effect stemming from installing the drains, and a low permeability and greater secondary consolidation settlement by the soft clay.

3 STUDY OF VERTICAL DRAINS AT THE DOCKYARD SITE

A second attempt was made with vertical drains from1975 to 1977, with the construction of a dockyard for the Royal Thai Navy. A test embankment was built (see Fig. 2a and Fig. 2b) to evaluate the performance and suitability of sand drains (sand wick type drains) of accelerating consolidation of the soft clay. Without an understanding of the recharge effect due to the sand wicks on the piezometric drawdown, doubts were cast on the pore pressure measurements as revealed below the natural terrain where the sand wick was installed, and this led to the installation of additional piezometers so that finally there were 166 piezometers monitoring the pore pressure below the clay surface. It was found that the installation of sand wicks recharged the area below the test embankment with and without drains, and erased the normal piezometric draw-down which normally existed in the Bangkok subsoils due to deep well pumping, as can be seen in the area which was not influenced by the test embankment location installed with sand wick drains. This re-charging effect was somehow not envisaged in the original planning and design of the test embankment, but it did give a valuable insight into the extensive deep well pumping in the Bangkok Plain, and the Piezometric drawdown that has resulted in the Bangkok subsoils as a consequence of excessive extraction of ground water.

3.1 Description of test embankment and soil profile

The performance of sand drains (sand wick type of drains) at the Naval Dockyard site, Pom Prachul, Thailand was investigated in 1975 by constructing an instrumented test embankment. The test site was situated at the mouth of the Chao Phraya River in SamutPrakarn province, approximately 20 km south of the city of Bangkok. The embankment, which was built in two stages, was 90 m long, 33 m wide, 2.35 m high and consisted of three sections; a section without drains, a section with drains 2.5 m apart, and a section with drains 1.5 m apart (as shown in Fig. 2a and Fig. 2b). A profile of the soil is shown in Fig. 2c. The sand drains consisted of 0.05 m diameter sand wicks which were installed to a depth of 17 m by the displacement method.

These sand wicks were constructed at the site by pouring sand inside a permeable membrane. First, a 75 mm inside diameter steel tube closed at one end was driven into the ground and the sand wick was lowered into the casing and then the casing was removed. 166 piezometers were installed below the test fill area and also outside it. Surface and sub-surface settlement points were installed to monitor settlement along the centre line and the edges of the test embankment. Three hydrostatic profile gauges were installed, that is, one along each central cross-section of a test section, and eleven magnetic

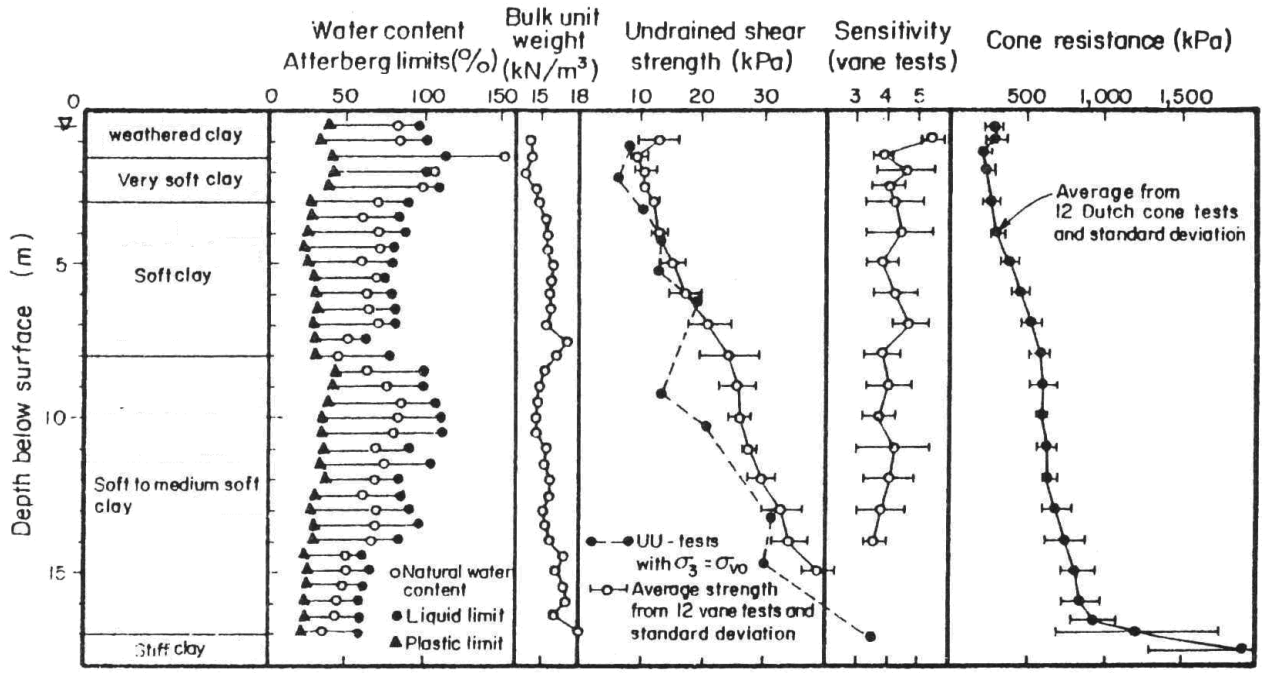

Fig. 2c General properties of Pom Prachul Clay at RTN Dockyard site (Balasubramaniam et al. 2005)

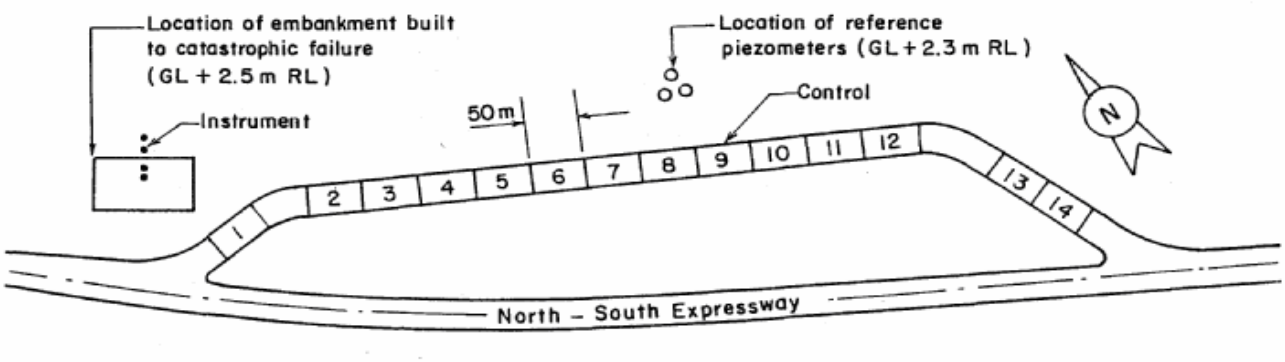

Method of Ground Improvement:

- Electro - Osmosis (6)
- Chemical Injection (1 & 4)
- Sand Sandwith (13)
- Preloading & Drains (11, 12 & 14)
- Micro Piles (3)
- Vacuum Preloading (10)
- Sand & Compaction Piles (8)
- Well - Paint Preloading (5)
- Prestressed Spun Piles (7)

Fig.3 Locations of Embankments (Indraratna et al. 1997)

movement plates were used to monitor lateral displacement along the gauge. Three inclinometer casings were installed along the centre line of each test section. A typical profile of the soil at this site is shown in Fig. 2c.

3.2 Pore pressure measurements below the test embankment

The loading pattern for the three test sections and the pore pressure observations are shown in Fig. 4a and the piezometric drawdown is shown in Fig. 4b. Before constructing the test embankment, a 0.35 m thick sand blanket was placed in the area, and this corresponded to a surcharge pressure of 5.5 kN/m2. The first stage of loading was carried out in 25 days to a fill height of 1.1 m and a surcharge pressure of 19 kN/m2. At the end of the first stage of loading the surcharge pressure was 24.5 kN/m2. After waiting for 60 days, the embankment was raised to 2.35 m (inclusive of the 0.35 m sand blanket). The second stage loading was for a one month period and the observations were continued for ten months.

The piezometers P41, P27, and P13 which were located at 7.5 m depths in the three sections indicated a consistent rise during the loading phase and a drop in values during the waiting period and under the time observed after the full surcharge. These piezometers measured the absolute values of the pore pressure and thus included the original ground water pressure before loading. As Fig. 4a shows the static ground water pressure was observed from the observation well where the effect of drawdown was ignored. The dummy piezometers installed at a location far away from the test embankment and without the influence of the sand wick and the surcharge will give the static water pressure inclusive of any possible drawdown due to deep well pumping. At this site the piezometric drawdown only began below 7.5 m and as such the hydrostatic water pressure indicated by the observation well and the dummy piezometers located at 7.5 m depths were more or less coincident, indicating very small drawdown.

All 166 piezometers indicated consistent pore pressures except for the active piezometers installed at depths of 10 to 15 m which indicated that the piezometric drawdown below the embankment was more or less erased by the sand drains which recharged the drawdown area back to its hydrostatic conditions. Thus at deeper depths the absolute values of the piezometer readings under the embankments will be a sum of the static water pressure without any drawdown and the excess pore pressure induced by the surcharge loading. In order to clarify the situation, additional piezometers were installed along the centre line of the longitudinal section of the test embankment from the northern edge corresponding to the closely spaced sand drain section and also along the edge of the eastern boundary of the test embankment. Fig. 5 shows the distance from the edge of the embankment in an easterly direction, up to which the drains have influenced erasing the draw-down. A similar phenomenon was noted in an northerly direction along the centre line, but in both directions the full draw down was only realised about 15 to 20 m away from the edges of the embankment. This would indicate that having the three sections side by side without any space in between them was a grave mistake when planning the overall test program. Ideally speaking the three sections must be separated from each other with a substantial allowance for the zone of influence of the drains to recharge the draw down area below the embankment. This was observed in the final planning of the test embankment with PVD at the Second Bangkok International Airport (SBIA) site in the 1994-1995 studies. The three test embankments at the SBIA site were separated from each other with substantial space between them.

3.3 Measured and computed settlements at the Dockyard site

The settlement records from 47 active settlement plates were studied and typical cases are plotted in Fig 6. In this Figure the surface settlement at the centre line of the three test sections were plotted with respect to time. Also shown in this Figure is the loading pattern with time in terms of the surcharge stress (Vertical stress increment). These settlement records are in accordance with the pore pressure dissipation shown in Fig. 4a. The section with closer drain spacing showed higher settlement than the one with wider spacing and the one with no drain. It has already been discussed that the wider spaced drain section was interfering with the section without a drain and therefore substantial lateral drainage would have taken place in this section due to the adjoining drain section with a wider spacing.

Using the elastic theory for increment in stresses below the test sections and the undrained modulus from CK0U triaxial tests, immediate settlements were computed and plotted in Fig. 7. It can be seen here that very little immediate settlement occurred below a depth of 11 m. The immediate surface settlement under the first stage loading and the second stage loading was computed to be 36 mm and 115 mm respectively. The total primary consolidation settlement under the embankment loading was calculated using the stress-strain curves from the Oedometer tests. Fig. 8 shows the variation of the primary consolidation settlement with depth. In Fig. 8 the consolidation settlements were computed from six series of consolidation tests performed with the Lever Arm Consolidometer, the Anteus Consolidometer, and the Bishop Consolidometer. In Series SC seven tests were conducted from 1 to 16 m with a 24-hour load increment duration, and a load increment duration of one. A similar series of tests were conducted in the Anteus Consolidometer as Test Series AC. Bishop Consolidometer was used in Test Series BC and the load increment duration and ratio were similar to the SC and AC series. In Test Series SI, small load increments were used in the Lever Arm Consolidometer to accurately determine the preconsolidation pressure. The measured settlements were in the drained section with drains set 1.5 m apart. These data indicate that even in the 1.5 m-drained section, primary consolidation was not yet completed.

The major lesson learnt from this trial embankment was that the sand wick drains recharged the zone that was originally under piezometric drawdown, so recharging the bottom layer of soft clay would have decreased the effective stress, which is why the settlements were smaller below the upper 5 m where there was no previous drawdown. Moreover, the recharging zone seemed to extend laterally up to a distance of about 15 m or so, and as such the section without drains would have been influenced by the drained section. It was therefore better to have had three separate sections spaced out to ensure minimum interference, and the data from each embankment truly represents a no-drain section and the sections with the wider and narrower spacing of drains.

4 MUAR CLAY TEST EMBANKMENTS

Several lessons were learnt from the analysis of the Muar clay test embankments. The well documented publications on the behaviour of the residual soil test embankment built to failure indicated how such a simple field problem can deviate from the known behaviour of sandfill test embankments. The inclusion of well compacted residual soil fill seemed to offer good tensile strength and would prevent the formation of tensile cracks at the base of the embankment. The predictions were presented in the "International Symposium on Trial Embankments on Malaysian Muar Clays," in November 1989, held in Kuala Lumpur, Malaysia. All the predictors were given soils with the same properties and field instrumentation results (Brand and Premchitt, 1989). Most experts also made poor predictions of settlement pore pressures and lateral movements.

The CRISP program as based on the critical state soil mechanics was better at predicting the coupled behaviour of the undrained and consolidation performance of these embankments. The Muar clay test embankments also illustrated that the Pads available in the market for accelerating the dissipation of pore pressures were not 100 percent effective, as expected from the classical theories of Barron and others. Hansbo in particular considered the non-Darcian flow of

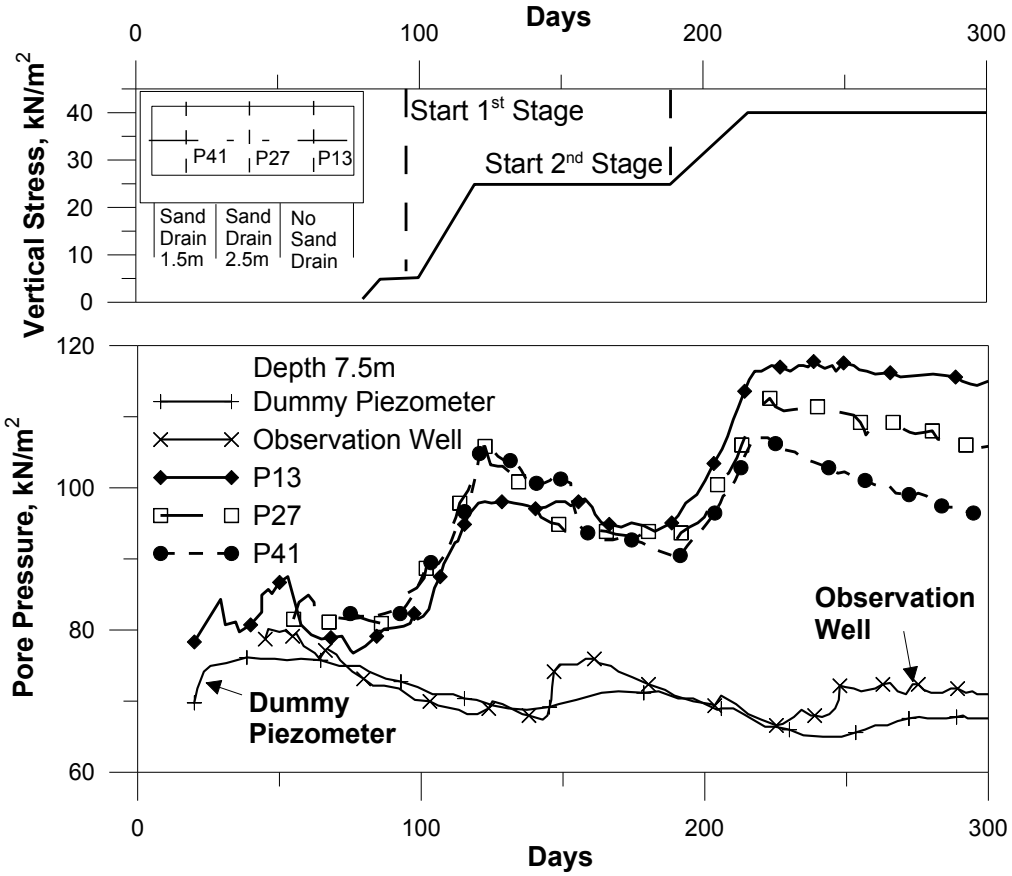

Fig. 4a Typical piezometer readings at RTN Dockyard site (Balasubramaniam et al. 2005)

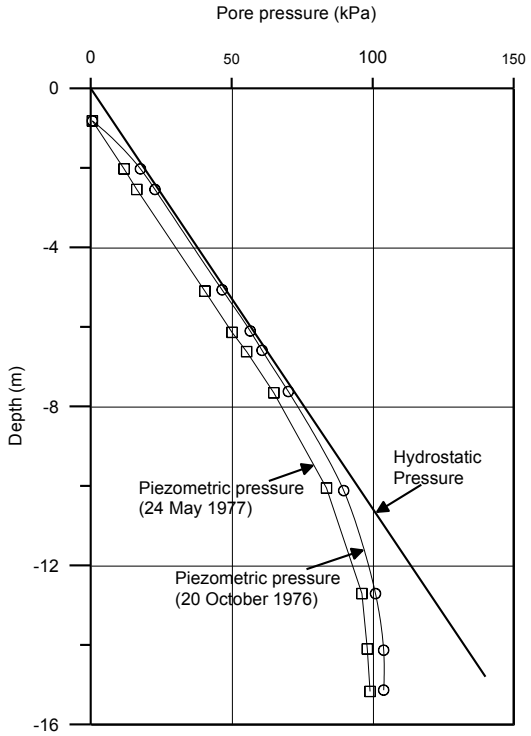

Fig. 4b Variation of Piezometric pressures with depth at RTN Dockyard site (Balasubramaniam et al. 2005)

water during consolidation with drains in clays, while several other authors studied the effect of smear and possible well resistance in the drains. The Muar clay test embankments also showed the defects that arose from using sand compaction piles, piled embankments, and electro-osmosis.

Further studies conducted at AIT on the creep behaviour of the Muar clay test embankments where continuous undrained creep occurred with the increase in lateral deformation indicated that the undrained creep in soft clays due to high embankments was quite substantial. In places where high embankments are constructed with residual soils, undrained creep plays an important role. Loganathan (1992) used the field deformation analysis to separate the immediate settlement from consolidation settlement during the loading stage and to separate the consolidation settlement and creep settlement during the performance stage. This method was different from the Asoka technique used to estimate consolidation settlement under one dimensional consolidation in particular. When high embankments are built in soft clays, creep is a major factor, and this makes it difficult to estimate the so-called residual settlement during the maintenance period in most road works and other projects. Fig. 3 and Fig. 9a contain details of the test embankments built at the Muar Plain. Details of the soil profile at the Muar test embankment site is shown in Fig. 9b.

The total settlement observed beneath an embankment subjected to step loading, is basically a combination of immediate settlement, consolidation settlement, and creep settlement. Establishing relationships between these components, after separating them from the total settlement observed in the field, will help to predict the settlement from relatively simple numerical computations. Separating the settlement components leads to a better understanding of the settlement mechanism and a far better design of step loading. Time-dependent deformation due to undrained creep can be quite large in clays that are normally consolidated and highly overconsolidated. The effects of creep are more important for horizontal deformation than for vertical deformation (Christian and Watt, 1972), although coupling drained creep with undrained creep could be analytically more cumbersome and would require soil data that are difficult to obtain. A new methodology called Field Deformation Analysis (FDA) based on the changes in the volume of foundation soil under embankment loading, was proposed by Loganathan (1992) to separate and quantify the settlement components. Shibata (1987) noted that significant volume changes occurred in the embankment during the construction and that its behaviour deviated significantly from undrained conditions. Ting et al. (1989) and Toh et al. (1989) used a similar concept; they considered the volumetric deformation of the foundation of an embankment under loading to separate the settlement components for the Malaysian embankments.

Total settlement observed during loading was a combination of immediate and consolidation settlement components. Fig. 10 shows the pattern of subsoil deformation stemming from undrained deformation which caused immediate settlement. Because this occurred in an undrained manner, the volume of settlement deformation, designated as AOC, should be equal to the volume of lateral deformation, designated as APM. Due to the dissipation of excess pore pressures, the process of consolidation occurred simultaneously. Fig. 10 also shows the ultimate deformation pattern of the embankment foundation at the end of loading, where the volume that changed vertically (ABC) and laterally (APMQA) was due to consolidation. It should be noted that the volumes referred to here are for the unit length of the embankment.

VvL(volume OAB) is the observed settlement volume in the field from settlement gauge readings, for half the embankment. The settlement volume VvL(volume OAB) at the end of each loading stage is the resultant of the change in volume due to immediate settlement (ViL= volume OAC) and consolidation settlement (VcL = volume CAB) as shown in Fig. 10. Since the loading period was comparatively small, creep settlement was ignored. The increase in lateral volume (volume APM) due to undrained deformation (immediate settlement) decreased during consolidation due to the dissipation of excess pore pressures (Christian and Watt, 1972). Let α be the ratio of the lateral volume reduction to the consolidation settlement volume. Then

α = Lateral consolidation volume/ settlement volume (1)

In Fig.10 VhL is the observed lateral volume change in the field from inclinometer measurements. The volume VhL measured at the end of loading is the resultant of lateral volume increase due to undrained deformation (ViL due to immediate settlement) and the lateral volume reduction during consolidation (αVcL). If Hj and Hj+1 correspond to the height of loading at two stages j and j+1, then α can be determined from

$$\alpha = \frac{\left[\frac{(V_{hl})_{j+1}}{H_{j+1}} - \frac{(V_{hL})_j}{H_j}\right]}{\left[\frac{(V_{vL})_j}{H_j} - \frac{(V_{vL})_{j+1}}{H_{j+1}}\right]} \qquad (2)$$

Similarly at two time stages tj and tj+1, the α factor during the consolidation stage (Fig. 10) can be obtained from

$$\alpha = \frac{\left[\frac{(V_{hC})_{j+1}}{t^{\gamma}_{j+1}} - \frac{(V_{hL})_j}{t^{\gamma}_j}\right]}{\left[\frac{(V_{vC})_j}{t^{\gamma}_j} - \frac{(V_{vC})_{j+1}}{t^{\gamma}_{j+1}}\right]} \qquad (3)$$

where V_{VC} and V_{hc} correspond to the settlement volume and lateral volume during consolidation.

Loganathan (1992) also defined a β factor during consolidation to describe the creep.

β = Lateral creep volume/ creep settlement volume (4)

VcC during the loading stage can be calculated as

$$V_{cC} = \frac{\beta V_{vC} - V_{hC}}{\alpha + \beta} \qquad (5)$$

Similarly, VcC during the loading stage can be calculated from

$$V_{crC} = \frac{\alpha V_{vC} + V_{hC}}{\alpha + \beta} \qquad (6)$$

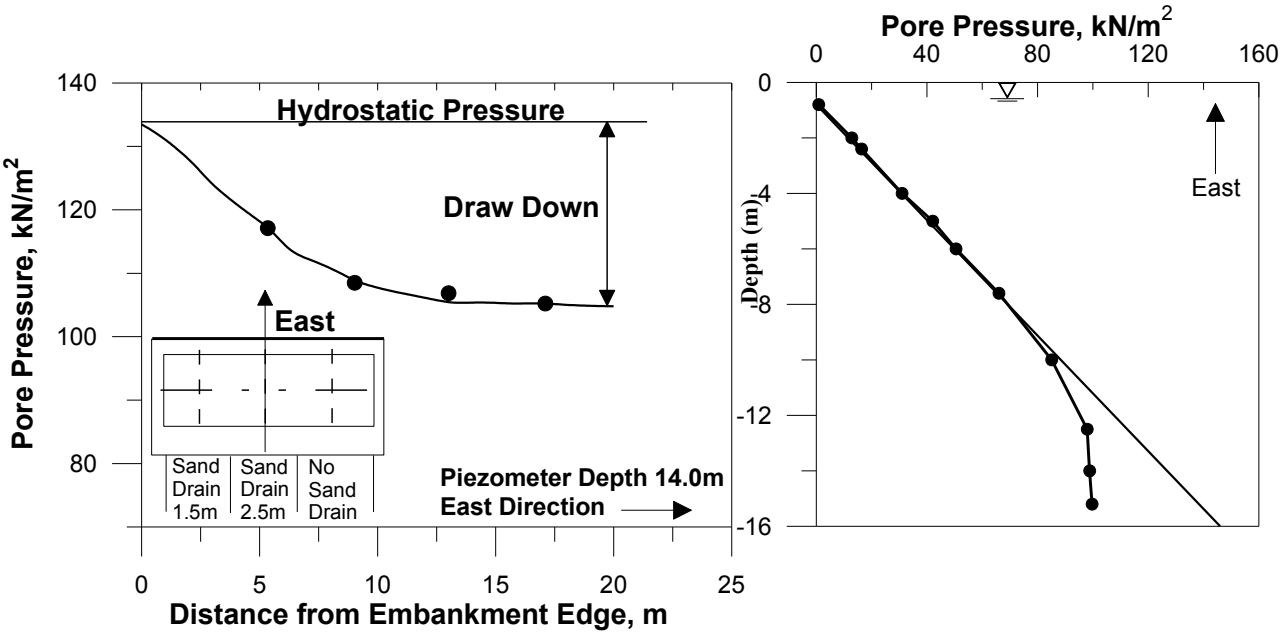

Fig.5 Piezometric pressure vs. distance from the edge of the embankment at RTN Dockyard site (East direction) (Balasubramaniam et al. 2005)

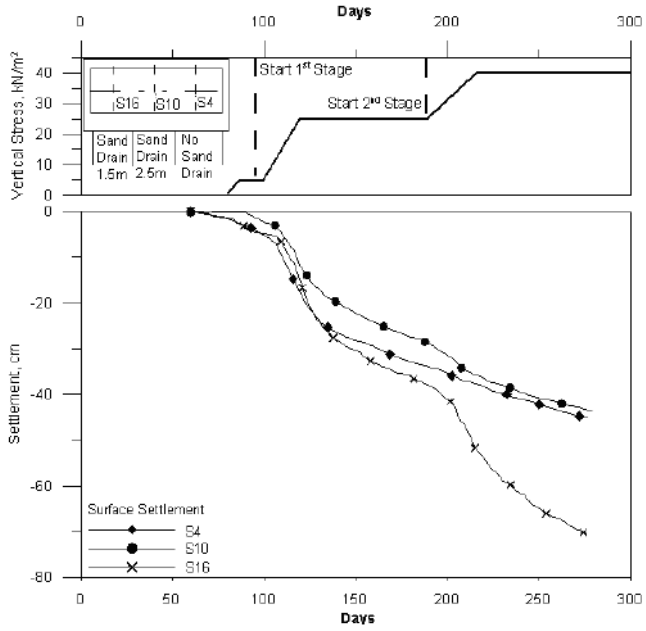

Fig. 6 Time settlement curves with staged construction schedule (Balasubramaniam et al. 2005)

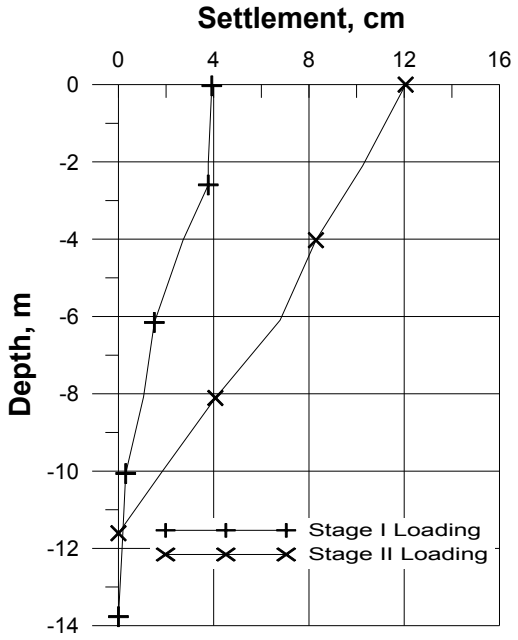

Fig.7 Immediate settlement below embankment at RTN Dockyard site (Balasubramaniam et al. 2005)

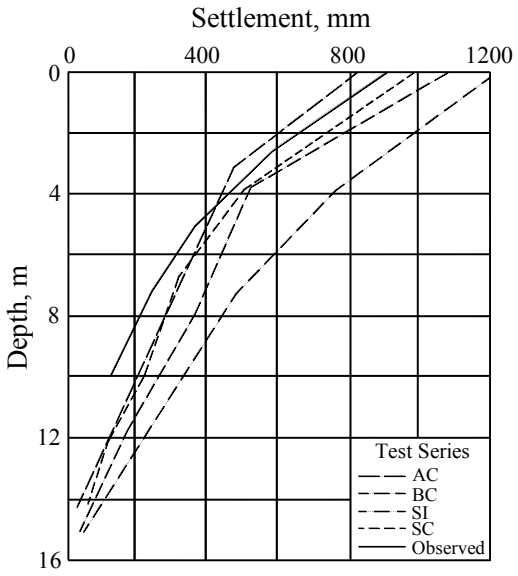

Fig.8. Consolidation settlement below the embankment as calculated at the RTN Dockyard site (Balasubramaniam et al. 2005)

Further details of these derivations can be found in Loganathan et al. (1993). In Fig.11 the creep settlement volume (VcrC) is denoted as volume EFAE. Similarly the lateral creep volume is represented as volume ARMSA

The normalised settlement with maximum settlement at the surface is presented in Fig. 12a and Fig. 12b. The empirical formulation for the 6 m and 3 m high embankments are shown in Eqs. (7) and (8) respectively:

$$S = -0.02z3+0.75z2-14.11z+102.83 \text{ with } r2=98 \text{ percent} \quad (7)$$

$$S = 0.02z3 +0.86z2-15.02z+103.74 \text{ with } r2=97 \text{ percent} \quad (8)$$

If the two sets of embankment data are combined then the combined relationship is

$$S = -0.02z3 +0.86z2-14.68z+103.38 \text{ with } r2=97 \text{ percent} \quad (9)$$

5 TEST EMBANKMENTS AT THE SBIA SITE IN BANGKOK

It became evident from the previous trials that the engineers in Bangkok were rather cautious about the potential use of vertical drains in the Bangkok plain, while the client, the Airport Authority of Thailand insisted that the 1994-1995 study must indicate beyond all doubt that most of the settlement experienced in the trial embankment must be consolidation type which would indicate that water had been removed from the soft clay to improve its strength and to ensure there was no possible hydraulic connections between the PVD used and the underlying sand strata which is experiencing substantial piezometric drawdown. These objectives were to be met by estimating the degree of consolidation from a direct measurement of settlement and from observation of the dissipation of pore pressure in the field. Furthermore, in-situ tests were conducted with vane apparatus to measure the in-situ increase in strength and the reduction of the water content from consolidation due to the use of PVD and surcharge. Additionally, the rate of settlement overtime needed to be plotted to indicate that the final settlement rate was somewhat comparable to that which one would consider acceptable at a rate similar to those experienced in secondary consolidation, and not the higher values corresponding to hydraulic connections.

The plan dimensions of the embankments were the same as the earlier study. The locations of the test embankments and the cross-section of embankment TS3 with PVD are shown in Fig. 13 and Fig. 14 respectively. These embankments were fully instrumented to measure the surface and subsurface settlements, pore pressures, lateral movements and heave. PVD were installed to 12 m depth and the spacing was 1.5, 1.2, and 1.0 m in the three embankments TS1, TS2 and TS3 respectively.

5.1 Settlement and Pore Pressure Plots

All three test embankments performed more or less in the same manner and as such, a detailed discussion will only be based on one (Test embankment TS 3 with PVD spacing at 1 m interval). For this embankment the settlement profile with depth and the pore pressure plots at various times are shown in Fig. 15 and Fig. 16 respectively. In Fig 15, the settlement profiles at the end of construction (270 days), after 450 days (June 95), and after 660 days (Feb 96) are shown.

Settlements were also independently computed from actual pore pressure dissipation. In Fig. 16, the dotted curve ABC represents the actual piezometric profile with draw down that was observed in September 1994 before the embankment was constructed. The full line curve DEF corresponds to the pore pressure profile after the full height of the embankment is reached with a surcharge of 75 kPa and prior to any pore water pressure dissipation. The pore pressure profile at the end of the construction period, in June 95 and in February 1996 is also shown. The final pore pressure after the dissipation of excess pore pressure and the recharged hydrostatic profile is MNPQ (NPQ is the assumed final recharged pore pressure profile, where there are no data points). Settlements were directly computed from these pore pressure dissipation curves.

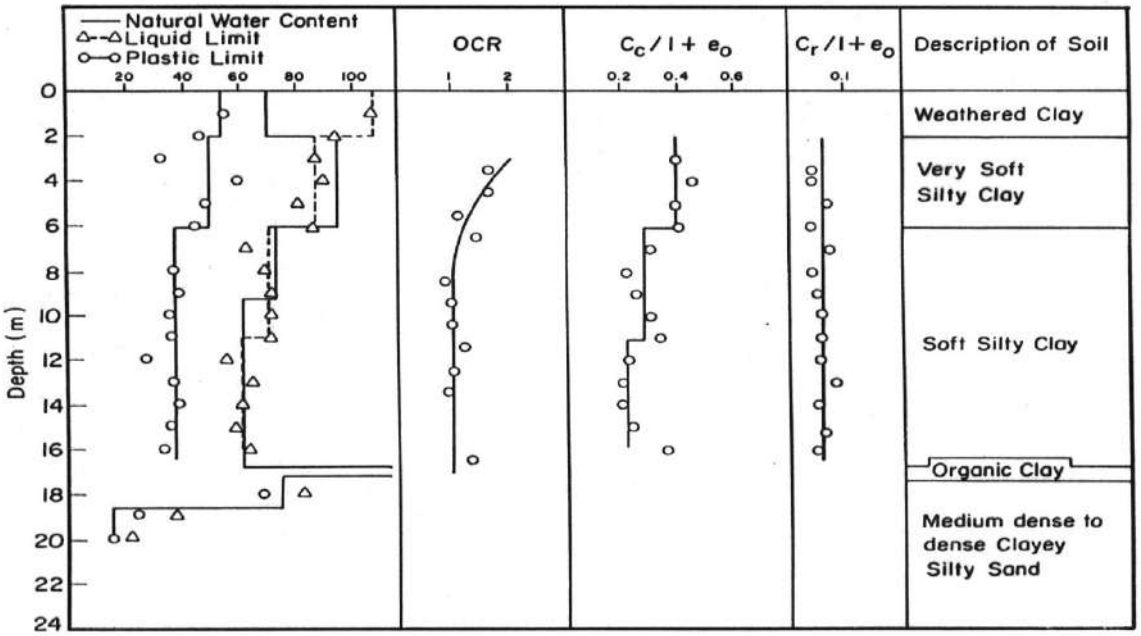

		Liquid Limit ω_L (%)	Plastic Limit ω_P (%)	Natural Water Content ω_n (%)	Plasticity Index	Grain Size (%)			$\frac{C_c}{1+e_o}$	$\frac{C}{1+e_o}$	Preconsolidation Pressure P_c (KPa)
+2.5 mRL						Clay	Silt	Sand			
+0.5	Weathered Crust	108	55	70		42	57	1	.24	.04	110
-5.5	Very Soft Silty Clay with Decated Leaves and Roots	90	40	100	50	48	52	0	.48	.04	40
-15.3	Soft Silty Clay with Traces of Shell Fragments Occasionally Sand Lenses	80	30	60	50	40	60	0	.31	.04	60
-15.9	Peaty Soil										
-19.9	Sandy silt / clay with Organic Matters					22	43	35			
	Dense Medium to Coarse Sand with Gravels SPT N = 21 to 37										

Fig. 9a Soil profile at Muar test embankment site (Indraratna et al. 1992)

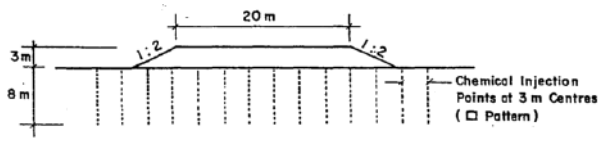

Scheme 3/1

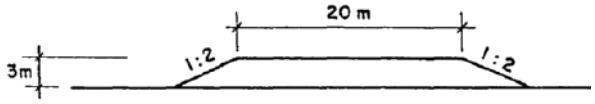

Scheme 3/2

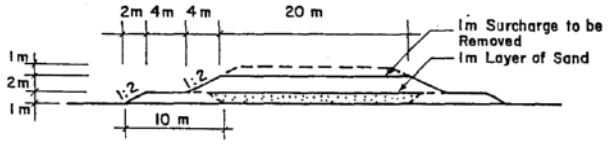

Scheme 3/3

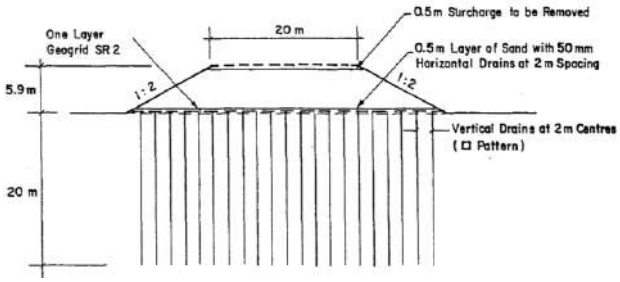

Scheme 3/4

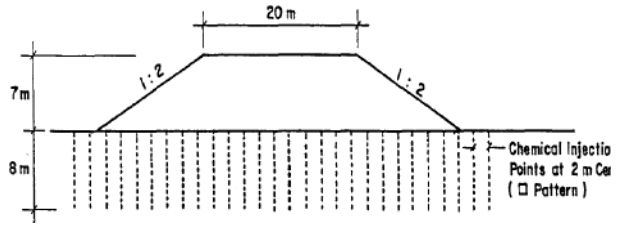

Scheme 6/1

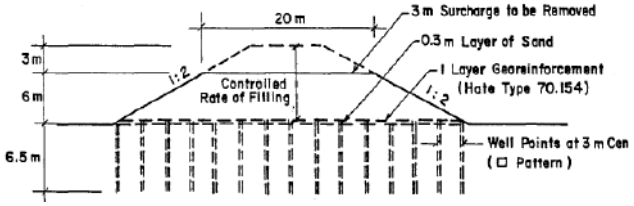

Scheme 6/2

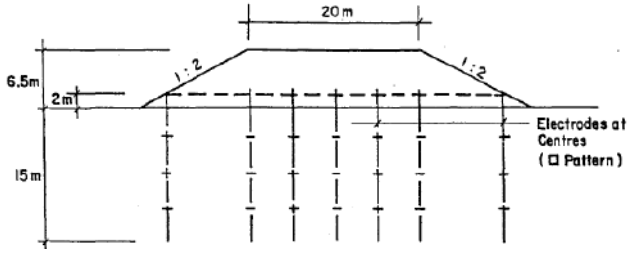

Scheme 6/3

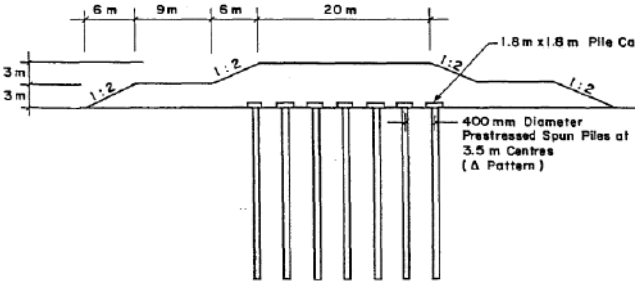

Scheme 6/4

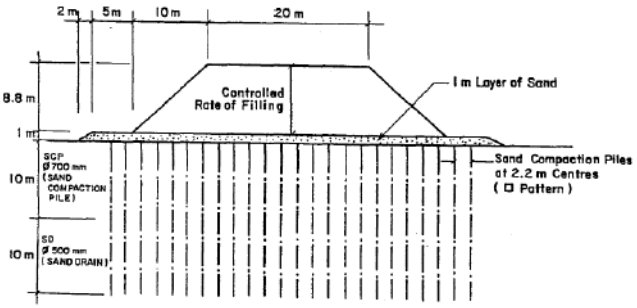

Scheme 6/5

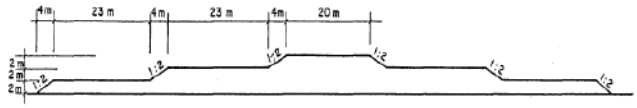

Scheme 6/6

Fig. 9b Malaysian Trial Embankment Schemes (Balasubramaniam et al. 2007)

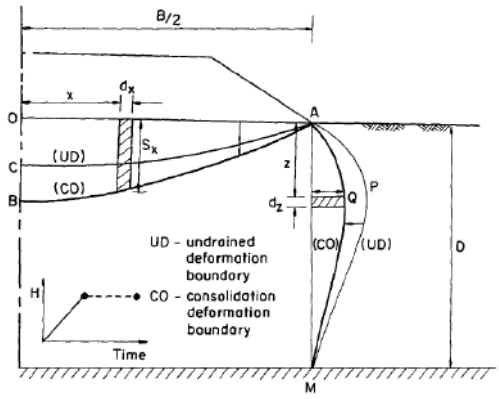

Fig. 10 Deformation Pattern of Embankment Foundation at End of Loading Stage

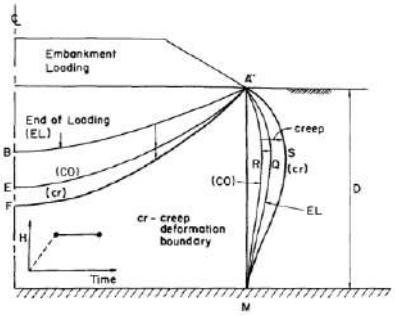

Fig. 11 Deformation Pattern of Embankment Foundation at End of Consolidation Stage

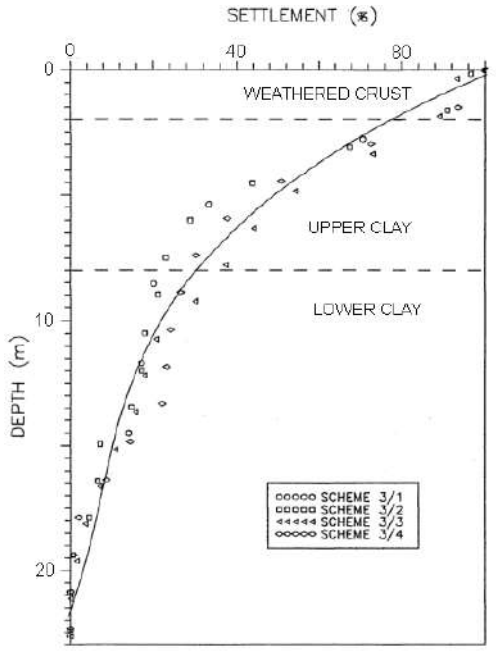

Fig. 12a Variation of Percentage Settlement with Depth for 3m High Embankments

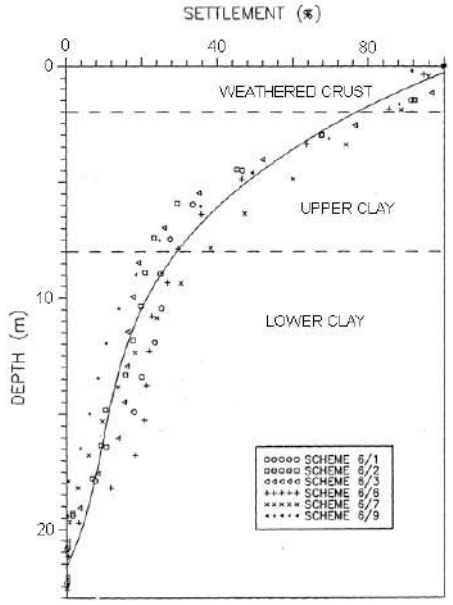

Fig. 12b Variation of Percentage Settlement with Depth for 6 m High Embankments

The degrees of consolidation computed from the pore pressure dissipations are illustrated in Fig. 17. Fig. 18 compares the degree of consolidation computed from the settlement measurements to those estimated from the dissipation of pore pressure. In Fig.18 the ordinate axis Up refers to the degree of consolidation computed from the pore pressure dissipation, while the abscissa axis refers to the degree of consolidation Us computed from the settlement measurements. With due allowance for a small percentage of secondary settlement and creep, the two degrees of consolidation seem to agree well because they are close to the 45 degree line. Due to the limited length of paper, the data related to the lateral movements are not presented here. The deformation due to lateral movement was less than 10 %, as estimated by the method used by Loganathan et al. (1993). The immediate settlement computed from the lateral movements, as adopted by the method where balancing the volume (Loganathan et al., 1993) was within 10 % of the measured vertical settlement. The rate of settlement and the rate of lateral movements were plotted in Fig. 19 and Fig. 20, and were found to decay with time. Also the settlement log-time plots in Fig. 21 for the TS1 and TS3 test embankments were found to be approaching a constant slope. An attempt was made to define the 100% primary consolidation time using the Casagrande type of settlement versus log-time plots. The points P and Q (shown in Fig. 21) correspond to the 100% primary consolidation for the Test Section TS3 and TS1 respectively. The data for TS2 is not shown because it would crowd out the data from the other two embankments. The final portions of the test data for the two embankments seemed to approach the secondary consolidation part as computed from the Casagrande settlement versus log-time plots. These results further confirmed that the PVD did not cause any hydraulic connection with the lower aquifers and the measured final settlement is of the same order as the secondary settlement.

Finally, the increase in the shear strength with time after consolidation in the field was measured with the vane shear apparatus, as plotted in Fig. 22.

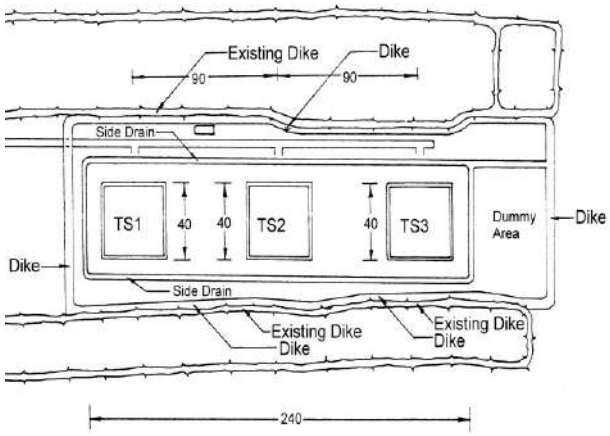

Fig. 13 Site plan of test embankments TS1, TS2 and TS3 at SBIA site (Balasubramaniam et al. 2007)

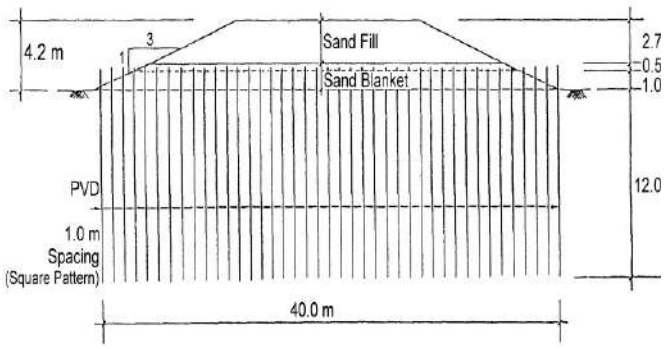

Fig. 14 Cross section TS3 showing PVD at SBIA site (Balasubramaniam et al. 2007)

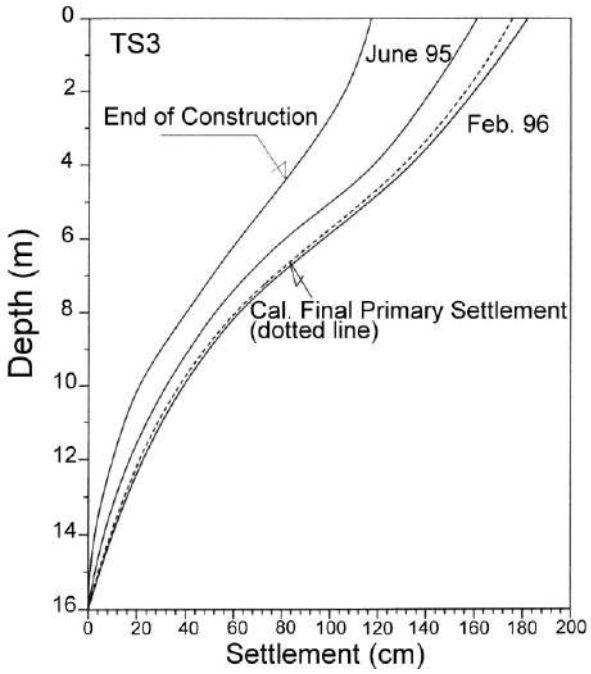

Fig. 15 Settlement plot of test embankment with PVD at SBIA site (Balasubramaniam et al. 2007)

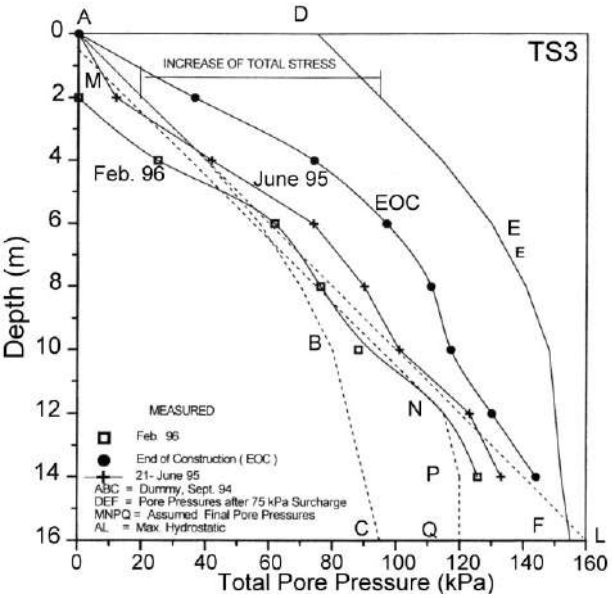

Fig. 16 Pore pressure profile of test embankment with PVD at SBIA site (Balasubramaniam et al. 2007)

6 CONCLUDING REMARKS

This paper set out to study the role of test embankments as a site investigation into the design and construction aspects of ground improvement works in soft clays. Test embankments in Bangkok, Thailand, and the Muar site in Malaysia and in Southeast Queensland were used as case studies. The work mainly emphasised the practical aspects related to stability and deformation, and even though research work on this subject has been there for more than

five decades, yet the Case A type of Prediction of the stability and settlement characteristics is still a challenging task.

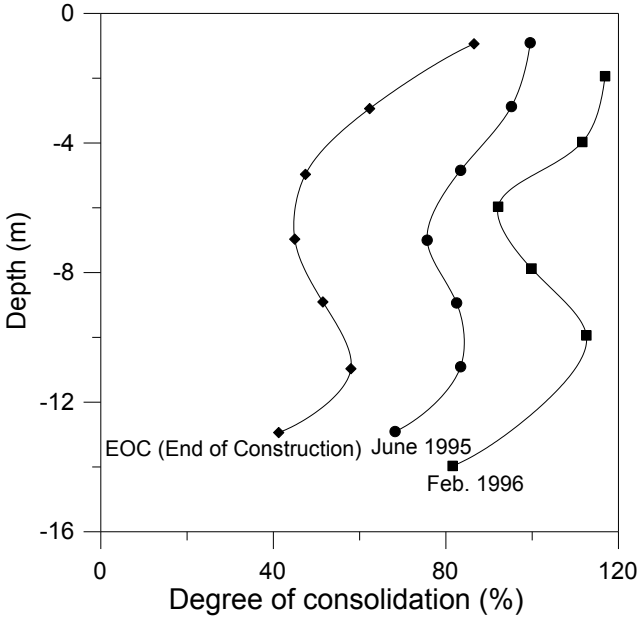

Fig. 17 Degree of consolidation from measured pore pressure at SBIA site (Balasubramaniam et al. 2007)

From the test embankment studies carried out in Bangkok with and without ground improvement, most of this experience was with embankments constructed using sand. Without any ground improvement, the failure height of these embankments was very modest and was in the range of 2.5 m to 3.5 m. Vane shear strengths were adequate enough to determine the stability of these embankments with a total stress analysis, although the Bjerrum's correction factor as based on the plasticity index was essential.

Data from three fully instrumented test embankments revealed that when vertical drains were used in the Bangkok Plain the piezometric draw-down which naturally exists in the Plain due to deep well pumping, was virtually eliminated in the upper clay layer. Moreover, the presence of sand and silt seams tended to assist lateral drainage and therefore test embankments with and without drains had to have large spaces between to eliminate any type of interference. The possibility of interference also remained in the soft clays of Southeast Queensland and elsewhere where the presence of sand and silt seams and the existence of piezometric drawdown had made it difficult for the vacuum drainage to be implemented successfully. Recent modifications and improvements to the sealing methods together with the use of Bentonite type cut off walls were not included in the studies made here. Test embankments built on soft clay with pre-fabricated vertical drains have performed successfully in accelerating the consolidation settlement when the PVD spacing was properly designed to take care of the smear effect and well resistance, as proposed by Hansbo and others. The spacing for the soft Bangkok clay was about 1.5 m. The immediate settlement observed was generally of the order of 10 %. The Asaoka method and a Field Deformation Analysis were also performed to confirm the magnitude of consolidation settlement and immediate settlement respectively. Computations of settlement from pore pressure dissipation and direct settlement measurements agreed well and the magnitude of long term secondary settlement was also computed from the field data.

The test embankment studies at the Muar site indicated the importance of the fill strength in the stability characteristics when well compacted residual soil was used. Also the Field Deformation Analysis successfully separated the consolidation settlement, the immediate settlement, and the long term creep settlements. The normalised settlement profile and the normalised lateral movement profiles for several ground improvement schemes were found to be

similar in shape. The use of sand compaction piles and pre-stressed piles were found to successfully minimise lateral deformation at the toe of the embankments.

In all the test embankment studies, predicting the observed behaviour was possible using the CRISP computer program and soft clay models of the type developed at Cambridge University

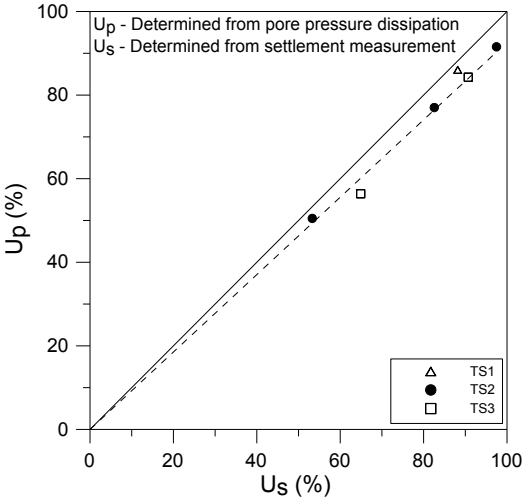

Fig. 18 Degree of consolidation computed from pore pressure dissipation and settlement measurements at SBIA site (Balasubramaniam et al. 2007)

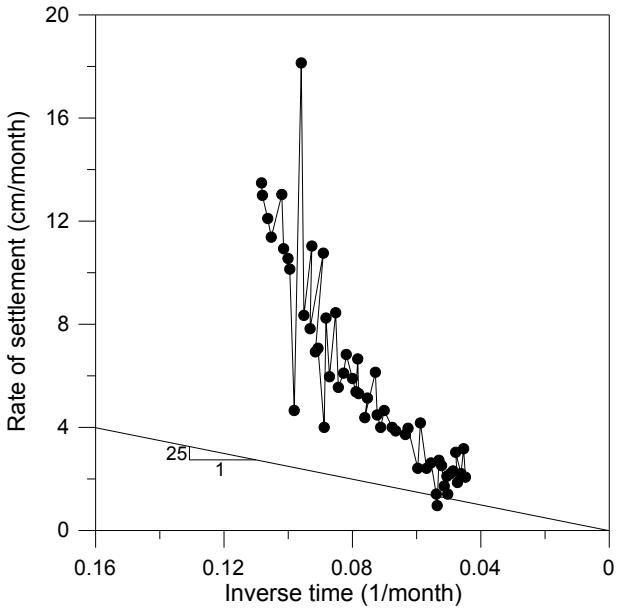

Fig. 19 Rate of settlement versus inverse time plot at SBIA site (Balasubramaniam et al. 2007)

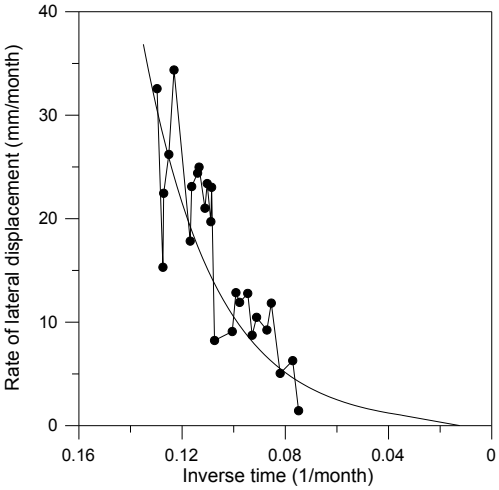

Fig. 20 Rate of lateral movement versus inverse time plot at SBIA site (Balasubramaniam et al. 2007)

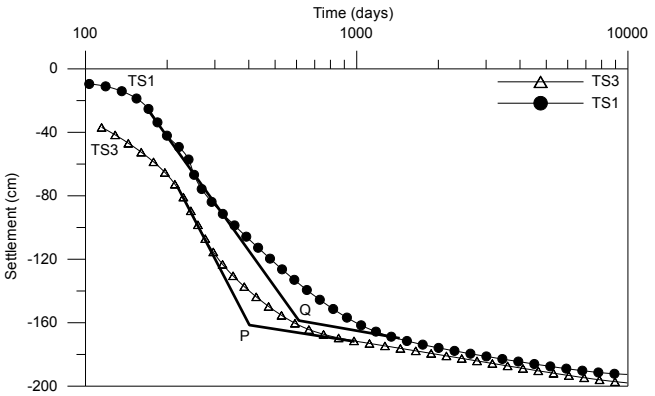

Fig. 21 Settlements versus log-time plot for embankments TS1 and TS3 at SBIA site (Balasubramaniam et al. 2007)

7 ACKNOWLEGEMENT

The work presented in this paper relates to the research work conducted by the first author over a period of 27 years at the Asian Institute of Technology as sponsored research projects and graduate thesis research work. The close collaboration that the first author enjoyed while having several discussions with the late OveEide of the Norwegian Geotechnical Institute, former colleagues Dr. ZaChiehMoh, Dr. Edward W Brand, Prof. PrinyaNutalaya, Dr. Peter Brenner, Drs Ting Wen Hui, OoiTeikAun, Chan Sin Fatt, Dr. Noppodol Phienwej, Dr. Seah, Mr.VasanthaWijekulasooriya, Dr. Chu Jian, Dr. Bo, Dr. Arul Rajah, and a large number of AIT Alumni and friends are gratefully acknowledged. The Royal Thai Navy and the Airport Authority of Thailand are thanked for engaging the first author and his team in carrying out the elaborate full-scaled field tests and the interpretation of the data presented in this paper. The first author is also most grateful to the large number of Master students and Research Associates at AIT who had helped him carry out the work presented in this paper over a thirty year period. A substantial component of the technical details presented in this paper can be found in earlier publications by the first author and his co-workers in the Journal of Geotechnical and Geoenvironmental Engineering ASCE and Canadian Geotechnical Journals and International Journal for Numerical and Analytical Methods in Geomechanics, since mid 1990's

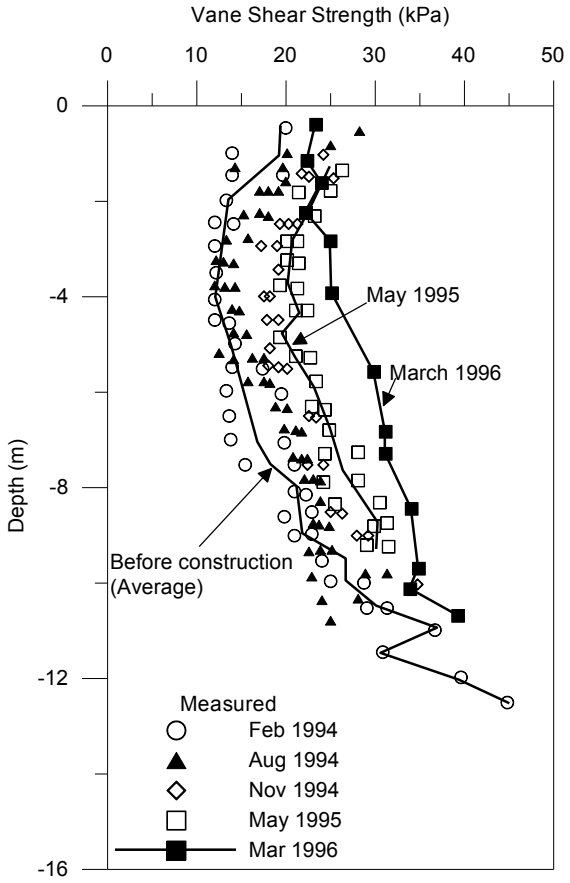

Fig. 22 Field vane shear strength as measured in embankment TS3 at SBIA site (Balasubramaniam et al. 2007)

8 REFERENCES

Balachandran,S. (1990). Simulation of a test embankment failure (Muar flood plain, Malaysia) using finite element techniques coupled with critical state soil mechanics, AIT M Eng thesis, Bangkok, Thailand.

Balasubramaniam, A. S., Oh, E. Y. N., Bolton, M. W.,Bergado D.T., Phienwej, N. (2005). Deep-well pumping in the Bangkok Plain and its influence on ground improvement development with surcharge and vertical drains. Ground Improvement 9, No. 4, 149–162.

Balasubramaniam, A. S., Huang, M., Bolton, M. W., Oh, E. Y. N., Bergado D.T., Phienwej, N. (2007). Interpretation and Analysis of Test Embankments in Soft Clays with and without Ground Improvement. Proceedings of the Sixteenth Southeast Asian Geotechnical Conference, in CD.

Brand, E.W., and Premchitt, J. (1989), Moderator's report for the predicted performance of the Muar test embankment, Proc. Int. Symp. Trial Embankment on Malaysian Marine clays, Kuala Lumpur, Malaysia, Vol.2, 1/32 -1/49.

Christian, L.T. and Watt,J.B. (1972), Undrained visco-elastic analysis of soil deformations, Application of the FEM in Geotechnical Engineering, Proc. Symp. Vicksburg, Mississippi, May, 2, 533-574.

Cox, J. B. (1967). A review of the engineering characteristics of the recent marine clays in Southeast Asia, Research Report No 6, Asian Institute of Technology, Bangkok, Thailand.

Eide, O. (1968). Geotechnical engineering problems with soft Bangkok clay on the NakhonSawan highway project.Pub. No 78, Norwegian Geotechnical Institute, Norway.

Eide, O. (1977). Exploration, sampling and insitu testing of soft clay in the Bangkok area, Proc. of International Symposium on Soft Clay, Thailand, 122-137.

Indraratna, B., Balasubramaniam, A. S. S and Sivaneswaran, N. (1997). Analysis of Settlement and Lateral Deformation of Soft Clay Foundation beneath Two Full-Scale Embankments, International Journal for Numerical and Analytical Methods in Geomechanics, Vol. 21, 599-618.

Indraratna, B., Balasubramaniam, A. and Balachandran, S. (1992). Performance of Test Embankment Constructed to Failure on Soft Clay. Journal of Geotechnical Engineering, ASCE, Vol. 118, No. 1, pp. 12-33.

Loganathan, N (1992). Analysis of test embankment on Malaysian Muar clays, AIT M Eng thesis, Bangkok Thailand.

Loganathan, N., Balasubramanaim, A. S., and Bergado, D. T. (1993). Deformation analysis of embankments, Journal of Geotechnical Engineering, ASCE, 119(8), 1185-1206.

Moh, Z.C., Brand, E.W. and Nelson, J.D. (1973), Performance of test sections for new Bangkok Airport at nong NgooHao, AIT Research Report to Northrop Airport Development Corporation.

Moh, Z. C., and Woo, S. M., (1987). Preconsolidation of Bangkok clay by non-displacement sand drains and surcharge, Proc. of 9th Southeast Asian Geotechnical Conference, Bangkok, Thailand, 1, 287-296.

Moh, Z. C., Nelson, J. D., and Brand, E. W. (1969). Strength and deformation behaviour of Bangkok clay, Proc. of 7th Int. Conf. On Soil Mechanics and Foundation Engineering, Mexico, 1, 287-295.

Muktabhant, C., Teerawong, P., and Tengamnuay, V. (1967). Engineering properties of Bangkok subsoils, Proc. of Southeast Asian Conference on Soil Engineering, Bangkok, 1, 1-7.

Ratnayake, A.M.P. (1991). Performance of test embankment with and without vertical drains at Muar Clays, Malaysia, AIT M Eng thesis, Bangkok, Thailand.

Shibata, T (1987), Lateral deformation of clay foundations, Discussion 6,Proc. 8th. Asian Regional Conf. on S.M.F.E., Kyoto, 2, 390-391.

Sivaneswaran, N. (1993). Performance of trial embankments on treated and untreated soft clay at the Muar Site, Malaysia. AIT M Eng thesis, Bangkok, Thailand.

Tavenas, F. and Leroueil, S. (1980), The behaviour of embankments on clay foundations, Canadian Geotech. Jour., vol 17, pp. 236-260.

Ting,W.H., Chan,S.F. and Kassim,K. (1989), Embankments with geogrid and vertical drains, Proc. Int. Symp. On Trial Embankments on Malaysian Marine Clays, Kuala Lumpur, 2.

Toh, C.T., Chee, S.K., Hudson, R.R., Loh, M.H., and Gue,S.S. (1989), 3m high control embankment on untreated soft ground, MHA. Int. Symp. On Trial Embankments on Malaysian Marine clays, Kuala Lumpur, 2.

THE APPLICATION OF VERTICAL DRAINS AND VACUUM PRELOADING FOR IMPROVING SOFT GROUND

C. Rujikiatkamjorn[1] and B. Indraratna[2]

1Associate Professor, Centre for Geomechanics and Railway Engineering, University of Wollongong, Wollongong City, Australia
cholacha@uow.edu.au
2Professor of Civil Engineering, School of Mining and Environmental Engineering
Research Director of Centre for Geomechanics and Railway Engineering, University of Wollongong, Wollongong City, Australia,
E-mail: indra@uow.edu.au

ABSTRACT: Much of the world's essential infrastructure is built along congested coastal belts that are composed of highly compressible and weak soils up to significant depths. Soft alluvial and marine clay deposits have very low bearing capacity and excessive settlement characteristics, with obvious design and maintenance implications on tall structures and large commercial buildings, as well as port and transport infrastructure. Stabilising these soft soils before commencing construction is essential for both long term and short term stability. Pre-construction consolidation of soft soils through the application of a surcharge load alone often takes too long, apart from which the load required to achieve more than 90% consolidation of these mostly low lying, permeable, and very thick clay deposits can be excessively high over a prolonged period. A system of vertical drains combined with vacuum pressure and surcharge preloading has become an attractive alternative in terms of both cost and effectiveness. This technique accelerates consolidation by promoting rapid radial flow which decreases the excess pore pressure while increasing the effective stress.

Over the past 15 years the second Author and his co-workers have developed numerous experimental, analytical, and numerical approaches that simulate the mechanics of prefabricated vertical drains (PVDs) and vacuum preloading, including two-dimensional and three-dimensional analyses, and more comprehensive design methods. These recent techniques have been applied to various real life projects in Australia and Southeast Asia. Some of the new design concepts include the role of overlapping smear zones due to PVD-mandrel penetration, pore pressure prediction based on the elliptical cavity expansion theory. These recent advances enable greater accuracy in the prediction of excess pore water pressure, and lateral and vertical displacement of the stabilised ground. This paper also presents an overview of the theoretical and practical developments and salient findings of soft ground improvement via PVD and vacuum preloading, with applications to selected case studies in Australia, Thailand, and China.

1 INTRODUCTION

Soft clay deposits usually possess a low bearing capacity, as well as excessive settlement characteristics, and therefore it is necessary to improve the existing soft soils before construction activities commence in order to prevent excessive and differential settlement (Richart, 1957). The use of vertical drains with preloading is a popular technique for improving soil because vertical drains accelerate consolidation by providing short horizontal drainage paths. For this reason they are employed worldwide in many soft soil improvement projects (Holtz et al., 1991; Indraratna et al., 1992; Indraratna and Redana, 2000; Chu et al. 2000; Chai et al., 2006; Indraratna et al. 2011). Prefabricated vertical drains (PVDs) have become an economical and viable ground improvement option because of their rapid installation with simple field equipment (Shang et al. 1998, Bo et al. 2003; Chai et al., 2010; Artidteang et al. 2011; Walker et al. 2009). In order to increase the stability of embankments, surcharge placement is usually a multi-stage exercise with rest periods between the loading stages so that consolidation and the associated gain in shear strength occur before the next lift (Jamiolkowski et al. 1983, Mesri and Khan 2012). This practice may not be possible with tight construction schedules or foundation soil with very low shear strength, which is why the application of a vacuum load in addition to surcharge fill can further accelerate the rate of settlement to obtain the desired settlement without increasing the excess pore pressure (Kjellman, 1952; Qian et al., 1992; Qiu et al. 2007; Saowapakpiboon et al. 2011, Indraratna et al. 2010a). This practice has been used for land reclamation and port projects (Tang and Shang 2000; Yan and Chu 2005; Chu and Yan, 2005, Chai et al. 2010; Saowapakpiboon et al. 2010; Indraratna et al. 2011). The PVDs distribute the vacuum pressure to deep layers of subsoil, thereby reducing the excess pore water pressure due to surcharge loading (Zhu and Miao 2002; Chai et al. 2009; Indraratna et al. 2010b). The consolidation process of vacuum preloading compared to conventional preloading is shown in Figure 1.

In this paper a modified radial consolidation theory that considers the effects of time dependent surcharge loading and vacuum pressure is proposed. The smear zone prediction using the Elliptical Cavity Expansion Theory is discussed based on the results of large scale laboratory tests. The equivalent (transformed) plane strain conversion is incorporated into finite element codes using the modified Cam-clay theory. Case histories are discussed and analysed, including the site of the Second Bangkok International Airport (Thailand) and the Port of Brisbane. The predictions are compared with the available field data.

2 THEORETICAL APPROACH

2.1 Development of Vacuum Consolidation Theories

The mechanism of vacuum-assisted consolidation is comparable to, but not the same as conventional surcharge. In earlier studies, vacuum preloading was often simulated with an equivalent surface load or by modifying the surface boundary condition. However, laboratory observations confirm that the vacuum pressure propagates downwards along the drains in addition to the uniformly applied surface suction. In the absence of vertical drain, Mohamedelhassan and Shang (2002) developed a vacuum and surcharge combined one-dimensional consolidation model based on the Terzaghi's consolidation theory. Indraratna et al (2004, 2005a) Geng et al. (2012) showed that when a vacuum pressure is applied in the field through PVDs, the suction head along the drain length may decrease with depth and thereby reduce its efficiency. A modified radial consolidation theory to include different vacuum pressure distribution patterns has been proposed. The results indicate that the efficiency of vertical drains depends on both the magnitude of vacuum pressure and its distribution. Chai et al. (2006; 2010) and Robinson et al. (2012) introduced an approximate method for calculating the ground settlement and inward lateral displacement induced by vacuum consolidation. Rujikiatkamjorn and Indraratna (2007; 2009) presented the design charts for vacuum consolidation.

magnitude of vacuum pressure and its distribution. Chai et al. (2006; 2010) and Robinson et al. (2012) introduced an approximate method for calculating the ground settlement and inward lateral displacement induced by vacuum consolidation. Rujikiatkamjorn and Indraratna (2007; 2009) presented the design charts for vacuum consolidation.

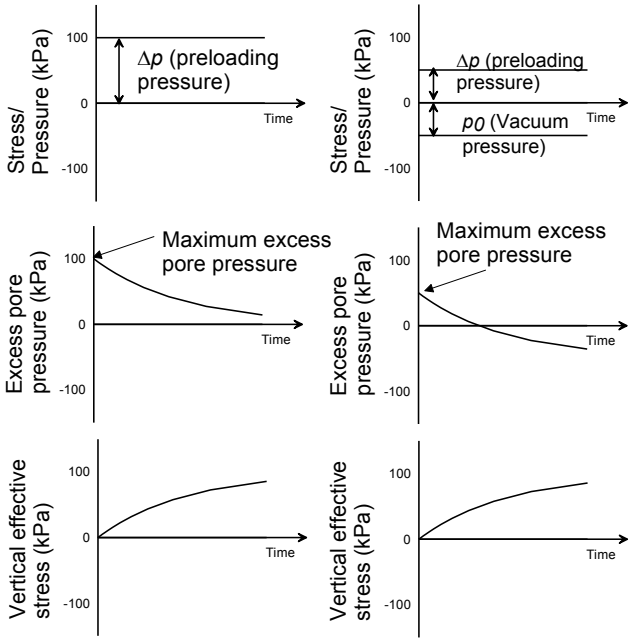

Figure 1 Consolidation process: (a) conventional loading (b) idealised vacuum preloading (modified from Indraratna et al. 2005c)

2.2 Solution for Axisymmetric Condition

A radial consolidation theory incorporating the smear effect and well resistance was proposed by Barron (1948) and Hansbo (1981). The application of a vacuum pressure with only a surcharge load along the surface (i.e. no vertical drains), was modelled by Mohamedelhassan and Shang (2002) based on one-dimensional consolidation. The above mathematical models are based on instantaneous loading and a constant coefficient of lateral permeability (kh). Lekha et al. (1998) further extended the solution by incorporating time dependent surcharge loading. Walker et al. (2009) proposed a spectral method for a vertical and redial consolidation analysis of stratified soils. Indraratna et al. (2005b) introduced the unit cell analysis for vacuum preloading under instantaneous loading. However, while an embankment is being constructed on soft clay, the fill surcharge is usually raised over time to attain the desired height. Therefore, a time dependent loading due to filling would be more appropriate than an instantaneous loading, especially during the initial stages of construction. In this Section the embankment load from filling (□t) is assumed to increase linearly up to a maximum value (□ at time t0 and kept constant thereafter (Figure 2a). The vacuum is applied at t=tvac. Figure 2b illustrates the unit cell adopted for analytical solutions with boundary conditions (Figure 2c).

Indraratna et al. (2011) proposed that the average excess pore pressure due to radial consolidation while considering the smear effect under time dependent surcharge ($\overline{u_L}$) can be expressed by:

$$\overline{u_L} = \frac{\mu d_e^2}{8c_h t_0}\left(1-\exp\left(\frac{-8c_h t}{\mu d_e^2}\right)\right)\sigma_1 \quad for \quad 0 \le t \le t_0$$

$$\overline{u_L} = \frac{\mu d_e^2}{8c_h t_0}\left(1-\exp\left(\frac{-8c_h t_0}{\mu d_e^2}\right)\exp\left(\frac{-8c_h (t-t_0)}{\mu d_e^2}\right)\right)\sigma_1 \quad for \quad t > t_0 \qquad (2)$$

where, d_e is the influence zone diameter, c_h is the coefficient of consolidation for horizontal drainage, σ_1 = applied surcharge pressure, t = time.

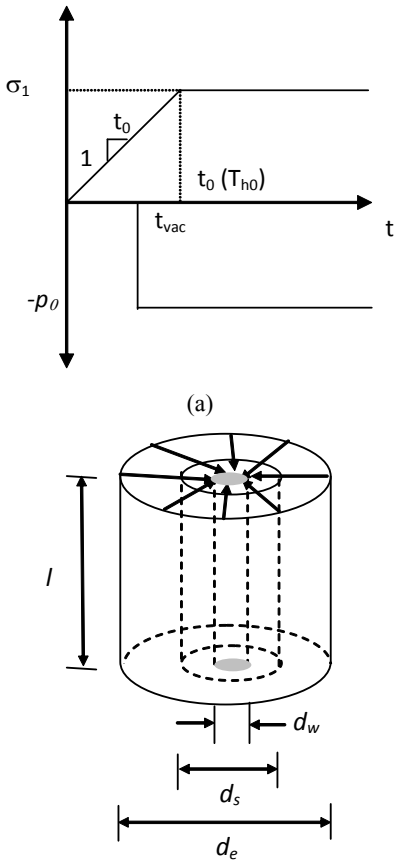

Figure 2 (a) time-dependent loading, (b) unit cell, and (c) boundary conditions

Recently, Indraratna et al. (2005b) showed that the average excess pore pressure under radial consolidation due to vacuum pressure (u_{vac}) alone could be determined from:

$$u_{vac} = 0, \qquad t < t_{vac} \tag{3}$$

$$u_{vac} = p_0 \exp\left(-\frac{-8c_h(t-t_{vac})}{\mu d_e^2}\right) - p_0, \qquad t \geq t_{vac} \tag{4}$$

where d_e = the diameter of the soil cylinder dewatered by a drain, d_s = the diameter of the smear zone, d_w = the equivalent diameter of the drain, k_s = horizontal soil permeability in the smear zone, μ = a group of parameters representing the geometry of the vertical drain system and the smear effect. Hansbo (1981) assumed the smear zone to have a reduced horizontal permeability that is constant throughout this zone. The μ parameter is given by:

$$\mu = \ln n/s + k_h/k'_h \ln s - 0.75 \tag{5a}$$

where, $n = \frac{d_e}{d_w}$, $s = \frac{d_s}{d_w}$, d_s =diameter of smear zone, d_w = equivalent diameter of drain, k_h = permeability in the undisturbed zone and k'_h = permeability in the smear zone.

However, laboratory testing conducted by Onoue et al. (1991), Indraratna and Redana (1998) and Sharma and Xiao (2000), using a large scale consolidometer, suggests that the disturbance in the 'smear zone' increases towards the drain (Figure 3). To obtain more accurate predictions, Walker and Indraratna (2006) employed a parabolic decay in horizontal permeability towards the drain to represent the actual variation of permeability in the smear zone. The μ parameter can be given by:

μ parameter can be given by:

$$\mu_p = \left[\begin{array}{l} \ln\left(\frac{n}{s}\right) - \frac{3}{4} + \frac{\kappa(s-1)^2}{\left(s^2 - 2\kappa s + \kappa\right)} \ln\left(\frac{s}{\sqrt{\kappa}}\right) \\ - \frac{s(s-1)\sqrt{\kappa(\kappa-1)}}{2\left(s^2 - 2\kappa s + \kappa\right)} \ln\left(\frac{\sqrt{\kappa} + \sqrt{\kappa-1}}{\sqrt{\kappa} - \sqrt{\kappa-1}}\right) \end{array}\right] \tag{5b}$$

In the above expression $\kappa = k_h/k_0$ and k_0 = minimum permeability in the smear zone.

The excess pore pressure at a given time t can determined based on the combination of Equations (1) to (5). For normally consolidated clay, the vertical settlement (ρ) can now be evaluated by the following equations:

$$\rho = \frac{HC_c}{1+e_0} \log\left(\frac{\sigma'}{\sigma'_i}\right) \tag{6}$$

where ρ = settlement at a given time, C_c = compression index, σ' = effective at a given time, σ'_i = initial effective stress, and H = thickness of compressible soil.

In order to predict excess pore pressures and associated settlements, Equations (1)-(6) can be used in conjunction with the soil properties of each layer and the thickness of the soil for each section.

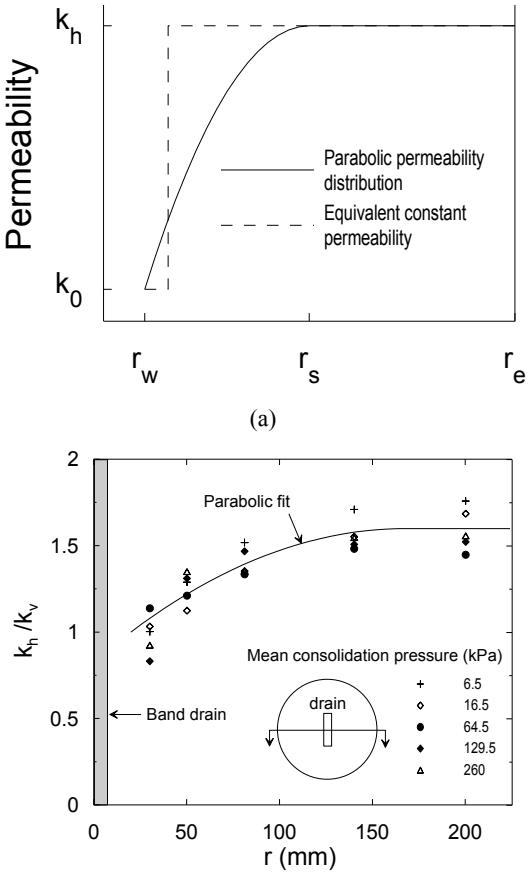

Figure 3 (a) Permeability distribution and (b) ratio of horizontal to vertical permeability (kh/kv) along radial distance from drain in large scale consolidometer (Walker and Indraratna, 2006) (re=de/2, rs=ds/2 and rw = dw/2)

2.3 Conversion Procedure for Equivalent Plane Strain Analysis

Indraratna and Redana (2000) and Indraratna et al. (2005a) showed that, based on the appropriate conversion procedure, and by considering the degree of consolidation at a given time step, plane stain multi-drain analysis can be used to predict the behaviour of soft soil improved by vertical drains and vacuum preloading. Using the geometric transformation in Figure 4, the corresponding ratio of the permeability of the smear zone to the undisturbed zone is obtained by (Indraratna et al., 2005a):

$$\frac{k'_{h,ps}}{k_{h,ps}} = \beta \Big/ \left(\frac{k_{h,ps}}{k_{h,ax}}\left[\ln\left(\frac{n}{s}\right) + \frac{k_{h,ax}}{k'_{h,ax}}\ln(s) - \frac{3}{4}\right] - \alpha\right) \tag{7}$$

where $\alpha = 0.67 \times (n-s)^3 / n^2(n-1)$, $\beta = \frac{2(s-1)}{n^2(n-1)}\left[n(n-s-1) + \frac{1}{3}\left(s^2+s+1\right)\right]$ and subscripts *ps* and *ax* represent plane strain and axisymmetric condition, respectively

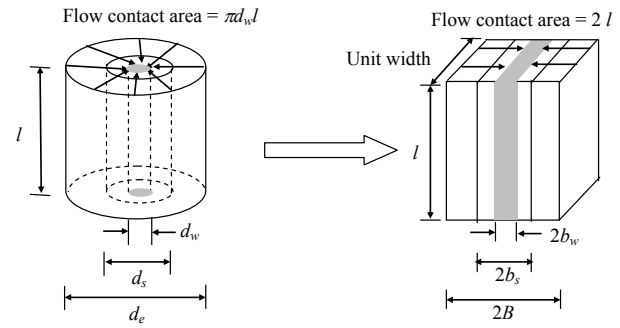

Figure 4 Unit cell analysis: (a) axisymmetric condition, (b) equivalent plane strain condition (after Indraratna et al., 2005a) (B=b_s, b_w= half width of unit cell, smear zone and drain, respectively under plane strain condition)

By ignoring the effects of both smear and well resistance, a simplified ratio of equivalent plane strain to axisymmetric permeability in the undisturbed zone can be attained based on the geometric equivalence (i.e. $d_w=2b_w$, $d_s=2b_s$, $d_e=2B$, in Figure 4, Indraratna et al., 2005) hence;

$$k_{h,ps} / k_{h,ax} = \frac{2}{3}\frac{(n-1)^2}{n^2} / \left[\ln(n) - 0.75\right] \tag{7a}$$

2.4 Consolidation Theory for Multi-layered Soil

Assuming time independent soil properties that vary spatially with depth, the governing equation for consolidation with combined vertical and radial drainage under instantaneous loading and equal strain conditions in a cylindrical unit cell can be derived as (Walker, 2006):

$$\frac{m_v}{\overline{m}_v}\frac{\partial \overline{u}}{\partial t} = -\left[dT_h \frac{\eta}{\overline{\eta}}\overline{u} - dT_v \frac{\partial}{\partial Z}\left(\frac{k_v}{\overline{k}_v}\frac{\partial \overline{u}}{\partial Z}\right)\right] \tag{8}$$

where $Z = \frac{z}{H}$, $dT_v = \frac{\overline{c}_v}{H^2}$, $dT_h = \frac{2\overline{\eta}}{\gamma_w \overline{m}_v}$, $\overline{c}_v = \frac{\overline{k}_v}{\gamma_w \overline{m}_v}$, $\eta = \frac{k_h}{r_e^2 \mu}$

In the preceding, $\overline{u}$ =average excess pore pressure for a given depth, t =time, z =depth, H =depth of soil, γ_w =unit weight of water, m_v =volume compressibility and k_v =vertical permeability. Equation (8) has been normalised with respect to convenient reference values of each property indicated by the over-bar notation. Vertical flow to the surface is based on the average hydraulic gradient. Walker (2006) presented solutions to Eq. (8) for multiple layers (see Figure 5) based on the spectral method. The three parameters k_v , m_v and η in the l^{th} layer, are described using the unit step (Heaviside) function (Walker, 2006):

$$\alpha(Z) = \alpha_l UnitStep(Z - Z_{l-1}) UnitStep(Z_l - Z) \tag{9}$$

The spectral method assumes a truncated series solution of N terms:

$$\overline{u}(Z,t) \approx \mathbf{\Phi A} \approx \begin{pmatrix} [\phi_1(Z) & \phi_2(Z) & \ldots & \phi_N(Z)]\times \\ [A_1(t) & A_2(t) & \ldots & A_N(t)]^T \end{pmatrix} \tag{10}$$

In the preceding, ϕ_j is a set of linearly independent basis-functions, and $A_j(t)$ are unknown coefficients. The basic functions were chosen to satisfy the boundary conditions. In the current analysis, for a pervious top and bottom (PTPB) $\overline{u}(0,t) = 0$ and $\overline{u}(H,t) = 0$, and for a pervious top and bottom (PTIB) $\overline{u}(0,t) = 0$ and $\partial \overline{u}(H,t)/\partial z = 0$. Suitable basis functions are thus:

$$\phi_j(Z) = \sin(M_j Z) \tag{10a}$$

where $M_j = \begin{cases} j\pi & \text{for PTPB} \\ \frac{\pi}{2}(2j-1) & \text{for PTIB} \end{cases}$

The Galerkin procedure requires that the error in Eq. (10) is orthogonal to each basis function, hence:

$$\int_0^1 \phi_i L(\mathbf{\Phi A})\, dZ = 0 \tag{11}$$

where L describes the differential operations in Eq. (11). Combining Eqs. (9), (10), (11) yields a set of coupled ordinary differential equations for A_j , which in matrix form reads:

$$\mathbf{\Gamma A'} = -\mathbf{\Psi A} \tag{12}$$

where

$$\mathbf{\Gamma}_{ij} = \Lambda^-_{ij} m_{vl} / \overline{m}_v$$

$$\mathbf{\Psi}_{ij} = dT_v M_j M_i \Lambda^+_{ij} k_{vl} / \overline{k}_v + dT_h \Lambda^-_{ij} \eta_l / \overline{\eta} \tag{12a}$$

$$\Lambda^{\pm}_{ij} = \begin{cases} SN(M_j - M_i) \pm SN(M_j + M_i) & i \neq j \\ (Z_l - Z_{l-1}) \pm SN(M_j + M_i) & i = j \end{cases},$$

$$SN[\beta] = (\sin(\beta Z_l) - \sin(\beta Z_{l-1}))/\beta \tag{12b}$$

Based on the eigen problem of Eq. (12), under instantaneous loading the solution to Eq. (11) is:

$$\overline{u}(Z,t) \approx \mathbf{\Phi v E}(\mathbf{\Gamma v})^{-1}[\theta_1 \quad \theta_2 \quad \ldots \quad \theta_N]^T \tag{13}$$

The diagonal matrix $\mathbf{E}$ (square matrix with non-diagonal terms equal to zero) $\mathbf{E}$ is:

$$\mathbf{E}(t) = \text{diag}[\exp(-\lambda_1 t) \quad \exp(-\lambda_2 t) \quad \cdots \quad \exp(-\lambda_N t)] \tag{13a}$$

where λ is an eigen value of matrix $\mathbf{\Gamma}^{-1}\mathbf{\Psi}$. The eigenvector associated with each eigen value makes up the columns matrix $\mathbf{v}$ (i.e. v_{i1} is the eigenvector associated with λ_1). $\mathbf{\theta}$ is a column vector defined by:

$$\theta_i = 2\left(1-\cos\left(M_i\right)\right)/M_i \tag{13b}$$

To find the average pore pressure between depth Z_1 and Z_2 the $\phi_j(Z)$ terms in $\mathbf{\Phi}$ are replaced with:

$$\bar{\phi}_j\left(Z_1,Z_2\right)=\begin{pmatrix}\cos\left(M_jZ_1\right)-\\ \cos\left(M_jZ_2\right)\end{pmatrix}\Big/M_j\left(Z_2-Z_1\right) \tag{13c}$$

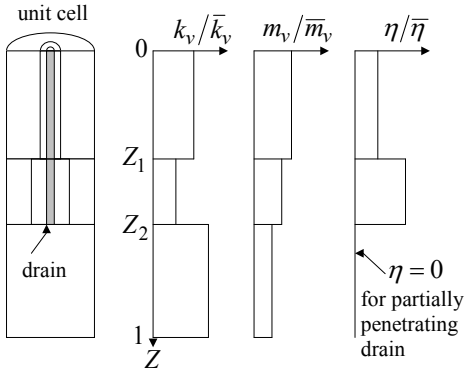

(a)

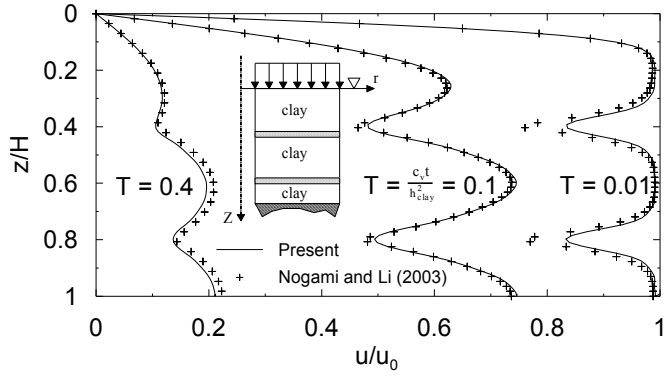

(b)

Figure 5 (a) Multi-layered consolidation properties and (b) model verification: multi-layer equal-strain vs free-strain (Walker et al. 2009)

The adoption of the current method via Equation (13c) allows one to apply a straight forward way of determining the average pore pressure values within a soil layer, across some layers, or across all layers. Nogami and Li (2003) developed a free strain approach for calculating the distribution of excess pore pressure for multi-layered soil having vertical and radial drainage. An example problem is presented with a soil system consisting of two identical layers of thin sand (height h_s) separating three identical layers of clay (height, h_c). The properties of the soil are described by the ratios: $k_{\text{sand}}h_sh_c/r_e^2k_v$ = 5, n = 20, $c_hh_c^2/c_vr_e^2$ = 1. The average excess pore water pressure calculated with the present approach, and that of Nogami and Li (2003), is compared in Figure 5b. Both methods are in close agreement except for slight deviations in the thin layers of sand at a low degree of consolidation. The close agreement shows that, as for homogenous ground (Hansbo, 1981; Barron, 1948), there is little difference between free strain and equal strain formulations.

3 DETERMINATION OF THE SMEAR ZONE AND LARGE SCALE LABORATORY TESTING

The term 'smear zone' is generally referred to as the disturbance that occurs when installing a vertical drain. This causes a substantial reduction in soil permeability around the drain, which in turn retards the rate of consolidation. In this section, the Cavity Expansion Theory is used to estimate the extent of the smear zone. The prediction is then compared with the laboratory results based on permeability and variations in the water content.

The extent of the "smear zone" caused by mandrel installation can be estimated using the elliptical cavity expansion theory incorporating the modified Cam-clay model (MCC) (Ghandeharioon et al. 2010). The detailed theoretical developments are explained elsewhere by Ghandeharioon et al. (2010), so only a brief summary is given below. The yielding criterion for soil obeying the MCC model is:

$$\eta = \mathrm{M}\sqrt{\left(p_c^{'}/p^{'}\right)-1} \tag{14}$$

Where, $p_c^{'}$: the stress representing the reference size of yield locus, $p^{'}$ = mean effective stress, M = slope of the critical state line and η = stress ratio. The relationship between the radial distance and its associated deviator stress can be determined by:

$$\ln\left(1-\frac{r_1^2-r_0^2}{r^2}\right)=\left[\begin{array}{l}\dfrac{q}{\sqrt{3}\,G}-\\ 2\sqrt{3}\,\dfrac{\kappa\Lambda}{\upsilon M}\left[\zeta-\tan^{-1}\left(\dfrac{\eta}{M}\right)\right.\\ \left.+\tan^{-1}\sqrt{n_p-1}\right]\end{array}\right] \tag{15}$$

$$\zeta=\frac{1}{2}\ln\frac{\left(\eta+M\right)\left(\sqrt{n_p-1}-1\right)}{\left(\eta-M\right)\left(\sqrt{n_p-1}+1\right)} \tag{15a}$$

$$q=\eta\,p^{'} \tag{15b}$$

$$\sigma_r=\sigma_{r_p}-\frac{2}{\sqrt{3}}\int_{r_p}^{r}q\frac{dr}{r} \tag{16}$$

$$\Delta u=\Delta p-\Delta p' \tag{17}$$

In the above expression, r = radius of the cavity, r_0 = initial radius of the cavity, G = Shear modulus, ν = Poisson's ratio, κ = slope of the over consolidation line, υ = specific volume, σ_{r_p} = total radial stress at the elastic-plastic boundary, Δu = excess pore water pressure and $\Lambda=1-\kappa/\lambda$ (λ is the slope of the normal consolidation line).

Based on Equations (15), q and p' can be calculated at any soil element inside the plastic region. Equation (16) is then used to derive the total stress state at that particular position, while noting

$$p=\sigma_r-\frac{q}{\sqrt{3}}$$

Finally, by using Equation (17), the value of excess pore pressure can be determined at the location being considered.

The extent of the smear zone can be defined either by the variation of permeability (Indraratna and Redana, 1998) or by the variation of the water content (Sathananthan and Indraratna, 2006) along the radial distance from the central drain. The permeability variation can be obtained from specimens recovered vertically and horizontally from the large-scale consolidation apparatus. In the field, the measurement of moisture content variation is more convenient. Consolidation tests were conducted to obtain the horizontal and vertical permeabilities under different pressures. Figure 6 shows the variation of the permeability ratio (kh/kv) and water content at different consolidation pressures along the radial distance, obtained from large scale laboratory consolidation. Here the radius of the smear zone is about 100mm or 2.5 times the radius of the mandrel, which is in agreement with the prediction using the cavity expansion theory.

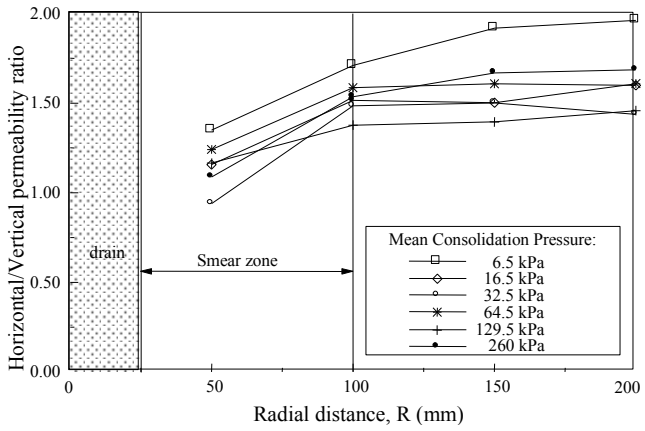

(a)

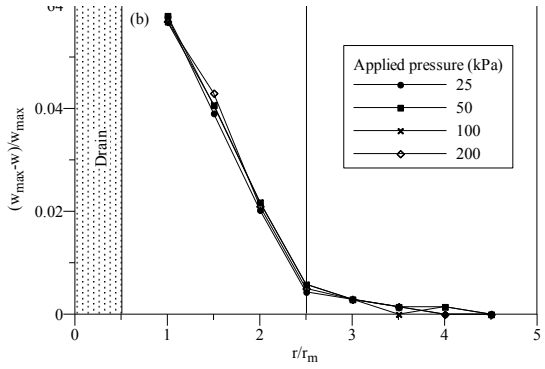

(b)

Figure 6 Smear zone determination (a) permeability approach (Indraratna and Redana, 1998); (b) water content approach (Sathananthan and Indraratna, 2006) (w = water content)

Figure 7 presents the analytical predictions of excess pore water pressure using the conventional cylindrical cavity expansion theory (CET) (Cao et al. 2001) and elliptical CET of the Authors (Ghandeharioon et al., 2010), compared with the results of the large scale laboratory tests. It is clear that the elliptical CET estimates the pore pressure during mandrel installation more accurately than the conventional cylindrical CET. By incorporating the laboratory test results on soil permeability, Ghandeharioon et al. (2010) proposed that the plastic shear strain normalised by the rigidity index, $I_r = \sqrt{3}\frac{G}{q_f}$, can be adopted to characterise the disturbed soil surrounding the mandrel driven prefabricated vertical drains (Figure 8).

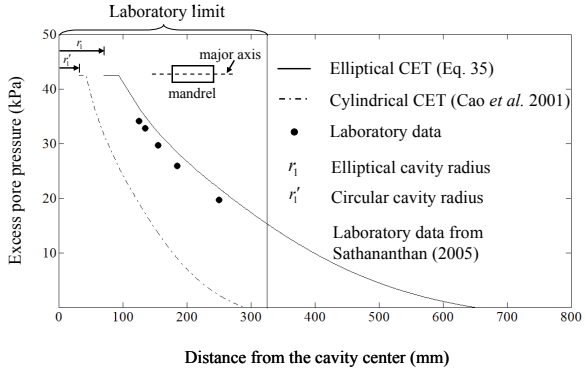

Figure 7 The patterns of distribution s predicted for excess pore pressure with the radial distance using elliptical CET and cylindrical CET along the major axis of the mandrel 0.5m below the soil surface, and measured when the tip of the mandrel's shoe passed the horizontal plane under consideration, with a pre-consolidation pressure = 30 kPa (Ghandeharioon et al. 2010)

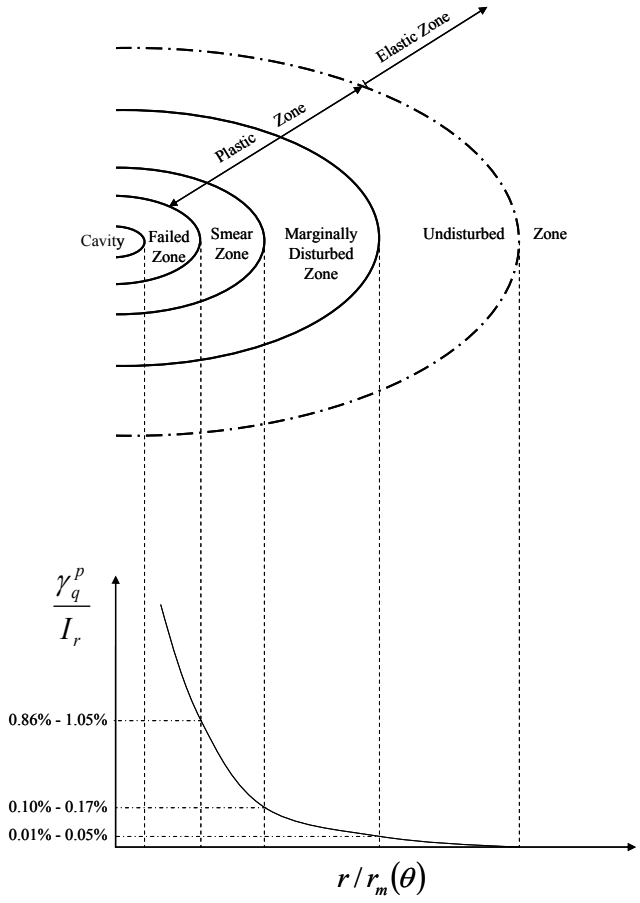

Figure 8 The distribution pattern for the ratio of the plastic shear strain to the rigidity index in relation to the radial distance normalised by the equivalent elliptical radius of the mandrel characterising the disturbed soil surrounding a PVD (Ghandeharioon et al. 2010)

Recently, Rujikiatkamjorn et al. (2013) made an attempt to employ a compression curve of soil to determine the smear zone. Figure 9(a) shows the degree of disturbance of soil structures against the radial distances after the drain was installed and the soil was loaded. The degree of disturbance of the partially disturbed soil, and as expected, the surrounding soil adjacent to the drain shows a higher degree of disturbance. Based on the model predictions for the relatively undisturbed region, the degree of disturbance can still be approximately 19% and 22%.

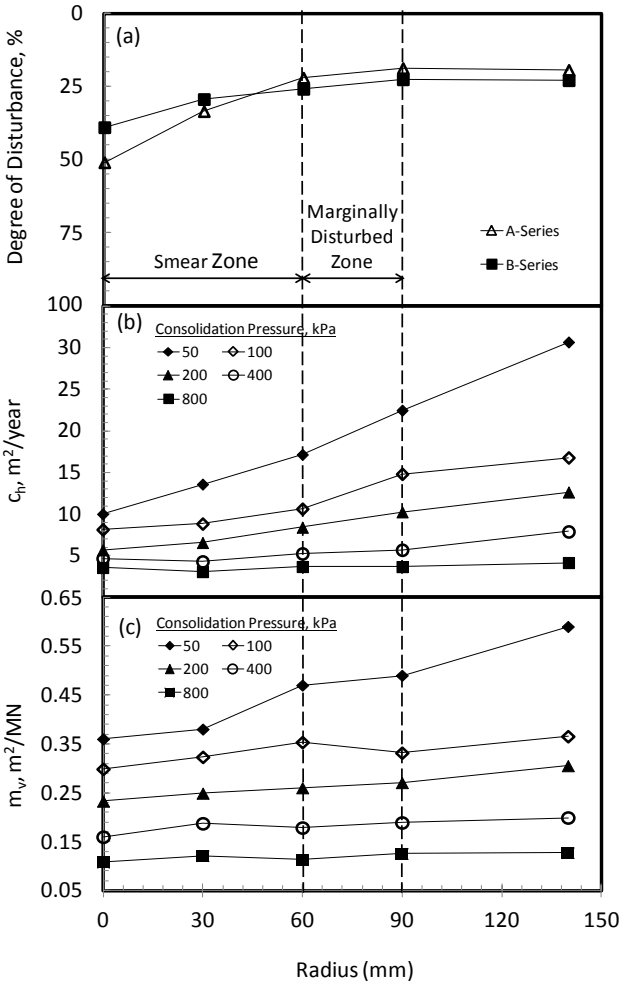

Figure 9 (a) Degree of disturbance, (b) Coefficient of consolidation (ch), and (c) Coefficient of volume change (mv) versus radial distance from the centre of the drain (Rujikiatkamjorn et al. 2013)

Walker and Indraratna (2007) investigated the effect of overlapping smear zones by incorporating a more realistic linear permeability distribution. As shown in Figure 10, two smear zones overlap when the spacing is less than the extent of the smear zone. Figure 10 shows the time required to reach 90% consolidation. A range of drain spacing values exist, across which the time required to reach a certain degree of consolidation does not change. It appears that this radius of minimum influence is 0.6 times the value of the radius of the linear smear zone assumed for non-overlapping smear zones.

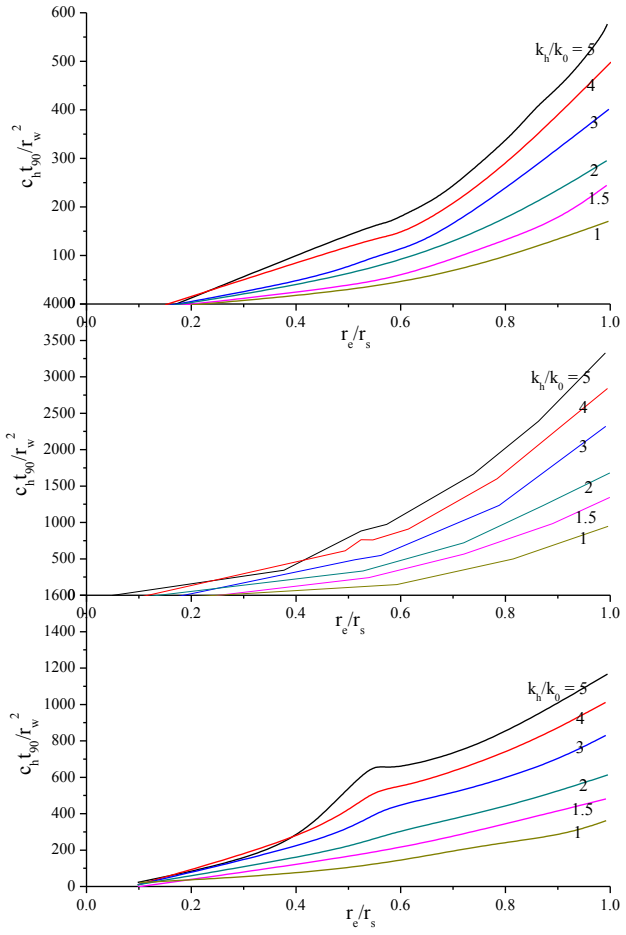

Figure 10 Time required for 90% consolidation for overlapping smear zones with linear variation of permeability (Walker and Indraratna, 2007)

4 COMPARISON OF MEMBRANE AND MEMBRANELESS VACUUM PRELOADING SYSTEMS

Numerical and analytical modelling of vacuum preloading while considering membrane-type and membraneless systems has been described earlier by Geng et al. (2012), where both vertical and horizontal drainage were captured to reflect in-situ conditions. The placing of the surface sand blanket and installation of a completely air tight membrane is imperative for the membrane type vacuum system, in order to create and sustain a desired uniform vacuum pressure on the surface of the soil, and thereby ensure a speedy propagation of this vacuum head down the PVDs to consolidate the clay layer. While a surface sand blanket has no real advantage except for traffic ability, for a membraneless system where a vacuum is applied directly onto the PVDs through a network of tubing, the absence of a membrane eliminates construction time and associated costs. The permeability of the layer of sand plays an important role in this process as it governs how effectively the vacuum pressure propagates from the boundary of the upper soil to the PVD's to consolidate the layer of clay. The roles of the permeability of the sand blanket in a membrane-type vacuum system and adverse effect of the loss of vacuum with depth in a membraneless type system have been analysed by Geng et al. (2012). Figure 11 illustrates the effect of the sand blanket permeability in a membrane system.

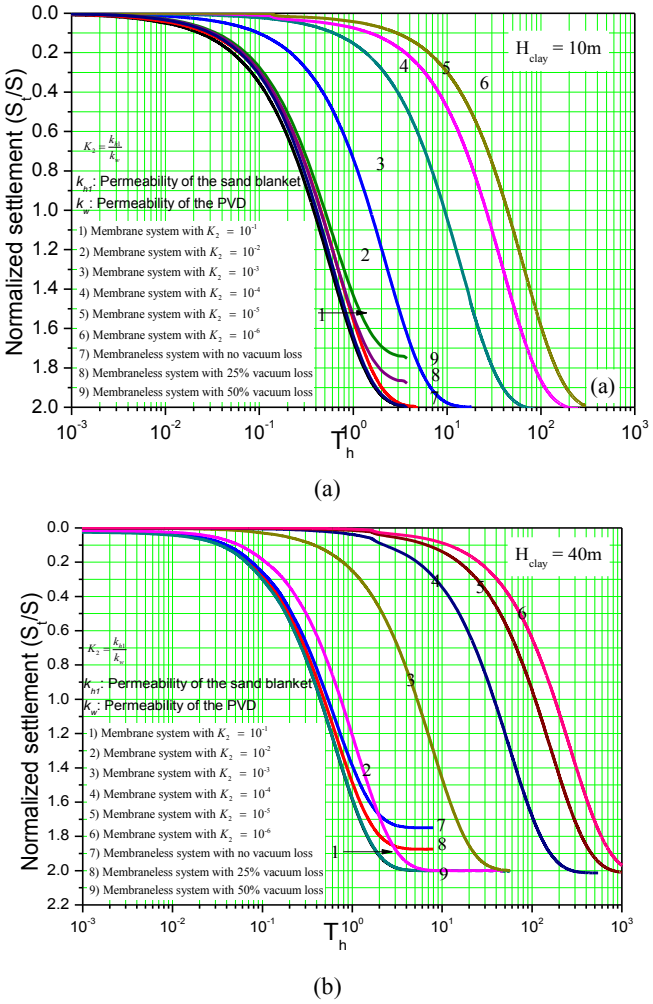

Figure 11 Normalised settlement-time factor curves for varying the permeability of the sand blanket (for membrane system) and the loss of vacuum (for membraneless system): (a) the thickness of the clay is 10 m; (b) the thickness of the clay is 40 m (after Geng et al. 2012)

As expected, when permeability decreases, the time for consolidation increases. For relatively short PVDs (less than 10 m), Figure 11a shows that the permeability of the sand blanket should not be less than 0.01 times the permeability of the PVD, and at least 104 times the permeability of the clay to maintain an acceptable consolidation time for a degree of consolidation (DOC) of 90%. With longer drains (Figure 11b), the permeability ratio of the sand blanket to PVD should be greater than 0.1, and the permeability ratio of the sand blanket to the clay layer should be at least 105. For a membraneless system, the possible reduction in vacuum along the length of long PVDs increases the consolidation time for a given DOC. Where there is no loss of vacuum with depth, the membraneless system is as efficient as the membrane-type (Figure 11), for relatively shallow (10 m) and very thick (40 m) layers of clay.

5 EFFECT OF REMOVING AND RE-APPLYING A VACUUM

A large scale consolidometer can be utilised to examine the effect of vacuum preloading in conjunction with the surcharge load (Indraratna et al. 2004). A large scale consolidation test was conducted by applying a vacuum pressure close to the theoretical maximum of 100kPa to the PVD and the soil surface through the centre hole in the rigid piston. A surcharge pressure was then applied in two stages, 50kPa, and 100kPa. The vacuum pressure was released for a short time in two stages over a 28 day period, to investigate the effect of unloading and reloading (Figure 12a).

The laboratory results indicated that the suction head decreased with the depth of the drain because a maximum suction of 100kPa could not be maintained along the entire length of the drain. The settlement associated with a combined vacuum and surcharge load is shown in Figure 12b, which clearly reflects the effect of removing and re-applying the vacuum by the corresponding gradient settlement plot. The above experimental procedure also showed that it is very difficult to sustain a vacuum pressure greater than 90 kPa, (the theoretical maximum is 100 kPa)

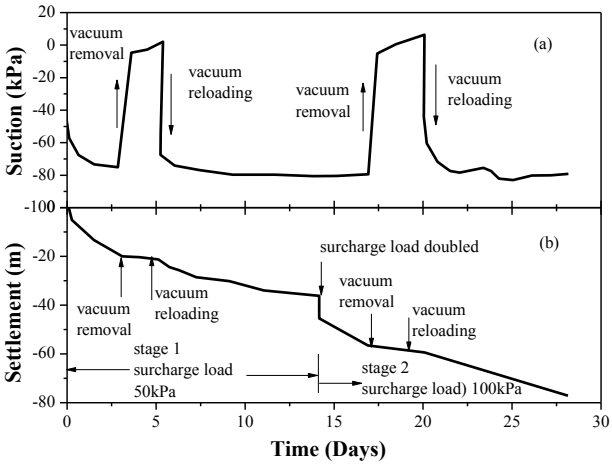

Figure 12 (a) Suction in the drain (240mm from bottom); (b) surface settlement surface settlement associated with simulated vacuum loading and removal (Indraratna et al. 2004)

6 EFFECT OF VACUUM CONSOLIDATION ON THE LATERAL YIELD OF SOFT CLAYS

In order to investigate the effect of a combined vacuum and surcharge load on lateral displacement, a simplified plane strain (2-D) finite element analysis could be used (Indraratna et al. 2008). The outward lateral compressive strain due to surcharge can be reduced by applying suction (vacuum preloading). The optimisation of vacuum and surcharge preloading pressure to obtain a given settlement must be considered in any numerical model to minimise lateral displacement at the embankment toe (Figure 13a), while identifying any tension zones where the vacuum pressure may be excessive.

As expected, the vacuum pressure alone can create inward lateral movement, whereas preloading without any vacuum may contribute to an unacceptable outward lateral movement. The particular situations for most clays is generally a combination of 40% surcharge preloading stress with a 60% vacuum, which seems to maintain a lateral displacement close to zero. Figure 13b presents the various profiles of surface settlement with an increasing surcharge loading. A vacuum alone may generate settlement up to 10m away from PVD treated boundary while the application of VP can minimise the value of soil heave beyond the embankment toe.

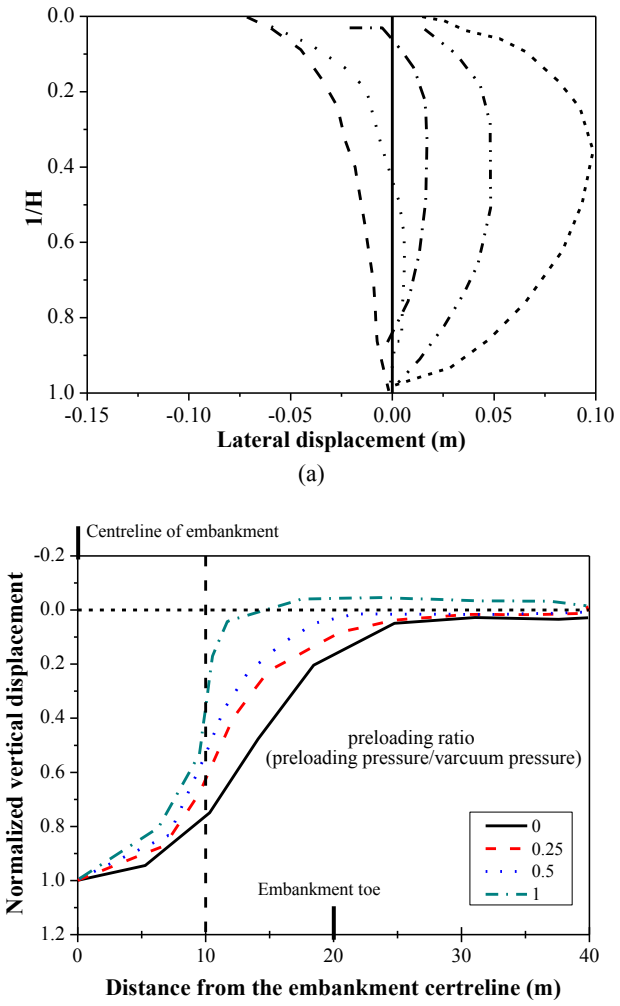

Figure 13 (a) Lateral displacements; and (b) surface settlement profiles (Indraratna et al. 2008)

7 APPLICATION TO CASE HISTORIES

7.1 Second Bangkok International Airport

Indraratna et al. (2004) analysed the performance of test embankments constructed at the Second Bangkok International Airport (SBIA), Thailand. At this site the use of vacuum preloading in lieu of high surcharge embankment as an alternative preloading technique was also studied. Table 1 summarises the typical modified Cam-clay parameters and equivalent plane strain permeability (using Eqs. 7-8) for the FEM analysis. A cross section of the embankment and typical finite element mesh used in the multi-drain analysis are given in Figure 14. The test embankment was raised and stabilised with PVDs installed in a triangular pattern with 1m spacing to a depth of 15m. The 100mm x 3mm PVDs (Mebra) were used.

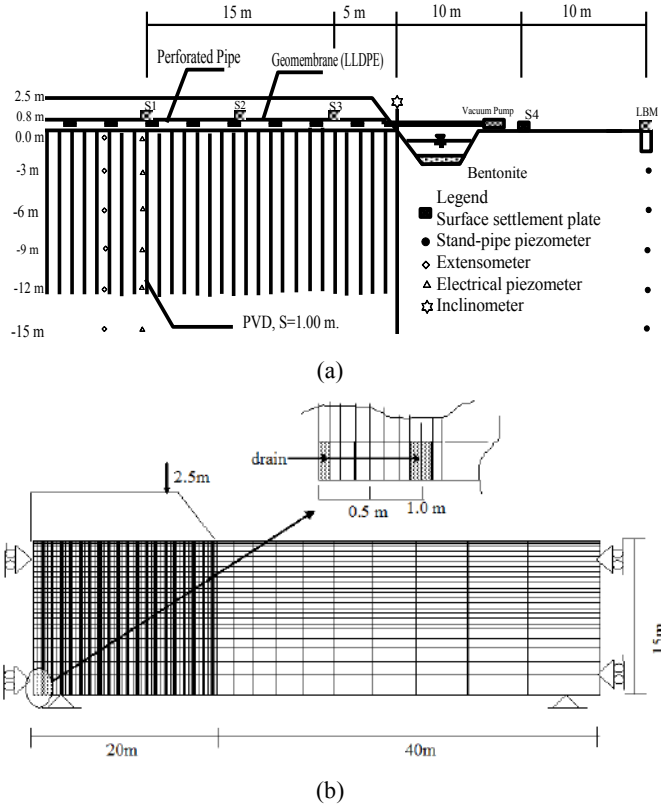

Figure 14 (a) Cross section of an embankment with profile of the subsoil and (b) finite element discretisation of the foundation of the embankment (Indraratna et al., 2004)

The embankment loading was simulated by the sequential construction history (Figure 15a). The following 4 models were considered and numerically evaluated under plane strain multi-drain analysis (Indraratna et al., 2004):

Model 1 –With the application of suction pressure (60 kPa) along the surface of the top soil, and along the length of the drain, a thin layer of unsaturated elements of predetermined constant half widths (30mm) was activated at the boundary of the drain.

Model 2– Similar to Model 1, with a constant 60 kPa suction along the surface of the top soil, but a linearly varying vacuum pressure (60 kPa at top and zero at bottom) applied along the depth of the drain.

Model 3 – Similar to Model 2, but the vacuum pressure was varied linearly with depth to zero at the bottom of the drain and varied with time (Figure 15b), as occurs in the field. The vacuum distribution with depth and time was measured at the drain interface. However, the predictions were made at the middle between 2 drains

Model 4– Conventional surcharge alone with no vacuum pressure.

Figure 15c shows the predicted settlement together with the measured settlement. The Model 3 predictions agreed well with the field data. The assumed time dependent variation of vacuum pressure based on surface measurements improves the accuracy of settlement predictions.

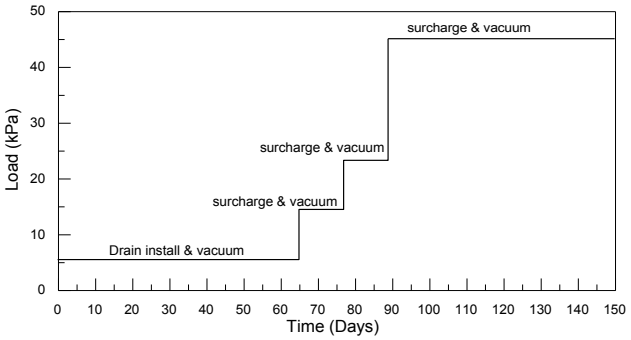

(a)

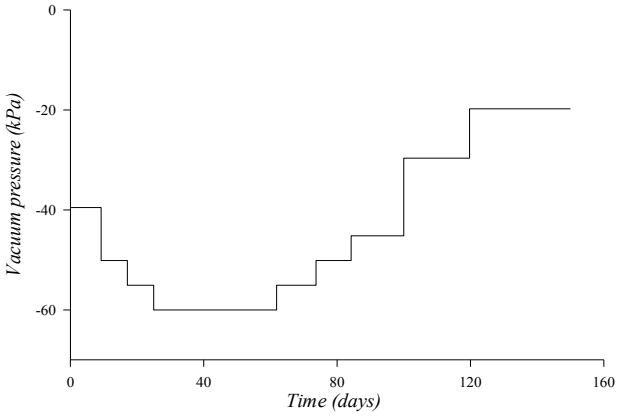

(b)

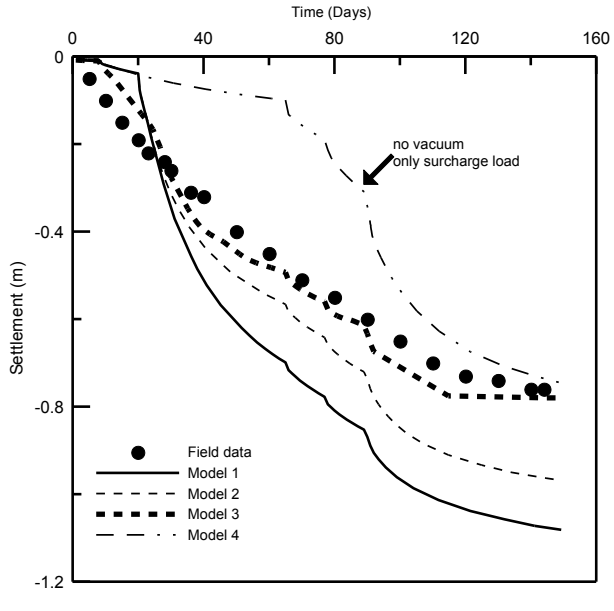

(c)

Figure 15 (a) Stage loading (b) variation of vacuum with time for Model 3 and (c) settlement predictions (Indraratna et al. 2004)

The measured and predicted excess pore pressures along the centreline of the embankment 3m below the ground surface are compared in Figure 16a. Model 3 shows that the time dependent variation in vacuum agrees with the field measurements. All the other models that did not consider the time dependent variation in vacuum pressure were unable to predict the field behaviour to an acceptable accuracy. Measured and predicted lateral deformation for the inclinometer installed away from the centreline of the embankment (after 150 days) is shown in Figure 16b. All 3 models incorporating vacuum pressure have caused 'inward' (radial) movement. The effect of the compacted crust is not clearly reflected by the field data, which suggests that the depth of the crust is no more than 1m in the field, whereas the numerical analysis assumed a 2m thick crust. The loss of the vacuum head increases the lateral movements more in line with Model 4.

Table 1 Critical state soil parameters used in the analysis (Indraratna et al., 2004)

Depth (m)	0-2.0	2.0-8.5	8.5-10.5	10.5-13.0	13-18
e_o	1.8	2.8	2.1	1.8	1.2
λ	0.3	0.73	0.5	0.3	0.1
κ	0.03	0.08	0.05	0.03	0.01
ν	0.3	0.3	0.25	0.25	0.25
M	1.2	1.0	1.2	1.4	1.4
$k_{h,ax}$ (m/s)	30 x10^{-8}	1.3 x10^{-8}	6.0 x10^{-9}	2.6 x10^{-9}	6.0 x10^{-10}
$k'_{h,ax}$ (m/s)	3.01 x10^{-9}	1.27 x10^{-9}	6.02 x 10^{-10}	2.55 x 10^{-10}	6.02 x10^{-11}
$k_{h,ps}$ (m/s)	8.98 x10^{-9}	3.80 x10^{-9}	1.80 x 10^{-9}	7.60 x 10^{-10}	4.15 x10^{-11}
$k'_{h,ps}$ (m/s)	5.86 x10^{-10}	2.48 x10^{-10}	1.17 x 10^{-10}	4.96 x 10^{-11}	2.71 x10^{-12}
γ (kN/m^3)	16.0	14.5	15.0	16.0	18.0

Note: e_o= initial void ratio

λ = slope of compression curve in semi-log scale

κ = slope of re-compression curve in semi-log scale

ν = Poisson's ratio

M= Slope of critical state line

k_h = permeability in undisturbed zone

k'_h = permeability in smear zone

γ = Unit weight of soil

ax and ps denote axisymmetric and plane strain condition, respectively

7.2 Port of Brisbane

The Port of Brisbane is one of the largest container ports in Australia and is located at the mouth of the Brisbane River. Due to an increased demand in commercial activities, a new outer area (235000 m2) close to the current port facilities is being reclaimed to maximise the land area and provide an additional number of berths suitable for bulk cargo and container handling. In this area the soil profile primarily consists of high compressible clay over 30m deep, with an undrained shear strength that is lower than 15kPa at shallow depths. The dredged mud used for reclamation has a much lower strength, depending on the time of placement and duration that the capping material has been in place. In the absence of surcharge preloading, it is estimated that the consolidation time is in excess of 50 years with vertical settlements of 2.5-4.0m. Therefore, vacuum consolidation with prefabricated vertical drains (PVDs) was recommended to accelerate the consolidation process and minimise lateral deformation adjacent to the Moreton Bay Marine Park (Indraratna et al. 2011).

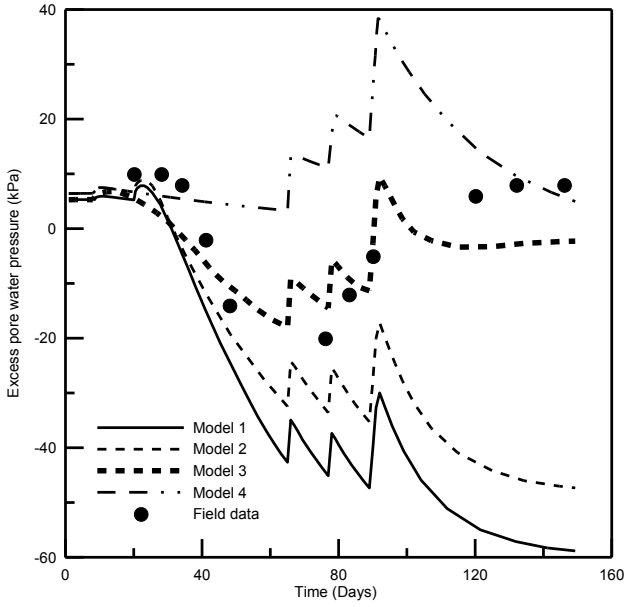

(a)

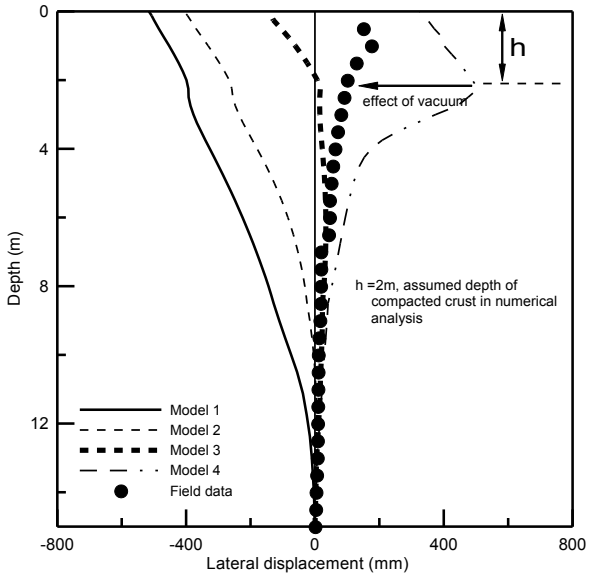

(b)

Figure 16 (a) Excess pore pressure predictions and (b) lateral displacement predictions (Indraratna et al. 2004)

To assess the performance of the vacuum system with a conventional system (PVD and surcharge load), a trial area (S3A) was sub-divided into WD1-WD5 (Non-vacuum areas) and VC1-VC2 (Vacuum areas) (Figure 17). The treatment area of the sub-divisions ranged from 1.5 to 11ha. To observe the ground behaviour, several instruments were installed including settlement plates, vibrating wire piezometers, magnetic extensometers, and inclinometers and their locations are shown in Figure 17. The inclinometers were critical because excessive lateral deformation adjacent to the Moreton bay Marine Park needed to be controlled. After drying, the mud is capped off with a 2-3m thick layer of dredged sand, which acts as a working platform for PVD installation rigs, whilst providing a drainage layer for the wick drains to discharge to. Table 2 summarises the PVD characteristics and types of treatment applied to each section. In non-vacuum areas, both circular and band shape drains were installed in a square pattern at a spacing of 1.1-1.3m. The length of drains varied from 6m to 27.5m across the site, as shown in Table 2a.

Table 2a PVD characteristics (Indraratna et al. 2011)

Section	**Drain type**	**Drain length** (m)	**Drain spacing in square pattern** (m)
WD1	Circular drains with 34mm diameter	14.5-18.5	1.1
WD2	Circular drains with 34mm diameter	22.5-27.5	1.3
WD3	Band drain Type -A (100×4 mm^2)	17.1-23.5	1.1
WD4	Band drains Type -A (100×4 mm^2)	27.0-28.7	1.3
WD5A	Band drains Type -B (100×4 mm^2)	6.0-8.0	1.2
WD5B	Band drains Type -B (100×4 mm^2)	13.5	1.1
VC1	Circular drains with 34mm diameter	14.0-26.5	1.2
VC2	Circular drains with 34mm diameter	15.5-22.5	1.2

Table 2b Clay thickness and improvement scheme (Indraratna et al. 2011)

Section	**Clay thickness(m)**	**Total fill height(m)**	**Treatment scheme**
WD1	12.0-15.5	5.2	Surcharge
WD2	20.0-23.5	7-7.2	Surcharge
WD3	14.0-17.0	4.3-4.6	Surcharge
WD4	22.5-24.5	6.1	Surcharge
WD5A	6.0-8.0	3.3	Surcharge
WD5B	9.5	5.5	Surcharge
VC1	9.0-21.0	3.2	Surcharge+ 70kPa vacuum
VC2	12.5-18.5	2.8	Surcharge+ 70kPa vacuum

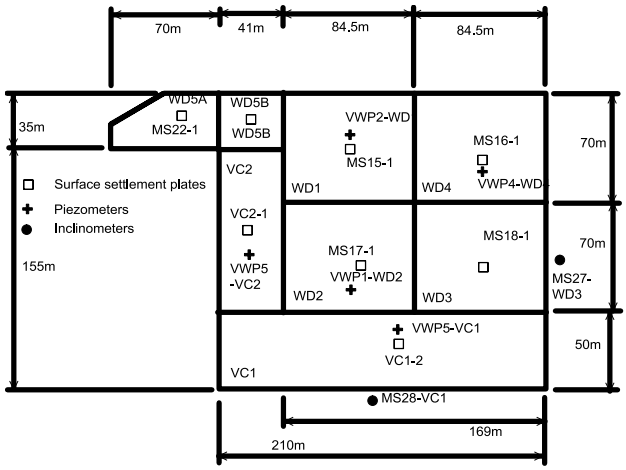

Figure 17 Site layout for S3A with instrumentation plan (Indraratna et al. 2011)

It can be observed that the trends are very similar where settlement occurs more rapidly at the initial stage of consolidation. The magnitude of ultimate settlement depends on the thickness of the clay and height of the embankment. The highest settlement is observed in the WD4 area where the clay is thickest (19-26m), whereas the lowest settlement belongs to WD5A area where the clay is relatively thin (8-12m). The measured lateral displacement normalised to total change in applied stress (vacuum plus surcharge load) for two inclinometer locations (VC1/MS28 and WD3/MS27) are shown in Figure 18. In VC1 and the WD3 area, the total load on the surface is similar. At the WD3 area, the total height of surcharge was 4-5m (90 kPa), whereas for the VC1 area the reduced surcharge pressure of 40 kPa (2m surcharge height) was supplemented with a vacuum pressure of 65 kPa. These plots indicate that the lateral movements are well controlled via isotropic consolidation by vacuum pressure.

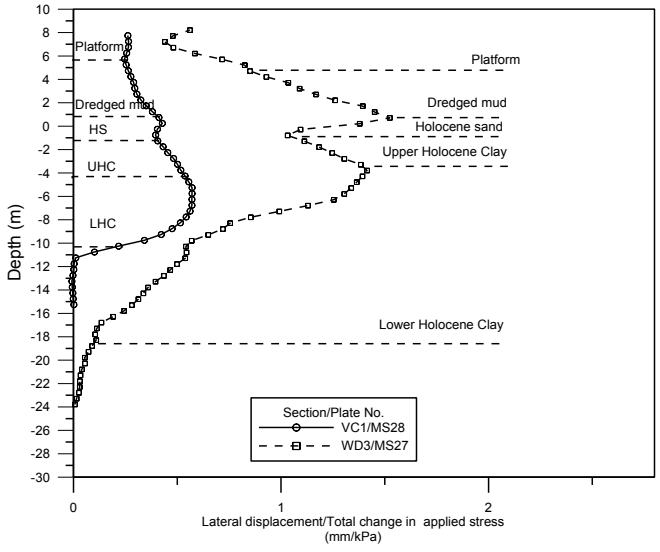

Figure 18 Comparison of lateral displacements at the toe of the embankment in vacuum and non-vacuum area after 400 days (Indraratna et al. 2011)

Figure 19 presents the predicted settlement and associated excess pore pressure with the measured data in Areas VC2. Overall, the comparisons between prediction and field observation show that the settlement and associated pore water pressure can be predicted very well.

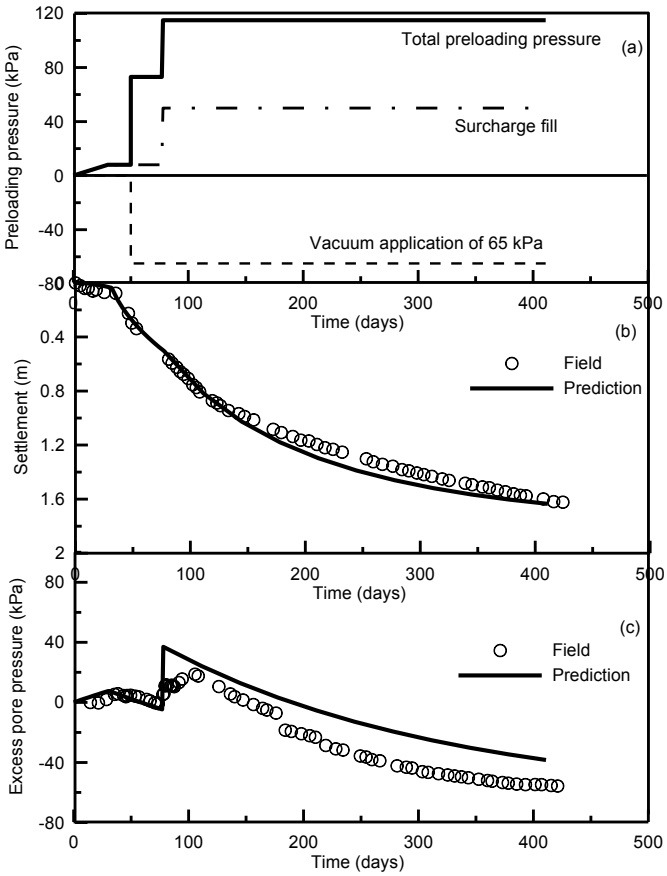

Figure 19 Comparison of lateral displacements at the toe of the embankment in vacuum and non-vacuum area after 400 days (Indraratna et al. 2011)

7.3 Tianjin Port

As reported by Chu and Yan (2005), Tianjin Port is 100 km from Beijing, China. Due to the rapid growth of the port, construction of a new dock on reclamation land was needed for a new storage facility. The site was reclaimed using clay dredged from the seabed and has formed the first top 3-4m of the soil deposit. The soft muddy clay underneath the reclaimed soil was 5m, followed by the soft muddy clay layer at a depth of 8.5-16m. A 6m thick stiff silty clay underlies the soft muddy clay layer. The soil profile and its related soil properties are shown in Figure 20, where the groundwater level is at the ground surface. The water contents of the soil layers are very close to or exceed their liquid limits, and the void ratio is in the range of 0.8-1.5. The field vane tests indicate that the undrained shear strength varies from about 20 to 40 kPa. More description of the project can be found in Yan and Chu (2005).

The storage facility covered an area of 7.5 hectares. The vacuum preloading method was chosen to improve the soil. The required preloading pressure to attain the desired settlement was 140 kPa. The nominal vacuum pressure was 80kPa. Therefore, a combined vacuum and fill surcharge preloading was employed to increase the shear strength of the soil before construction. During construction, the site was subdivided into three sections, as shown in Figure 21. Figure 22 presents the vertical cross-section and the locations of field instrumentation for Section II, which included the settlement gauges, pore water pressure transducers, multi-level gauges, inclinometers and piezometers. The settlement gauges were placed at various depths to measure subsurface settlements. The piezometers were installed under the test embankment to a maximum depth of 16 m. PVDs (100 mm × 3 mm) 20m long were installed at 1m spacing in a square pattern. A 0.3m sand blanket served as a platform for installing the PVDs and for placing the horizontal pipes needed to distribute

the vacuum pressure. The steel mandrel driven drains were installed using a static rig. Horizontal drainage consisted of 100mm diameter corrugated pipes wrapped in geotextile filters were installed in both directions and then covered with air tight membranes. Within the scope of this paper, the results for the analysis of Sections II and III are presented.

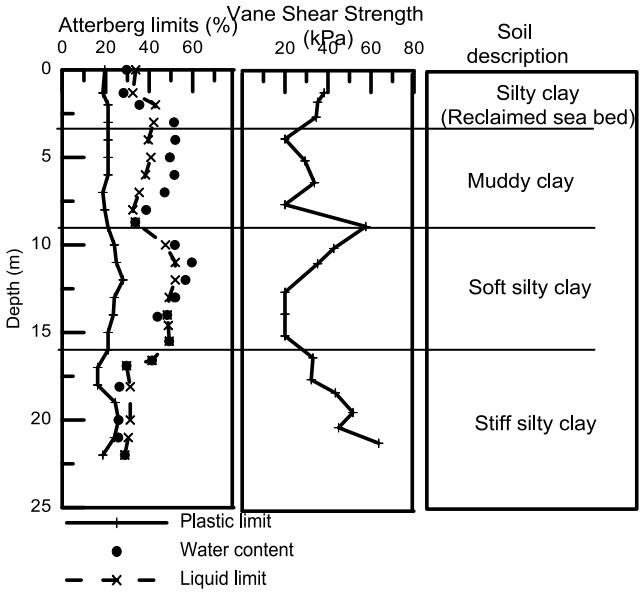

Figure 20 Soil properties and profile at Tianjin port (adopted from Yan and Chu, 2003)

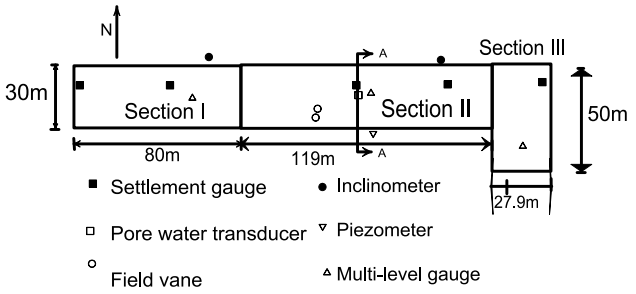

Figure 21 Field instrumentation plan for the trial embankments at Tianjin Port (adopted from Rujikiatkamjorn et al. 2008)

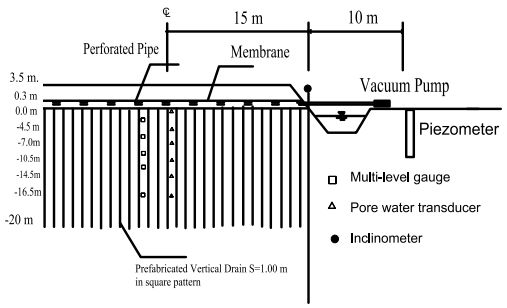

Figure 22 Vertical cross section A-A and locations of field instruments

A finite element program (ABAQUS v.6.5.1) coupled with Biot consolidation theory was used to simulate the 3D multi-drain analysis. As the aspect ratio of Section II was about 4, no differential deformation was expected along the length of Section II. Therefore, only half a row of PVDs with their influence zone was simulated. The 3D finite element mesh composes of 90000 C3D8RP solid elements (8-node tri-linear displacement and pore pressure) (Figure 23). Only a quarter of the embankment area in Section III (15x25m2) was used in the model because of the symmetry and very low aspect ratio. The 3D finite element mesh consisted of 101160 C3D8RP solid elements (Figure 23). The four lateral displacement boundaries at x=0, x=45m, y=0 and y=34m were fixed and were considered to be impermeable boundaries. The displacement boundary at z=20m was set to be zero in all the x, y and z directions. A total of 350 individual PVDs were created. To simulate the actual band drain boundary, the pore pressure was set along the 100 mm drain width to a negative value for vacuum pressure. As observed by Indraratna and Rujikiatkamjorn (2004), the cross sectional area of the smear zone associated with the shape of mandrel can be considered to be elliptical. In the analysis a 150 x 200mm2 rectangular smear zone was used to simplify the 3D mesh and to avoid an unfavourable shaped mesh (Figure 23). The area of this rectangular smear zone is equivalent to a 200mm diameter smear zone or twice the equivalent diameter of the mandrel. According to the laboratory results discussed by Indraratna and Redana (1998) and Sathananthan and Indraratna (2006), the ratio of kh/ks may vary from 1.5-2.0, but in the field it can vary from 1.5 to 5, depending on the type of drain, the soil properties and the installation procedures (Bo et al. 2003). The well resistance was neglected due to the very high discharge capacity of the drain, i.e. qw>120m3/year (Indraratna and Redana 2000).

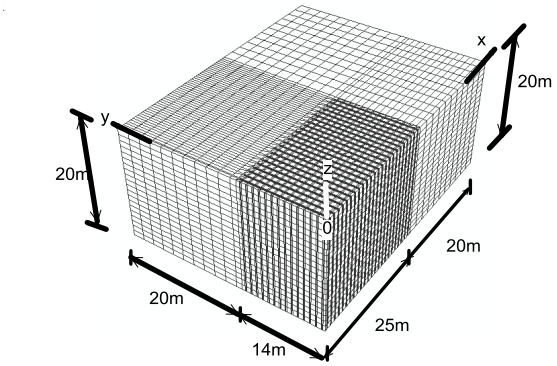

Figure 23 3D Finite element mesh for Section III (a) isometric view

In this section, the predictions based on the 3D and equivalent 2D plane strain finite element analyses are compared with the field measurements. Figure 24 shows a comparison between the predicted and recorded field settlements at the centreline of the embankment together with the loading history for Sections II and III, respectively. The predicted settlements agree with the field data. The surface settlement profiles at the end of 6 months for Section III are shown on Figure 24 along x=0 and y=0 planes (ref. Figure 23) in comparison with the 2D analysis.

Figure 25 presents the comparison between the measured and predicted lateral movements at the toe of the embankment (Section III) after 180 days. The negative lateral displacement denotes an inward soil movement towards the centreline of the embankment. The predictions from 2D and 3D agree well with the measured data. The lateral displacement predictions from 2D and 3D analysis for Section III are almost the same along both centrelines of the embankment (x and y directions) (Figure 25).

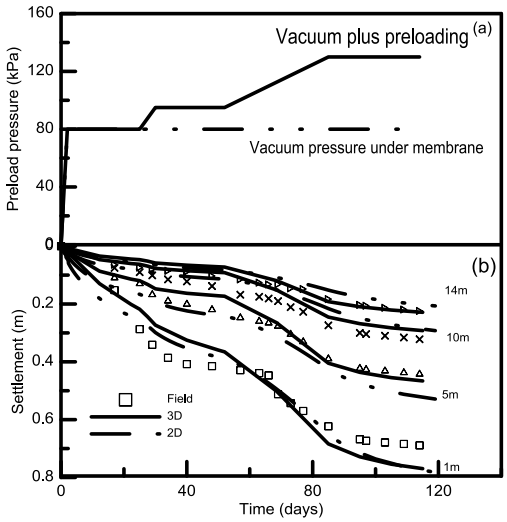

Figure 24 Section II (a) Loading history and (b) Consolidation settlements

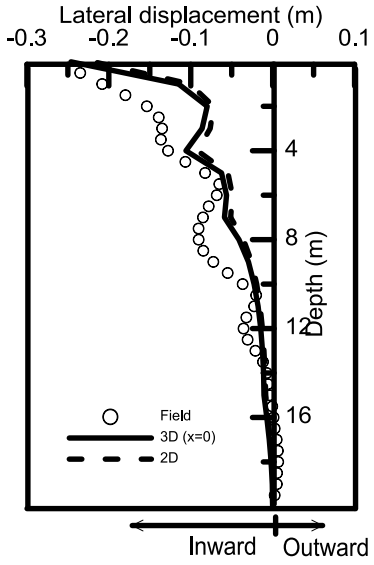

Figure 25 Lateral displacements at embankment toe Section III at 180th day

8 CONCLUSIONS

A system of vertical drains combined with vacuum preloading is an effective method for accelerating soil consolidation by promoting radial flow. The spectral method was used to predict the consolidation of layered soil. The variation of horizontal permeability coefficient (kh) with the stress level was also included. The parabolic decay of horizontal permeability in the smear zone associated with the installation of the drains was considered to represent the actual variation. The elliptical cavity expansion theory was used to predict the extent of the smear zone and it was found to be in agreement with the laboratory data, based on the permeability and water content approaches. The application of a vacuum pressure increases the rate of pore pressure dissipation due to the increased hydraulic gradient towards the drain.

There are two types of vacuum preloading systems; (a) a membrane system with an airtight membrane over the drainage layer and, (b) a membraneless system (a vacuum system is connected to individual PVD). Their effectiveness varies depending on the types of soil treated and characteristics of the vacuum and drain. The analytical solutions of both systems under time dependent surcharge loading were presented in this paper. It can be seen that the proposed solution also included a loss of vacuum along the length of the drain. The general solutions of pore water pressure, settlement, and the degree of consolidation were derived by applying the powerful spectral technique. There is no doubt that a system of vacuum assisted consolidation via PVDs is a useful and practical approach for accelerating radial consolidation.

Generally, the length of PVD can be reduced to 80% of the layer thickness without significantly affecting the time for settlement. With surcharge preloading combined with vacuum pressure, the length of PVD can only be reduced by 0.1 of the entire thickness of soft clay. It can be seen that vacuum preloading alone may not be effective when there is a permeable layer at the bottom of the clay. The applications of the proposed solutions were validated through various case studies.

9 ACKNOWLEDGEMENTS

The authors wish to thank the Australian Research Council for its support. A number of current and past PhD students, namely, Dr. I. Redana, Dr. C. Bamunawita, Dr. R. Walker, Dr. A. Ghandeharioon, Dr. I. Sathananthan, Dr. K. Kianfar and Mr M. Ardana have also contributed to the contents of this paper. A substantial component of the technical details presented in this paper can be found in earlier publications by the first author and his co-workers (albeit different interpretations) in the Géotechnique, ICE, ASCE, Canadian Geotechnical Journals and Geotechnical Engineering Journal of the SEAGS & AGSSEA, since mid 1990's.

10 REFERENCES

Artidteang, S., Bergado, D.T., Saowapakpiboon, J., Teerachaikulpanich, N., and Kumar, A. (2011) "Enhancement of efficiency of prefabricated vertical drains using surcharge, vacuum and heat preloading". Geosynthetics International, ,118, issue 1, pp35-47.

Barron, R.A. (1948) "Consolidation of fine-grained soils by drain wells", Transactions ASCE, 113, pp718-754.

Bo, M.W., Chu, J., Low, B.K. and Choa, V. (2003) "Soil improvement; prefabricated vertical drain techniques", Thomson Learning, Singapore, 341 p.

Cao, L. F., Teh, C. I., and Chang, M. F. (2001) "Undrained Cavity Expansion in Modified Cam Clay I: Theoretical Analysis", Géotechnique, 51, Issue 4, pp323-334.

Chai, J.C., Carter, J.P., and Hayashi, S. (2005) "Ground Deformation Induced by Vacuum Consolidation" Journal of Geotechnical and Geoenvironmental Engineering, ASCE,131, Issue 12, pp187–192.

Chai, J. C., Miura, N., Kirekawa, T. and Hino, T. (2009) "Optimum PVD installation depth for two-way drainage deposit", Geomechanics and Engineering, 1, Issue 3, pp179-192.

Chai, J. C., Carter, J. P. and Hayashi, S. (2006) "Vacuum consolidation and its combination with embankment loading", Canadian Geotechnical Journal, 43, Issue 10, 985-996.

Chai, J., Hong, Z., and Shen, S. (2010) "Vacuum-drain consolidation induced pressure distribution and ground deformation", Geotextiles and Geomembranes, 28, Issue 6,pp525-535.

Chu, J., and Yan, S.W. (2005) "Application of vacuum preloading method in soil improvement", Ground Improvement-Case Histories, Indraratna, B. & Chu, J. (Eds.), Elsevier, pp91-118.

Chu, J., Yan, S.W. and Yang, H. (2000) "Soil improvement by the vacuum preloading method for an oil storage station", 50, Issue 6, pp625-632.

Ghandeharioon, A., Indraratna, B., and Rujikiatkamjorn, C. (2010) "Analysis of soil disturbance associated with mandrel-driven prefabricated vertical drains using an elliptical cavity expansion theory", International Journal of Geomechanics, ASCE, 10, Issue 2, pp53-64.

Geng, X. Y., Indraratna, B. and Rujikiatkamjorn, C. (2012) "Analytical solutions for a single vertical drain with vacuum and time-dependent surcharge preloading in membrane and membraneless systems", International Journal of Geomechanics, ASCE, 12, Issue 1,pp27-42.

Hansbo, S. (1981)."Consolidation of fine-grained soils by prefabricated drains and lime column installation", Proceedings of 10th International Conference on Soil Mechanics and Foundation Engineering, Balkema (Rotterdam) 3, pp677-682.

Holtz, R.D., Jamiolkowski, M.B., Lancellotta, R., and Pedroni, R. (1991) "Prefabricated Vertical Drains: Design and Performance", CIRIA: London; 1-131.

Indraratna, B. and Redana, I. W. (1998) "Laboratory determination of smear zone due to vertical drain installation." J.Geotech. and Geoenviron. Eng, 124, Issue 2, pp180-185.

Indraratna, B., and Redana, I.W. (2000) "Numerical modeling of vertical drains with smear and well resistance installed in soft clay", Canadian Geotechnical Journal, 37,pp133-145.

Indraratna, B., Balasubramaniam, A. S., and Balachandran, S. (1992) "Performance of test embankment constructed to failure on soft marine clay", Journal of Geotechnical Engineering, ASCE, 118, Issue 1,pp12-33.

Indraratna, B., Bamunawita, C., and Khabbaz, H. (2004) "Numerical modeling of vacuum preloading and field applications", Canadian Geotechnical Journal, 41, pp1098-1110.

Indraratna, B., Rujikiatkamjorn C., and Sathananthan, I. (2005a) "Analytical and numerical solutions for a single vertical drain including the effects of vacuum preloading", Canadian Geotechnical Journal, 42, pp994-1014.

Indraratna, B., Rujikiatkamjorn C., and Sathananthan, I. (2005b) "Radial consolidation of clay using compressibility indices and varying horizontal permeability", Canadian Geotechnical Journal, 42, pp1330-1341.

Indraratna, B., Rujikiatkamjorn C., Balasubramaniam, A. S. and Wijeyakulasuriya, V. (2005c) "Predictions and observations of soft clay foundations stabilized with geosynthetic drains and vacuum surcharge". Ground Improvement – Case Histories Book (Volume 3), Edited by Indraratna, B. and Chu, J., Elsevier, London, pp199-230.

Indraratna, B., Rujikiatkamjorn, C., Ameratunga, J., and Boyle, P. (2011) "Performance and Prediction of Vacuum Combined Surcharge Consolidation at Port of Brisbane", J. of Geotechnical & Geoenvironmental Engineering, ASCE, 137, Issue 11, pp1009-1018.

Indraratna, B., Geng, X., Rujikiatkamjorn, C. (2010a) "Review of methods of analysis for the use of vacuum preloading and vertical drains for soft clay improvement", Geomechanics and Geoengineering, 5, Issue 4, pp223-236.

Indraratna, B., Rujikiatkamjorn, C., Kelly, R. and Buys, H. (2010b) "Sustainable soil improvement via vacuum preloading", Ground Improvement, 163, Issue 1, pp31-42.

Indraratna, B., and Rujikiatkamjorn, C. (2008) "Effects of partially penetrating prefabricated vertical drains and loading patterns on vacuum consolidation". In K. R. Reddy, M. V. Khire and A. N. Alshawabkeh (Eds.), GeoCongress (pp. 596-603). USA: ASCE.

Jamiolkowski, M., Lancellotta, R., and Wolski, W. (1983) "Precompression and speeding up consolidation", Proc. 8th ECSMFE, pp1201-1206.

Kjellman, W. (1952) "Consolidation of clayey soils by atmospheric pressure", Proceedings of a conference on soil stabilization, Massachusetts Institute of Technology, Boston, pp258-263.

Lekha, K.R., Krishnaswamy, N.R. and Basak, P. (1998) "Consolidation of clay by sand drain under time-dependent loading", J. Geotech. Engng., ASCE, 124, Issue 1, pp91-94.

Mesri, G. and Khan, A.Q. (2012) "Ground improvement using vacuum loading together with vertical drains", ASCE. Journal of Geotechnical and Geoenvironmental Engineering, 138, Issue 6, pp680-689.

Mohamedelhassan, E., and Shang, J.Q. (2002) "Vacuum and surcharge combined one-dimensional consolidation of clay soils",Can. Geotech. J. 39, pp1126-1138.

Nogami, T. and M. Li (2003) "Consolidation of clay with a system of vertical and horizontal drains", J. of Geotechnical and Geoenvironmental Engineering, ASCE, 129, Issue 9, pp838-848.

Onoue, A., Ting, N.-H., Germaine, J. T. and Whitman, R. V. (1991) "Permeability of disturbed zone around vertical drains", Proc. ASCE Geotech.Engng.Congress.2, pp879-890.

Qian, J.H., Zhao, W.B., Cheung, Y.K. and Lee, P.K.K. (1992) "The theory and practice of vacuum preloading", Computers and Geotechnics, 13,pp103-118.

Qiu, Q. C., Mo, H. H., and Dong, Z. L. (2007) "Vacuum pressure distribution and pore pressure variation in ground improved by vacuum preloading", Canadian Geotechnical Journal, 44, Issue 12,pp1433-1445.

Richart, F.E. (1957) "A review of the theories for sand drains", Journal of the Soil Mechanics and Foundations Division, ASCE, 83, Issue 3, pp1-38.

Robinson, R. G., Indraratna, B. and Rujikiatkamjorn, C. (2012) "Final state of soils under vacuum preloading", Canadian Geotechnical Journal, 49, Issue 6, 729-739.

Rujikiatkamjorn C. and Indraratna, B. (2007) "Analytical solutions and design curves for vacuum-assisted consolidation with both vertical and horizontal drainage", Canadian Geotechnical Journal, 44, pp188-200.

Rujikiatkamjorn C. and Indraratna, B. (2009) "Design procedure for vertical drains considering a linear variation of lateral permeability within the smear zone", Canadian Geotechnical Journal, 46, Issue 3, pp270-280.

Rujikiatkamjorn, C. Ardana, M., Indraratna, B., and Leroueil, S. (2013) "Conceptual Model Describing Smear Zone Caused by Mandrel Action", Géotechnique (Accepted, February 2013).

Saowapakpiboon, J., Bergado, D. T., Youwai, S., Chai, J. C., Wanthong, P. and Voottipruex, P (2010) "Measured and predicted performance of prefabricated vertical drains (PVDs) with and without vacuum preloading", Geotextiles and Geomembranes, 28, Issue 1, pp1-11.

Saowapakpiboon, J., Bergado, D. T., Voottipruex, P., Lam, L. G. andNakakuma, K. (2011) "PVD improvement combined with surcharge and vacuum preloading including simulations", Geotextiles and Geomembranes, 29, Issue 1, pp74-82.

Sathananthan, I. (2005). "Modelling of Vertical Drains with Smear Installed in Soft Clay", PhD Thesis, University of Wollongong, 264p.

Sathananthan, I. and Indraratna, B. (2006) "Laboratory Evaluation of Smear Zone and Correlation between Permeability and Moisture Content", Journal of Geotechnical and Geoenvironmental Engineering, ASCE, 132, Issue 7, pp942-945.

Sharma, J. S. and Xiao, D. (2000) "Characterization of a smear zone around vertical drains by large-scale laboratory tests", Can. Geotech. J., 37, Issue 6, 1265-1271.

Shang, J.Q., Tang, M., and Miao, Z. (1998) "Vacuum preloading

consolidation of reclaimed land: a case study", Canadian Geotechnical Journal, 35, pp740-749.

Tang, M., and Shang, J. Q. (2000) "Vacuum preloading consolidation of Yaoqiang Airport runway", Géotechnique, 50, Issue 6, pp613-623.

Walker, R. (2006) "Analytical solutions for modeling soft soil consolidation by vertical drains", PhD Thesis, University of Wollongong, 242p.

Walker, R. and Indraratna, B. (2006) "Vertical drain consolidation with parabolic distribution of permeability in smear zone", J. of Geotechnical & Geoenvironmental Engineering, ASCE, 132, Issue 7, pp937-941.

Walker, R. and Indraratna, B. (2007) "Vertical drain consolidation with overlapping smear zones", Géotechnique, 57 (5): 463-467.

Walker, R., Indraratna, B., and Sivakugan, N. (2009) "Vertical and radial consolidation analysis of multi layered soil using the spectral method", J. of Geotechnical & Geoenvironmental Engineering, ASCE, 135, Issue 5, pp657-663.

Yan, S. W. and Chu, J. (2005) "Soil improvement for a storage yard using the combined vacuum and fill preloading method", Canadian Geotechnical Journal, 42, Issue 4, pp1094-1104.

Zhu, S. L. and Miao, Z. H. (2002) "Recent development and improvement of vacuum preloading method for improving soft soil", Ground Improvement, 6, Issue 2, pp79-83.

USE OF SHOCK MATS FOR MITIGATING DEGRADATION OF RAILROAD BALLAST

B. Indraratna[1], S. Nimbalkar[2], S.K. Navaratnarajah[3], C. Rujikiatkamjorn[4] and T. Neville[5]

1 Professor of Civil Engineering and Research Director, Centre for Geomechanics and Railway Engineering, Program Leader, ARC Centre of Excellence for Geotechnical Science and Engineering, University of Wollongong, Australia.
2 Research Fellow,Centre for Geomechanics and Railway Engineering, University of Wollongong, Australia.
Email: sanjayn@uow.edu.au
3 PhD Candidate, Centre for Geomechanics and Railway Engineering, University of Wollongong, Australia.
4 Associate Professor, School of Civil, Mining and Environmental Engineering, University of Wollongong, Australia.
5 Senior Geotechnical Engineer, Australian Rail Track Cooperation Ltd, Broadmeadow, NSW 2292, Australia

ABSTRACT: In Australia, increasing demand for High Speed Rail (HSR) and heavier freight transport is a technical and economic challenge for practicing engineers, designers and researchers. Because of this increased train speed and axle load, high undue stresses are transferred to the ballast and underlying formation. Ballast degradation is a major factor affecting track longevity and stability. Use of energy absorbing shock mats to reduce noise and vibrations is an established practice. The shock mat is sometimes called as Under Sleeper Pad (USP) and Under Ballast Mat (UBM) depending upon their placement position. However, studies to analyse their effectiveness in minimising ballast degradation are limited. A series of large-scale laboratory tests were conducted on ballast using a high-capacity drop-weight impact testing equipment to understand the performance of energy absorbing shock mats in the attenuation of impact loads and subsequent mitigation of ballast degradation. A numerical model was developed based on the modified stress-dilatancy approach to capture particle breakage during impact loading. Model predictions are compared with laboratory results. This paper presents state-of-the-art review of laboratory studies and numerical modelling illustrating benefits of USPs and UBMs in the practice.

Keywords: Ballast, Impact load, Shock mats, Degradation, Deformation

1 INTRODUCTION

Energy absorbing mats such as Under Sleeper Pad (USP) and Under Ballast Mats (UBM) are resilient pads placed under the sleepers and under the ballast, respectively. The most significant applications of these resilient pads in railways are: 1) reduce the structure-borne vibration and noise to protect nearby structures and 2) reduce the ballast degradation to improve stability and maintain track geometry, thereby increasing the service life of the rail track. The resilient material used as the USP and UBM to improvethe overall vertical elasticity of the track substructure. In recent years, use of elastomeric soft pads underneath concrete sleepers have become increasingly popular and is the primary focus of track research (Marschnig and Veit 2011).

The elastic pad embedded under the sleeper avoids a hard interface with the ballast, allowing the ballast to bed into the padding material. This increases the contact surface area of the ballast with other interfaces such as, USP (increases the contact area of ballast with sleeper), and UBM (increases the contact area of ballast with sub-ballast or formation soil). Consequently, this avoids excessive contact forces between the interfaces and ballast particles, leading to increased stability, less settlement and reduced wear of the track sub-structure. In the case of USP, it extends the bending length of the rails. Therefore, the axle load from the train is distributed over a larger number of sleepers compare with sleepers without USPs. Since the compression load distributed over large area (Figure 1), it further reduces the force acting on sleeper-ballast interface and inter-ballast particle forces(Bolmsvik 2005; Plášek et al. 2007; Loy 2008; Dahlberg 2010).

The wheel and rail irregularities such as wheel flat, rail corrugation, dipped rail, defective rail weld, insulation joints and rail expansion gap causes higher impact load than the cyclic load exerted by moving wheels (Nielsen and Johansson 2000; Bruni et al. 2009; Nimbalkar et al. 2012). Change of stiffness where the track passages from ballasted track to the bridge approach, track transition locations such as road crossing and change of subgrade condition (weak subgrade to bedrock) is accelerating track degradation due to this high impact loading (Li and Davis 2005; Nimbalkar et al. 2012). Therefore the use of energy absorbing resilient pads in the track structure to attenuate the rail track degradation is becoming increasingly popular in rail road industries (Esveld 2001). This paper presents overview of various methods of analysis on use of shock mats in track structures in recent years. Few preliminary research studies on the assessment of shock mats using large scale impact testing equipment at the University of Wollongong, Australia are also presented.

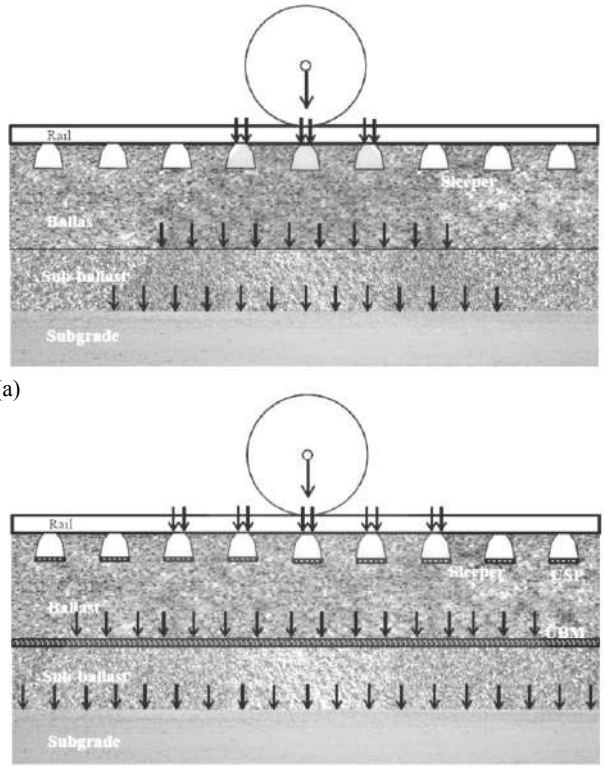

Figure 1. Distribution of Axle Load.
(a) Without Shock Mats; (b) With Shock Mats

2. LITERATURE SURVEY

2.1 History: Development of shock mats

The track improvements by using shock mats have been in use since 1980s and it is increasingly in use last 10 to 20 years specially in Central Europe (Bolmsvik 2005; Schneider et al. 2011). Initially it was used to reduce vibrations transmitted from the rail track to nearby buildings, then it has been in wide use to reduce the sleeper-ballast contact stresses. Since 2005, in Austria,USPs are used as a standard component in turnouts to improve track quality and reduce rail corrugation growth on small radius curves in category A tracks (curve radius >250m and traffic load >30,000 tons/day)(Schneider et al. 2011). Recent studies by Loy (2008) and Marschnig and Veit (2011) confirms the use of USP lessening the maintenance requirements and thereby dramatically reducing Life Cycle Cost (LCC) of track structure. Indraratna et al. (2012) found that the use of shock mats reduced up to 50% strain of the ballast layer subjected to impact forces owing to the wheel rail imperfections. Detailed overview of important studies on the use of shock mats in rail track improvement is presented in the following sections.

2.2 Shock Mats for Vibration reduction

In the beginning of 1980s, thin elastic pads as a USP material was used to cover the wooden sleeper to minimize the vibration transmitted to the houses near the rail tracks. Then in 1990s, the French railway started the testing by introducing thin layer of polyurethane as a USP material to minimize the sleeper-ballast contact stresses (Bolmsvik 2005). A study by Auersch (2006) suggest that the ballast mats (i.e. UBM) are an efficient measure to reduce the vibration near the rail tracks. In his study, numerical method of track dynamics using three dimensional and an improved simple two dimensional FEM models were used to analyse ballast track with and without ballast mat. Auersch (2006) reported that the resonance frequency depend on the stiffness of the ballast mat and the insertion of an elastic mat under the ballast layer shifts the vehicle–track resonance frequency between 20 and 50 Hz, thereby considerably improving the reduction of dynamic forces. Loy (2008) reported that the use of USP significantly improve the ballast track vibration behaviour compared with traditional track without USPs, especially the frequencies above 40 Hz. Medium frequency range of 50-150 Hz vibration tend to liquefy the ballast material and become unstable. Therefore, the use of USP is a beneficial effect on the stability of ballasted track. A research study by Loy (2012) on mitigating vibration by USP suggest that appropriate USPs can reduce the vibration and also improve the track bed geometry. A sandwich type of USP consist of a soft and acoustically highly-effective elastic layer embedded to the concrete sleeper on one side and a visco-plastic material layer on the ballast side recommended to cater for above two requirements.

2.3 Reduction of Life Cycle Cost

The Austrian mainline network sections data analysed by the Technical University of Graz shows that the installation of padded sleepers significantly reduce the LCC for the track (Marschnig and Veit 2011). This can be achieved by three main cost portions (1) prolonged service life by reducing depreciation, (2) higher track availability by reducing obstructions of operational cost and (3)reduced maintenance needs as shown in Figure 2. Therefore, Marschnig and Veit (2011) concluded that the use of soft padded track system is a major step towards cost efficient and sustainable ballasted track.

Since the stiffness of the track is reduced by the installation of USPs on concrete sleepers which lesser the corrugation in small-radii tight curves and reduce the higher maintenance cost required at the curves. Soft padded concrete sleepers reduce the ballast wear and extend the intervals between two tamping cycle by at least 2 and thereby increase the service life of the ballast (Marschnig and Veit 2011). The comfort of the rail transport also increase by the soft padded sleepers in the track structure.

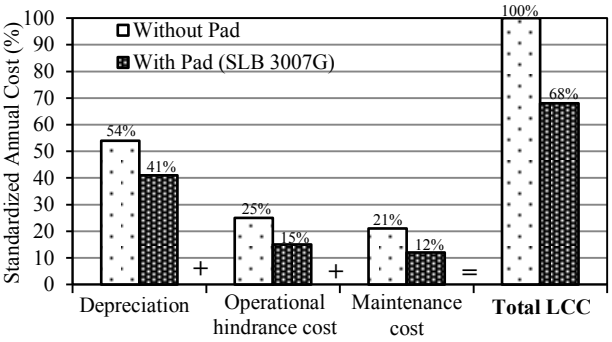

Figure 2 Breakdown of Normalized Annual Cost (data sourced from www.getzner.com)

2.4 Mitigating Ballast Degradation

Ballast is a major load bearing layer in the track bed which also facilitate the water draining easily from top of the track bed to the underlying formation or adjacent native ground. As the speed of the rail and the axle load increases, the ballast material used in the track bed needs considerable maintenance or a way of protect the ballast from high stresses. Limiting the generated stress on ballast is an economical option which many railway agencies and authorities are currently more interested on. This can be achieved by the use of energy absorbing shock mats such as USP and UBM. As mentioned previously, the use of USP in the concrete sleepers reduces the ballast stresses by two mechanisms: 1) Increase the contact area of the ballast to concrete sleeper interface, and 2) increase the number of load bearing sleepers per axle load (Bolmsvik 2005; Dahlberg 2010). Each of two mechanisms reduces the maximum load carried by each sleeper and thereby reduces the ballast stresses. Bolmsvik (2005) reported that USP increase the contact area of ballast to the sleeper by more than 36% for soft USP (stiffness 30 kN/mm) and by more than 18% for stiff USP (stiffness 70 kN/mm), which is otherwise far lower than 12%. As of the study by Loy (2008), the contact area between the sleeper and the ballast increases 30-35% with sleeper pads which is 5-8% without sleeper pads, at a bedding modulus C=0.2 N/mm³ and reducing the pressure on the ballast by 10-25%. Dahlberg (2010) found that the higher stiff tracks transmit the wheel–rail contact forces to the ballast through fewer number of the sleepers. Therefore, the ballast-sleeper contact stress is very high. This can be minimized by introducing USPs which distribute the stresses over more number of sleepers and thereby decrease the ballast stresses. The maximum contact force 57 kN without USP is reduced to 48 kN, 32 kN and 22 kN for stiff pad (stiffness 3000 kN/mm), medium stiff pad (stiffness 400 kN/mm) and soft pad (stiffness 50 kN/mm), respectively (Figure 3). It was concluded from the study by Dahlberg (2010) due to significant reduction of ballast stresses, these USPs can be used to protect the ballast material in the track bed and the detrimental effects of hanging sleepers can also be reduced by these USPs.

2.5 Field Study on Use of Shock Mats

An extensive full-scale field test to investigate the influence of under sleeper pads(USPs) on track quality and track dynamics was conducted by Schneider et al. (2011) on the Schweizerische Bundesbahnen test site at Kiesen in Switzerland. This study concluded that the placement of USPs in a ballasted track changes the track performance. The track settlement increased with time when track was without USPs, and needed renewal of sleepers and re-tamping of ballast. The settlement restarted over again when the track was loaded. But when USPs were used, the track settlement appeared to decrease with time. The authors reported that the varying subgrade condition between padded and unpadded test track sites made it difficult to draw any specific

recommendation. It was also mentioned in the study, the resilient layer reduced sleeper flexural strains but increased rail and sleeper accelerations and the contact forces between the USP and the ballast bed were related to the stiffness of the USPs.

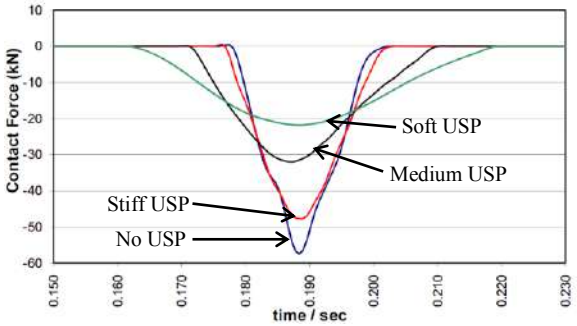

Figure 3Sleeper/ballast contact force
(data sourced from Dahlberg 2010)

3. DYNAMIC WHEEL-RAIL IMPACT FORCES

The wheel and rail undergo significant irregularities during the life time of the track structure. These irregularities are discrete in nature and usually at the surface of the rail and wheel. The higher frequency forces created by these irregularities are known as dynamic wheel-rail impact forces, which are higher in magnitude than quasi-static forces. If the wheel and rail surfaces are in good condition, then the wheel-rail contact force would be similar to the static wheel load (Steffens 2005).

3.1 Sources of impact load

The wheel-rail impact forces are caused by various sources such as wheel flat, wheel shells, worn wheel and rail, dipped rails, turnouts, crossings, insulated joints, expansion gap between two rail segments, rail joint misalignment, imperfect rail weld and rail corrugation (Indraratna et al. 2011). Figure 4 shows some of typical sources of irregularities.

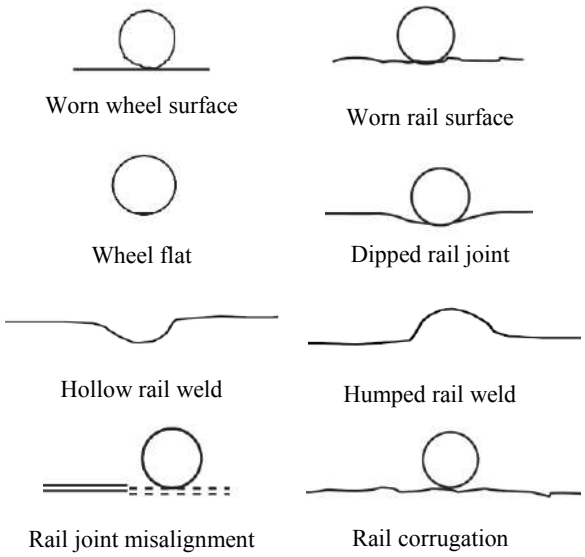

Figure 4 Wheel-Rail Irregularities causes impact forces

These abnormalities on the wheel and rail can generate large impact forces between wheel and rail. The impact load caused by defects on the wheel subsequently rotates with each wheel rotation and roll over when the defects are in the rail. A large wheel impact forces generated at the turnout and crossings due to traversing of wheel over the rail discontinuity (Anastasopoulos et al. 2009). Besides, the rapid change of track stiffness at the road crossing, bridge approach and track transition such as concrete slab track merging to ballasted track or vice versa, the rise of high impact energy accelerate the track degradation and settlement (Li and Davis 2005). The magnitude of the impact forces is very high within the very short (2–10 msec) impulse duration (Lee et al. 2005). Therefore, the effects of impact forces are very significant in the design and utilization of concrete sleepers as parts of the railway track structures (Kumaran et al. 2002).

3.2 Impact Forces

Usually, the track degradation is driven by the wheel/rail impact loads, referred to as static load and peak loads. Two distinct types of peaks (1) an instantaneous sharp peak; and (2) a much longer duration gradual peak of smaller magnitude were observed during impact loading. Jenkins et al. (1974) termed these force peaks as P1 and P2, respectively. These P1 and P2 are respond to how a wheel rolling over a short-pitch irregular defects. These notations were adopted by industry and are in common use today to describe limitations on forces applied to the track structure (Indraratna et al. 2011). P1 and P2 forces observed from wheel/rail impact force time histories when the train vehicle passes a typical rail joint on Chinese mainline tracks at various train speeds are shown in Figure 5 (Zhai and Cai 1997).

The P1 force is due to the inertia of the rail and sleepers resisting the downward motion of the wheel and compression of the contact zone between the wheel and rail and the force is a very high frequency (>100 Hz) force of less than half a millisecond in length. Its effects are mostly filtered out by the rail and sleepers, therefore, its direct effect on ballast or subgrade settlement is very minimum (Frederick and Round 1985). On the other hand, the P2 force occurs at a lower frequency (30 – 90 Hz) than the P1 force, but in comparison to static forces this P2 force still classified as high frequency force. This P2 force is due to the downward movement of the vehicle unsprung mass and the rail/sleeper mass and causing compression of the ballast mass underneath the sleeper which increases the contact stresses, and the loads on sleepers and ballast. Therefore, the P2 forces are of great interest to the track designers.

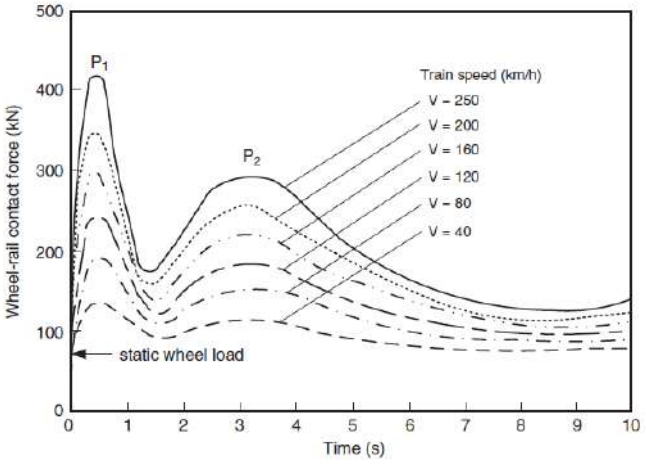

Figure 5 Wheel/Rail Impact Force
(data sourced from Zhai and Cai 1997)

Since the P_2 forces are of greater importance in the assessment of track degradation, Jenkins et al. (1974) proposed a theoretical equation to calculate P_2 forces at dipped joints. The P_2 force in the equation shown below is dependent on the vehicle unsprung mass, track mass, track stiffness, vehicle speed and joint dip angle.

$$P_2 = P_0 + 2\alpha V_m \sqrt{\frac{M_u}{M_u + M_t}} \cdot \left[1 - \frac{C_t \pi}{4\sqrt{K_t (M_u + M_t)}}\right] \cdot \sqrt{K_t M_u} \quad (1)$$

where:
P_0 = Vehicle static single wheel load (kN)
Mu = Vehicle unsprung mass (kg)
2α = Total joint angle (rad)

V = Speed of vehicle (m/s)

$K_t = 2K_{td}\beta$ = Equivalent track stiffness (MN/m)

$C_t = \frac{3C_{td}\beta}{2}$ = Equivalent track damping(kNs/m)

$M_t = \frac{3M_{td}\beta}{2}$ = Equivalent track mass (kg)

$\beta = \left(\frac{K_{td}}{4EI}\right)^{-0.25}$ = Effective track length (m)

K_{td} = Ballast Stiffness per metre (MN/m/m)

C_{td} = Ballast Damping per metre (kNs/m/m)

M_{td} = Rail + Sleeper mass per metre (kg/m)

Internationally similar limits are placed for the safety of the track. The British Rail Safety and Standards Board (RSSB) Railway Group Standard (GM/TT0088):Permissible Track Forces for Railway Vehicles (1993) states that when a vehicle (Class 55 Deltic locomotive) negotiates a vertical ramp discontinuity at its maximum design operating speed (160 km/h) the total P2 force produced should not exceed 322 kN per wheel. Australian standards recommend Jenkins's formula to calculate P2 forces and specify the guidelines shown in Table 1 to limit P2 forces as a function of track and vehicle characteristics (Indraratna et al. 2011).

Table 1 Limiting P_2 forces (QR 2001; RIC 2002; ARA 2003)

Track Class	Maximum P_2 Force Locomotives (kN)	Maximum P_2 Force Other Rolling Stock(kN)	K_t (MN/m)	C_t (kNs/m)	M_t (kg)
1	295	230	110	52.5	135
2	230	230	110	48	117
3	200	230	95.8	45.9	106
4	180	180	90.3	43.2	95
5	130	130	83.6	40	85

4. Laboratory testing

In this study the use of energy absorbing shock mats to mitigate the ballast degradation under impact loading was assessed by a series of laboratory testing. The typical dynamic stresses in the range of 400-600 kPa caused by wheel-flat and dipped rail (Jenkins et al. 1974; Steffens and Murray 2005; Indraratna et al. 2010)was simulated by using the large-scale impact load test facility available at the University of Wollongong, Australia.

4.1 Test apparatus, Impact Loading and Instrumentations

The impact loading test facility available at the University of Wollongong (Figure 6) is a high capacity drop weight impact test machine. It can be hoisted mechanically to the height which corresponds to the required impact load magnitude and drop height through guided roller on vertical column fixed to the strong concrete floor. The efficiency of the hammer velocity is 98% due to the friction of the guiding column (Kaewunruen and Remennikov 2010). Therefore, the actual hammer drop height (h=V^2/2g) is calculated multiplying the theoretical drop height by a factor 1.04 (i.e., 1/0.982). The free fall drop hammer is a weight of 592 kg and it can be dropped from a maximum height of 6 m from the base of the concrete floor. The impact load was measured and recorded by a dynamic load cell of a capacity of 1,200 kN mounted at the bottom of the hammer and connected to a data acquisition system. Ballast deformation and transient acceleration of the impact loads were captured by a piezoelectric accelerometer of a capacity of 10,000g (g is the gravitational acceleration) connected at the top of the sample load plate shown in Figure 7.

4.2 Material Specifications

The materials used in this study are the ballast, shock mats and the weak and hard base. The specifications of these materials are given in following sections.

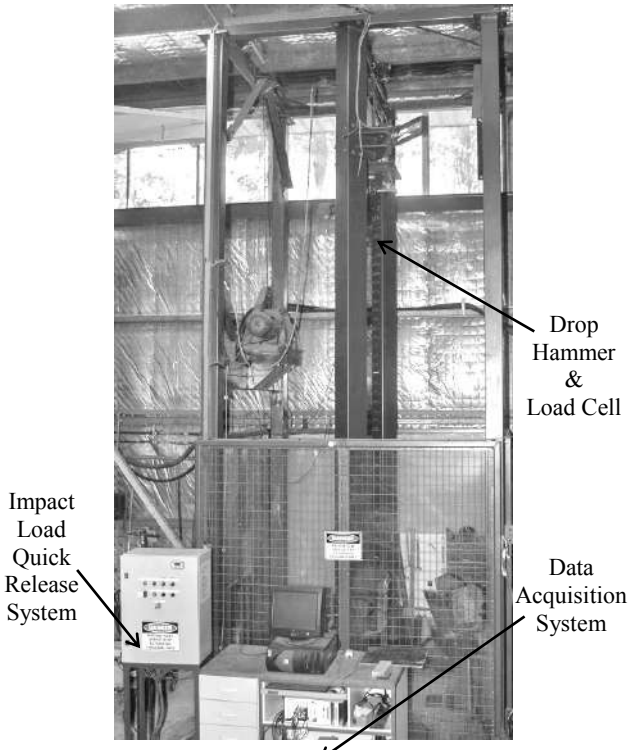

Figure 6 Impact load Testing Apparatus

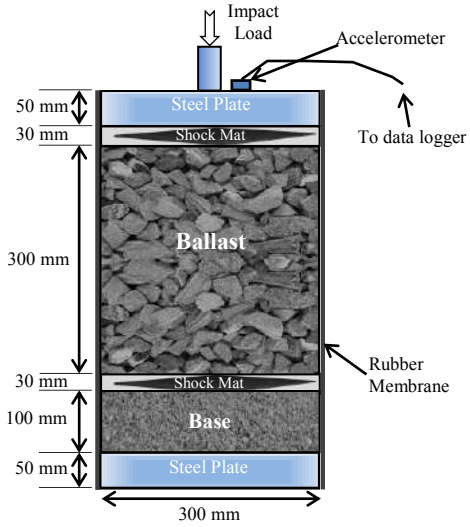

Figure 7 Schematic Diagram of the Test Specimen

4.2.1 Ballast

The railway ballast material commonly used in New South Wales (NSW), Australia is Latite basalt, a common igneous rock can be found in the south cost of NSW and closer to Wollongong City, Australia. The aggregates made from crushed volcanic basalt are dark, fine grained and very dense with sharp angular corners suitable for fresh railway ballast material. The physical and index properties of the fresh ballast were evaluated as per AS 2758.7 (1996) and discussed by Indraratna et al. (1998) in a previous study. The ballast material for this study was prepared in accordance with current practice in Australia as per AS 2758.7 (1996). The raw ballast material was thoroughly cleaned by water and dried before sieving. The particle size distribution (PSD) of the ballast material is shown in Figure 8. The basic martial parameters from the PSD are listed in Table 2.

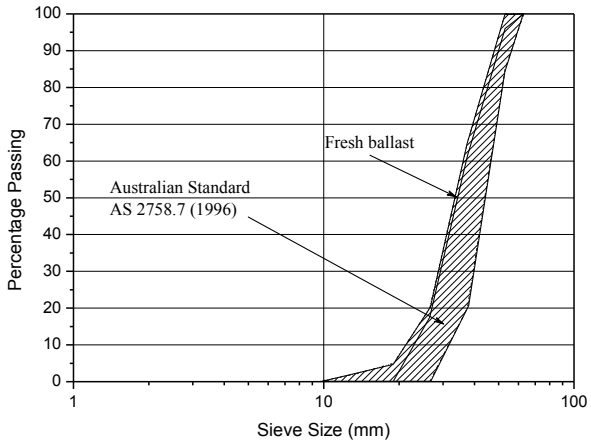

Figure 8 Particle Size Distribution (PSD) of the ballast material

4.2.2 Sand Subgrade

In order to simulate a typical weak base condition, a thin layer of sand subgrade cushion was used in the laboratory testing. The sand parameters are listed in Table 2.

4.2.3 Shock Mats

There are many manufacturers of the USP and UBM around the world and some of the manufacturers listed by (Bolmsvik 2005). One of such manufacturer's USP and UBM with its material parameters are shown in Figure 9 (a). USPs are generally stiffer than UBMs as they are placed adjacent to higher stress zones i.e. sleeper-ballast interface. The rubber shock mats used in this study was a 10 mm thick made of recycled rubber granulates of 1 to 3 mm particle size, bound by polyurethane elastomer compound. A sample of shock mat and its material parameters are shown in Figure 9 (b).

Under Sleeper Pad (USP)
Thickness including mounting mesh = approx. 15 mm
Weight = 4.2 kg/m^2
Bedding Modulus
C_{stat}= 0.22 N/mm^3
Tear Strength of the connection
USP-Concrete Sleeper
Minimum = 0.4 N/mm^2
Average = 0.5 N/mm^2

Under Ballast Mat (UBM)
Thickness = approx. 17 mm
Weight = 10.5 kg/m^2
Specific Static Stiffness
C_{stat}= 0.15 N/mm^3
Tensile Strength = 1.3 N/mm^2

(a)

Recycled Rubber Shock Mat
Tensile Strength = 600 kN/m^2
Tensile Strain at Failure = 80%
Modulus at 10% compressive strain = 3800 kN/m^2

(b)

Figure 9 (a) Sample of USP and UBM; (b) Shock Mat used for laboratory testings in this study

Table 2Material Parameters of Ballast and Sand

Parameters	Fresh Ballast	Sand Subgrade
Particle Shape	Angular	-
Type of Gradation	Uniformly graded	Poorly graded
Max. particle size, mm (D_{max})	63.0	4.75
Min. particle size, mm (D_{min})	19.0	0.075
Effective size, mm (D_{10})	24.0	0.24
Uniformity Coefficient (C_u)	1.6	2.3
Coefficient of Gradation (C_c)	1.0	1.0

4.3 Laboratory Test Setup

The thickness of the ballast layer in Australian rail track is 250-300 mm (the lower thicknesses are at the bridge deck). Therefore a 300 mm thick ballast layer was selected as the specimen height in this study. 300 mm ballast thickness is found to be more realistically simulating site condition as per the previous study on ballast material conducted on large scale triaxial or cubical test apparatus by Brown et al. (2007) and Indraratna et al. (2007).The inclusion of shock mats at the top and bottom of ballast layer brings the total height of the track foundation more realistic value. In order to simulate the field density (approximately 1560 kg/m3) for heavy haul tracks, the ballast material was compacted in several layers by using a rubber padded hammer. The low lateral confining pressure for the ballast was simulated by placing a cylindrical rubber membrane around the specimen. The rubber membrane (thickness of 7 mm) was capable of prevent piercing or cutting the membrane by sharp corners of ballast particles.

The two types of base condition used were, 1) relatively weak base represented by a 100 mm thick sand layer vibro-compacted to a density of 1620 kg/m3and placed under the ballast bed, 2) hard base condition represented by a rigid steel plate of thickness 50 mm. This hard base condition is represented by the tracks running on steel bridge deck or track foundation located on hard bed rock. Three layers of shock mats (total thickness of 30 mm) were used at the top and bottom of the ballast specimen (Figure 7).

4.4 Test Procedure

Each test specimens were placed on the concrete floor under the impact load hammer. The hammer was hoisted to the required drop height and released by an electronic quick release system. The ballast specimens were tested with and without shock mats placed at the top and the bottom of the ballast layer. The impact loading was repeated for 10 times for each sample. It was found that the strain due to impact loading is attenuating after certain number of blows (typical 8 or 9 blows). Automatic triggering of impact loading signal was enabled and data at sampling frequency of 50,000 Hz was collected by the data acquisition system. To remove the noise in the data, the raw impact load-time history data were digitally filtered using low-pass fourth order Butterworth filter with a cut-off frequency of 2,000 Hz. Ballast deformation and transient acceleration of the impact load data were collected by data acquisition system by the piezoelectric accelerometer connected at the top of the sample plate.

4.5 Impact load-time history

The impact load was dropped on the sample and after the first impact the hammer rebounded on the sample couple of time then the impact load attenuated with time as shown in Figure 10. Two distinct types of peaks were observed during impact loading and named as P1 and P2 as per Jenkins et al. (1974). The peak P1 related to the multiple impacts including the first impact from the free fall hammer drop and the hit from rebounded hammer. The single peak P2 is related to the mechanical resistance of the ballast leading to its significant compression (Saxton et al. 1974). The P2 peak is lesser than the

instantaneous P1 peaks. It is evident from Figure 10, the shock mats are attenuating the impact force (reduces the P2 peak) and extending the time duration of impact load.

U.K. Railway group standards recommends considering P2 force in the track design criteria as it is the direct influence on the degradation of track bed. Therefore the P2 forces variation with continuous impact loading is the major concern in this study with respect to ballast degradation. The P2 forces plotted with each blow is shown in Figure 11 showed a gradual increase with the increased number of blows. As the ballast particle get rearranged and become a densely packed after each blow, which offer a higher inertial resistance, leads to increased P2 force values. When ballast particle rearrange and stabilise completely, the changes of P2 forces become insignificant. This is apparent from Figure 11, the changes of P2 forces very minor after 8th blow.

By comparing the impact forces with and without shock mats, the results shows that the shock mats attenuated the impact forces for both base conditions. It is also evident from the results shown in Figure 11 for the weak base without shock mat and hard base with shock mat, the weak base itself acted as a shock absorbing material. Therefore, the impact forces were more distinct for hard base.

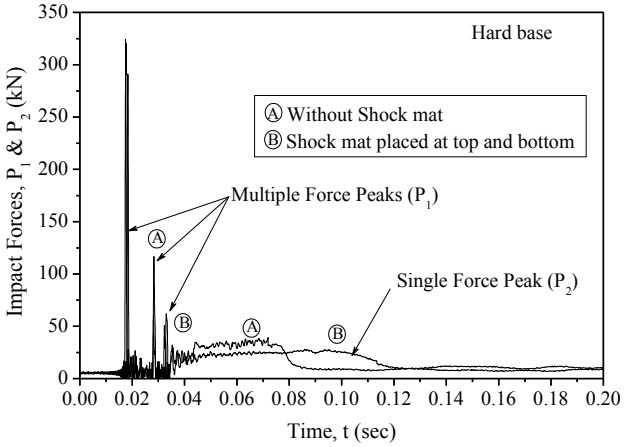

Figure 10 Impact Load-Time Histories (Hard base)

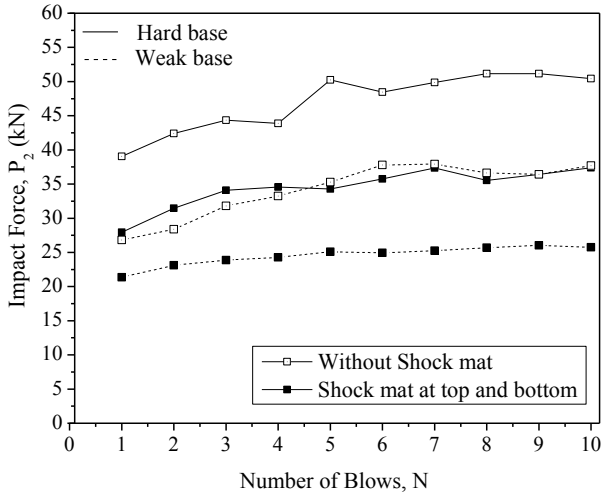

Figure 11P_2 force variation with number of blows (data sourced from Nimbalkar et al. 2012)

4.6 Ballast deformation and strain response

Vertical and lateral deformation data were collected after each impact blow. The shear strain (ε_q) and volumetric strain (ε_v) for axisymmetric loading were calculated by using the following equation by Timoshenko and Goodier (1951).

$$\varepsilon_q = \frac{2}{3}(\varepsilon_1 - \varepsilon_3) \quad (2)$$

$$\varepsilon_v = (\varepsilon_1 + 2\varepsilon_3) \quad (3)$$

The variation of shear and volumetric strain with the number of impact blows are shown in Figure 12a and 12b, respectively. In general both the shear and volumetric strains increased in the initial impact loadings and eventually become constant at the end of impact blows 9 and 10. This is because the ballast layer displays a strong tendency to compact under repetitive loading due to rearrangement, reorientation and breakage of corners of the ballast particles (Lackenby et al. 2007; Indraratna et al. 2010) and become stable when the ballast particles are completely rearranged and densified.

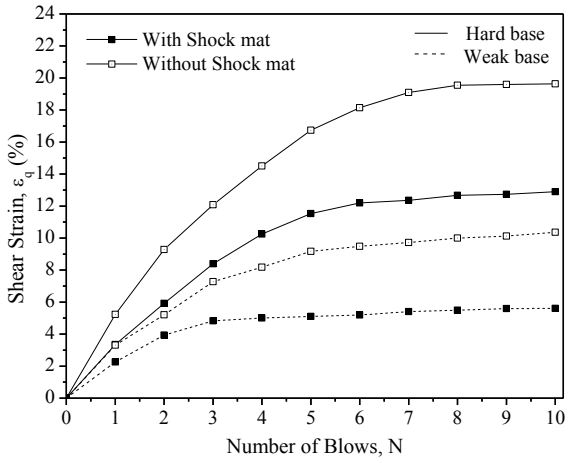

(a)

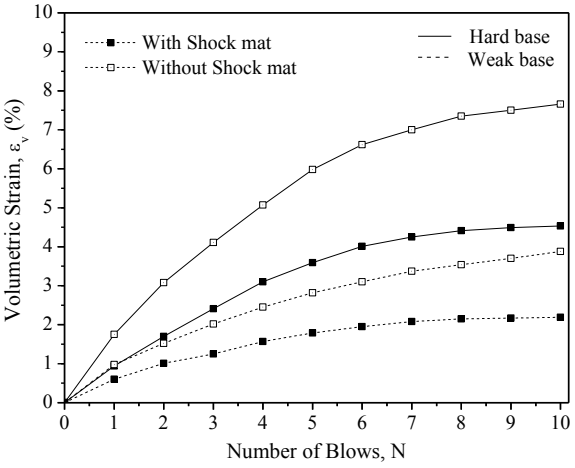

(b)

Figure 12 Permanent strain response of ballast with and without shock mat:(a) shear strain; (b) volumetric strain (data sourced from Nimbalkar et al. 2012)

The inclusion of shock mats in the ballast bed reduced the shear and volumetric strain of the ballast layer. The permanent strains were more pronounced for the hard base condition. However when shock mats are placed at the top and bottom of the ballast layer the shear and the volumetric strains are reduced in the order 40% to 50%. The ballast breakage can be related to the number of blows as well as accumulated impulse (area under the transient impact loading curve). In order to abbreviate in view of scope of this paper, Figures 11 and 12 are plotted against number of blows.

4.7 Ballast Breakage under Impact Loading

Ballast particle breakage takes place under repetitive impact loading. Initially, breakage of corners of the angular ballast at the inter-particle contacts takes place, followed by complete fracture of the particles depends on the strength of the raw ballast and level of the load increase. This affects the overall deformation characteristics and ultimate strength of the ballast layer(Selig and Waters 1994; Indraratna et al. 2011).This breakage of ballast particles contributes to increased vertical and lateral deformations and differential track settlement. To quantify the particle breakage under impact loading, an evaluation of ballast breakage was performed. After 10 impact blow, the ballast from the specimen was recovered and particle size analysis was performed to compare the degraded ballast with the fresh ballast initially used in the testing. To quantify the ballast breakage, the following equation from the method proposed for Ballast Breakage Index (BBI) by Indraratna et al. (2005) was used.

$$BBI = \frac{A}{(A+B)} \tag{4}$$

The parameters defining the BBI are shown in Figure 13. The BBI for both hard and weak base condition with and without shock mats are summarized in Table 3. The values shown in parentheses in Table 3 are the percentage reduction of BBI by the use of shock mats at the top and the bottom of the ballast layer.

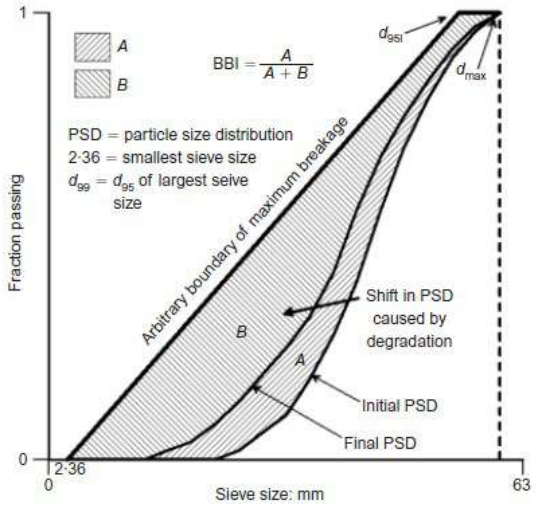

Figure 13 Determination of Ballast Breakage Index (BBI) (after Indraratna et al. 2005)

Table 3Ballast Breakage after 10 impact blows

Base Condition	Ballast Breakage Index (BBI)	
	Without Shock Mats	With Shock Mats (placed at top and bottom of ballast)
Hard	0.170	0.091 (reduced by 46.5%)
Weak	0.080	0.028 (reduced by 65.0%)

It is evident from the BBI values reported in Table 3 that the use of shock mats considerably reduced the breakage of ballast particle under impact loadings. The hard base condition induced relatively higher breakage than the weaker base condition. This is due to the concentration of non-uniform stresses developing at the corners of the sharp angular ballast increasing by the higher resistive hard base. When shock mats placed at the top and bottom of ballast layer, the ballast breakage was reduced by about 46.5% for hard base condition. The same reduction for the weak base condition was relatively higher and about 65%. This is due to the weak base itself act as a shock absorbing layer.

5. NUMERICAL MODELLING

The dynamic response of this layered system attributed to transient impact load is analyzed by a 2-dimentional (2D) axisymmetric dynamic finite element analysis by using PLAXIS(PLAXIS 2D: Ver. 8.6).The main features of this dynamic finite element analysis includes, introduction of modified stress-dilatancy relationship to capture the ballast particle degradation and incorporation of material damping for various track materials tested. The specimen of this study was modeled as an elasto-plastic model of a composite layered system including ballast, shock mat,base and steel plate. A typical axisymmetric specimen model simulated in finite element discretization using PLAXIS 2D is shown in Figure 14. All 3 layers are modeled using 15-node cubic strain elements and the interaction between granular media and the shock mats are modelled using 5-node interface elements. The 15-point cubic element provides a fourth order interpolation for displacements. The numerical integration by the Gaussian scheme involves 12 Gauss points.

The digitally filtered (by using a low-pass Butterworth filter) transient impact load-time histories obtained from the laboratory testings are used for the dynamic finite element analysis. Lateral distributed loads are applied to the right boundary to represent the confining effects of thick rubber membrane (Henkel and Gilbert 1952). The following boundary conditions are adopted for the numerical analysis. The left (axis of symmetry) and bottom boundaries are restrained in lateral and vertical directions, respectively. The top and right boundaries are free to move.The node at the left bottom corner of the mesh is restrained in both vertical and horizontal directions (pinned support - standard fixity).The right and bottom boundaries are considered adsorbent boundaries. Two different soil models have been adopted are (1) classical Mohr-Coulomb elastic-perfectly-plastic model for the basematerial and (2) isotropic Hardening Soil model(Schanz et al. 1999) for ballast. The constitutive model parameters adopted here are based on the available laboratory test results.

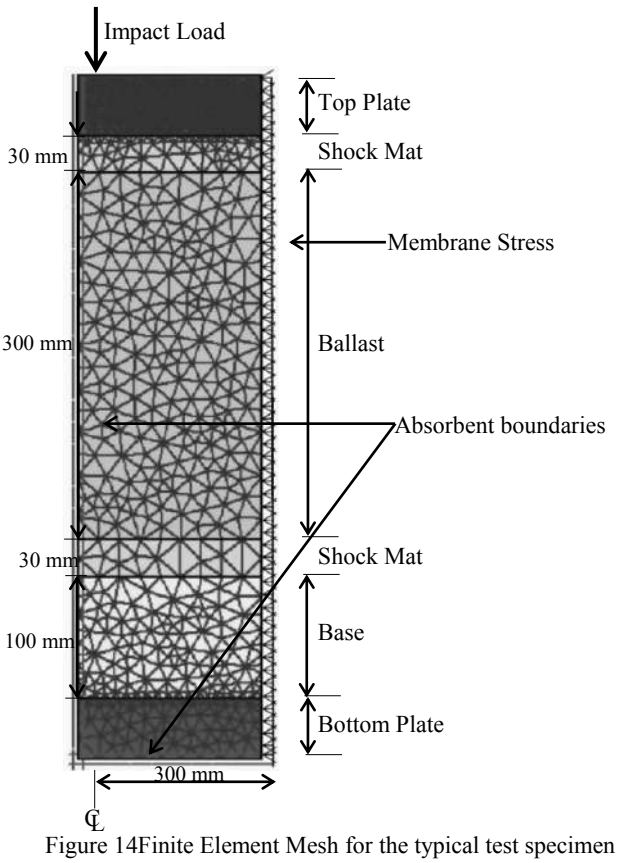

Figure 14Finite Element Mesh for the typical test specimen

5.1 Mohr-Coulomb Elasto-Plastic model

The Mohr-Coulomb (MC) model is used to represent the weak base. The following key parameters and values were used to represent a relatively weak base (i.e., poorly graded sand).

$E = 45\,MPa,\ \ \nu = 0.33,\ \ c' = 0,\ \ \varphi' = 24^o\ \ and\ \ \psi = 0.$

5.2 Hardening Soil Model

The hardening soil (HS) model is used to simulate the strain-hardening behaviour of ballast under impact loading.The mobilised friction angle $\phi'_m$is defined as follows:

$$\sin\varphi'_m = \frac{q}{q + 2\sigma'_3} \tag{5}$$

The mobilised dilatancy angle $\psi_m$is given by(Nimbalkar et al. 2012):

$$\sin\psi_m = \frac{\left(\sin\phi'_m - \sin\phi'_{cv}\right) - \left\{\dfrac{\kappa\left(dBBI\right)\left(1-\sin\phi'_m\right)}{2\sigma'_3 d\varepsilon_1^p\left(1+\tan^2\phi'_{cv}\right)}\right\}}{\left(1-\sin\phi'_m\ \sin\phi'_{cv}\right) - \left\{\dfrac{\kappa\left(dBBI\right)\left(1-\sin\phi'_m\right)}{2\sigma'_3 d\varepsilon_1^p\left(1+\tan^2\phi'_{cv}\right)}\right\}} \tag{6}$$

The symbols are explained in the notation section of this paper. Further details of the HS material parameters and breakage parameters are given in Table 4.

Table 4Ballast Parameters for HS Model Simulation

Material Parameters	Hard Base		Weak Base	
	Sample 1	Sample 2	Sample 3	Sample 4
E_{50}^{ref} (MPa)	11.04	13.12	12.43	15.10
E_{oed}^{ref} (MPa)	11.04	13.12	12.43	15.10
E_{ur}^{ref} (MPa)	10.20	12.09	12.53	14.80
ϕ'_p (degrees)	73.34	73.60	74.81	75.83
ψ (degrees)	21.27	16.15	18.20	14.58
P_{ref} (kN/m^2)	19.70	12.67	10.65	6.06
$\left(dBBI/d\varepsilon_1^p\right)_f$	0.81	0.68	0.73	0.47
κ	882.44	728.54	664.45	674.72
$\left(dE_B/d\varepsilon_1^p\right)_f$ (kNm/m^3)	714.78	495.41	485.05	317.12

5.3 Linear Elastic Model and Interface Elements

Steel plates located at the top and bottom of the test sample are considered as linear elastic. The shock mat is also modelled as a linear elastic material. Zero-thickness interface elements are used to model the frictional behaviour between various layers and are simulated by 5-nodeline elements. The following material parameters were used for Steel and shock mat.

$Steel:\qquad E = 210\,GPa,\ \nu = 0.15,\ \gamma = 77\,kN/m^3$

$Shock\ Mat: E = 6.12\ MPa,\ \nu = 0.48,\ \gamma = 12.04\,kN/m^3$

5.4 Finite Element Model Predictions

Figure 15 shows the finite element model prediction of the axial strain using the impact pulse data obtained in the laboratory impact testing. The axial strain values are compared with laboratory measured data for with and without the placement of shock mats for both hard and weak baseconditions. As from Figure 15, the finite element analysis able to predict the strain hardening behaviour of ballast under repeated impact load. The FE simulation is closely captured the plastic yielding of the ballast which influenced by amount of vicious damping of the ballast material. The close comparison of FE model predicted and laboratory measured axial strain values reveal that the influence of P1 forces on the response of the ballast is negligible, as the digitally filtered P2 force load-time history was used as an input for the finite element analysis.

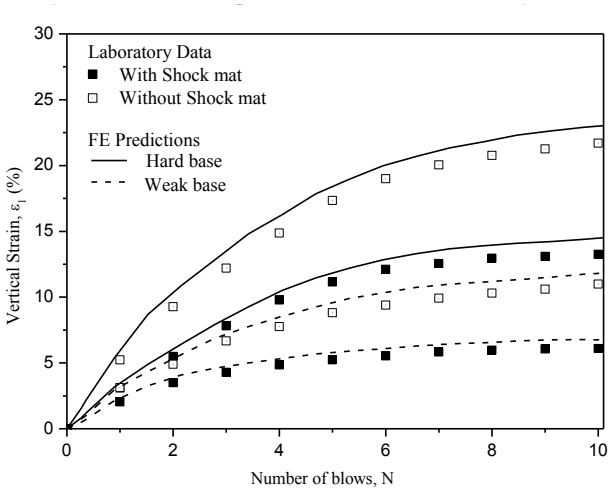

Figure 15 Axial Strain: Measured vs FE predicted values (data sourced from Nimbalkar et al. 2012)

6. CONCLUSION

The performance of ballasted track with shock mats has been described through laboratory experiments and numerical models. The impact load causes accelerated ballast breakage was confirmed by experiment and numerical model data. Two base conditions tested in this study confirm that the hard base conditions such as bridge deck, rail track-road crossing and track on rock foundation cause comparatively higher ballast degradation compare to weak base condition. Initially, the impact induced strain of the ballast is very high and it eventually stabilizes and become constant after certain number of load application.

The insertion of shock mats at the top and bottom of the ballast reduces the impact induced stresses on ballast and considerably reduces the ballast degradation. As the hard base condition produces more breakage, the benefits of shock mats are greater in hard base conditions compared to weak bases. Weak base itself act as a shock absorbing layer, therefore the use of additional shock mats are not more pronounced for softer foundations. The finite element model analysis is capable of predicting strain responses measured for ballast under impact loading with and without shock mats. It is evident from this study, by placing shock mats, loads on the ballast bed can be reduced by a more homogenous mounting of the sleepers and ballast and track stability can be improved. This leads to reduced track misalignment, which in turn leads to a reduced number of maintenance operations.

Results could vary for different PSD and impact force P1 and P2. Also in reality, material used for USP and UBM can vary, usually stiffer mats preferred under sleeper. No study has yet been reported

on quantitative or qualitative analysis of ballast degradation by placing USP and UBM under cycling loading condition. Currently an investigation is undertaken at the University of Wollongong testing facility to evaluate the effectiveness of USP and UBM in mitigating ballast degradation.

7. ACKNOWLEDGMENTS

The authors wish to thank the Australian Research Council for its financial support. The support provided by University of Peradeniya, Sri Lanka offering the study leave to conduct doctoral work of Sinniah K. Navaratnarajah is gratefully acknowledged. The assistance provided by senior technical officers, Alan Grant, Cameron Neilson and Ian Bridge is also much appreciated.A significant portion of the contents have been reproduced with kind permission from the Journal of Geotechnical and Geoenvironmental Engineering ASCE, International Journal of Geomechanics, ASCE, ASTM Geotechnical Testing Journal, Geotechnique, and Canadian Geotechnical Journal.

8. NOTATION

The symbols used in this paper are listed below:

A	=	Shift in the PSD curve after the test
B	=	Potential breakage or the area between the arbitraryboundary of maximum breakage and the final PSD
C_c	=	Coefficient of curvature
C_u	=	Coefficient of uniformity
c'	=	Cohesion (kPa)
D_{10}	=	Effective particle size (mm)
dE_B	=	Incremental energy consumption by particle breakage per unit volume (kN·m/m^3)
D_{max}	=	Maximum particle size (mm)
D_{min}	=	Minimum particle size (mm)
E	=	Young's modulus (kPa)
E_{oed}	=	Stress-dependent tangent stiffness modulus for primary loading (kPa)
E_{ur}	=	Stress-dependent secant stiffness modulus for unloading and reloading (kPa)
E_{50}	=	Stress-dependent secant stiffness modulus for primary loading (kPa)
κ	=	Constant of proportionality
N	=	Number of blows
P_1	=	High-frequency impact force (kN)
P_2	=	Low-frequency impact force (kN)
P_{ref}	=	Reference pressure (kPa)
q	=	Deviator stress (kPa)
γ	=	Unit weight (kN/m^3)
ε_q	=	Shear strain
ε_v	=	Volumetric strain
ε_1	=	Average vertical strain (major principal strain) in ballast layer
ε_3	=	Average lateral strain (minor principal strain) in ballast layer
v	=	Poisson's ratio
σ'_1	=	Major principal effective stress (kPa)
σ'_3	=	Minor principal effective stress (kPa)
ϕ'		Friction angle (degree)
ϕ'_{cv}	=	Friction angle at critical state (degree)
ϕ'_m	=	Mobilized friction angle (degree)
ϕ'_p	=	Peak friction angle obtained from peak stress ratio, $(\sigma'_1/\sigma'_3)_f$ (degree)
ψ	=	Dilatancy angle (degree)
ψ_m	=	Mobilized dilatancy angle (degree)

9. REFERENCES

Anastasopoulos, I., Alfi, S., Gazetas, G., Bruni, S. and Van Leuven, A. (2009) "Numerical and Experimental Assessment of Advanced Concepts to Reduce Noise and Vibration on Urban Railway Turnouts." Journal of Transportation Engineering, 135, (5), pp. 279-287.

ARA (2003), Code of Practice for the Defined Interstate Rail Network, Volume 4: Track, Civil and Electrical Infrastructure, Part 1: Identification and Classification of Wheel defects, Australasian Railway Association.

Auersch, L. (2006) "Dynamic axle loads on tracks with and without ballast mats: numerical results of three-dimensional vehicle-track-soil models." Proceedings of the Institution of Mechanical Engineers Part F-Journal of Rail and Rapid Transit, 220, (2), pp. 169-183.

Bolmsvik, R. (2005) "Influence of USP on the track response—a literature survey."

Brown, S. F., Kwan, J. and Thom, N. H. (2007) "Identifying the key parameters that influence geogrid reinforcement of railway ballast." Geotextiles and Geomembranes, 25, (6), pp. 326-335.

Bruni, S., Anastasopoulos, I., Alfi, S., Van Leuven, A., Apostolou, M. and Gazetas, G. (2009) "Train-Induced Vibrations on Urban Metro and Tram Turnouts." Journal of Transportation Engineering, 135, (7), pp. 397-405.

Dahlberg, T. (2010) "Railway Track Stiffness Variations – Consequences and Countermeasures." International Journal of Civil Engineering, 8, (1), pp. 1-12.

Esveld, C. (2001). Modern railway track. MRT-Production, The Netherlands.

Frederick, C. O. and Round, D. J. (1985). Vertical Track Loading. Track Technology: Proceedings of a Conference, University of Nottingham, UK, Thomas Telford Ltd, pp. 135-149.

GM/TT0088 Rail Safety and Standards Board (1993) "Permissible track forces for railway vehicles", Group Standard, Issue 1, Revision A. Rail Safety and Standards Board, London.

Henkel, D. J. and Gilbert, G. D. (1952) "The Effect Measured of the Rubber Membrane on the Triaxial Compression Strength of Clay Samples." Géotechnique, 3, pp. 20-29.

Indraratna, B., Ionescu, D. and Christie, H. (1998) "Shear Behavior of Railway Ballast Based on Large-Scale Triaxial Tests." Journal of Geotechnical and Geoenvironmental Engineering, 124, (5), pp. 439-449.

Indraratna, B., Lackenby, J. and Christie, D. (2005) "Effect of confining pressure on the degradation of ballast under cyclic loading." Géotechnique 55, 325-328.

Indraratna, B., Nimbalkar, S., Christie, D., Rujikiatkamjorn, C. and Vinod, J. (2010) "Field Assessment of the Performance of a Ballasted Rail Track with and without Geosynthetics." Journal of Geotechnical and Geoenvironmental Engineering, 136, (7), pp. 907-917.

Indraratna, B., Nimbalkar, S. and Rujikiatkamjorn, C. (2012). Performance evaluation of shock mats and synthetic grids in the improvement of rail ballast pp. 47-62.

Indraratna, B., Salim, W. and Rujikiatkamjorn, C. (2011). Advanced Rail Geotechnology: Ballasted Track. CRC Press/Balkema, Rotterdam, Netherlands.

Indraratna, B., Shahin, M. A. and Salim, W. (2007) "Stabilisation of granular media and formation soil using geosynthetics with special reference to railway engineering." Proceedings of the ICE - Ground Improvement 11, 27-43.

Jenkins, H. M., Stephenson, J. E., Clayton, G. A., Moorland, J. W. and Lyon, D. (1974) "The effect of track and vehicle parameters on wheel/rail vertical dynamic forces." Railway Engineering Journal, 3, (1), pp. 2-16.

Kaewunruen, S. and Remennikov, A. (2010) "Dynamic Crack Propagations in Prestressed Concrete Sleepers in Railway Track Systems Subjected to Severe Impact Loads." Journal of Structural Engineering, 136, (6), pp. 749-754.

Kumaran, G., Menon, D. and Nair, K. K. (2002) "Evaluation of dynamic load on railtrack sleepers based on vehicle-track modeling and analysis." International Journal of Structural Stability and Dynamics, 02, (03), pp. 355-374.

Lackenby, J., Indraratna, B., McDowell, G. and Christie, D. (2007) "Effect of confining pressure on ballast degradation and deformation under cyclic triaxial loading." Géotechnique 57, 527-536.

Lee, M. L., Chiu, W. K. and Koss, L. L. (2005) "A Numerical Study into the Reconstruction of Impact Forces on Railway Track-like Structures." Structural Health Monitoring, 4, (1), pp. 19-45.

Li, D. and Davis, D. (2005) "Transition of Railroad Bridge Approaches." Journal of Geotechnical and Geoenvironmental Engineering, 131, (11), pp. 1392-1398.

Loy, H. (2008). "Under Sleeper Pads: improving track quality while reducing operational costs." European Railway Review, Issue 4.

Loy, H. (2012) "Mitigating vibration using under-sleeper pads." Railway Gazette International, 168, (4), pp. 40-42.

Marschnig, S. and Veit, P. (2011) "Making a case for under-sleeper pads." International Railway Journal, 51, (1), pp. 27-29.

Nielsen, J. C. O. and Johansson, A. (2000) "Out-of-round railway wheels - a literature survey." Proceedings of the Institution of Mechanical Engineers Part F-Journal of Rail and Rapid Transit, 214, (2), pp. 79-91.

Nimbalkar, S., Indraratna, B., Dash, S. and Christie, D. (2012) "Improved Performance of Railway Ballast under Impact Loads Using Shock Mats." Journal of Geotechnical and Geoenvironmental Engineering, 138, (3), pp. 281-294.

Plášek, O., Svoboda, R. and Hruzíková, M. (2007).Assembly of under sleeper pads in turnouts for the homogenization of vertical rail deflectionsCentre for Integrated Design of Advanced Structures, Czech Republic.

QR (2001), STD/0026/TEC Rollingstock Dynamic Performance, Safety Management System, Version: 2, Queensland Rail.

RIC (2002), RSU120 General Interface Requirements, Version: 2.0, Rail Infrastructure Corporation (Rail Corp).

Saxton, H. J., Ireland, D. R. and Server, W. L. (1974). "Analysis and control of inertial effects during instrumented impact testing." ASTM Spec. Tech. Publ., American Society of Testing and Materials, Philadelphia, pp. 50-73.

Schanz, T., Vermeer, P. A. and Bonnier, P. G. (1999). The hardening soil model: Formulation and verification. Beyond 2000 in Computational Geotechnics Balkema, Rotterdam, A A Balkema Publishers, pp. 281-296.

Schneider, P., Bolmsvik, R. and Nielsen, J. C. O. (2011) "In situ performance of a ballasted railway track with under sleeper pads." Proceedings of the Institution of Mechanical Engineers, Part F: Journal of Rail and Rapid Transit, 225, (3), pp. 299-309.

Selig, E. T. and Waters, J. M. (1994). Track Geotechnology and Substructure Management. Thomas Telford, London.

Steffens, D. and Murray, M. (2005). Establishing meaningful results from models of railway track dynamic behaviour. Proceedings of 8th IHHA Conference, Rio de Janeiro, Brazil, pp. 41-50.

Steffens, D. M. (2005)."Identification and development of a model of railway track dynamic behaviour." Master of Engineering Thesis,School of Built Environment,Queensland University of Technology, Australia.

Timoshenko, S. and Goodier, J. N. (1951). Theory of Elasticity. McGraw-Hill book Company.

Zhai, W. and Cai, Z. (1997) "Dynamic interaction between a lumped mass vehicle and a discretely supported continuous rail track." Computers & Structures, 63, (5), pp. 987-997.

GROUND IMPROVEMENT TO MITIGATE EARTHQUAKE-INDUCED SOIL LIQUEFACTION HAZARDS

D. Wijewickreme[1]

1Professor of Civil Engineering, Department of Civil Engineering
University of British Columbia, Vancouver, Canada E-mail: dharmaw@civil.ubc.ca

ABSTRACT: Ground improvement is commonly used as a means to enhance the geotechnical engineering performance of structures under anticipated design loads. In essence, the objective is to increase the stiffness and/or strength properties of soil through ground improvement, and in turn, to resist the system loads while keeping the deformations within acceptable limits from a performance point of view. In addition to operational loads, permanent ground displacements and/or loss of bearing capacity due to earthquake-induced liquefaction are key geotechnical hazards to structures founded on loose saturated granular soils in seismically active areas. Typical methods of ground improvement against liquefaction-induced geotechnical hazards include: dynamic compaction, vibro-replacement using stone columns, compaction piling, preloading, blast densification, and compaction grouting. There is field evidence to suggest that ground improvement is effective in reducing seismic damage to facilities. A number of published geotechnical case histories involving ground improvement for mitigating liquefaction induced geotechnical hazards, originating from the Lower Mainland of British Columbia, Canada, which is located in a moderate to high seismic risk region, are reviewed. In particular, current approaches for the prediction of earthquake-induced ground deformations, considerations in governing the selection of suitable ground improvement methods, and applicability of such methods to address typical engineering situations are highlighted using the case histories.

1 INTRODUCTION

Enhancing geotechnical stiffness and strength properties is critical to controlling settlements and bearing capacity of structures founded or supported on soils. A variety of techniques evolved in the past few decades are commonly used for improving ground and, in turn, the properties of soils (Mitchell, 1981; JGS, 1998).

Some of the ground improvement measures are directly aimed at reducing the risk of soil liquefaction in seismically active areas. As noted by Youd and Perkins (1978), regions underlain by relatively young marine, deltaic, and alluvial soil deposits are considered to be susceptible to liquefaction and large ground movements when subjected to earthquake shaking. Liquefaction would trigger loss of shear strength and reduction in deformation modulus (stiffness) in soils. As such, earthquake-induced permanent ground displacements and/or loss of bearing capacity are some key geotechnical hazards to structures located at sites underlain by liquefiable soils (MCEER, 1999; O'Rourke and Hamada, 1992). The observed performance of sites following major earthquake events [e.g., 1964 Niigata (Japan), 1995 Hyogoken Nanbu (Kobe, Japan), 1999 Kocaeli (Turkey), 2001 Nisqually (Washington State, USA)] indicates that the sites with improved ground had generally less susceptibility to earthquake-induced permanent ground deformations and resulting damage than the sites that had not been densified (Mitchell et al., 1998; Hausler and Sitar, 2001; Hausler and Koelling, 2004). Typical ground improvement measures include dynamic deep compaction, vibro-replacement using stone columns, compaction piling, explosive compaction, and compaction grouting.

In general, there are four ways to consider in improving the seismic performance against an identified geotechnical hazard: (a) avoid the hazard by relocation; (b) isolate the structure from the hazard; (c) accommodate the hazard by strengthening the structure; and (d) reduce the hazard using ground improvement. Typically, all of the above options are considered in developing retrofit concepts. When ground improvement is considered as the desired option, the selection of the most suitable remedial option is governed by many factors including: soil conditions, equipment/space restrictions, issues related to the protection of existing structures during ground improvement, operational constraints, environmental regulatory requirements, and land availability.

In this paper, a number of published geotechnical case histories involving ground improvement for mitigating liquefaction induced geotechnical hazards, originating from the Lower Mainland of British Columbia (BC), Canada, which is located in a moderate to high seismic risk region, are reviewed. Considerations governing the selection of suitable ground improvement methods and applicability of such methods to address typical engineering situations are highlighted using these case histories. The paper draws particularly from publications of previous involvement by the author on ground improvement against earthquake-induced soil liquefaction and associated hazards (Wijewickreme et al. 2002; Wijewickreme et al. 2005; Wijewickreme and Atukorala, 2006).

2 BURIED GAS PIPELINE SITE

A case history on the seismic upgrading of a buried natural gas pipeline gate station site in Vancouver, BC, is presented in this section. The gate station is part of a major natural gas transmission system. Prevention of loss of pipeline pressure integrity under earthquake loading corresponding to an equivalent return period 2,000 years was used as the performance criterion for the acceptability of pipeline performance. Liquefaction-induced ground deformations were identified as significant hazards to the pipelines entering the gate station and associated facilities.

2.1 Site Description and Subsurface Soil Conditions

The gate station site is generally rectangular in plan (~100 m x 75 m) and located on the North Bank of the North Arm of the Fraser River (see Fig. 1) in Vancouver, BC, Canada. As illustrated, two transmission pipelines 20 in. and 24 in. diameter (i.e., NPS 20 and NPS 24 pipes) enter the gate station below the riverbed from the south. The site topography within the station compound and also in the east-west direction is generally flat. Prior to ground improvement, the river bank sloped down towards the south at slopes ranging 1H:1V to 3H:1V (horizontal: vertical) within the rip-rap area which extended to about 6 m below crest level. The riverbed below this level sloped southward at an average gradient of about 8% to the horizontal.

Fig. 2 presents the inferred soil stratigraphy at the site, developed based on a geotechnical field investigation. A combination of the methods of electric cone penetration testing (CPT), mud-rotary drilling, and solid-stem auger drilling was used in this investigation. The upper soils within the station consisted of about 2 to 3 m of loose to compact sand to sandy silt fill material. The upper fill materials in the northern part of the gate station were found to be underlain by a layer of very soft to soft silt (Liquid limit, LL = 38%; Plasticity

index, PI = 11%; Water content, w = 40%) extending to depths in the order of 6 to 8 m below the ground surface. The silt zone is underlain by a compact to dense sand stratum, which, in turn, was found to overlie a stratum of very dense sand and gravel at a depth of about 9 m below the ground surface. Within the southern shoreline of the gate station, the soils underlying the upper fill materials primarily consisted of loose to compact sand extending to depths of up to 12 m below the ground surface. Underlying these soils, compact to dense sand with some gravel was encountered. These strata are underlain by dense glacial till-like material that was encountered at a depth of about 14 m below the ground surface. CPT testing within the river adjacent to the site also indicates the presence of sandy soils, below a 2-m thickness of silt and clayey silt, and extending down to a depth of about 9 m below the riverbed. These materials are underlain by a compact to dense soil stratum. The groundwater level at the site was assessed to be located at depths of about 1 to 3 m below the ground surface at the site.

2.2 Geotechnical Performance under Earthquake Loading

The seismic response of the site was assessed using the one-dimensional wave propagation program SHAKE (Schnabel et al., 1972), and charts developed by Seed et al. (1985) were used to assess the liquefaction potential of the site soils. The results indicated that the loose to compact sands in the southern portion of the site would liquefy under the levels of seismic loading investigated. The loose sandy soils at the site extending to a depth of about 12 m was found to be potentially liquefiable (see Fig. 2). An earthquake magnitude of M7 (representing 10 to 15 cycles of loading) was used in the liquefaction assessment corresponding to the considered seismic hazard level.

The stability of the gate station under post-liquefaction condition was analysed, using both circular and non-circular failure surfaces, to investigate the potential for a flow slide condition at the site. The post-liquefaction shear strength parameters for potentially liquefiable zones were mainly selected based on a review of number of previously published results of laboratory post-cyclic monotonic simple shear test data. Potential slip zones with significant encroachment into the station compound (failure zones extending landwards about 30 m from the river bank) were computed to have a post-liquefaction factor of safety less than 1.0 even without application of any seismic inertia forces. This suggested a high risk of a flow slide as a result of earthquake shaking leading to very large deformations for the southern part of the site.

Ground displacement analyses were conducted using a number of methods available at the time to assess the magnitude and patterns of the relative ground movements in the area north of the predicted flow slide zone. In particular, the liquefaction-induced free-field ground displacements were calculated using the computer program developed by Houston et al. (1987), sliding block method by Newmark (1965), the empirical MLR method developed by Bartlett and Youd (1992), and a mechanistic finite element approach by Byrne et al. (1992).

The predictions from all analysis techniques indicated that, for the seismic loadings corresponding to all the risk levels considered in the study, large ground displacements (in excess of 3 m) towards the river would influence an area extending to about 30 m north from the crest of the river bank. The ground displacements for the non-liquefiable silty zones within the northern half of the site were computed to be less than about 0.1 m. Along with lateral ground movements, significant vertical ground movements were expected to

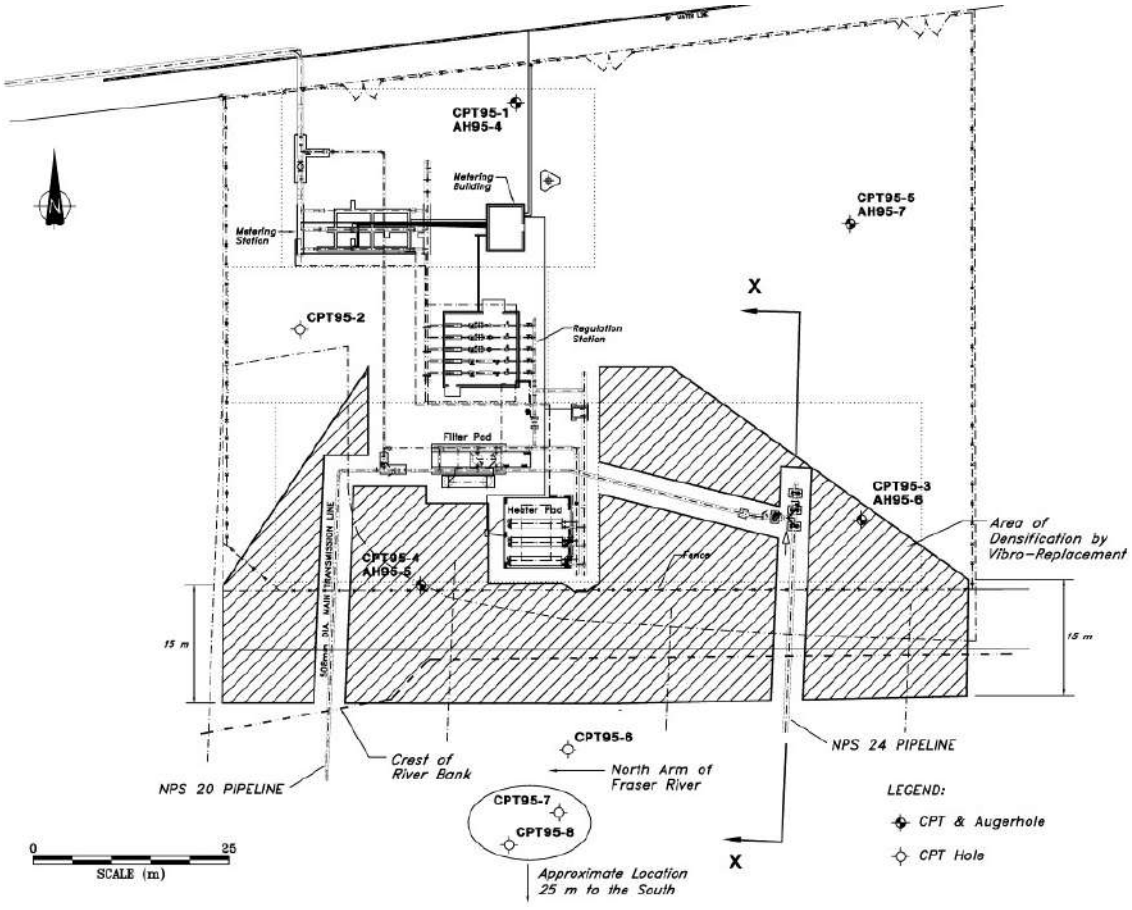

Fig. 1. Site plan showing existing structures, pipeline configurations, and geotechnical testhole locations.

occur within the southern area of the site.

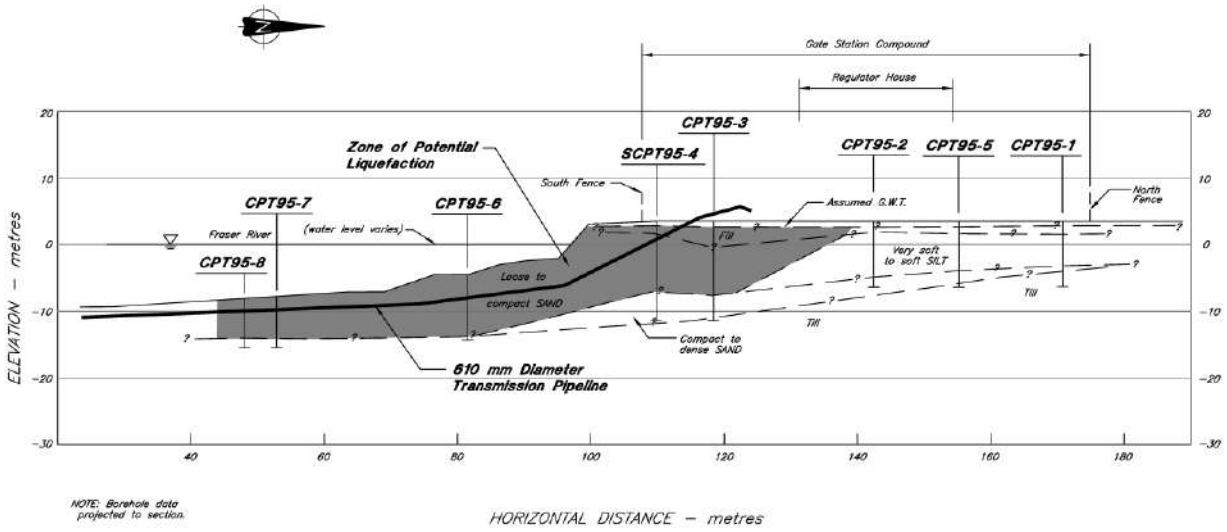

Fig. 2. Profile of soil stratigraphy, predicted zone of potential liquefaction, and alignment of 610 mm diameter pipeline.

Maximum computed ground deformations derived from the geotechnical analyses were compared with the computed pipe structural deformation capacities. The computed large ground displacements and resulting differential displacements at the gate station from earthquake-induced liquefaction were found to well exceed the estimated capacity of the pipelines; this, in turn, indicated that the risk of damage to the station piping under earthquake loading would be well above the acceptance criteria. The only remedial measures deemed practical for the gate station involved improving the ground conditions.

The effectiveness of ground improvement in reducing the liquefaction-induced ground displacements at the site was assessed again using slope stability and finite element analysis. The results indicated that the introduction of an in-ground densified barrier, likely in the order of 15 to 20 m wide, would reduce the expected large earthquake-induced ground movements in the vicinity of the gate station to a level below the tolerable ground deformation of the pipelines. In addition to the ground improvement, the shoreline slope was configured to a gentler slope to improve the riverbank slope stability.

2.3 Ground Improvement Using Vibro-replacement

The selection of the most suitable ground improvement technique was governed by several factors such as soil conditions, equipment space restrictions, pipeline protection issues, environmental regulatory requirements, land availability etc. Based on an evaluation of these considerations, the method of vibro-replacement was considered to be the most suitable technique of ground densification for use at the gate station site.

Two hundred and seventy three (273) stone columns were installed (using the method of vibro-replacement) in a triangular pattern at 3 m centre-to-centre spacing to cover the plan area shown in Fig. 1 to improve the overburden soils. A poker type V-23 vibrator with a rated energy of 165 hp was used to install the stone columns using the top feed method (see Fig. 3). All stone columns extended to the top of the underlying hard stratum to depths between 8 and 16 m below the existing ground surface, with an average depth of about 14 m. The average amperage output during construction of individual stone columns was about 150 A, with peak outputs ranging from 170 to 260 A. Boulders, concrete and timber obstructions were encountered during column installation at some locations, generally at depths of some 3 to 6 m below the existing ground surface preventing the installation of some 20 stone columns. Of these locations, some columns were successfully installed at alternate locations by relocating within 1.5 m of the design location. In general, attempts were made to relocate stone columns rather than locally excavating the obstruction.

Field verification testing was performed at selected centroids of the stone column pattern using CPT testing during the progress of densification. The results of the post-densification testing together with review of the stone column installation details indicated that the cone tip resistance (Qt) values generally exceeded pre-specified performance Qt criteria (ranged between 100 and 125 bars for clean sand zones). Some of the initial CPTs, carried out within about 14

Fig. 3. Poker type V-23 vibrator (photo taken just before insertion at the stone-column location with water jets started).

days from the time of stone column installation, indicated that the specified Q_t requirement was not satisfied in certain zones of silty

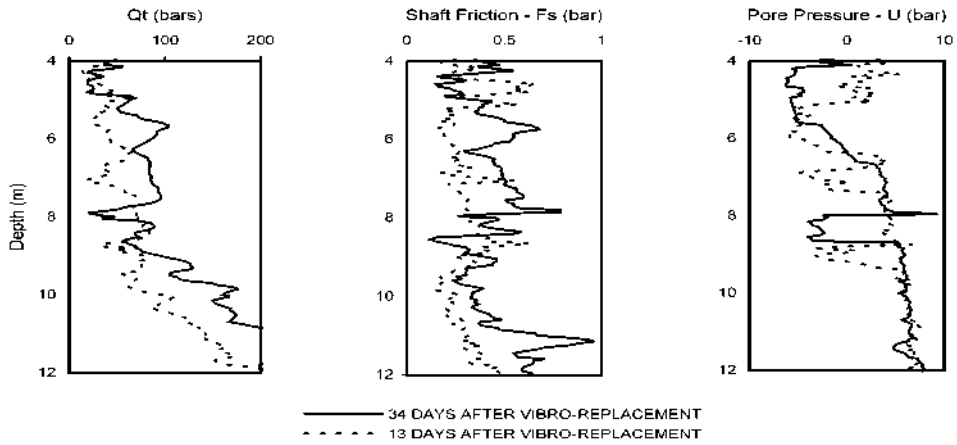

Fig. 4. Results of post-densification electric cone penetration tests at the centroid of adjacent stone column triangular patterns (comparison between results from tests conducted 13 and 34 days after installation).

fine sand (Note: Qt requirements were corrected the for silt content); however, repeat testing carried out in the same area after about five weeks from the installation of the stone columns indicated that the Qt values had increased significantly from the initial post-densification values, and met the specified criteria for silty sands (see Fig. 4).

3 HIGHWAY BRIDGE CROSSING SITE

This case history describes some of the retrofit work adopted to enhance the seismic performance of the foundation soils of a major 1.3 km long, 6-lane bridge on a highway in Vancouver, BC. The primary focus was to minimize the risk of bridge collapse following the design earthquake corresponding to a seismic event having an annual probability of exceedance of 1/475 (or a return period of 475 years). The site-specific ground motions were characterized by a uniform hazard firm-ground response spectrum with a peak horizontal ground acceleration of 0.20 g and a design earthquake of magnitude M7. In order to achieve the project requirements, a displacement-based design approach was used, and, in turn, ground improvement was designed to limit ground deformations at locations that are identified as critical.

3.1 Site Description and Subsurface Soil Conditions

The north side of the bridge is underlain by coarse granular soils (i.e., primarily sand and gravel) arising from an alluvial fan of a river stream deposit (see Fig. 5). Due to the coarse nature of site soils, a number of different techniques were utilized to characterize the subsurface soils. These included conventional drilling with rotary methods, Becker Penetration percussion testing with energy measurements, downhole shear wave velocity testing, seismic refraction profiling, and Sonic drilling (http://www.prosoniccorp.com) and sampling.

Becker Penetration Testing (BPT) consists of driving a closed-toe steel pipe that is 169 mm (6.65 in) in diameter using an ICE 180 diesel hammer that delivers 11 kN-m of rated maximum energy per blow. The number of blows required to drive the steel pipe are recorded over penetration increments of 0.3 m and these blow counts along with hammer energy levels were later converted to equivalent Standard Penetration Test (SPT) blow counts following the procedures outlined by Harder and Seed (1986). The conventional SPT sampler, due its relatively smaller diameter [50 mm (2 in.) outer diameter], could give rise to unrealistically high penetration resistance values in coarse granular soils. Therefore, BPT with a relatively larger diameter penetrating tool is often adopted in the characterization of coarse-grained soils.

The presence of low permeability layers of soil within the generally coarse-grained overburden soils was considered a concern, and this

coarse-grained overburden soils was considered a concern, and this

Fig. 5. Bridge site – the alluvial fan can be seen on the left (i.e., north abutment).

aspect was investigated using the method of Sonic drilling, where continuous samples of soils were obtained that provided information on soil stratification. This was considered important since low permeability soil layers can potentially lead to severe post-liquefaction behaviour. Based on ground response analyses, the foundation soils were identified as having a high risk of liquefaction under the design earthquake ground shaking. The analytical results indicated that soil liquefaction may extend to depths varying from 15 to 20 m below the existing ground surface.

3.2 Design of Ground Densification Configurations

Rigorous ground response analyses were undertaken to optimize the ground densification requirements taking into consideration the displacements that can be tolerated by the bridge foundations. In particular, free-field ground response analyses as well as soil-structure interaction analyses were undertaken to assess the bridge foundation performance under the 475-year ground motions using the computer code FLAC (Version 3.4, 1998). A cyclic stress-strain model that was capable of simulating sequential liquefaction in accord with the commonly used liquefaction resistance chart (Seed et al. 1985;

Youd et al. 2001) was used in the analysis of ground deformations. The results were compared with empirical methods of estimating ground deformations and were in good agreement. For most of the critical foundations, liquefaction was not predicted below the pile foundations, and the main geotechnical hazard was noted to arise from liquefaction-induced lateral spreading. A ground improvement program involving the construction of in-ground densified zones (barriers) at selected critical locations along the bridge alignment was assessed to be sufficient to reduce the lateral displacements to acceptable levels.

3.3 Ground Improvement Program

Ground improvement using vibro-replacement was selected as the most cost-effective method of treatment in areas where the available headroom was sufficient for the use of construction equipment. The proximity of the work to existing settlement sensitive bridge foundations, depth of treatment required, available headroom beneath bridge deck, and cost of treatment were critical factors in making this decision. Since ground improvement was required mostly in over-water areas, the stone columns were constructed using the bottom-feed, "wet" method of construction. The amperage build-up and depth of probe penetration were monitored during stone column construction. The contractor elected to install the stone columns using a square grid pattern at a centre-to-centre spacing of 3 m. A total of 365 stone columns were installed. Robust equipment that can sustain amperage readings as high as 300 A for longer durations in the order of 10 to 30 seconds were required for this site with highly coarse-grained soils.

The post-improvement testing was carried out using the Becker Hammer. An HAV-180 rig with 169 mm (6 5/8th inch) casing was utilized for all post-improvement verification testing. Bounce chamber pressure was measured with depth of probe penetration in order to obtain necessary parameters for the inference of equivalent SPT (N1)60 values. Typical post-improvement penetration resistance measurements obtained at the centroid of the vibro-columns are shown in Fig. 6. The results indicated that the stone column spacing and procedure were more than adequate to achieve the target SPT penetration resistance specified.

4 FOUNDATIONS AT AN INDUSTRIAL PLANT

The ground improvement work undertaken in the preparation of foundations for a kiln line and two large-diameter material storage silos (i.e., clinker silo and cement silo) at a major cement plant are presented herein. The peak horizontal firm-ground acceleration for the site was estimated to be 0.22g for the design seismic risk level corresponding to a 475-year return period. Foundation systems involved a combination of ground treatments including: piling, replacement of weak soils, and densification of liquefiable soils.

4.1 Site Description and Subsurface Soil Conditions

The site area is flat, and it is located on the river bank of a major river, and the plan locations of the two silos in relation to the existing plant layout are identified in Fig. 7. The general soil conditions at the site comprise soft/loose deltaic soils that are susceptible to liquefaction. They can be described in terms of four main stratigraphic units. The upper unit comprises granular river sand fills in the order of 3 m in thickness. Underlying the fills is a deltaic deposit comprising interlayered fine sandy silts, silty sands, and clayey silts extending to depths ranging from 4.0 m to 6.5 m below the ground surface. Based on the geotechnical test data, these deposits were considered to be loose to compact and/or soft to firm. Underlying the deltaic soils, river sand deposit with occasional loose silt/silty sand layering was encountered. The measured cone penetration resistance indicated that the sand deposit within about the upper 15-20 m is in a loose to compact condition whereas the sands beneath this depth level, generally, are inferred to be in a compact to dense state. The river sand extends to a depth of about 30 to 35 m below the ground surface. A thick compressible marine deposit comprising inter-layered sands, silty sands, sandy silts, and occasional layers of clayey silt exists below. The marine deposit is inferred to extend to a depth in the order of 250 m below the ground surface, below which very dense Pleistocene sediments (glacial till or drift) are expected to be encountered. The ground water level was inferred to be about 3 m below the ground surface on an

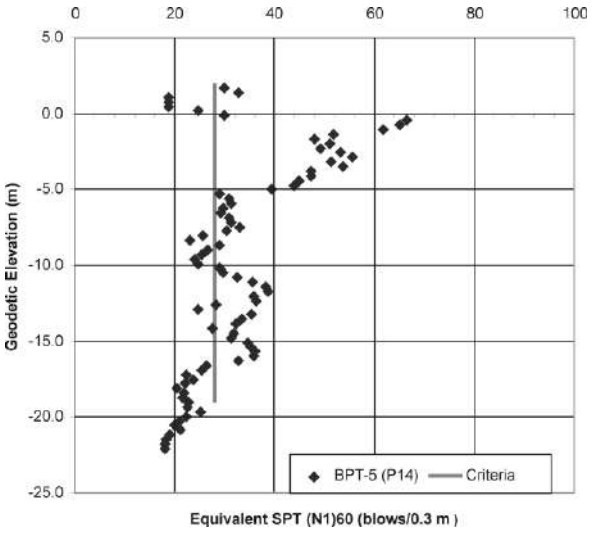

Fig. 6. Typical post-improvement penetration resistance profile compared with specification for required densification.

average basis, although the groundwater level at the site is expected to vary with the seasonal precipitation as well as the tidal variations of the nearby river.

4.2 Clinker Silo

The clinker silo was built east of an existing silo foundation (i.e., called B-silos) as shown in Fig. 7. The clinker silo has a diameter of 45 m and the foundation had to be designed to support an average maximum bearing pressure of 500 kPa under static loading conditions. Ground response analysis indicated that a soil zone extending to a depth of about 18 m below the ground surface at the clinker silo location is potentially liquefiable under the design seismic loading. Total vertical ground settlements up to 350 mm due to the dissipation of excess pore pressures, and lateral ground displacements in the order of 0.5 m were predicted under design earthquake loading. Bearing capacity requirements under both static and seismic loading could be best satisfied if ground improvement measures were undertaken and the silo was then founded within the improved alluvial deposits. Various foundation options including timber, concrete, and steel piling as well as shallow foundation options with ground improvement, were considered. With the piling alternative, a pattern of closely spaced lower capacity piles were needed to achieve the required densification. If piles were to be used, it was also noted that there might be a requirement for installation of vertical drains to relieve excess pore water pressures under earthquake loading.

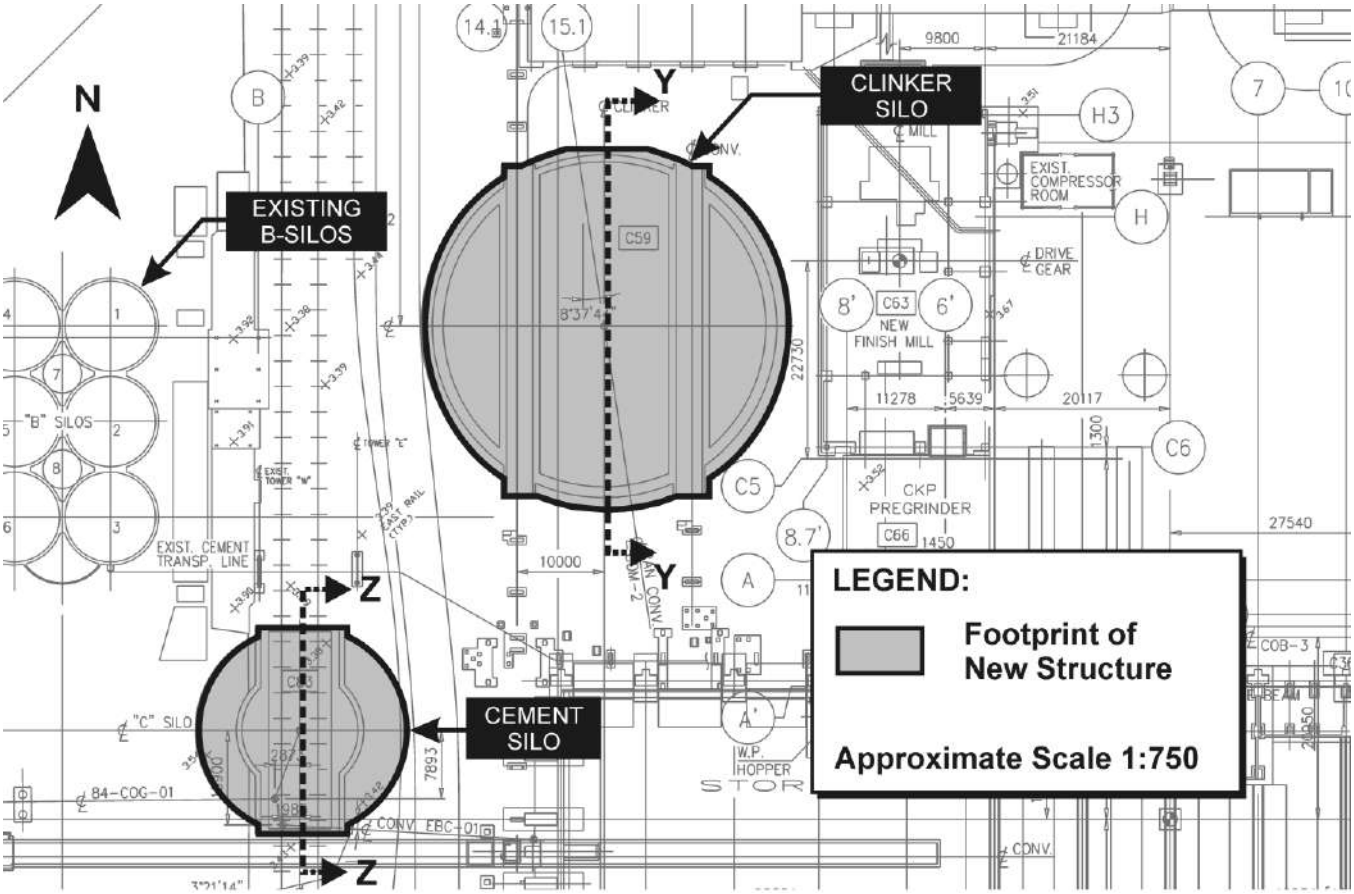

Fig. 7. Plan layout of structures

Ground improvement using vibro-replacement was selected as the most suitable option, because drainage is also improved with this technique. It was determined that the upper deltaic deposits, however, could not be effectively treated using the method of vibro-replacement. As such, the silty soils within the stress influence zone of the structure (extending about 2 m beyond the foundation perimeter to a depth of about 5 m below the foundation level) were sub-excavated prior to performing ground densification. Because of the relatively shallow groundwater level, the excavation work was performed with dewatering. The excavation was backfilled using locally available relatively coarse clean sand. Vibro-replacement was then undertaken to treat a zone extending horizontally about 10 m beyond the perimeter of the clinker silo foundation and also extending vertically down to a depth of 18 m below the existing ground surface as shown in Figure 8. The vibro-replacement would not densify the upper portion of the sand fill due to lack of confinement and groundwater. As such, about 1 m of the sand fill was removed upon completion of vibro replacement work, and the excavation base was raised to the design slab underside elevation using 75 minus well-graded crushed rockfill compacted to 100% of standard Proctor maximum dry density. The 1.5-m thick raft for the clinker silo was founded on the compacted rockfill as prepared above (see Fig. 8 for a schematic cross-section).

4.3 Cement Silo

The cement silo was constructed immediately south west of the new clinker silo (see Fig. 7). The silo was constructed on a relatively stiff circular raft foundation 25 m in diameter, to withstand a design average maximum bearing pressure of 300 kPa under static loading conditions. The underside of the raft foundation was located at a depth of about 3 m below the ground surface.

The soil conditions at the cement silo are similar to those at the clinker silo with the estimated potentially liquefiable soil zone

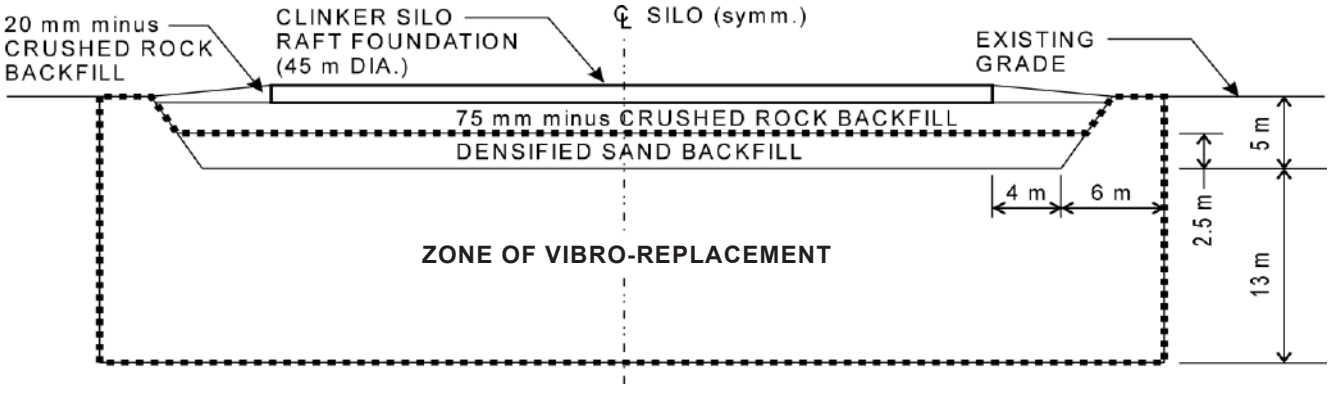

Fig. 8. Foundation system: clinker silo – Section Y-Y (see Fig. 6-1 for section location).

extending to a depth of about 20 m below the ground surface. Unlike at the clinker silo, partial excavation of the weak upper silty soils and support of the raft on a densified subgrade was not considered feasible for the cement silo foundation due to the close proximity of adjacent existing facilities as well as the need to resist potential uplift foundation loads from the silo. For this reason, it was decided that the cement silo raft would be supported on piles. Two alternative options were considered: (a) install piles into the compact to dense alluvial soils at depths below 21 m; (b) install relatively short piles 10 to 12 m, with densification of the loose subsoils below the pile tip levels to a depth of 21 m prior to pile driving (see Zone 'A' in Fig. 9). In both options, the piles would be installed at a relatively close spacing so that the looser soils between the piles would be compacted, and an annular zone of ground treatment around the foundation footprint would be undertaken to mitigate effects of liquefaction (similar to the circumferential ground treatment at the clinker silo). Option (b) was identified as the more cost-effective and preferred design.

It was determined that the critical lateral loading for the cement silo would occur under earthquake shaking conditions. The response of the silo foundation under lateral loading was analysed accounting for both soil-pile and pile group interaction effects to provide necessary input for final structural design. It was specified in the construction contract that the lower Zone 'A' shown in Fig. 9 be densified with suitable provisions to facilitate subsequent installation of expanded-base piles through the upper Zone 'B' (i.e., the Zone 'A' to be treated without excessively densifying the upper Zone 'B'). A total of 123 expanded-base piles with shaft diameter of 508 mm and with a design compression capacity of 1070 kN/pile were specified. The annular zone of soil within 10 m outside the footprint of the foundation extending to a depth of 21 m below the existing ground surface was densified using vibro-replacement (see Fig. 9, Zone 'C').

After installing some 30 expanded-base piles, it was determined that the construction progress was slower than anticipated; this appeared to be a result of not carefully limiting the densification of the upper Zone 'B' during the densification of the lower Zone 'A' prior to the pile installation process. Because of this difficulty, the contractor proposed the installation of 508 mm diameter (open-ended) steel piles instead of the specified expanded-base piles. This alternative steel pile option was accepted (by the design team and the owner) subject to contractor achieving the required vertical capacity and lateral fixity as per original design. As a result, the remaining 90 pile locations for the cement silo foundation was completed using steel pipe piles; pile driving analyser (PDA) testing was conducted on selected piles to confirm the axial capacities achieved.

4.4 Kiln Line

The new kiln line was to be constructed immediately north of an existing kiln line located immediately north of clinker silo. The new kiln line comprises several units: raw grinding mill, homogenizing silo, pre-heater/coal mill, kiln piers, and cooler. The most prominent feature of the kiln line is the pre-heater tower that has a height in the order of 115 m.

These structures are linearly aligned from east to west extending over a distance of about 150 m. The kiln pier No. 2, pre-heater, and homogenizing silo was constructed on a pile-supported raft foundation (~ 38 m x 70 m), and the cooler building and the kiln pier No. 1 was supported on a similar but separate raft foundation (~ 23 m x 55m). The underside of the rafts was located at a depth of 2.7 m below the ground surface. The raw grinding mill and its building were supported on separate pile foundations, with the building pile caps, at column locations, tied together by grade beams and a suspended-grade slab. The design bearing pressures for each foundation footprint is summarized in Table 1.

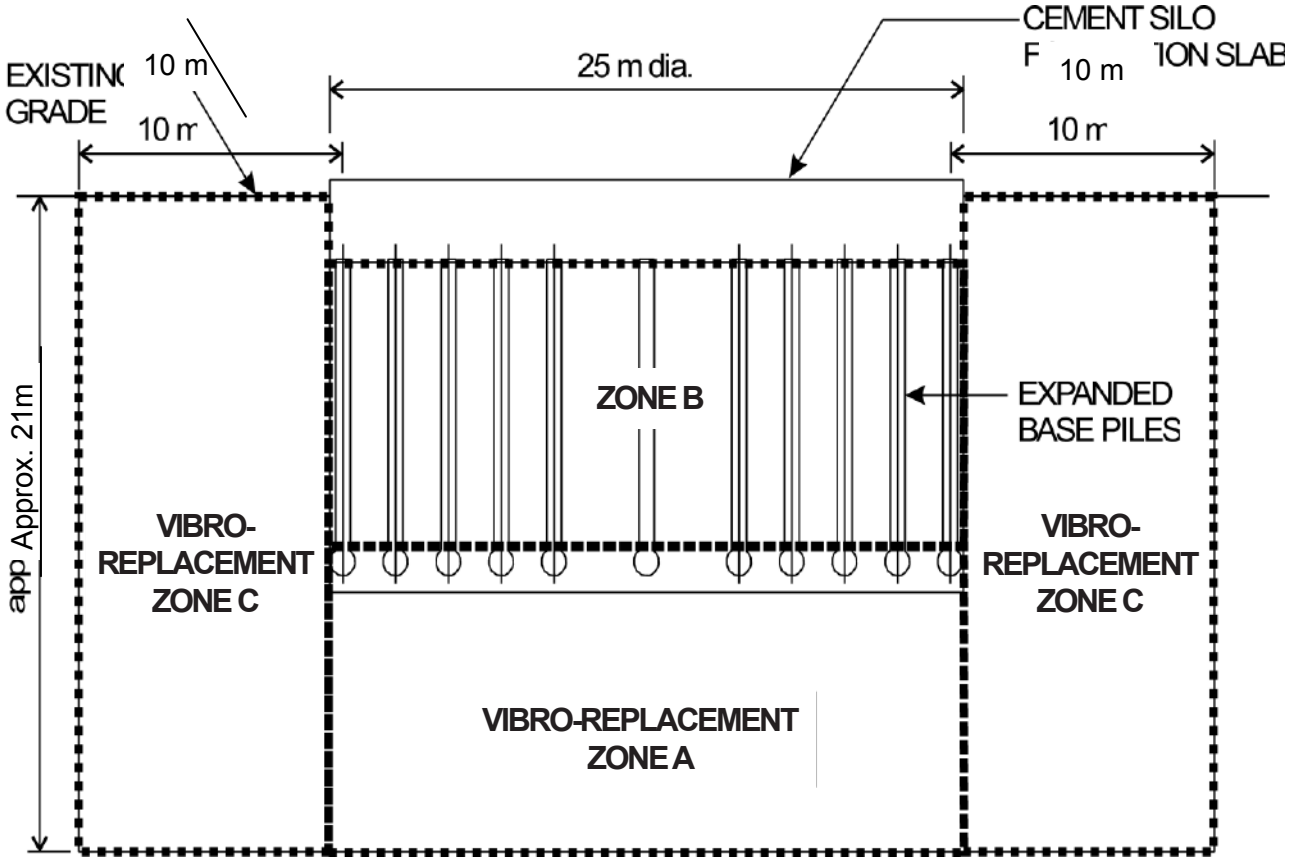

Fig. 9. Foundation system - cement silo – Section Z--Z (see Fig. 6-1 for section location).

Table 1. Foundation details - Kiln Line

Kiln Line Structure	Gross Bearing Pressure (kPa)
Cooler	80
Kiln Pier # 1	280
Kiln Pier # 2	280
Pre-heater/Coal Mill	115
Homo Silo	240
Raw Mill	65

It was identified that the performance of the kiln line is sensitive to post-construction settlements, especially differential settlements between adjacent foundations and across the larger foundations. The allowable differential settlements are quite limited because of the requirement for strict tolerances on tilt. In addition to the expected settlements within the upper soil strata, settlements due to the compressibility of the deep marine deposit (located below ~30 m depth) were also a key consideration. The anticipated lateral loadings from wind and earthquake shaking on the tall pre-heater tower were the other critical concerns.

In consideration of the sensitivities to differential settlements and the lateral loadings, it was concluded that it would be prudent to support all the kiln line structures on piled foundations. Expanded-base cast-in-place concrete piles or closed-end steel pipe piles were considered most suitable for the support of the kiln line structures. It was noted that the existing kiln line at the plant is also supported on expanded-base piles; because of this valuable site-specific experience combined with the assessed advantage in terms of potential cost savings, the use of expanded-base piles were selected over the steel pile option. It was estimated that an allowable vertical geotechnical load capacity of up to 1070 kN per pile could be allowed on a 508-mm shaft diameter expanded-base pile installed with its base at a depth of about 10 to 12 m below the existing ground surface.

Based on these design considerations, the kiln line foundations were supported using over 600 expanded-base piles (shaft diameter varying from 406 mm to 559 mm) with centre-to-centre horizontal pile spacing varying from 2.0 m to 2.6 m. Pile spacing was chosen to avoid significant reduction in pile group efficiency, and to minimize the risk of damage to adjacent piles during installation.

A pile-supported system for the kiln line essentially eliminated the settlement concerns arising from the upper layers. However, it was recognized that settlements, below the pile tips, within the occasional looser zones of the alluvial deposits would still be a concern. Since these looser zones within the alluvial deposits would not be far below the piled zone, it was considered that any settlements arising within these zones could potentially translate into differential settlements along the kiln line. In consideration of this, preloading of the site, up to heights in the order of 6 m, was recommended, and this work was undertaken to remove at least a portion of the post-construction differential settlements due to local variations in soil conditions.

It was accepted that below-ground slabs and walls, pile caps, as well as piles would provide the required passive soil resistance against lateral loads primarily arising due to wind and earthquake loading. It was noted that liquefaction-induced horizontal ground displacements are the key controlling parameter in terms of lateral load performance of the foundation. Seismic ground response analyses indicated that the loose Fraser River sands, within the upper 10 to 12 m, (i.e. approximately above the pile base levels) have a high risk of liquefaction and it would lead to "free-field" lateral ground movements in the order of 0.5 m. Detailed soil-pile interaction analyses indicated that expanded-base piles would be subjected to unacceptably large bending moments under these ground displacements. Reduction of the potential for lateral ground displacements was considered essential, and installation of ground improvement barriers around the footprint of the kiln line was judged to be the most effective form of achieving this objective. As a result, ground improvement using vibro-replacement (installation of stone columns) was undertaken immediately outside the foundation footprints extending over a horizontal distance of 6 m and to a depth of about 12 m below the ground surface (see Figure

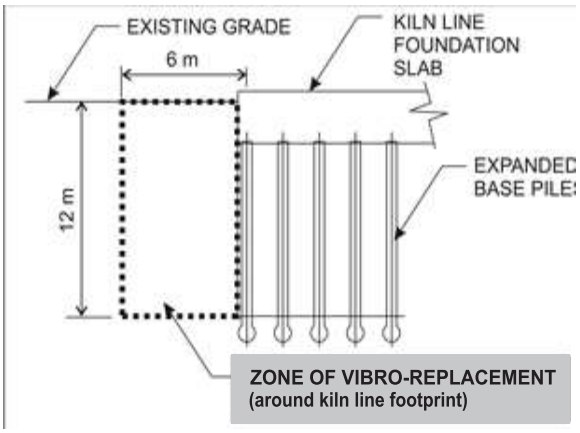

Fig.10. Foundation system – kiln line

5 CONCLUSIONS

Liquefaction is one of the main causes of geotechnical hazards to facilities located in seismically active regions. The options to improve the seismic performance of a given structure against liquefaction-induced geotechnical hazard are: (a) relocate to avoid the hazard; (b) isolate from the hazard; (c) tolerate the hazard (by strengthening); and (d) eliminate the hazard (using ground improvement). With respect to the elimination of the hazard, ground improvement is emerging as one of the widely adopted mitigative measures to minimize the risk of liquefaction. Commonly used ground improvement measures include dynamic compaction, vibro-replacement using stone columns, compaction piling, blast densification, and compaction grouting.

Using a number of case histories from the Greater Vancouver Region of British Columbia, Canada, which is located in a moderate to high seismic risk region, several engineering considerations in relation to ground improvement to mitigate liquefaction-induced geotechnical hazards are illustrated. The case histories correspond to ground improvement carried out using vibro-replacement, preloading, piling, and combinations of one or more of the above methods. The protected foundations and/or structures belong to key industrial plants, highways, and pipeline systems. Some of the key observations/findings are as follows:

1. In seismic mitigation works, the design philosophy revolves around displacement-based design.

2. The ground improvement configurations commonly used in practice include: (i) in-ground densified barrier(s) aligned perpendicular to the direction of ground movement; (ii) densification of wide-area footprints beneath and/or around foundation footprints to improve bearing capacity failures and the impacts from lateral spreading.

3. The selection of the most suitable ground improvement option is governed by many factors including: soil conditions, equipment/space restrictions, issues related to the protection of existing structures during ground improvement, operational constraints, environmental regulatory requirements, and land availability.

4. The method of vibro-replacement using stone columns can be effectively used to densify coarse-grained soils within about 25 m below existing ground level. The method has also become attractive because of the potential availability of drainage through stone columns for the dissipation of excess pore water pressures in addition to the densification effect.

5. Heavily-loaded structures can be founded on compressible deposits by careful selection of site treatments such as preloading, piling, and vibro-replacement. In addition to reducing the compressibility of soils, such treatments can be used to effectively reduce the liquefaction susceptibility of upper loose soils under seismic loading. .

6 ACKNOWLEDGEMENTS

The author is grateful to the BC Ministry of Transportation, Terasen Gas Utility Ltd., Lafarge Canada Inc., and Golder Associates Ltd. for granting permission to publish the technical information associated with the case histories. The author's involvement in the projects presented herein took place during his tenure at Golder Associates Ltd. between 1990 and 2000. The important contributions to the engineering projects cited herein made by the author's former colleagues Mr. Trevor Fitzell, P.Eng. and Dr. Upul Atukorala, P.Eng. of Golder Associates Ltd., as project team members, are respectfully acknowledged.

7 REFERENCES

Bartlett, S.F. & Youd, T.L. (1992). Empirical analysis of horizontal ground displacement generated by liquefaction-induced lateral spreads. Technical Report NCEER-92-0021, National Center for Earthquake Engineering Research, State University of New York, Buffalo, N.Y.

Byrne, P.M., Jitno, H. & Salgado, F. (1992). Earthquake induced displacements of soil-structures systems. Proceedings 10th World Conference, Earthquake Engineering, 19-24 July. Madrid, Spain, A.A. Balkema, Rotterdam, pp. 1407-1411.

FLAC. (1998). Fast Lagrangian Análysis of Continua. Itasca Consulting, Ithaca, Minnesota, USA.

Harder, L.S. & Seed, H.B. (1986). Determination of penetration resistance for coarse-grained soils using the Becker hammer drill. Earthquake Engineering Research Center Report No. UCB/EERC-86/06, University of California, Berkeley, California, U.S.A.

Hausler, E.A. & Koelling, M. (2004). Performance of improved ground during the 2001 Nisqually Earthquake. Proceedings of the 5th International Conference on Case Histories in Geotechnical Engineering, Paper No 3.27.

Hausler, E.A. & Sitar, N. (2001). Performance of soil improvement techniques in earthquakes. Proceedings of the 4th International Conference on Recent Advances in Geotechnical Earthquake Engineering and Soil Dynamics, Paper No. 10.15.

Houston, S. L., Houston, W. N. & Padilla J. M. (1987). Microcomputer-aided evaluation of earthquake induced permanent slope displacements. Microcomputers in Civil Engineering 2, Elsevier Science Publishing Co. pp. 207-222.

Japanese Geotechnical Society (eds.). (1998). Remedial measures against soil liquefaction: From investigation and design to implementation, A.A. Balkema, Rotterdam.

MCEER. (1999). Proceedings of the Seventh U.S.-Japan Workshop on Earthquake Resistant Design of Lifeline Facilities and Countermeasures for Soil Liquefaction, San Francisco, California, Technical Report MCEER-99-0019, Multidisciplinary Center for Earthquake Engineering Research, State University of New York, Buffalo, N.Y.

Mitchell, J.K. (1981). Soil improvement - State-of-the art report. Proceedings of the 10th International Conference on Soil Mechanics and Foundation Engineering, Stockholm, Vol. 4, pp. 509-565.

Mitchell, J.K., Cooke, H.G. & Schaeffer, J.A. (1998). Design considerations in ground improvement for seismic risk mitigation. Geotechnical Special Publication No. 75, Geotechnical Earthquake Engineering and Soil Dynamics III, Specialty Conference, American Society of Civil Engineers, pp. 580-613.

Newmark, N.M. (1965). Effects of earthquake on dams and embankments - Rankine Lecture. Gĕotechnique, Vol. 15, No. 2, pp. 139-160.

O'Rourke, T.D. & Hamada, M.(eds.). (1992). Case studies of liquefaction and lifelines performance during past earthquakes: United States case studies. Technical Report NCEER-92-0002, Vol. 2, National Centre for Earthquake Engineering Research, State University of New York, Buffalo, N.Y.

Schnabel, P.B., Lysmer, J. & Seed, H.B. (1972). SHAKE: A computer program for earthquake response analysis of horizontally layered sites. University of California, Berkeley, California, Earthquake Engineering Research Center, Report No. EERC 72-12.

Seed, H.B., Tokimatsu, K., Harder, L.F. & Chung, R.M. (1985). The influence of SPT procedures in soil liquefaction resistance evaluations. J. Geotech. Eng., ASCE, Vol. 111, No. 12, pp. 1425-1445.

Wijewickreme, D., Fitzell, T.P. & Smith, D. (2002). Foundation Systems for the Modernization of Lafarge Canada Richmond Cement Plant - Geotechnical Engineering Considerations, Proc. 55th Canadian Geotechnical Conference, Niagara Falls, Ontario, October 2002, Paper No. G131.

Wijewickreme, D., Honegger, D.G., Mitchell, A., & Fitzell, T.P. (2005). Seismic Vulnerability Assessment and Retrofit of a Major Natural Gas Transmission System: A Case History, Earthquake Spectra, Journal of the Earthquake Engineering Research Institute (EERI), Vol. 21, No. 2: 539-567.

Wijewickreme, D. & Atukorala, U. (2006). Ground Improvement For Mitigating Liquefaction-Induced Geotechnical Hazards, Eds. B. Indraratna & C. Jian, Elsevier Publishers (UK) (43 pages).

Youd, T.L. & Perkins, D.M. (1978). Mapping of liquefaction severity index. J. Geotech. Eng., ASCE, Vol. 113, No. 11, pp. 1374-1392.

Youd, T.L., Idriss, I. M., Andrus, R. D., Arango, I., Castro, G., Christian, J.T., Dobry, R., Finn, W.D.L., Harder Jr., L.F., Hynes, M.E., Ishihara, K., Koester, J.P., Liao, S.S.C, Marcuson III, W.F., Martin, G.R., Mitchell, J.K., Moriwaki, Y., Power, M.S., Robertson, P.K., Seed, R.B., & Stokoe II, K.H. (2001). Liquefaction Resistance of Soils: Summary Report from the 1996 NCEER and 1998 NCEER/NSF Workshops on Evaluation of Liquefaction Resistance of Soils, J. Geotech. Geoenvir. Eng., ASCE, Vol. 127, No. 10, pp. 817-833.

PERFORMANCE OF HIGHWAY EMBANKMENTS CONSTRUCTED OVER SRI LANKAN PEATY SOILS

W. A. Karunawardena[1] and M. Toki[2]

1 Director General, National Building Research Organization, Sri Lanka and Senior Geotechnical Engineer, Southern Transport Development Project , Oriental Consultants Co., Ltd., Japan

2 Team Leader, Southern Transport Development Project, Oriental Consultants Co., Ltd., Japan

ABSTRACT: The construction of the Southern Expressway in Sri Lanka involved extensive ground improvement work as many parts of the Expressway traverses through flood plains and marshy ground consisting of very soft peat, organic soils, and clays. Depending on the ground conditions, various ground improvement methods including remove and replacement, preloading, preloading with vertical drains, dynamic compaction and vacuum consolidation were applied to improve the soft soil to build the embankments with heights varying from 2 m to 12 m. In this project, embankments of about 4 km in length were constructed by improving the peaty soil basically by the application of the heavy tamping method. The length of the embankments that were built by improving the peaty soil by vacuum assisted surcharging is around 2.5 km. The details of the field instrumentation program and field monitoring program to assess the soft ground improvement are presented. The performance of the ground improvement was evaluated in terms of the degree of consolidation, improvement of the physical and engineering properties, and increase in preconsolidation pressure and gain in shear strength of the peaty soil. The results of the post construction surface settlement monitoring of the expressway carried out up to date reconfirm that the ground improvement work was very successful and the expected residual settlements are well below the allowable limit of the contract.

1 INTRODUCTION

The Southern Highway is Sri Lanka's first E Class highway that links the Sri Lankan capital Colombo with Matara, a major city in the south of the island as shown in Figure 1. The length of 96 km section from Colombo to Galle had been completed and opened to traffic in November 2011. Many parts of the highway traverse through flood plains and marshy ground consisting of very soft peat, organic soils, and clays. Especially, in the major flood plain of Welipenna River, Bentota River and Gingaga River areas, thick peat and organic clay deposits were found. These problematic soils have low shear strength, high compressibility and low bearing capacity, and therefore it needs to be improved to avoid excessive settlement and prevent stability failure during expressway embankment construction. Also, these peaty soils posses high creep settlements and therefore it is necessary to improve the soft ground to control the post construction settlements (Karunawardena 2007). Many ground improvement methods have been used on soft soil to improve its bearing capacity and to minimize the anticipated settlement in this section of Southern Expressway Project. Ground improvement methods such as surcharging, surcharging with pre-fabricated vertical drains, rock replacement, heavy tamping, vacuum consolidation and piled embankment have been used to improve the soft soil in order to control the post construction settlements and to ensure the stability of the highway embankment.

This paper presents the ground improvement methods applied in a section of the Southern Expressway between Ch.0+000 km to Ch.66+160 km to improve the peaty soil, with some background information on the design methodology. In the first 34 km of the highway, about 50% of the area is covered by soft ground and from 34 km to 66 km, the distance covered by the soft ground is around 12 km. In this project, embankments of about 4 km in length were constructed by improving the peaty soil basically by the application of heavy tamping method. The length of the embankments that were built by improving the peaty soil by vacuum assisted surcharging was around 2.5 km. The problems encountered during ground improvement work and embankment construction and the solutions given for the same are highlighted and discussed. The details of the laboratory and field investigations carried out before and after ground improvement, field instrumentation program and field monitoring program that was carried out during and after construction of highway embankment to assess the soft ground improvement are presented.

Figure 1. Location map of the Southern Expressway

2 DETAILS OF THE SUBSOIL PROFILE

Many geotechnical investigations have been carried out since the inception of the project in order to assess the condition of the soft ground. At the preliminary stage, to provide information to bidders and to facilitate initial designs, boreholes were carried out at 500 m intervals. After commencement, boreholes were carried out at about every 50 m interval in order to provide the necessary information for the detailed design.

Site investigation consisted of bore holes with Standard Penetration Test (SPT), hand augering, Cone Penetration Test with pore pressure measurement (CPTu) as in-situ testing and a series of laboratory testing such as index property tests, unconsolidated undrained triaxial compression tests and conventional consolidation tests.

The investigation identified that the soft ground area of the highway

mainly consisted of peat, organic clay, alluvial clay and loose sand deposits. The distribution of soft soil deposits along the highway trace from Kottawa to Kurundugahahetekma is shown in Figure 2.

Silty clay and silty sand were found as top soil in most of the lowland areas up to a depth of 1.5 m to 3.0 m. This was followed by sand to lateritic soil and the thickness of the layers varied from 1 m to 5 m.

In the flood plains of Panape, Kalu Ganga, Welipenna and Bentota river areas sub soil consisting of mainly peat, organic clay, very soft inorganic clay and silt layers was found. The total average thickness of the compressible layer was in the range of 4 m to 11 m. In some areas loose silty sand layers were present under the above compressible layers. In the valley areas between hillocks, instead of cohesive inorganic clays, very loose to loose silt and sand were found ranging from 0.5 m to 4m thickness. The details of the Geotechnical properties of the subsoil have been given by Karunawardena and Nithiwana (2009) and Karunawardena and Toki (2011).

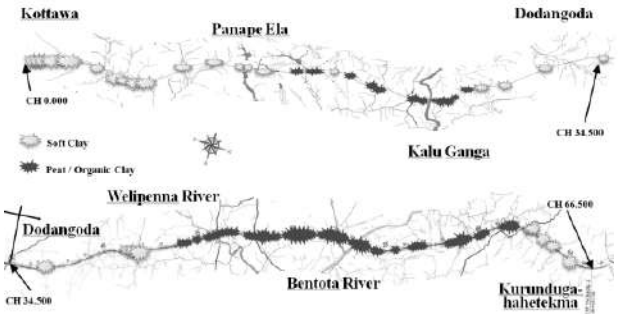

Figure 2. Distribution of soft ground areas

3 DESIGN OF SOFT GROUND IMPROVEMENT

Soft ground improvement design had to be carried out in order to control the settlements and to ensure the stability of the highway embankment as required in the technical specification. According to the technical specification, the embankment had to be designed and constructed by improving the soft ground in order to control the continued settlement to 15cm at the road center after a period of 3 years following the acceptance of the paving. In addition, the maximum residual differential settlement had to be not more than 0.3% change in grade over longitudinally within three years after construction. In order to achieve the above criteria, most or all of the primary settlement and some of the secondary settlement that would have occurred under the final embankment height alone were forced to take place by improving the soft ground.

The soft ground was improved mainly by using the following methods based on the subsoil conditions. Soft clay of shallow thickness was improved by placing a surcharge load. Shallow peat and organic clay deposits were removed and replaced with rock in order to support the embankments. The subsoil with relatively thick soft clay layers were improved by installing vertical drains and placing a surcharge load. The embankments on the relatively thick peat and organic deposits were constructed by improving the ground by heavy tamping method and the vacuum consolidation method from sections 0.0 km to 34.5 km and from 34.5 km to 66.5 km respectively.

In rock replacement method, all compressible layers of the sub soil were removed and replaced with rock, completely eliminating the settlements. In the ground improvement method of application of surcharge load with or without vertical drains, future settlement of the highway embankment was controlled as required in the contract by designing of an appropriate surcharge load. Most or all of the primary settlement and some of the secondary settlement that would have occurred under the final embankment height alone were forced to take place under the surcharge load. In addition, it was expected that the soil beneath the embankment would become over consolidated or stiffer due to the surcharging of ground. The aim of applying the surcharge was to eliminate 100% of primary consolidation settlement and enough secondary settlement such that the residual settlement is within acceptable performance limits. The residual settlement for a given length of time after construction was estimated as the remaining secondary settlement that occurs during the required time after the eliminated equivalent time of secondary compression has elapsed. In the design of surcharge, it was expected to have 1.1 over consolidation ratio (OCR) for inorganic clays and 1.2 to 1.3 for peat and organic clays in order to reduce the secondary settlements during the operation period.

Special treatments were done in the construction of bridge and under pass approaches in soft ground areas in order to create a smooth transferring of expected differential settlements between the approach embankment and the bridge deck. The approach area with thin peat layer was replaced with rock and the approach embankments on thick peat layers were constructed with using the Geogrid Reinforced Piled Embankment technique in order to have a smooth gradient between the approach embankment and the bridge deck.

4 EMBANKMENT CONSTRUCTION ON PEATY SOIL

Embankments over peaty deposits in the Southern Expressway between Ch. 0.000 km to Ch 34.500 km were constructed by improving the peaty soil using the heavy tamping method whereas vacuum consolidation technique was applied to improve the peaty soil in the section between Ch.34.500 km to 66.500 km. This Chapter presents the details of the heavy tamping method and the vacuum consolidation techniques applied in the project.

4.1 Heavy Tamping Method

Heavy tamping method resulted in a quick decrease in void ratio of the peaty soil and instantaneous settlement of ground under impact. Heavy tamping method was designed to enforce the settlements that would be caused by the construction of earth embankment on soft ground by applying impact energy. Different energy levels had to be imparted by considering the anticipated settlement of the compressible layer under the respective designed embankment heights. In the estimation of settlements, all primary consolidation settlements and secondary settlements at the end of 3 years after construction were considered. The estimated settlement of peaty soil layers of different thickness under various embankment heights is shown in Figure 3. In the calculation of settlement, the values of 0.428, 0.0428, 0.05, and 20 kPa were used for the parameters $c_c/(1+e_0)$, $c_r/((1+e_0)$, c_α , and P_c respectively where c_c is the compression index, e_0 is the initial void ratio, c_r is the recompression index, c_α is the coefficient of secondary consolidation and P_c is the preconsolidation pressure.

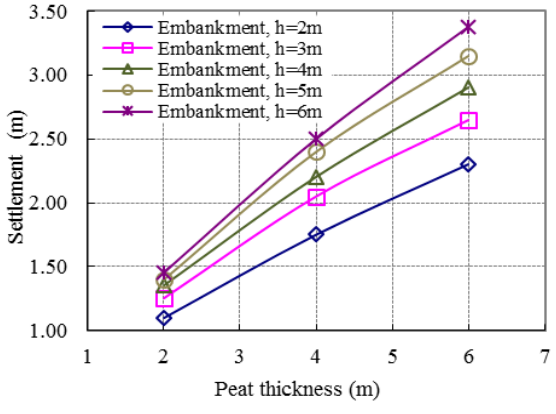

Figure 3. Predicted settlement in peaty clay due to different embankment heights.

The energy level required to enforce the designed settlement was estimated using the graph shown in Figure 4. First, the soft soil, which was to be consolidated, was overlain by a working platform of lateritic soil to facilitate the movement of machinery. Then, a strong type fibre drain (band drain) was installed by a machine in soft subsoil in a square pattern with a spacing of 1 m. The required energy was applied to the soil by dropping a large weight on the ground surface repeatedly in phases on a grid pattern over the entire full base width of the embankment using multiple passes. A high energy level was applied in 5 phases whereas only 4 phases were used to apply a low energy requirement.

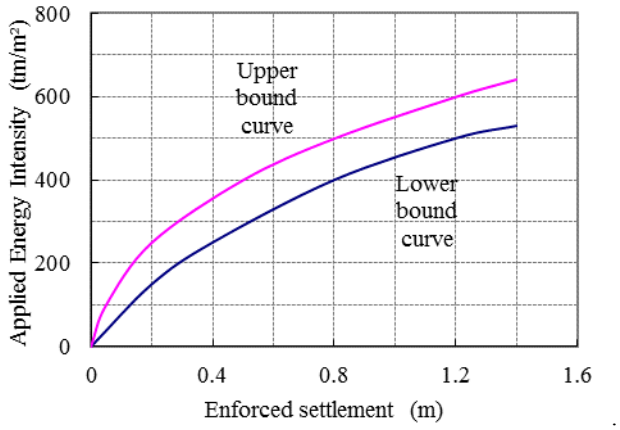

Figure 4. Relationship between the enforced settlement and applied energy

The energy intensity per phase was gradually increased from 15% - 20% of the total energy intensity to 30% - 40% at the last phase prior to the ironing phase. The spacing of the prints of the pounder dropped on the square grid was estimated as 2H to 2.5H, where H is the thickness of the compressible layer. As the ground strength improved the spacing was reduced in the subsequent phases. In the ironing phase, a smaller drop height was used at very close spacing for removing surface unevenness and to compact the soil at shallow depths.

During tamping, once the depth of the crater formed by the drop of pounder exceeded the height of the pounder, the crater was back filled and leveled with soil. The dimension of the crater was recorded in order to calculate the volume of soil introduced. The above process was continued in all phases of tamping operation. Using the crater fill volumes, the enforced settlements were calculated and if the enforced settlement was less than the required then another phase of tamping was introduced until the required settlement was achieved.

The weight of the pounder was 15 tons and it was built by stacking and bolting a series of 25 mm thick mild steel plates, 2 m by 2 m in plan area. A 60 ton capacity mobile crane that was equipped with an automatic lifting and release mechanism of the pounder was used in the tamping operation. The height of drop is governed by the pounder dimension, crane capacity and boom configuration and hence, was found to be a maximum 8 m in this operation. The depth of improvement generally depends on the total amount of energy applied to the soil, which is a function of the weight of the tamper and the drop height as shown in the following equation as reported by Lukas (1995).

$$D = n\sqrt{(WH)} \qquad (1)$$

In the above equation, D is the depth of soft/loose soil to be improved, W is the weight of the tamper (pounder) in tons, H is the height of drop in m and n is a constant ranging from 0.3 to 0.6 and for the peaty soils found in the site it was taken as 0.35. According to the above data, the practically possible improvement depth that could be achieved in the present operation was about 3.5 m to 4 m. However, according to the investigation, it was observed that the soft compressible layer thickness was higher than above in most of the locations and therefore the underneath deeper soft layers were not improved properly by heavy tamping. These underneath deeper soft layers were improved after the heavy tamping operation by keeping a surcharge load for a sufficient period of time. Figure 5 illustrates the major steps in the heavy tamping ground improvement adopted in the project.

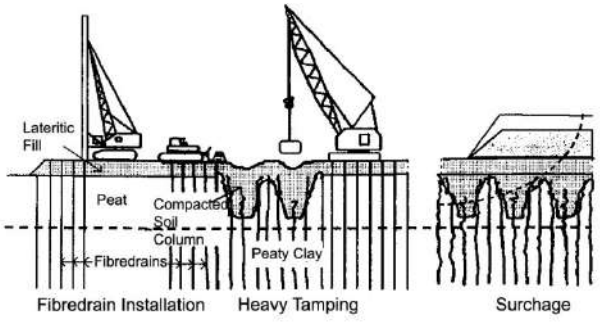

Figure 5. Major steps in heavy tamping ground improvement.

4.2 Effect of the Fiber drain Installation for the Tamping Energy

The in situ permeability of peat is relatively higher than that of ordinary clays and therefore, it was assumed that quick dissipation of excess pore water pressure would occur within the peat during the tamping operation. However, it was noted that the process of pore water pressure dissipation was rather slow and therefore no further densification can be achieved by imparting additional energy to the soils. This could have been due to the rapid reduction of permeability of the peaty soil as a result of damage to the structure of the soil, presence of substantial amount of clay content and long drainage paths. Therefore, it was noted that the energy level required to achieve the designed enforced settlement was very high as the excess pore pressure was not allowed to dissipate as expected. Having experienced the above difficulty, it was decided to install special strong type fibre drains in the peaty soil prior to the tamping in order to eliminate the development of high excess pore water pressure during the heavy tamping operation.

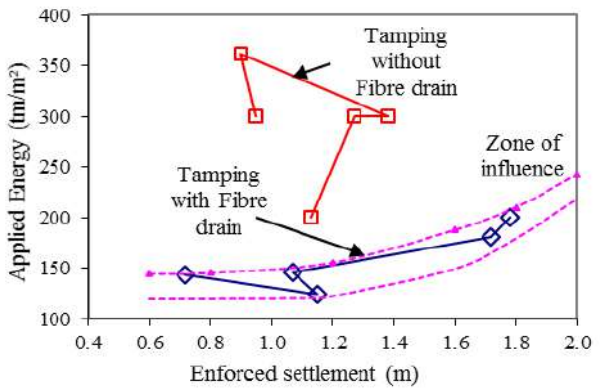

Figure 6. Comparison of Applied energy vs. Enforced settlement with and without fibre drains

Figure 6 shows the applied tamping energy level in order to achieve the designed enforced settlement with and without fibre drain installation in similar ground conditions. As shown in Figure 6, the energy that was required to achieve the designed enforced settlement in fibre drain installed peaty ground was significantly lower than the energy required without fibre drains. This clearly shows that part of the applied energy was wasted in compressing the 'incompressible' water. Therefore, provision of a strong band drain such as fibre drains to withstand heavy tamping impact is useful in reducing the required tamping energy level as described by Karunaratne (2007).

4.3 Vacuum Consolidation Method

The length of the embankments that were built by improving the peaty soil by vacuum assisted surcharging is around 2.5 km. The above length was divided into Sections. The base width of a section was 40 m and the length varied between 50 m to 70 m. The average height was around 8 m, with the crest width of 22 m and side slope of 1 vertical: 1.5 horizontal.

The vacuum consolidation was carried out using the "Compact Vacuum Consolidation" (CVC) patent by Maruyama Industry, Japan. A brief description of the method adopted at the site is given below and the schematic construction is shown in Figure 7.

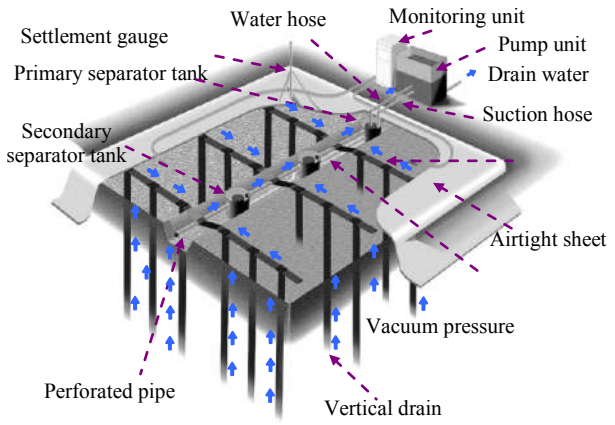

Figure 7. Schematic construction of compact vacuum Consolidation

In the application of vacuum consolidation method, about a 1.0 m to 1.5 m thick fill was constructed on the original ground surface to form a working platform for the band drain installation machine. Band drains were installed by a machine up to a designed depth from the original ground surface in a square pattern with a spacing of 1 m. Thereafter, flexible horizontal drains (300 mm wide and 4 mm thick) were laid on top of the fill with a horizontal spacing of 1 m and then connected to the vertical band drains in order to ensure adequate horizontal drainage capacity. Subsequently, the tank system was installed and connected to the designed pipe systems. Small ditches were excavated perpendicular to the horizontal drains at 20 m intervals and filled with aggregates after placing perforated pipes. Instrumentation such as settlement plates, displacement stakes, electrical piezometers and differential settlement gauges were also installed at the designed depths. After installation of vertical drains, horizontal drains, perforated pipes and separator tanks, the surface of the treatment area was covered by a protection sheet. Thereafter, an air tight sheet was laid on top and the periphery trench system was constructed to provide air tightness and the necessary anchorage at the boundary of the treatment area. Vacuum pressure was then applied using a vacuum pumping system patented by Maruyama Industry Co. Ltd, Japan by connecting the suction and water hoses to the vacuum pump. After confirming that there were no leaks through the air tight sheet, filling was commenced.

The fill was applied in stages, partly due to the stability consideration and partly due to practical constrains in transporting the required high quality fill material with an average compacted unit weight of 18kN/m3. It was expected to apply the surcharge by means of a vacuum pressure of 70kPa to compensate the primary consolidation settlements and to minimize the secondary settlements that can take place in the proposed highway embankment. However, in some areas the applied vacuum pressure was less than the designed value and therefore the above designed surcharge was applied by means of both vacuum pressure and embankment fills. The designed load was kept until the expected settlement completed.

5 FIELD MONITORING PROGRAM

An extensive monitoring program was carried out to understand the field behavior of the foundation soil due to the different ground improvement methods. The improvement of the soft ground was monitored through the measurement of settlement and the excess pore water pressure during the construction period. Settlement plates were installed at the top of the soft layer or on top of the pioneer layer and piezometers were installed at the middle of the soft layer. The settlement stakes were installed near the toe of the embankments to check the stability during the construction. In addition to the above, in the areas improved by vacuum consolidation, a vacuum pressure monitoring unit was used to measure the vacuum pressure at the pump and under the air tight sheet. Also, a water discharge meter was used to measure the rate and the total discharged water flow due to the vacuum operation. An automatic data acquisition unit was connected with the piezometer, vacuum pressure monitoring unit and water discharge meter to keep continuous records. The locations of the instrumentation in one of the CVC improvement Sections are shown in Figure 8 with the treatment area dimensions.

Installed instruments were monitored at selected time intervals to investigate the performance of the expected ground improvement process and the stability of the embankments. The filling rates and the vacuum pressure were adjusted when the stability of the embankment was seen to be at risk, based on the field monitoring data. During the first two weeks of the vacuum operation, the vertical settlement and lateral movement devices were monitored twice a day and the frequency of monitoring was increased with the progress of the embankment construction work. After construction of the embankment up to the required level, monitoring frequency was reduced to once a week. But daily records of the vacuum pressure at pump and under the sheet as well as piezometer readings were taken from the beginning to the completion date of the treatment.

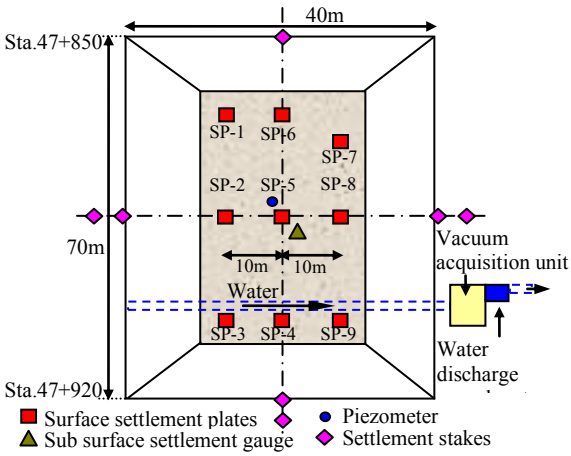

Figure 8. Plan of the embankment and instrumentation layout

The loading curve that shows the placement of the fill, the surface settlement of the settlement gauge installed under the center of the embankment, the observed vacuum pressure under the sheet and the pore water pressure (PWP) in the piezometer installed in the middle of the peat layer, water discharge rate and cumulative water discharge with time for one of the CVC improvement area are shown in Figures 9(a), 9(b), 9(c) and 9(d) respectively.

6 ASSESSMENT OF THE SOFT GROUND IMPROVEMENT

The performance of the ground improvement was evaluated in terms of the degree of consolidation, improvement of the physical and engineering properties, increase in preconsolidation pressure and gain in shear strength of the peaty soil.

6.1 Estimation of degree of Consolidation

The ground improvement achieved was investigated by calculating the degree of consolidation using the observed field settlements before termination of the vacuum operation and the removal of surcharge. The degree of consolidation is calculated as the ratio of the current settlement to the expected ultimate primary settlement. In the present work, ultimate primary settlement and the degree of consolidation were estimated by the method outlined in Asaoka (1978) and hyperbolic method described in Tan et al. (1991) using the measured field settlement data.

The graphical plot of the Asaoka method based on the observed settlement under the center of embankment (SP 5) at vacuum consolidated ground improvement section from Ch.47+850 km to Ch. 47+920 km is shown in Figure 10.

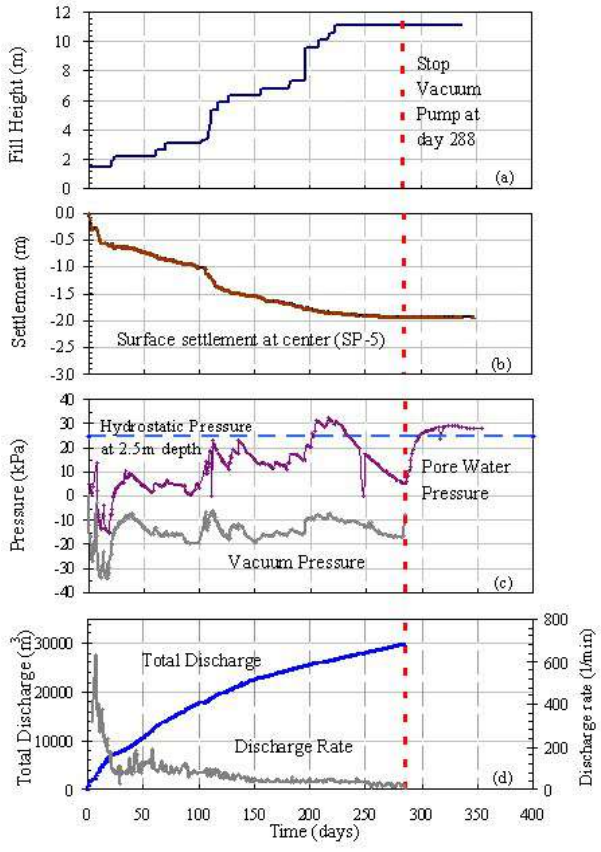

Figure 9. Field monitoring data

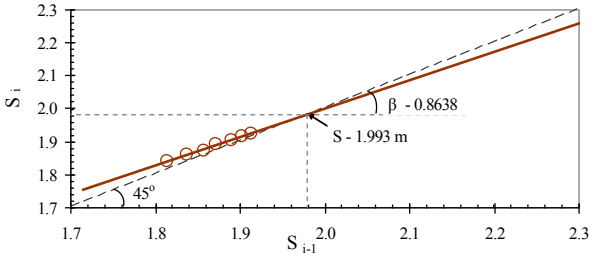

Figure 10. Graphical plot of Asaoka method

It is seen that at the end of CVC treatment the achieved degree of consolidation is around 97%. The degree of consolidation was also calculated based on the pore water pressure measurements (PWP), and laboratory consolidation testing of peaty samples after the treatment program. The comparison of the degree of consolidation for each method is shown in Table 1.

Table 1. Estimation of the degree of consolidation

Location	Degree of Consolidation		
	Asaoka Method	Laboratory Data	PWP
Ch. 45+380 – Ch. 45+430	97.83%	83.10% 73.87%	79.46%
Ch. 47+850 – Ch. 47+920	97.10%	100.00% 100.00%	100.00%
Ch. 52+950 – Ch. 53+000	97.57%	80.21% 90.91%	100.00%
Ch. 53+660 – Ch. 53+730	96.65%	96.70% 83.62%	68.71%

If the degree of consolidation from the PWP measurement is assumed to be accurate, Asaoka Method accurately estimates the degree of consolidation in treatment areas 47 + 850 to 47 + 920 and 52 + 950 to 53 + 00 whereas Asaoka method over predicts the degree of consolidation in treatment areas 45 + 380 to 45 + 430 and 53 + 660 to 53 + 730. However, in treatment area 53 + 660 to 53 + 730 the degree of consolidation from the laboratory test results agree very well with the same estimated from the Asaoka method. Therefore, based on this investigation it can be concluded that the degree of consolidation estimated from the Asaoka method is reasonably accurate.

In order to assess the secondary settlements, for each monitoring point, the long-term settlement was predicted by extrapolating the secondary settlement rate over a period of 3 years. Predictions were made by preparing a plot of displacement against log (time) for each settlement plate, with the best-fit line through the data extended to define the likely settlement after 3 years. The surcharge was removed only after confirming the residual settlement by considering both the primary and secondary consolidation settlements as described above.

6.2 Improvement of Physical and Mechanical Properties of Peat

Site investigation was carried out to assess the actual ground improvement in the areas improved by the heavy tamping and vacuum consolidation method just before the removal of surcharge. Investigation was carried out in the improved as well as the adjacent unimproved area in order to assess the ground improvement. Site investigation comprised of advancing of bore holes with Standard Penetration Test (SPT), collection of undisturbed soil samples, performing of Field Vane Shear Test Cone Penetration Test (CPT) and performing of laboratory tests. The improvement of physical and mechanical properties of peat due to heavy tamping improvement

is described in Karunawardena and Toki (2011). The location of the investigations carried out at CVC improved areas of Ch. 47+ 850 to Ch. 47+920 is shown in figure 11. The observed subsoil profile deduced from the borehole investigation is shown in Figure 12. In the same figure recorded SPT values are also plotted along the depth.

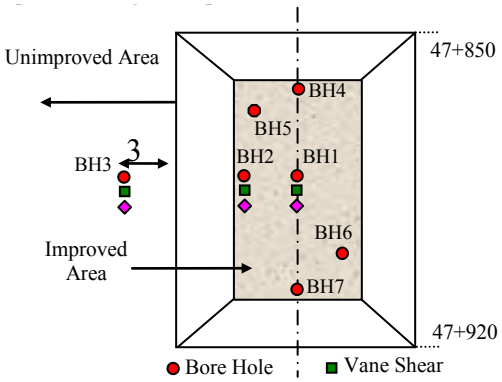

Figure 11. Investigation locations

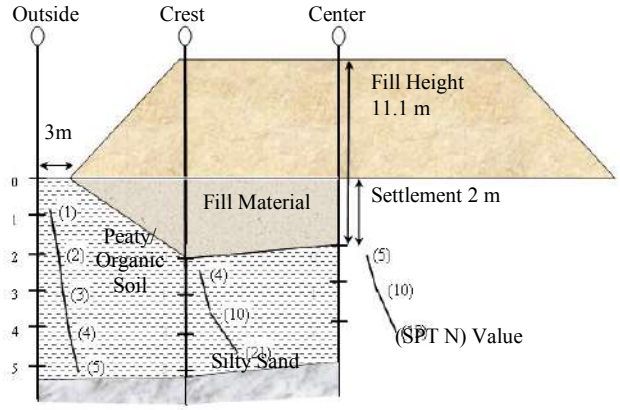

Figure 12. Subsoil profile of improved and unimproved area

The observed change in the peaty soil layer thickness, the changes in water content and void ratio due to CVC ground improvement are given in Table 2. Accordingly, the initial thickness of the peat layer has been reduced by 50%-60% after ground improvement. The above reduction reasonably agreed with the percentage change of water content and void ratio values obtained from peaty soil collected from the improved and unimproved areas. The summary of laboratory test results from the peat samples collected from the improved and unimproved area of Ch.47+850 to Ch.47+920 is given in Table 3. Consolidation tests revealed the significant reduction in the compression index which is proportional to primary consolidation settlement. The compression index of the peat layer has reduced from a range of 2.65 to 2.13, to as low as 0.90 as a result of the ground improvement. The average reduced value is about 1.65.

The reduction of secondary compression is very important as the secondary compression phenomenon is dominant in the peaty soil. The results of long term consolidation tests carried out in the improved and unimproved peaty samples are shown in Table 3. It reveals that the coefficient of secondary consolidation has reduced from a range of 0.10 to 0.13 to a range of 0.03 to 0.06. Subsequently the ratio of has decreased from 0.050 to 0.029 due to ground improvement. The estimation carried out based on the above information assures that the residual settlement would be less than 150 mm by the end of 3 years after construction as required in the contract Karunawardena and Nithiwana (2009).

Table 2 Change in peat thickness, water content and void ratio due to CVC improvement

Location	Peat Layer Thickness (m)		Water Content (%)		Void Ratio		% Change in Thickness of Peat	% Change of Water Content	% Change of Void Ratio
	Initial	Final	Initial	Final	Initial	Final			
Ch.45+380-Ch.45+430	7.70	2.30	378.3 406.8	163.6 137.3	6.83 10.11	3.916 3.805	70.13	56.75 66.25	42.66 62.36
Ch.47+850-Ch.47+920	4.70	2.00	370 398	141.0 168.0	5.54 5.58	1.810 1.940	57.45	61.89 57.79	67.33 65.23
Ch.52+950-Ch.53+000	5.85	2.85	378.3 471.2	175.7 105.8	4.10 9.35	1.900 2.580	51.28	53.56 77.55	53.66 72.41
Ch.53+660-Ch.53+730	5.25	2.76	111.6 122.9	86.6 79.7	3.06 2.66	1.810 2.000	47.43	22.40 35.15	40.85 24.81

Table 3. Summary of laboratory test results

Location	Depth (m)	W_n %	e_o	c_c	c_α	c_u (kPa)
Improved Area – BH1	3.0	227	4.21	1.80	0.055	85
	3.5	266	4.50	1.95	0.061	120
Improved Area – BH2, 5	3.5	141	1.81	0.90	0.037	55
	4.5	168	1.94	1.94	0.048	70
Unimproved Area – BH3	2.5	370	5.54	2.13	0.110	22
	3.5	398	5.58	2.65	0.120	33

6.3 ncrease in Preconsolidation Pressure and Undrained Shear Strength

It is expected that the subsoil behaves in an over consolidated state during the service life of the structure after the completion of ground improvement. This can be verified by the pre-consolidation pressure determined through the 1-D consolidation test. Consolidation tests carried out from section Ch.47+850 to Ch.47+920 indicated that the preconsolidation pressure of the peaty soil found under the embankment has increased from 28 kPa – 38 kPa range to 160 kPa – 180 kPa range after ground improvement as shown in Figure 12. The expected load induced on the peaty layer due to the proposed embankment is around 145 kN/m^2. Therefore, the subsoil will behave under the over consolidated state with an Over Consolidation Ratio (OCR) of 1.2 to 1.3 during the service life of the highway and hence will only give rise to very small settlements in the future.

Consolidation test results related to some other sections also indicated that the pre-consolidation pressure of the peaty soil found under the embankment has increased as shown in Table 4. Table 4 also shows the expected load induced on the peaty layer due to the proposed embankment and the subsoil over consolidation ratio. According to the data in Table 4, the sub soil will behave under the over consolidated state with an Over Consolidation Ratio (OCR) of 0.98 to 1.33. It should be noted here that even though the applied vacuum pressure and the fill surcharge load is adequate to yield an OCR value in the range of 1.2 to 1.3, sometimes the calculated OCR is less than that the anticipated value. This might be due to the inaccurate Pc value obtained from the consolidation test as a result of sample disturbance.

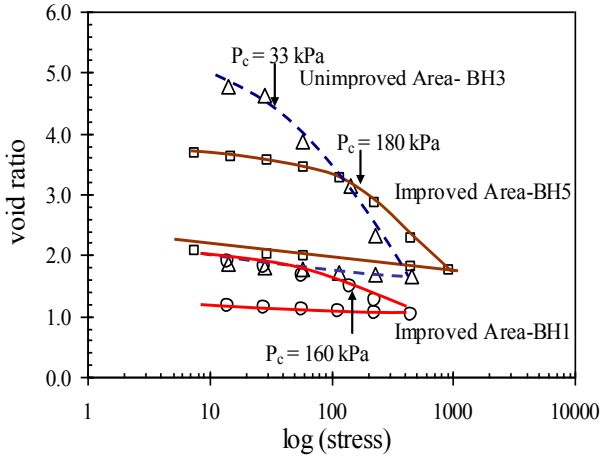

Figure 12. Consolidation Test Results

The SPT and Field Vane Shear results indicate that the strength has improved in the compressible layer due to the ground improvement and as a result the status of the compressible layer has been changed from very soft to medium stiff state. The strength gained due to ground improvement was investigated by calculating the ratio between the increments of undrained shear strength of peaty soil and the effective stress . The undrained cohesion of the peaty soil was determined from unconsolidated un-drained triaxial tests and the preconsolidation pressure was obtained from oedometer tests on undisturbed soil samples. The ratio between the increment of undrained shear strength of peaty soil and the effective stress after the treatment program was obtained to be 0.25 to 0.49.

7 OBSERVED SETTLEMENT AFTER PAVEMENT CONSTRUCTION

The surface settlement of the highway embankment constructed over the improved soft ground was monitored by installing the settlement markers at 50 m intervals after construction of the road pavement. The observed total surface settlement up to September 2012, ten months after opening to traffic, is shown in Figure 13.

Table 4. Increase in preconsolidation pressure and undrained shear strength

Location	Expected Load (kPa)	P_c (kPa)	OCR	C_u (kPa)	$(\Delta c_u / \Delta \sigma'_v$
Ch.45+380- Ch.45+430	160.0	180	1.13	79.0	0.49
		160	1.00	57.0	0.36
Ch.47+850- Ch.47+920	145.0	200	1.37	55.0	0.36
		180	1.25	70.0	0.45
Ch.52+950- Ch.53+000	152.5	150	0.98	41.5	0.27
		170	1.11	38.2	0.25
Ch.53+660- Ch.53+730	150.0	170	1.13	54.0	0.36
		147	0.98	50.5	0.34

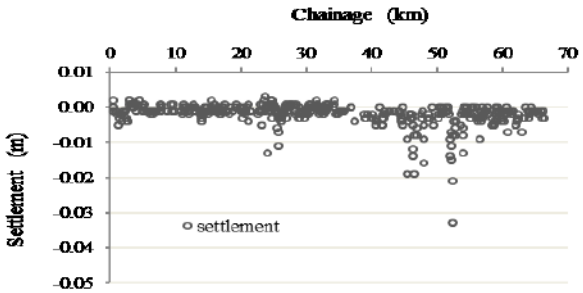

Figure 13. Results of the surface settlement monitoring

Initially, for about a 6 month period, before the road was opened to traffic, surface settlement was monitored at both the center and the edge of the embankment. The observed settlements were in the range of 0 mm to 5 mm in most of the ground improved sections except at very few locations where high embankments were constructed over thick peat deposits by improving the vacuum consolidation method. The observed surface settlement in those areas was around 10 mm to 20 mm at end of six months after the construction of the pavement. After the highway was opened to traffic in November 2011, settlement monitoring was carried out only along the edge of the highway embankment considering safety reasons.

The observed settlement was less than 5 mm in most of the sections and in only two locations the settlement exceeded 20 mm. The maximum observed settlement was 35 mm and the settlement prediction using the monitoring data indicates that the estimated residual settlement is less than 15 mm at the end of 3 years after the handing over of the project.

8 CONCLUSION

This paper presents successful application of ground improvement work carried out in the construction of Southern Highway project in Sri Lanka. Ground improvement methods such as heavy tamping method and vacuum consolidation techniques were applied to construct the high embankments over thick peaty deposits. In both methods, a surcharge load had been applied to over consolidate the peaty soil. Field monitoring data obtained during the construction period indicates that the primary consolidation settlement due to final load of the highway embankment has already been completed and the secondary settlement had been reduced to control the residual settlement within acceptable performance limits. Investigations carried out at the site show that both physical and mechanical properties of the peat have improved significantly and the peaty soil will behave in an over consolidated state with a ratio of 1.2 to 1.3 during the service life of the highway. The results of the post construction surface settlement monitoring of the expressway carried out up to date reconfirm that the ground improvement work was successful and the expected residual settlements are well below the allowable limit in the contract.

9 ACKNOWLEDGEMENT

The authors are grateful to the Road Development Authority of Sri Lanka, for the necessary approval and support extended towards writing this paper.

10 REFERENCES

Asaoka, A. Observational Procedure of Settlement Prediction. Soil and Foundation, (1978), 18(4): 87-101

Karunawardena, A. Consolidation Analysis of Sri Lankan Peaty Clay using Elasto-viscoplastic Theory. Doctoral Thesis, Kyoto University, Japan. (2007).

Karunawardena, A. and Nithiwana, W. Construction of a trial embankment on peaty ground using vacuum consolidation method for a highway construction project in Sri Lanka. Proc., 17th Int. Conf. on Soil Mechanics and Geotechnical Engineering. Alexandria,Vol. 3. . (2009), pp. 2200-2203

Karunawardena, A. and Toki, M. Application of the Heavy Tamping Method on Sri Lankan Peaty Clay for the Construction of a Highway Embankment. Proc. of 14th Asian Regional Conference on Soil Mechanics and Geotechnical Engineering, Hong Kong, China. (2011)

Karunaratne, G.P. Technical report on Heavy Tamping Trial, Oriental Consultants Co., Ltd., Japan, Southern Transport Development Project, JABIC founded Section, Sri Lanka (2007).

Lukas, R. G. Geotechnical Engineering Circular No. 1, Dynamic Compaction, Federal Highway Report. FHWA-SA-95-037, U.S.A. (1995)

Tan, T.S., Inoue, T. & Lee, S.L. Hyperbolic method for consolidation analysis, Journal of Geotechnical Engineering, ASCE (1991),117(11): 1723–1737

DESIGN AND PERFORMANCE OF BRIDGE APPROACHES CONSTRUCTED USING GEOGRID-REINFORCED PILED EMBANKMENT METHOD

W. A. Karunawardena[1] and W.S.N.M Wedikkarage[2]

1 Director General, National Building Research Organization, Sri Lanka
2 Former Geotechnical Engineer, National Building Research Organization, Sri Lanka

ABSTRACT: The specified maximum allowable residual settlement under an embankment fill could be far too excessive and fatal at bridge approaches for high speed vehicles. Therefore, it is necessary that there should not be any settlement at the adjacent embankment near the bridge deck and not more than about 10 mm settlement at the opposite end of the embankment, say 20 m away.As such, it is understood that the embankment for the bridge approach must be improved adequately in order to achieve the above objectives. This paper reports a case history of the design and performance of geogrid- reinforced piled embankments constructed at the bridge approaches in the Southern Expressway project in Sri Lanka. In the present work, geosynthetic reinforcement has been successfully incorporated with pile foundations to improve settlement performance. The load from the embankment is effectively transferred to the columns using multiple layers of geosynthetic reinforcement embedded in the gravel mat, which acts as a load transfer platform that bridges over the piles and reduces the differential settlement at the surface of the embankment. In this paper the information about the project, the design methodology, the numerical analysis, and details of the construction together with the results of the field settlement monitoring carried out during and after embankment construction are presented.

Keywords: soft ground, peat, differential settlement, geogrid-reinforced piled embankment, pile foundations

1 INTRODUCTION

The Southern Highway is Sri Lanka's first E Class highway that links the Sri Lanka's Commercial Capital Colombo with Matara, a major city in the south of the island. The length of 96 km section from Colombo to Galle had been completed and opened to traffic in November 2011. Many parts of the highway traverse through flood plains and marshy ground consisting of very soft peat, organic soils, and clays. Especially, in the major flood plain of Welipenna River, Bentota River and Gingaga River areas, where thick peat and organic clay deposits were found. Many ground improvement methods such as surcharging, surcharging with pre-fabricated vertical drains, rock replacement, heavy tamping and vacuum consolidation were used to improve the soft soil in order to control the post construction settlements and to ensure the stability of the highway embankment. According to the technical specification, the embankment had to be designed and constructed by improving the soft ground in order to control the continued settlement within 15cm at the road center after a period of 3 years following the acceptance of the pavement. The application of the above soft ground improvement methods and performance of highway road embankments constructed using different ground improvement techniques have been described by Karunawardena and Toki (2013).

In addition to the above soft ground improvement work, special treatments were done in the construction of bridge and underpass approaches in soft ground areas in order to create a smooth transferring of expected differential settlements between the approach embankment and the bridge deck. There are about 18 nos. bridges and underpass approaches located in the soft ground areas within the first 34 km of Sothern Expressway trace and four of them are on major flood plains and contain a thick deposit of very soft highly compressible peat. To mitigate the settlement effect, rock replacement method was carried out as the ground improvement for the bridge and the underpass approach locations which consist of thin layers of soft soils in the subsurface. Alternatively, Geogrid Reinforced Piled Embankment (GRPE) has been proposed for the bridge approach locations which consist of very soft to soft, highly compressible soil layers of high thickness. This paper reports a case history of the design and performance of geogrid- reinforced piled embankment constructed at the Panape (Figure 1) bridge approach in the Southern Expressway project in Sri Lanka.

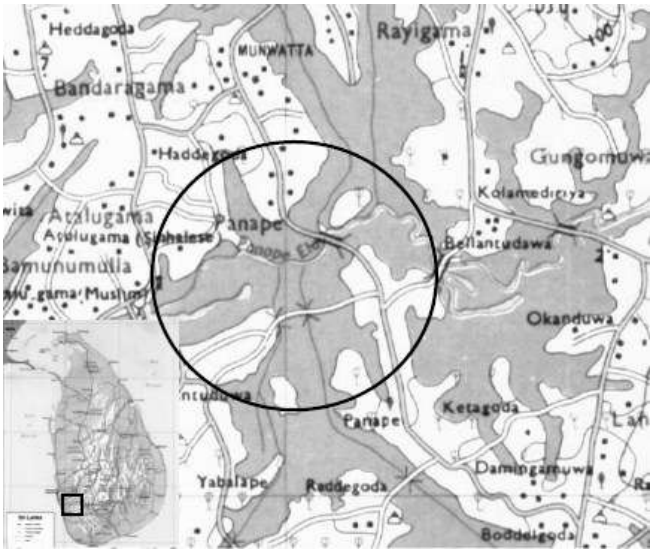

Figure 1. Location map of the bridge approach

2 SUBSOIL CONDITION

The Panape Bridge is located at Ch.16.195 km in Southern Highway route. The site area is a typical low lying marshy land. The subsurface of the site was investigated by carrying out two boreholes at Ch16+236 and Ch 16+255. Boreholes were advanced through the overburden and driven down to the competent rock layer. Standard Penetration Tests (SPT) were performed in the overburden soil and disturbed and undisturbed soil samples were collected at different depths to obtain soil profile and parameters required for the design. Figure 2 shows the assumed subsurface

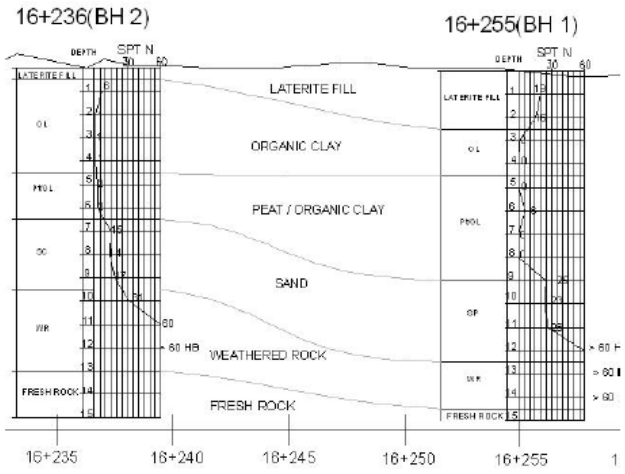

Figure 2. Idealized subsoil profile at the location

Investigations revealed that the subsoil is composed of soft organic clay layer followed by very soft peat layer with some decayed wooden pieces. Total thickness of the above organic clay and peat layers is around 6.5 m and these compressible layers are underlain by layers of sand, about 3 m in thickness. The summary of the laboratory tests are given in the Table 1.

Table 1. Summary of laboratory tests

Borehole Location	16+255	16+236
Consolidation test		
Depth /m	4.0~4.6	5.5~6.1
C_c	1.8	1.24
σ'_c	65	68
Triaxial Test		
Depth /m	-	3.5~4.1
c'	-	8.85
φ'	-	25.4
Unconfined compressive strength test		
Depth/(m)	15.7 ~ 16.7	13.95 ~ 14.95
UCS/(N/mm²)	20.36	11.9

3 DESIGN CONCEPT

A bridge approach must be constructed to allow road way to meet the elevation of the bridge. Therefore, it is necessary to provide smooth transition (reduced differential settlement) at bridge approaches and the bridge. This can be achieved by transferring the differential settlement between the embankments and the bridge deck to an adequate length to ensure a smooth riding surface. Long et.al (1998) classified the approach embankment–bridge structure interface movements qualitatively as given in Table 2 and the approximated differential settlements related to each rating are also given in the same table.

By referring to the data given in Table 2, it was intended to limit the settlement to less than 20mm near the bridge and less than 150mm at 20m away from the bridge by constructing a Geogrid Reinforced Piled Embankment (GRPE) in the bridge approach area.

The Geogrid Reinforced Piled Embankment (GRPE) consists of vertical piles, pile caps and a load transfer platform (LTP) which is reinforced by geosynthetics (geogrids/geotextiles).The load from the embankment, road pavement, and vehicles are transferred to piles through the LTP and the piles transfer that load to the hard bearing stratum bypassing the soft soil deposits. The mechanism of transferring of the load to the piles in this system is performed by the arching action of the soil in LTP. The arching action is further enhanced by the geosynthetics in the LTP. The arching action is effectively mobilized in the granular soils and hence it is very important to use a granular material in the LTP. The pile spacing, load transfer platform thickness and required tensile strength of the geogrids/geotextiles were determined to comply with the design requirements.

Table 2. Classification of approach/bridge interface description (Long et al, 1998)

Qualitative visual rating	Approach/ Bridge Interface Description	Approximate differential settlement/(mm)
0	No bump	0
1	Slight bump	25
2	Moderate bump, readily recognizable	50
3	Significance bump, required repair	75
4	Large bump, safety hazard	>75

3.1 Arrangement of Piles

The design of pile arrangement is mainly based on required settlement profile. 400x400 mm2 square precast concrete piles with a precast concrete pile cap with 0.8m x 0.8m dimensions were used in the construction of GRPE system. Piles were driven into the weathered rock at a grid spacing increasing from 2.5 m to 3.0 m.

A closed spacing is maintained near the bridge approach to minimize the differential settlement between the bridge deck and approach embankment. Pile spacing is then increased with the increase of distance away from the approach slab to ensure the smooth transition of differential settlement to an adequate distance without creating an abrupt vertical jump at the beginning of the bridge approach

3.2 Design of Load Transfer Platform

The load transfer platform (LTP) transfers the load to piles. It is assumed that this reinforced LTP acts as a beam, which transfers the load to piles (Collin 2004). Accordingly, in the design of LTP, it

3.3 Length of Treatment from Bridge

The settlement of the pavement should be gradually changing from zero at the approach slab to a maximum of only 150 mm anywhere else, at the end of three years after construction. To limit the maximum gradient to 1% a treated length of 15m from the approach slab is needed and to eliminate abrupt deformation (settlement) at the junction of the piled embankment and the embankment beyond, a transition length is needed.

Therefore,it was intended to use GRPE for an average length of 25m from the bridge, which complied with the specified limits. The last 10m of the GRPE is considered as a de-skewing section due the skewness of the bridge abutment.

3.4 Estimation of Tensile Strength of Geosynthetic Material

There are few methods developed to determine the required tensile strength of geogrids in the LTP. The method proposed in BS 8006 (1995) is widely used. Han (1999) proposed a method to estimate the required tensile strength of geogrids based on case studies related to GRPE and the information in Figure 3 is developed based on that method. Figure 3 was used to estimate the tensile strength of the geogrid material.

As shown in Figure 3, if there is no contribution from foundation soil and for 6.5 m high embankment, tension in reinforcement will be 600 kN/m. With bulk safety factor of three (3) for the damages during installation, long term creep, chemical degradation and biological degradation, ultimate tensile strength of geogrids was taken as 1800 kN/m.Therefore, 3 numbers of geogrids with 600 kN/m of ultimate tensile strength were embedded in the LTP at 300mm vertical spacing.

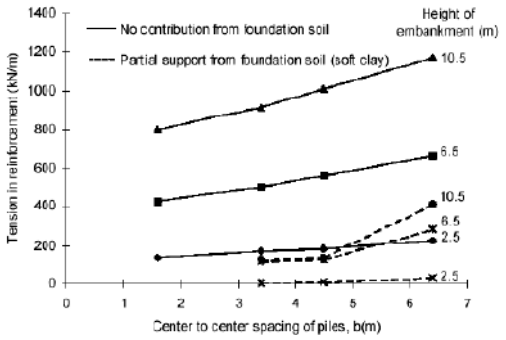

Figure 3. Variation of tensile strength of the reinforcement with other parameters

was considered that a minimum of three layers of reinforcements had to be used to create the platform, the spacing between the layers of reinforcement was 200- 450 mm, the platform thickness was equal to one half the clear span between piles, and the soil arch was fully developed within the depth of the platform. Therefore, the thickness of the LTP was selected as 1.2m, which was tentatively half of the pile spacing. A granular material is compulsory to be in the LTP and hence dense graded aggregate base course (ABC) material was planned to be used for LTP.

4 DETAILED ANALYSIS

The current problem is mainly related to deformation of soft soil under a very complex load transferring system and even more complex geometry due to the skewness of the bridge approach. There is very few or almost no closed form solution to estimate deformations of this kind of a problem.

The application of three dimensional Finite Element (FE) analyses would be ideal for the analysis of deformations. However, the analysis would require very powerful computers and longer time. Even if it is used, the results may not differ very much when compared with a two dimensional model. Therefore, carrying out a two dimensional FE Analysis is worth and a software package called PLAXIS 8.2 2D was used for the analysis. In the finite element analysis, the problem was solved as a two-dimensional plane strain problem with a symmetry condition applied at the center of the embankment ¬using the with plane strain condition. Numerical modeling enables the analysis of embankment loading soil behavior in various conditions without resorting to simplified assumptions. This helps to understand the behavior of the displacement and stresses in the subsoil and the piles, total lateral movement of the soil, axial forces in the pile and the tension in the geogrids. The method of analysis, important materials involved in the construction of GRPE system are described in the following section.

4.1 Foundation Soils

Soft peaty clay and organic clay was modeled using soft soil model which is readily available in the software program. It is based on the Cam-Clay theory and required parameters other than shear strength parameter (cohesion, c' friction angle (Φ') and dilatancy angle (φ)) are modified compression index (λ*), modified recompression index (κ*) and initial void ratio,e_o. The relationship of λ* and κ* with laboratory consolidation test results are as follows.

$$\lambda^* = \frac{Cc}{2.3(1+e_o)} \qquad \kappa^* = \frac{C_r}{2.3(1+e_o)} \qquad (1)$$

Clayey sand, bedrock, embankment and gravel mat was modeled assuming linear elastic-perfectly plastic behavior which was modeled using Mohr Coulomb model. Relevant soil parameters are tabulated in Table 3. The foundation and embankment soil were modeled using 711 triangular elements.

Table 3 provides material parameters of soils for FE analysis.

Parameter	Symbol	Unit	Peat /Organic Clay	Clayey Sand	WR /fresh rock	Embankment fill	LTP
Saturated unit weight	γ_{sat}	kN/m³	10.3	16	22	20	20
Dry unit Weight	γ_{dry}	kN/m³	3	14	22	18	20
Horizontal Permeability	k_x	m/Day	1.5	0.864	0.009	0.086	8640
Vertical Permeability	k_y	m/Day	1.5	0.864	0.009	0.086	8640
Young's Modulus	E	MN/m²	10	40	4200	30	175
Poisson's Ratio	N	-	0.4	0.25	0.2	0.35	0.2
Cohesion	c'	kN/m²	5	5	1000	20	0
Friction Angle	φ'	o	20	30	45	30	40
Compression index	C_C	-	1.25	-	-	-	-
Swell Index	C_S	-	0.1	-	-	-	-

4.2 Piles and Geogrids

Piles were modeled as plate element and geogrids were modeled using geogrid element in the software program. Relevant material parameters are tabulated in Table 4 and 5 respectively.

Table 4-Properties of plate element (pile)

Pile spacing	2.5m	3m
Elastic modulus, E /GPa	20	20
Area, A /m^2	0.16	0.16
Moment of inertia, I /(m^4/m)	2.184×10^{-5}	1.264×10^{-5}
EA /(kN/m)	1 280 000	1 066 666.7
EI /(kNm^2/m)	436.8	252.8

Table 5-Properties of Geogrids

Tensile strength, T /kNm	600
Allowable strain, ϵ /%	6
EA	1000

4.3 Model Analysis 1- Settlement of the embankment without any treatment

The analysis was carried out to verify the model performance of predicting soft soil behavior. FE model was developed considering the normal embankment construction without any ground improvement i.e. consolidation settlement of the soft soils due to embankment loading.

The total settlement after the application of full load was 3.6 m. Karunarathna (2007) developed some curves for the variation of consolidation settlement of peat/peaty clay deposits with the embankment height and thickness of said soft soil deposit as in Figure 4. From that curve also, same settlement can be obtained and hence it can be considered as the validation of the developed FE model. Figure 5 presents deformation contours for the analysis 1.

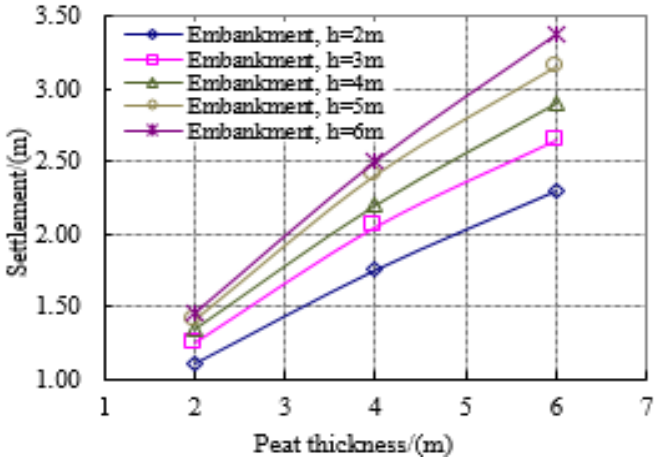

Figure 4. Variation of consolidation settlement with peat thickness and embankment height (Karunarathna, 2007)

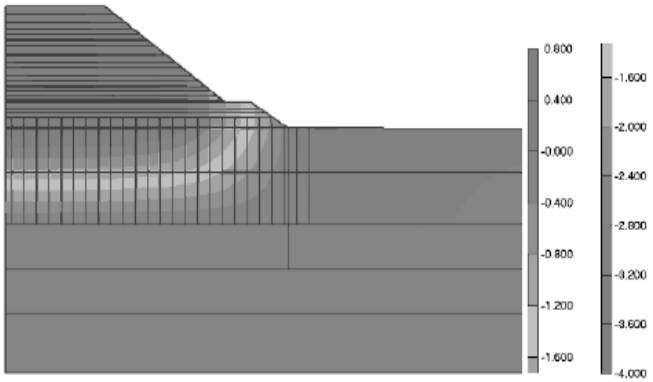

Figure 5. Settlement color contours without any treatment

4.4 Analysis 2- Analysis of GRPE

The schematic diagram of the GRPE system, which was analyzed, is presented in Figure 6. The main components of GRPE and relevant material properties are given in that Figure.

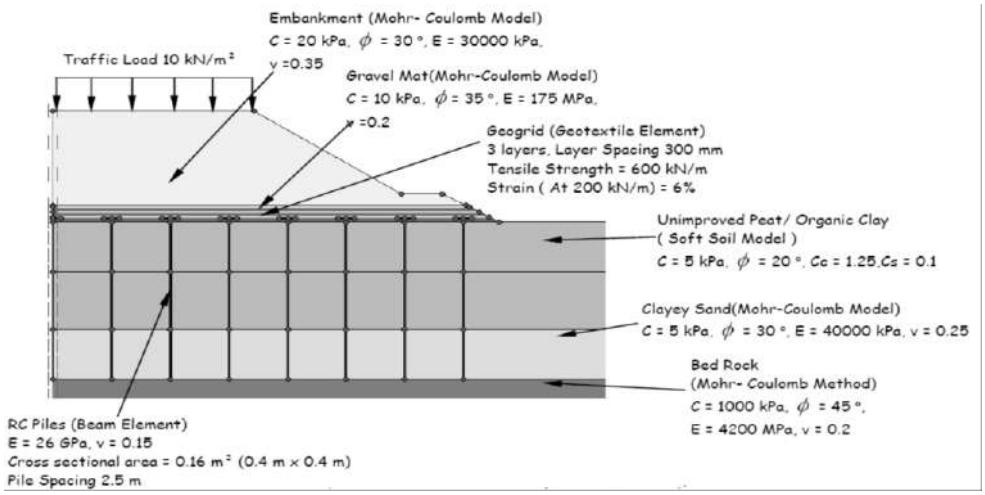

Figure 6. Schematic diagram of GRPE model

Figure 7 and Figure 8 provide the analysis results of GRPE for different pile spacing, namely 2.5m and 3.0m respectively. Pile spacing of 2.5 m represents the area close to the bridge and 3.0 m spacing away from the bridge. As mentioned above, stage construction procedure was used in the analysis in order to simulate the actual construction process.

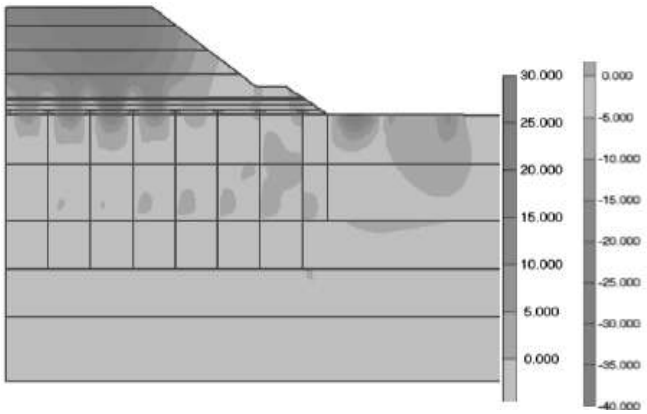

Figure 7. Plot of vertical displacements of 2.5 m pile space section

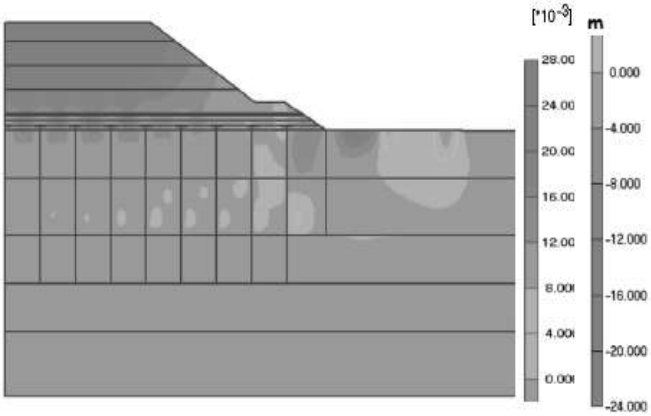

Figure 8. Plot of vertical displacements of 3.0 m pile space section (shadings)

4.5 Results of the Analysis

Table 6 gives the predicted settlement after completion of each construction phase.The predicted maximum settlement is about 20 mm near the bridge and 31 mm away from the bridge. Settlement after three years after completing the construction of GRPE can be estimated using stage construction option in PLAXIS. Accordingly, after the construction of the embankment, only 4 mm of settlement will occur in three year period near the bridge approach and only 7mm away from the bridge approach.

Table 6 - Settlement after each construction stage

Stage	Load application	Time Interval of load application /(Days)	Settlement of the top of the embankment	
			2.5 m pile spacing	3.0 m pile spacing
Initial stage	Existing ground + Driven piles + Geogrid + Gravel Mat (1.2 m Thick)	0	0	0
Stage 1	Initial stage +Embankment(1.5m)	21	2	2
Stage 2	Stage 1+Embankment (1.5 m)	21	5	6
Stage 3	Stage 2+Embankment (1.5 m)	21	10	15
Stage 4	Stage 3+Embankment (0.8 m)	21	16	24
Stage 5	Stage 4+ Open to traffic	21	20	30
Stage 6	Stage 5+ Open to traffic	200	20	31
Stage 7	Stage 6+ Open to traffic	800	20	31

4.6 Differential Settlement

Differential settlement is defined as the difference in the settlement at the center of the pile and at the mid span of the pile spacing. The observed differential settlement at the embankment top was almost zero. Differential settlement at pile top level is about 10 mm and 14 mm for 2.5 m and 3.0 m pile spacing respectively. As such, the anticipated differential settlement in the embankment is within the acceptable limits. It can be seen that the differential settlement decreases from the pile head to the top of the embankment. This is due to the development of soil arching at the pile head and the efficient load transfer mechanism created by the load transfer platform constructed with geogrids on top of the pile. According to the analysis, there has been no discernible differential settlement noticed at the site since the construction.

The final design drawing and the approximate settlement profile in longitudinal direction are presented in Figure 9 and 10 respectively.

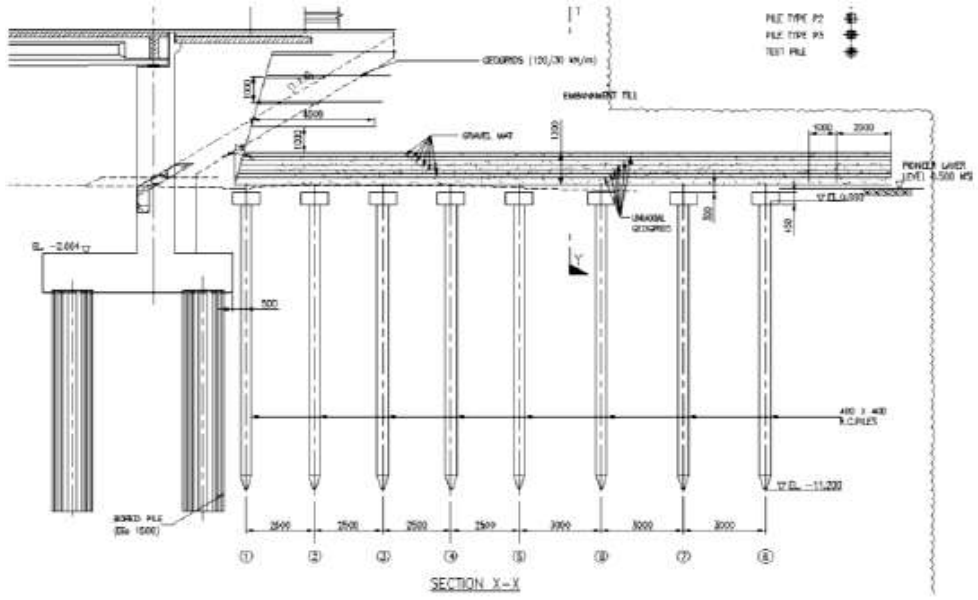

Figure 9. Final Design Drawing

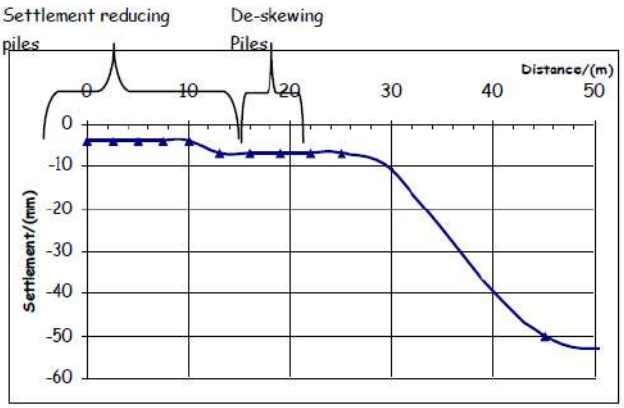

Figure 10. Settlement in longitudinal section of embankment

4.7 Stresses and the Deformation in Geogrid

The load transfer platform consists of 1.2 m gravel mat comprising of three layers of biaxial geogrids with strength of 600 kPa. The mobile tensile strength of geogrids placed on 3m pile spacing is shown in Figure 11. It indicates that more tensile strength has been mobilized in the geogrids at the edge of the pile.

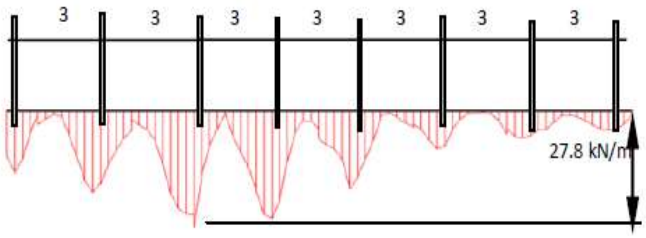

Figure 11. Mobilized Tensile Strength in 1st geogrid from top

4.8 Mobilized Strain

The estimated vertical displacements of the geogrid placed on 3.0 m pile spacing are shown in Figure 12.The calculated maximum total strain is 0.3 %. Gangakhedkar (2004) reported that to avoid long term localized deformations at the surface of the embankment, the long term strain should be kept to a minimum strain value of 2 % for the permanent construction work, which agrees with the calculated value.

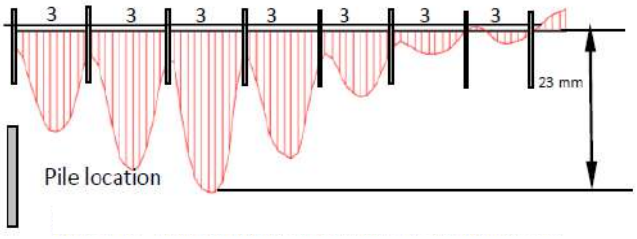

Figure 12. Vertical displacements in 1st geogrid from top

5 OBSERVED SETTLEMENT DURING AND AFTER CONSTRUCTION

To verify the design and to check the performance of the embankment, monitoring of settlement was carried out. Settlement was monitored during and after construction of the embankment. Figure 13 shows the observed settlement values of the settlement plate installed at the top of the LTP during the construction period of the embankment. As shown in the figure, the observed settlement reasonably agrees with the predicted settlement shown in Figure 12. Also, the results of the surface settlement monitoring indicate that the observed settlements were in the range of 0 m to 3 m one year after the road was opened to traffic.

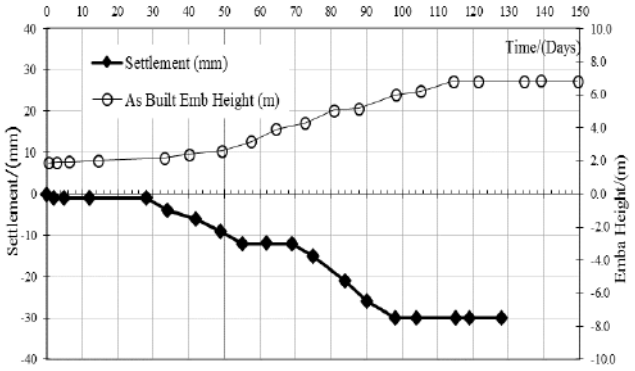

Figure 13. Observed settlement during the construction

6 CONCLUSION AND RECOMMENDATIONS

For comfortable rides, elimination of differential settlement between the embankment and the approach slab is very important. At a distance of about 20 m from the slab, the settlement should be comparable with the treated ground settlement under the embankment fill which is 150 mm. Settlement of the untreated ground is large and soft ground treatment is therefore essential to limit the differential settlement in the approach embankment.

The proposed GPRE system for construction of bridge approaches reduces the total settlement of the embankment; more importantly, the differential settlement between the pile and foundation soil is very small and hence upward lunges, which may be created due to the settlement between the bridge deck and the embankment, will be eliminated. The conceptual design or preliminary design for the situation was carried out based on published data and guidelines. Then the system was analyzed with a validated FE model and it was found that the specified design criteria were met. The results of the settlement monitoring carried out during and after construction of bridge approach embankment indicates that the settlement performance of bridge approach is satisfactory and confirms to the design criteria

References

British Standard BS 8006, 1995, Code of Practice for Strengthened/ Reinforced Soils and Other Fills. British Standard Institution, London.

Collin, J. G. 2004. Column Support Embankment Design Consideration, Proc 5th Annual Geotechnical Conference, University of Minnesota, Minneapolis, MN, February 27, 2004.

Gangkhedkar R. 2004. Geosynthetic Reinforced Pile Supported Embankments, Thesis for Degree of Master of Engineering, University of Florida.

Han J. 1999. Design and Construction of Embankment on Geosynthetic Reinforced Platforms Supported by piles, Invited Speaker, Proc.1999 ASCE/ PaDOT Geotechnical Seminar, Hershey, PA.

Hoppe E.J. 1999.Guidelines for the use, design, and construction of bridge approach slabs, Virginia Transportation Research Council, Charlottesville, Virginia.

Karunarathne G. P. 2007. Technical Report on Geogrid Reinforced Piled Embankment for Bridge Approaches for STDP Package 1.

Karunawardena, A. &Toki, M, 2013, Design and Performance of Highway Embankments Constructed Over Sri Lankan Peaty Soils. Proc. 18th Int. Conf. on Soil Mechanics and Geotechnical Engineering, Paris, p. 2949-2952.

Long, J. H., Stark T.D., Olson S.M., & Samara E.M. 1998. Differential movement at embankment–bridge structure interface in Illinois, Transportation Research Record Illinois Department of Transportation, Illinois.

PRACTICE OF REINFORCED EMBANKMENT ON HARD FOUNDATION - A CASE STUDY OF PHITSANULOK, THAILAND

P. Baral[1*], D.T. Bergado[2], C. Rujikiatkamjorn[3] and A.S. Balasubramaniam[4]

1 PhD Candidate, Centre for Geomechanics and Railway Engineering, Faculty of Engineering, University of Wollongong, NSW, Australia. (Corresponding Author, Email- pb994@uowmail.edu.au)*

2 Professor, School of Engineering and Technology, Asian Institute of Technology, Pathumthani, Thailand.

3 Associate Professor, Centre for Geomechanics and Railway Engineering, Faculty of Engineering, University of Wollongong, NSW, Australia.

4 Professor, Centre for Infrastructure Engineering and Management, School of Engineering, Griffith University, QLD, Australia.

ABSTRACT: A full scale reinforced test embankment was designed and constructed by Department of Highways (DOH) on hard foundation (i.e. Soil stratum containing relatively stiff to very stiff clay) in Phitsanulok Province, Thailand. Two types of reinforcements were used. One side, called reinforced steep slope (RSS) with folded polymer facing at an angle of 70 degrees from the horizontal, was reinforced with polymeric reinforcements consisting of polyester (PET), polypropylene (PP) and high density polyethelene (HDPE). The other side, called mechanically stabilized earth wall (MSEW) with vertical segmental concrete facing, was reinforced with metallic reinforcement consisting of metallic strips (MS) and steel wire grids (SWG). The behaviour of the RSS and MSEW slopes were observed, back-analysed by sensitivity analysis and compared with the predictions from FEM PLAXIS 3D simulations. As expected the vertical settlements were very small for the hard foundation. The corresponding lateral movements from the RSS side were much larger than the MSEW side due to the higher stiffnesses of the former than the later. The magnitudes of the reinforcing material stiffnesses decrease in the following order: metallic strips (MS), steel wire grids (SWG), polypropylene (PP) high density polyethelene (HDPE) and polyester (PET). The polymeric reinforcements have comparable ultimate tensile strengths at 100 KN/m. The predictions from the FEM PLAXIS 3D simulations were in good agreement with the field measurements in terms of vertical and lateral deformations as well as strains in the reinforcements.

1 INTRODUCTION

In past years, many researchers studied the behaviour of several reinforced earth structures (i.e. mechanically stabilised earth wall/ embankment) on Bangkok soft soil. Most of them were constructed in the premises of AIT campus. The fully instrumented steel grid reinforced embankment was constructed in the campus of Asian Institute of Technology in March 1989. The backfill of this reinforced embankment were clayey sand, lateritic and weathered clay whereas the reinforcement used was steel grid. Shivashankar (1991) observed the behaviour of a welded wire wall with poor quality, cohesive-friction backfills on soft Bangkok clay.

Later on, In May, 1993, another embankment was constructed in AIT campus with polymer grid reinforcement as a reinforcing material. The reinforcement used in this embankment was Tenax TT 201 geogrid SAMP, which is uniaxial oriented polymer grid reinforcement (Alfaro, 1996). Furthermore, Long (1996) studied about the behaviour of a geotextile reinforced embankment on soft ground. This study was focussed on the interaction parameter between soil and geotextile reinforcement, the localized mobilization of geotextile reinforcement force related with slip failure, the performance behaviour of geotextile reinforced embankment on soft ground and the closed-form solution for rotational stability analysis of reinforced embankment. Similarly, Voottipruex (2000) studied the behaviour of full scale embankment built in AIT campus which was reinforced with hexagonal wire mesh upto 6m with 10 degree inclined of gabion facing. The facing consisted of large rectangular wire baskets wired all together and was filled with rock and height of each basket was 1m. Two types of reinforcements, galvanized coated and PVC coated with unequal aperture size, were used in the two different sections along the length of the wall.

Furthermore, Lai et al (2006) performed the full scale MSE embankment laid on fully instrumented Deep Mixing Method DMM improved ground. The behaviour of the full scale test embankment showed that deep mixing improvement method reduced the settlement of reinforced soil test embankment by 70 %, which was an effective finding. Tanchaisawat (2008) performed the study about the interaction between geogrid and tire chips-sand mixture, performances of full scale geogrid reinforced test embankment and numerical simulation of this full scale test embankment. The results revealed that the aperture sizes of geogrid affected most for the direct shear resistance of geogrids. He concluded that larger aperture size may lead to higher direct shear resistance.

Recently, Artidteanget al (2014) has studied the behaviour of a full-scale test embankment constructed in AIT campus with silty sand backfill on soft ground reinforced with kenaf limited life geotextiles (LLGs) and found that the time to achieve 90 % degree of consolidation for this embankment was lesser than the estimated life of kenaf LLGs. The main finding of this research was utilization of kenaf LLGs as soil reinforcement for short-term application.

Moreover, Cisneros(1989), Abiera (1991), Mir (1996), Kabiling (1997), Modmoltin (1998), Wongsawanon (1998), Srikongsri (1999), Visudmedanukul (2000), Asanprakit (2000), Kongkitkul (2001), Supawiwat (2002), Youwai (2003), Rittirong (2003) , Prempramote (2005), Tin (2009) and Nualkiang (2011) studied and analysed the behaviour of various reinforced earth embankment and its components during their research in AIT.

A full-scale test embankment was constructed in Phitsanulok Province, Thailand on hard ground using five different types of reinforcing materials (polymeric on one side and metallic on the other side). The reinforced steep slope (RSS) was reinforced with polymeric material with folded soil bags as the facing material, and the mechanically stabilised earth (MSE) wall was reinforced with metallic reinforcement with precast concrete panels as the facing material. This embankment was fully instrumented with piezometers, settlement plates, inclinometers, total pressure cells and strain gauges and subjected to careful field monitoring to obtain high-quality data. The aim of this study was to compare the behaviour of polymeric- and metallic-reinforced embankments on hard foundation with 3D numerical simulations conducted using PLAXIS 3D. Particular attention was given to the lateral displacements, vertical settlements, total vertical pressures and tensile forces in the reinforcement.

2 DESCRIPTION OF THE EMBANKMENT AND INSTRUMENTATION

A 6-m-high reinforced earth embankment was constructed and designed by the Department of Highways (DOHs) of Thailand near Highway No. 11 (Phitsanulok-Uttaradit) in Phitsanulok Province in central Thailand. The test embankment was 18 m long and 15 m wide at the top. On one side, the reinforced steep slope (RSS) was constructed with a face sloping 70 degrees from the horizontal and consisting of folded soil bags. On the other side, the mechanically stabilised earth wall (MSEW) was installed with vertical concrete panels as the facing. Three types of polymeric geogrids reinforcement were installed in the reinforced steep slope (RSS) facing, and two types of metallic reinforcement were installed in the mechanically stabilised earth wall (MSEW) facing. The three types of polymeric geogrid reinforcement were polyester (PET), high-density polyethylene (HDPE) and polypropylene (PP). The two types of metallic reinforcement were steel wire grids (SWG) and metallic strips (MS). The vertical spacing was 0.5 m and the length of the reinforcement was 5 m.Thegrid spacing for MSEW wall was 0.375m for the first layer of reinforcement and 0.5m for the remaining layer. Extensive field instrumentation program was established to monitor both the behavior and performance for the embankment/wall, geogrid reinforcement and steel reinforcement and subsoil condition. Subsoil instrumentation was installed prior to the construction of the embankment/wall. Monitoring work was carried out during and after the construction completion. The monitoring instruments installed to check the vertical and horizontal displacements, stresses, excess pore water pressures, depth to the groundwater table and strains in the reinforcing material included inclinometers, settlement plates, total pressure cells, standpipe piezometers, vibrating-wire strain gauges and fibre optic strain gauges. The instruments include 5 inclinometers, 45 settlement plates, 6 total pressure cells, 5 standpipe piezometers, 2 reference benchmarks and 5 instrument houses. In addition, two observation wells were installed to measure the fluctuation in the depth to the groundwater table. The plan and cross section of the MSE wall/embankment with the location monitoring instruments are shown in Figs. 1 and 2, respectively.

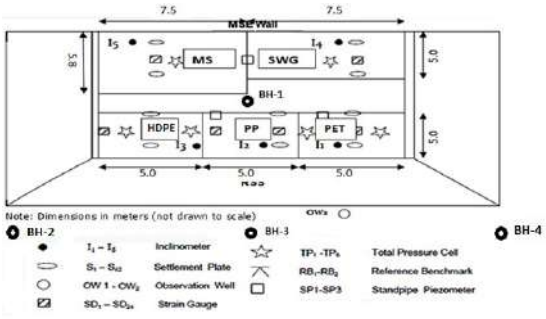

Figure 1.Plan of MSE wall/embankment.

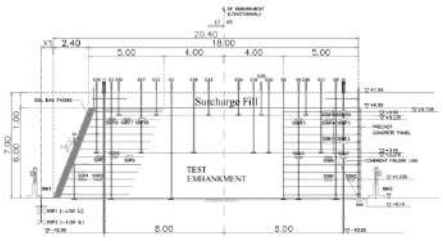

Figure 2.Cross section of MSE wall/embankment indicating the location of the monitoring instrument.

3 SUB-SOIL PROPERTIES

3.1 Foundation Soil

The soil profile in Phitsanulok Province generally consists of hard ground. One borehole (BH-1) was located in the middle of the embankment. Three additional boreholes were bored adjacent to the embankment near the RSS facing to obtain more data on the soil profile for the 3D model of the embankment foundation. These additional boreholes were designated as BH-2, BH-3 and BH-4. The borehole locations are shown in Fig. 1. Figures 3 indicate the soil profiles corresponding to BH-1 to BH-4, respectively. The depth of the groundwater was 2 m below the ground surface. From fig. 3, an abrupt change in soil profile was noticed if we observed BH-1 data on the first 3m layer and the deeper stratum (11m-20m) but other three borehole showed the consistent result in terms of SPT value.

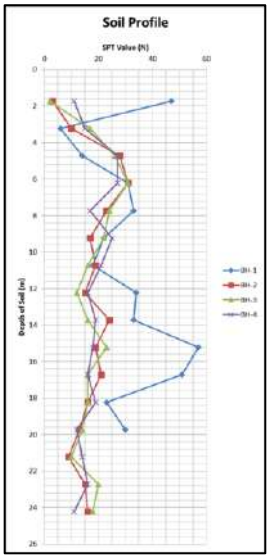

Figure 3. Soil profile SPT value (considering BH 1-4)

4 COMPONENETS OF MSE WALL/EMBANKMENT

4.1 Backfill Properties

The backfill materials used in this embankment consisted of 50% lateritic soil mixed with 50% silty sand (by volume). The backfill material was classified as poorly graded sand (SP). It had an optimum moisture content of 7.8%, a maximum dry unit weight 19.62 kN/m3. A friction angle of 42 degrees and a cohesion of 80 kPa were measured in a direct shear test. Effective friction angles of 32.8 degrees and 37 degrees and effective cohesions of 0 and 20 kPa were measured in two different consolidated undrained (CU) triaxial tests. The properties of the backfill material are tabulated in Table 1.

Table 1. Properties of backfill material

Atterberg Limit Test	LL = 20.8%, PL=17.3%, PI=3.5%.
Sieve Analysis Test	Sample No. 1 Percent finer (#200 sieve) = 0.94% Cu = 40, Cc = 0.34

	Sample No. 2 Percent finer (#200 sieve) = 0.14% Cu = 42.86, Cc = 0.55		
Unified Classification	Poorly graded sand (SP)		
AASHTO Classification	A-2-4(0)		
Compaction Test	Maximum dry density ($\gamma_{d,max}$) = 19.62 kN/m^3 Optimum water content (OMC) = 7.8 %		
California Bearing Ratio (CBR) Test	CBR = 50.5%		
Direct Shear Test	Friction angle = 42 degrees cohesion = 80 kPa		
Triaxial Test (CU test)	Test No. 1	Friction angle = 32.8 degrees cohesion = 0 kPa	
	Test No. 2	Friction angle = 37 degrees cohesion = 20 kPa	

4.2 Reinforcements

Two types of reinforcement, namely polymeric and metallic reinforcement, were used in the reinforced embankment. The polymeric reinforcement types used were high-density polyethylene (HDPE), polypropylene (PP) and polyester (PET). The metallic reinforcement consisted of metallic strips (MS) and steel wire grids (SWG). The properties of the reinforcement are tabulated in Table 2. The reinforcing materials used in the embankment are shown in Fig. 4. The MSEW facing with metallic reinforcement and the RSS facing with polymeric reinforcement are shown in Fig. 5.

Table 2. Properties of reinforcing material

Material Name	Tensile Strength (kN/m)	Thickness (mm)	Normal Stiffness, EA (kN/m)	Type
Metallic Strip (MS)	277.6	4.00	88,000	-
Steel Wire Grid (SWG)	128.1	6.00	35,000	-
Polyester (PET)	83.6	1.50	925	**Miragrid GX80/30**
Polypropylene (PP)	91.9	1.45	1,360	**Secugrid 80/80 Q1**
High-Density Polyethylene (HDPE)	85.8	1.91	1,320	**TT 090 SAMP**

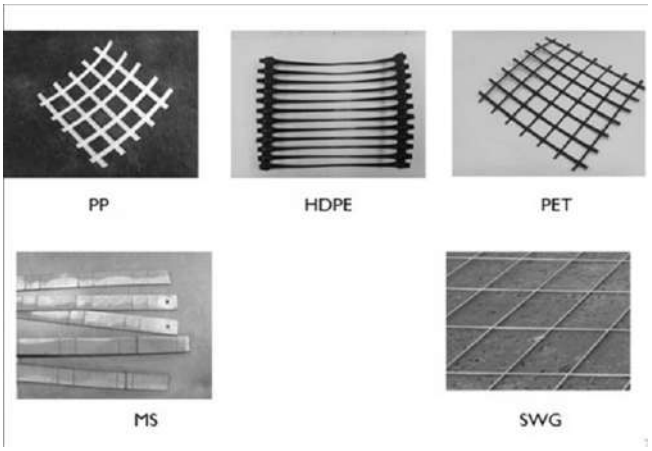

Figure 4.Reinforcing materials.

Figure 5. Photograph showing vertical face and sloping face showing metallic and polymeric reinforcements respectively.

4.3 Precast Concrete Panel

The vertical facing used in the MSEW portion of the embankment consisted of segmental precast concrete blocks 1.5 m × 1.5 m × 0.15m in size. The model parameters used in the numerical analysis for the precast concrete panels are summarised in Table 3. Interface element was placed in between soil element and concrete panel during simulation.

Table 3. Properties of concrete panel facing

Parameter	Name	Value	Unit
Type of behaviour	Material type	Elastic	
Normal stiffness	EA	42,000,000	kN/m
Flexural rigidity	EI	78,500	kN.m^2/m
Equivalent thickness	d	0.15	M
Weight	w	3.6	kN/m/m
Poisson's ratio	υ	0.15	-
Model		Plate	

4.4 Interface Shear Strength

The interaction between the backfill soil and the reinforcing materials, namely, the metallic strips (MS), steel wire grids (SWG), polyester (PET), polypropylene (PP) and high-density polyethylene (HDPE), was assessed by conducting large-scale direct shear tests.

The interface coefficients, Rinter, of the different types of reinforcing materials and the backfill soil shear strength are tabulated in Table 4. The large-scale direct shear tests were conducted under different normal stresses (i.e., 30, 60 and 90 kPa) and revealed that the maximum interface shear stresses between the steel wire grids and soil were highest, followed by the interface shear stresses between soil and soil, between metallic strips and soil, and between the three types of geogrids and soil.

Table 4. Interface coefficient (R_{inter}) and soil shear strength used in PLAXIS 3D

Soil to	Friction angle	Cohesion (kPa)	R_{inter}
Soil	40	23	1.00
Steel strip (MS)	36	23	0.87
Steel wire grid (SWG)	40	28	1.00
Miragrid GX80/30 PET	33	21	0.79
Secugrid 80/80 Q1 PP	35	25	0.83
TT 090 SAMP HDPE	33	24	0.77

5 CONSTRUCTION OF FULL SCALE MSE WALL

Full scale MSE wall was constructed with full instrumentation program as outlined in section 2. Preliminary design based on proposed wall geometry was carried out prior the execution of the construction work. Geogrid, steel grid and steel strip as the reinforcement for the MSE wall was prepared in the desired length prior the installation work.

5.1 Preliminary Design of MSE Wall/Embankment

Preliminary design of the MSE wall was carried out based on the external and internal stability analysis of the geometry of the wall. Limit equilibrium method of analysis was adopted for the preliminary design by assuming the interaction of the reinforcement with the backfill material based on the laboratory test data carried out in AIT. Silty sand mixed with lateritic soil(1 : 1 by volume) sourced from Phitsanulok is used as backfill material.

The wall height assumed for the preliminary design is 6m with vertical facing. Vertical spacing of5 (five) type of reinforcement adopted is 0.50 m and horizontal spacing for only steel strip is 0.50 m center to center of the 0.05 m wide strip of reinforcement. Precast concrete facing panel of 1.50m height, 1.50m width and 0.15m thickness and with surface area of 2.25 m2is used for the construction of the wall. Concrete strength of facing panel was 30 MP_a.

The internal stability, tension in the reinforcement behind the failure surface was checked against the lateral internal earth pressures. The lateral earth pressure coefficient was assumed to be uniform throughout the height of the wall at the value corresponding to the at rest condition (K_o). The effects of compaction were ignored in this preliminary design. The total pullout resistance inclusive of the friction over the reinforcement behind the failure surface was checked to be greater than the driving forces due to the internal lateral earth pressure. Also, the maximum tension force in each layer of reinforcement at the peak pullout resistance was checked not to exceed its yield point.

The external stability was examined using the conventional Bishop's method of slope stability analysis. A conservative estimate of minimum factor of safety is assessed to be around 1.5. The soil strength was assumed to be fully mobilized along the potential failure surface. Factor of safety was defined as the maximum reinforcement force available divided by the force required for stability to give a factor of safety of unity.

5.2 Construction Method

Site clearing and leveling works were carried out for the marking of the position of the proposed MSE wall/embankment. First course of pre-cast concrete facing panels were placed into position using lifting equipment. During the installation of the precast concrete facing panel, vertical and horizontal alignment of each panel was inspected using a spirit level. Adjustment of the verticality of the facing panel was carried out with the help of securing wooden wedges in between the facing panel. Clamp made of timber and steel rod complete with fastener was used to secure the positioning of each facing panel from movement.

Geogrid reinforcement form delivered in roll form (approximately 100m per roll) from the factory. It was cut by length of 7.0m each and optical fiber with sensors was installed at designated locations of the selected geogrid reinforcement at the site.

Steel grid and steel strip with 5.0m length was installed and connected to concrete panel facing. Vibrating wire strain gauges were fixed to steel reinforcement at designated locations at the site.

The first course of backfill material (silty sand) was spread at the rear of the precast concrete facing panel. Compaction of backfill material to 95% proctor density of the backfill material was carried out by a vibratory compactor. A small vibratory compactor was utilized to carry out the compaction work at narrow area with interference of the instruments installed. After the completion of the compaction work, (1) the first layer of steel grid reinforcement was installed into position and attached to the precast concrete facing panel by lap joint mechanism (Fig.6). The lap joint mechanism was secured by inserting a 10mm diameter deformed steel bar across the lap fold mesh. Steel grid was installed horizontally along the wall. The effective length of the reinforcements was 5.0m after deducting for the connection. (2) the first layer of steel strip reinforcement was installed into position and attached to the precast concrete facing panel by using a 12mm diameter galvanized bolt (Fig.7). (3) the first layer of geogrid reinforcement was installed into position and turn up geogrid reinforcement at the face of the slope and return the reinforcement a minimum of 1 m into the embankment below the next reinforcement layer (Fig. 8). This embankment was required soil bag with grass seed at the face to retain backfill materials (Fig. 9).

Subsequent course of backfill material measuring of 0.50m thick were spread over the plan surface area covering the embankment. Similar compaction work was carried out before the next course of precast concrete facing panel was installed. The procedure as mentioned above was repeated until the full height of 6.0m was achieved.

During the construction of the embankment, field density test at various selected places were carried out using sand cone replacement method to ensure compaction was carried out to minimum of 95% standard proctor density.

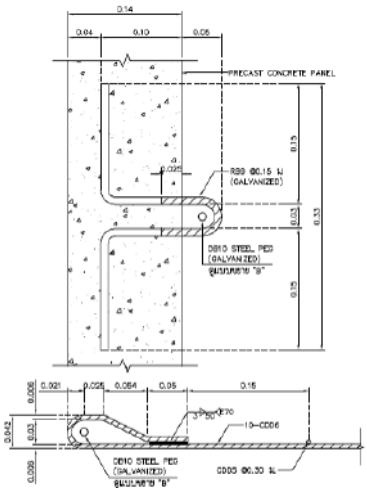

Figure 6.The connection between concrete facing and steel grid reinforcement

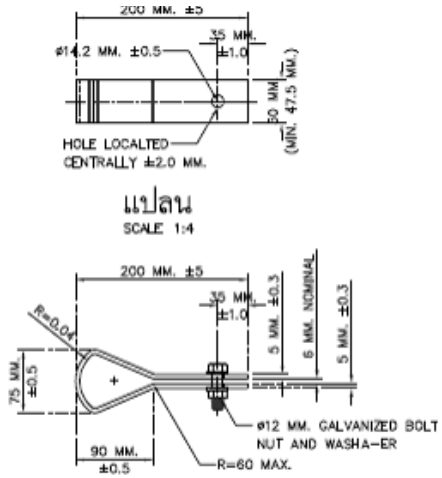

Figure 7.The connection between concrete facing and steel strip reinforcement

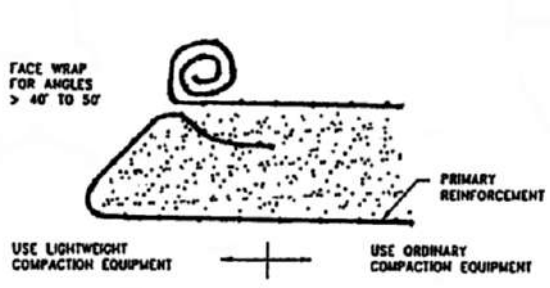

Figure 8.The wrap face construction of geogrid reinforcement

Figure 9.The wrap face construction of geogrid reinforcement

6 NUMERICAL SIMULATION AND STAGED CONSTRUCTION

PLAXIS 3D (Version 2011) was utilised as the 3D FEM numerical simulation tool for the embankment.In order to minimise the effects of test embankment boundaries, the PLAXIS 3D discretisation was formulated and the boundary conditions were specified at distances of two times the length and width of the reinforced embankment in the x and y directions, respectively, as well as at a distance of four times the height of the reinforced embankment in the z direction. A finite element mesh was created (Fig. 10) to carry out the finite element analysis of the embankment using PLAXIS 3D, and the material properties of the embankment components were established (Table 5). The generation of an appropriate finite element mesh and the generation of properties and boundary conditions on an element level were automatically performed by the PLAXIS mesh generator based on the input of the geometry model. The total number of elements and nodes in PLAXIS 3D model was found to be 101325 and 148547, respectively whereas the average size of the element was found to be 1.646m. Soil properties as determined from tests on samples from four boreholes were used as the main inputs for the foundation soils in the FEM model. The water level was fixed at 2 m below the ground surface. The polymeric and metallic reinforcements were characterised as geogrids, with their corresponding properties, whereas the precast concrete panels were characterised as plate elements. A surcharge load equivalent to 1.2-m-thick fill was placed at the top of the embankment 113 days after the start of construction and the modelling was allowed to run for 186 days (125 days for construction and 61 days for consolidation analysis). The total period (186 days) was divided into 16 stages for the modelling of the mechanically stabilised earth wall. The staged construction and consolidation stages were modelled by placing the backfill material, along with the corresponding reinforcement, at incremental depths of 0.5 m per stage, until the embankment reached its sufficient height, followed by 0.25 m of cover. The embankment was then loaded with a surcharge equivalent to a 1.2-m-thick fill 113 days after the start of its construction, and consolidation was allowed to proceed for 61 days. The loading time curve is plotted in Fig. 11.

Table 5. Material conditions and parameters used in PLAXIS 3D.

Soil Description	Model	Condition	γ_{sat} (kN/m^3)	γ_{unsat}(kN/m^3)	υ	E (kPa)	c' (kPa)	Φ' (^{o})	k_x (m/day)	k_y (m/day)
Backfill	M-C	Drained	22.7	21	0.3	20,000	10	37	0.8	0.4
Clayey sandy silt to clayey silty fine sand	M-C	Drained	19	17	0.3	18,000	1	33	0.001	0.0005
Medium dense clayey sand	M-C	Drained	18	16	0.3	37,500	5	34	0.001	0.0005
Stiff to very stiff clay	M-C	Undrained A	17	15	0.35	40,000	50	24	0.00002	0.00001
Very stiff clay	M-C	Undrained A	17	15	0.35	50,000	80	26	0.00004	0.00002
Hard clay	M-C	Undrained A	17.5	15.5	0.35	80,000	100	28	0.00004	0.00002

Note: Undrained A uses the effective parameters for stiffness and strength in PLAXIS 3D.

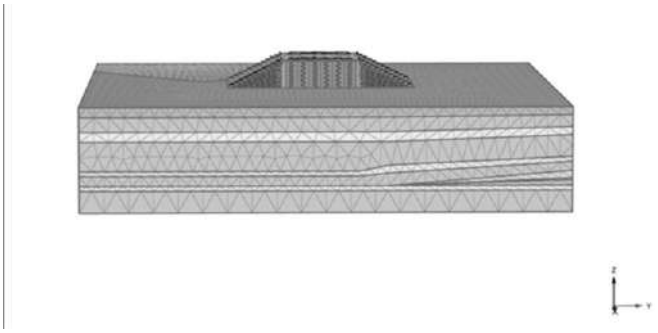

Figure 10.3D Discretisation model of MSE wall/embankment.

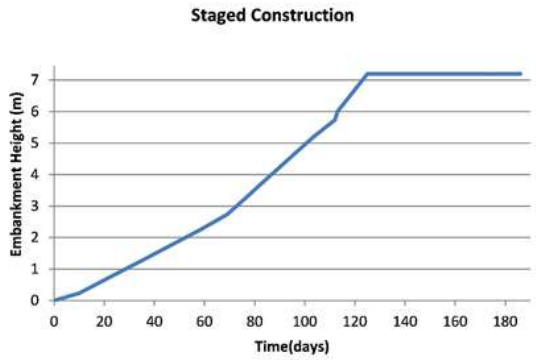

Figure 11. Construction details of MSE wall/embankment.

7 RESULTS AND DISSCUSSIONS

7.1 Lateral Deformation

The lateral deformation of each type of polymeric reinforcement (i.e., PET, PP and HDPE) on the RSS side and each type of metallic reinforcement (i.e., MS and SWG) on the MSEW side obtained from field measurements using inclinometers is compared with the numerical simulation results at 186 days after the end of the construction. Inclinometers I3 and I5 refer to the inclinometers installed in the PE and MS, respectively. Figures 12 and 13 show the measured and simulated lateral deformations of the PE (on polymeric side) and MS (on metallic side) reinforcement, respectively. Large lateral displacements at the top of the PP, PET, and HDPE geogrid reinforcement (i.e RSS facing) at 186 days were noted after the 1.2-m-thick surcharge was added.The horizontal field deformation indicated by inclinometers for all polymeric and metallic reinforcements agreed well with simulation data and larger deformation were noticed for successfully simulated polymeric reinforcements in comparison with metallic reinforcements due to higher stiffness of the metallic reinforcements. In addition, larger deformation was observed on the top of the embankment after the 1.2-m-thick surcharge has been added, which was confirmed by tilting of embankment on topmost part in field too as shown in Fig. 14.In general, the simulation results agreed well with the field observations and polymeric reinforcements were successfully simulated than metallic reinforcements in terms of lateral deformation.

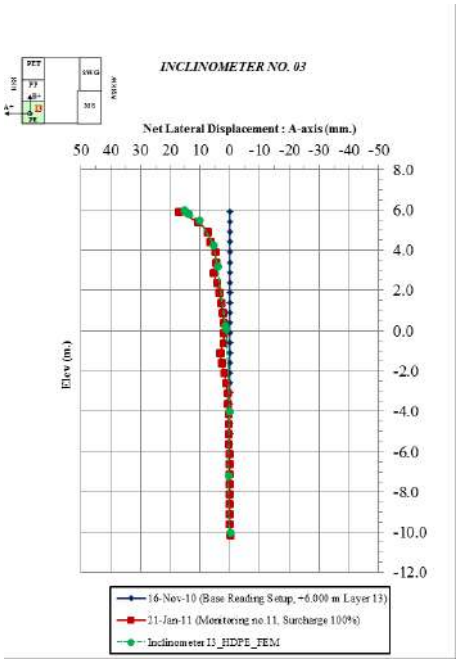

Figure 12.Inclinometer readings at the facing of the high-density polyethylene (HDPE) geogrid reinforcement.

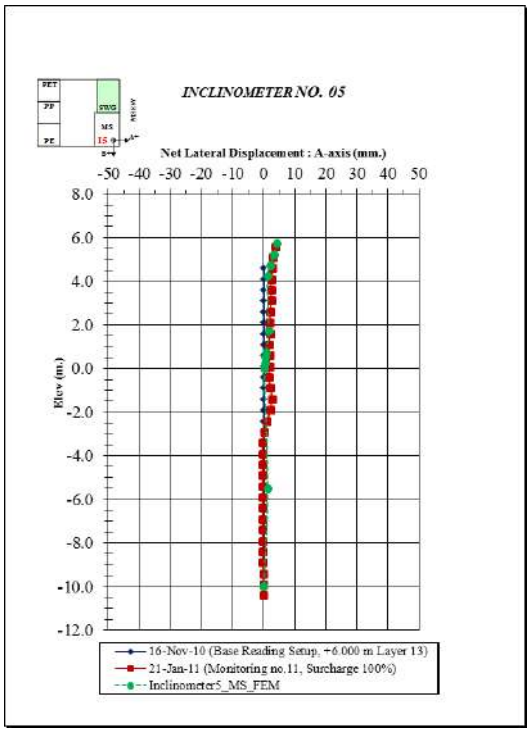

Figure 13. Inclinometer readings at the facing of the metallic strip (MS) reinforcement.

Figure 14. Figure showing tilt of inclinometer at the top of RSS facing.

7.2 Vertical Deformation

Surface and subsurface settlement plates were installed in the embankment at different locations to measure vertical settlements. The maximum settlement at the base of the embankment (Level 0.00 m) ranged from 60 to 80 mm 186 days after construction. The compression of the foundation was found to increase slightly towards the facing, as shown in Fig. 15a for the PE-MS section. Similarly, the compression of the embankment (Level 0.00 m to Level 5.50 m) varied between 20 to 40 mm, as shown in Fig. 15b, 16b and 17b for the PE-MS section. Due to the hard ground foundation, the magnitudes of the vertical settlements were relatively low. The settlement profile of the PE-MS section at different levels of the embankment (0.00 m at the base of the embankment and 5.50 m at the top of embankment) are plotted together with the simulated data in Fig. 15a,b. Overall, the simulation results are consistent with the vertical deformations measured in the field and the value of settlement is found to be low as the embankment was constructed on hard ground.

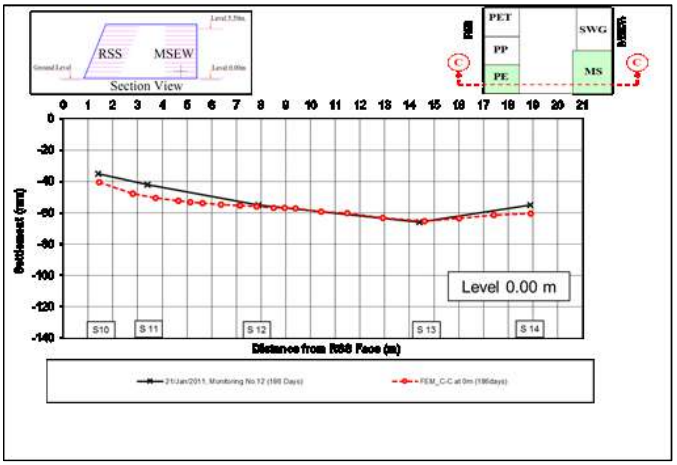

(a) Compression of the foundation 186 days after construction (Level 0.00 m).

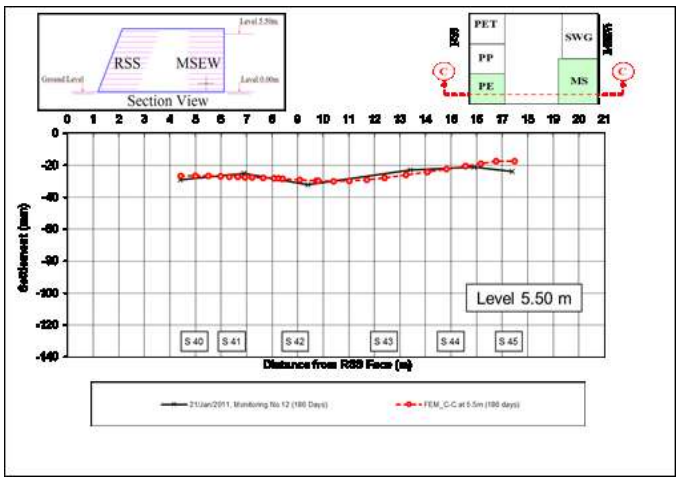

(b) Compression of the embankment (Level 0.00 m to Level 5.50 m) 186 days after construction.

Figure 15.Compression profile of the PE-MS section.

7.3 Strains in the Reinforcements

The measured and simulated strains in the metallic and polymeric reinforcement were in good agreement. The strains were measured using vibrating-wire strain gauges in the metallic reinforcement (SWG and MS) and using fibre optic strain gauges in the polymer geogrids (PET, PP and HDPE). For the metallic reinforcement, the strains were lower than the geogrid strains because the metallic reinforcement was much stiffer than the polymer geogrids. The measured and simulated strains in the metallic strips (MS) after 125 and 186 daysare plotted in Fig. 16whereas the corresponding strains in the polymer geogridHDPE are plotted in Fig. 17. In general, good agreement was observed between the measured and simulated strains. The line of maximum strain corresponded to bilinear rather than linear behaviour.Theoretically, the strains should be zero at the end of embankment (at a distance of 5m from the facing) but due to the difficulties and inaccuracies associated with sensitive strain gauges, there is certain value of strain at the end of reinforcements (see Figs. 16 and 17).

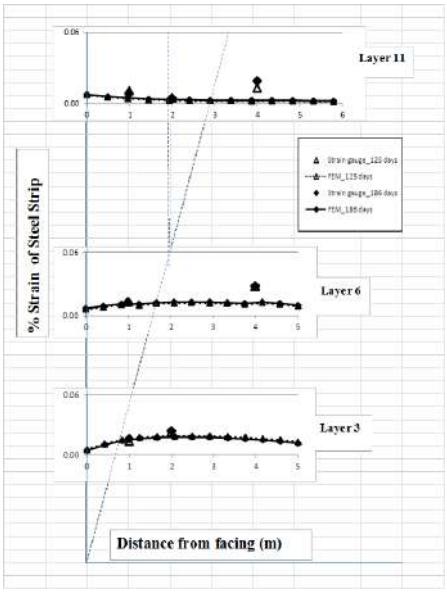

Figure16.Strains in metallic strip (MS) reinforcement.

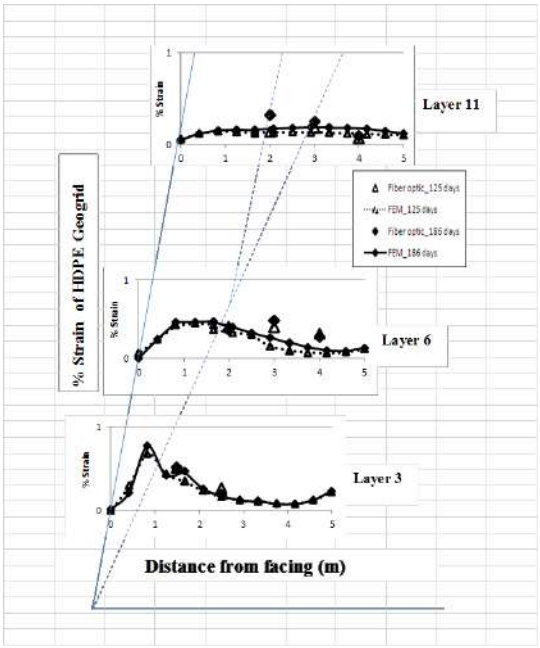

Figure17.Strains in high-density polyethylene (HDPE) geogrid reinforcement.

7.4 Total Pressure Cells

Total pressure cells were installed at various locations at the base of the embankment at level 0.00 m (see Fig. 18). The total pressure cell TP2 indicated that the highest total pressure measured was 275 kPa after 186 days, while the maximum total pressure recorded by TP5 was 175 kPa. These values are abnormally higher than the weight of the embankment. The pressures measured by TP1, TP3, TP4 and TP6 ranged from 130 to 150 kPa, which are consistent with the weight of the embankment. The variation in the total pressures measured by the 6 pressure cells at ground level are compared with the results from the 3D simulations in Fig. 18. There was an unexpectedly high value recorded for TP2, which might have been due to some problem with the instrumentation. This issue can be confirmed by plotting the polynomial distribution of total pressures from each of the pressure cells with respect to embankment height, as shown in Fig. 19. The total pressures after surcharge and after consolidation were almost constant and good agreement between the measured and simulated values were obtained.

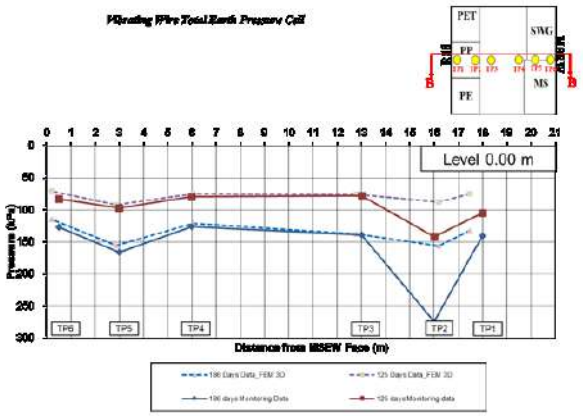

Figure 18. Observed data from total pressure cells 125 days and 186 days after the start of construction.

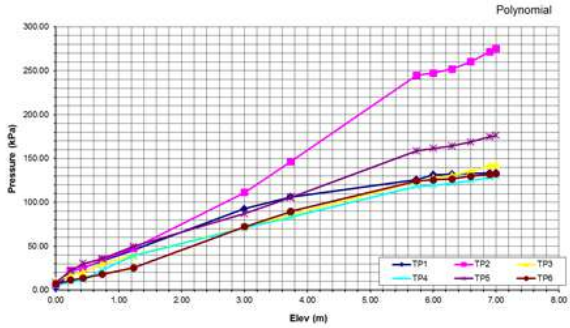

Figure 19. Polynomial distribution of total pressures corresponding to each pressure cell.

7.5 Piezometers

The observed pore water pressures were discussed to explain the settlement process of embankment. The predicted pore water pressures by one-dimensional method and Skempton's method were compared to the observed data.

Porewater pressures were obtained from piezometers during and after construction. The build up of excess pore water pressures was observed and the maximum pore water pressure was obtained. The observed excess pore water pressures are plotted in Fig. 20.

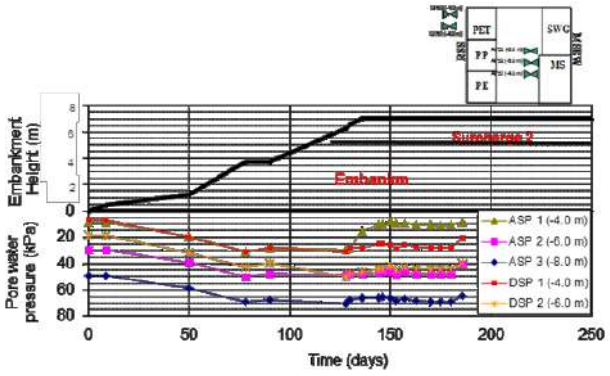

Figure 20.Pore water pressure measurements

8 CONCLUSIONS

A full-scale reinforced embankment was designed and constructed on a hard foundation in Phitsanulok, Thailand, with polymeric reinforcement on one side and metallic reinforcement on the other side. The metallic reinforcement in the mechanically stabilised earth wall (MSEW) facing consisted of metallic strips (MS) and steel wire grids (SWG) whereas the polymer reinforcement in the reinforced steep slope (RSS) facing consisted of polypropylene (PP), high-density polyethylene (HDPE) and polyester (PET) geogrids. The behaviour of both the metallic and polymeric reinforcement was monitored and observed. The lateral and vertical embankment deformations in the MSEW facing were very small, according to the field monitoring results. The deformations of the RSS facing were much greater than those in the MSEW facing because the polymeric reinforcement was not as stiff as the metallic reinforcement. The reinforcing materials can be listed in the following descending order in terms of stiffness: metallic strips (MS), steel wire grids (SWG), polypropylene (PP), high-density polyethylene (HDPE) and polyester (PET). The measured lateral and vertical deformations for both facings, with the different types of reinforcement, agreed well with those predicted from the numerical simulation using PLAXIS 3D. The data from the total pressure cells showed that the total pressures after surcharge (125 days) and after consolidation (186 days) were almost the same and that the measured and simulated values were in good agreement, except for the total pressure measured by cell TP2, which was found to have an instrument error. Furthermore, the strains in the metallic reinforcement and polymeric reinforcement agreed well with the strains predicted from the simulation. The line of maximum strain for both the metallic and polymeric reinforcement exhibited bilinear behaviour as expected. Although the embankment was made up of mixed soils and abrupt changes were noted in the soil profile at the field site, the simulations from PLAXIS 3D were able to simulate the overall embankment behaviour and good agreement was observed between the field measurements and simulation results.

9 ACKNOWLEDGEMENTS

The authors wish to thank the Department of Highway (DOH) and International Engineering Consultants (IEC), Thailand for their support.

10 REFERENCES

Abiera, H. O.(1991)“Mechanically stabilized earth using TENSAR, bamboo and steel grid reinforcements with lateritic soil as backfill”, M. Eng. Thesis GT-90-21, Asian Institute of Technology, Bangkok, Thailand.

Alfaro, M. C.(1996)“Reinforced soil wall-embankment system on soft foundation using inextensible and extensible grid reinforcements”, PhDThesis, Saga University, Japan.

Artidteang, S., Bergado, D.T., Chaiyaput, S and Tanchaisawat, T. (2014) “Embankment reinforced with limited life geotextiles on soft clay”, Ground Improvement(AOP article).

Asanprakit, A.(2000)“Analytical model on the distributions of frictional and bearing resistance as well as deformations of hexagonal wire mesh reinforcement with weathered Bangkok clay backfill”, M. Eng. Thesis No.GE-99-13, Asian Institute of Technology, Bangkok, Thailand.

Cisneros, C. B.(1989)“Pullout resistance of steel grids with weathered clay as backfill material”, M. Eng. Thesis No. GT-88-7, Asian Institute of Technology, Bangkok, Thailand

Kabiling, M. B.(1997)“Pullout capacity of different hexagonal link wire sizes and configurations on sandy and volcanic ash (Lahar) backfills”,M.Eng. Thesis No.GE-96-4, Asian Institute of Technology, Thailand.

Kongkikul, W.(2001)“Numerical and analytical modeling on pullout capacity and interaction of in-soil pullout tests between hexagonal wire mesh reinforcement and silty sand”,M.Eng Thesis, Asian Institute of Technology, Thailand.

Lai, Y. P., Bergado, D. T., Lorenzo, G. A. and Duangchan, T. (2006) “Full-scale reinforced embankment on deep jet mixing improved ground”, Ground Improvement, 10, Issue4, pp153-164.

Long, P.V. (1996)“Behavior of geotextile reinforced embankment on soft ground”,PhD Thesis GE-96-1, Asian Institute of Technology, Thailand.

Mir, E.N.(1996)“Pullout and direct shear test of hexagonal wire mesh reinforcements in various fill materials including lahar from mt. Pinatubo, Philippines”,M.Eng. Thesis No.GE-95-18, Asian Institute of Technology, Thailand.

Modmoltin, C. (1998)“Behavior of hexagonal wire mesh reinforcement in full scale embankment load during pullout test”, M. Eng. Thesis No.GE-97-6, Asian Institute of Technology, Bangkok, Thailand.

Nualkliang, M.(2011)“Behavior of MSE wall/embankment with geogrid and metallic reinforcements on hard foundation”, M. Eng. Thesis No.GE-10-5, Asian Institute of Technology, Bangkok, Thailand.

Prempramote, S.(2005)“Interaction between geogrid reinforcement and tire chip-sand mixture”, M.Eng Thesis No. GE-04-12, Asian Institute of Technology, Thailand.

Rittirong, A.(2003)“Large triaxial test of shredded rubber tire with and without sand mixture and the constitutive model verification”, M. Eng. Thesis No.GE-02-13, Asian Institute of Technology, Bangkok, Thailand.

Shivashankar, R.(1991)“Behavior of mechanically stabilized earth (MSE) embankment with poor quality backfills on soft clay deposits, including a study of the pullout resistances. PhD Thesis, Asian Institute of Technology, Bangkok, Thailand

Srikongsri, A.(1999)“Analytical model for interaction between hexagonal wire mesh and silty sand backfill”, M. Eng. Thesis No.GE-98-14, Asian Institute of Technology, Bangkok Thailand.

Supawiwat, N.(2002)“Behavior of shredded rubber tires with and without sand, its interaction with hexagonal wire reinforcement and their numerical simulation”, M.Eng. Thesis GE-01-14, Asian Institute of Technology, Thailand.

Tanchaisawat, T.(2008)“Interactions and performances of geogrid reinforced tire chips-sand lightweight embankment on soft ground”, PhD Thesis No.GE-07-01, AIT, Bangkok, Thailand.

Tin, N. (2009)“Factors affecting the kinked steel grid reinforcement and modification of K-stiffness Method in MSE structures on soft ground”, M. Eng. Thesis No.GE-08-03, AIT, Bangkok, Thailand.

Visudmedanukul, P(2000). “FEM analysis on the interaction mechanism between hexagonal wire mesh reinforcement and silty sand backfill”, M. Eng. Thesis No.GE-99-6, Asian Institute of Technology, Bangkok, Thailand.

Voottipruex P.(2000)“Interaction of hexagonal wire reinforcement with silty sand backfill soil and behaviorof full scale embankment reinforced with hexagonal wire mesh”,PhD Thesis No. GE-99-01, Asian Institute of Technology, Thailand.

Wongsawanon, T.(1998)“Interaction between hexagonal wire mesh reinforcement and silty sand backfill”, M.Eng. Thesis No. GE-97-14, Asian Institute of Technology, Thailand.

Youwai, S. (2003)“Strength and deformation characteristics of reinforced rubber tire chip with and without sand mixtures and its application on reinforced wall simulation”,PhD Thesis No. GE-03-2, Asian Institute of Technology, Bangkok, Thailand.

SUBGRADE SOIL STABILISATION USING NATIVE VEGETATION

M. Pallewattha[1], B. Indraratna[2], B. Fatahi[3],C. Rujikiatkamjorn[4] and U. Pathirage[5]

1 PhD Candidate, School of Civil, Mining & Environmental Engineering, University of Wollongong, Australia. E-mail: map804@uowmail.edu.au

2 Professor of Civil Engineering, School of Mining and Environmental Engineering
Research Director of Centre for Geomechanics and Railway Engineering, University of Wollongong, Wollongong City, Australia, E-mail: indra@uow.edu.au

3 Senior Lecturer of Geotechnical Engineering at University of Technology, Sydney. Australia, E-mail: behzad.fatahi@uts.edu.au

4Associate Professor, Centre for Geomechanics and Railway Engineering, University of Wollongong, Wollongong City, Australia
5Research Fellow, School of Civil, Mining & Environmental Engineering, University of Wollongong, Australia.

ABSTRACT: Current demand of infrastructure facilities along metropolitan areas has led to construction of earth structures, major highways and railways on soft soils. Subsequently civil engineering is in a more challenging situation to discover more cost effective, reliable and sustainable methods for ground improvement. The green corridor concept, or ground improvement using native vegetation, can be considered as often a more effective method. Even though this is considered as a new idea, the use of vegetation in hill slopes to prevent erosion and to give some stability has long been known, but without proper engineering quantification of the stabilisation. Trees are capable of increasing the matric suction of the soil subgrade underneath the substructure throughroot water uptake, in conjunction with the tree canopy evapotranspiration. At the same time, these trees are capable of providing significant mechanical reinforcement through the anchoring effect provided by the root network plus the additional cohesive increment due to hair roots generating osmotic suction.

Much of the previous research carried out to quantify the mechanical strength generated by tree roots has been mainly based on empiricism. Empirical relations have been developed for given tree species grown under known soil conditions. The extrapolation of such empirical relations from one tree-soil system to another can be misleading. At the same time, the effect of transpiration by the tree canopy and its influence on the sustained suction equilibrium generated at the root zone for stabilising soft subgrade has not been considered rationally in the design of rail corridors. To accommodate the above natural phenomena, a novel and rational computational model has been developed to quantify the overall suction effect provided by the tree roots and its continual link with the rate and magnitude of canopy evapo-transpiration. Root based suction of a tree improves the shear strength and accelerates the pore water pressure dissipation. In addition it may alter the potential failure conditions of the soil-root system from a saturated to an unsaturated domain. Therefore, it is necessary for the root based suction and the mechanical properties of the root network to be analysed within a coupled multiphase framework. Accordingly, this paper will present a model developed to capture the root based suction and the importance of the combined effect of the root reinforcement and suction.

1 INTRODUCTION

Ground improvement using native vegetation is an economic, environmental friendly and expedient, method which can be used in most geotechnical engineering projects after a thorough engineering quantification of subsequent effects. In the process of 'Ground improvement using native vegetation' tree roots look after the most important fragments of the process.

Tree roots provide mechanical strengthening to the soil by the anchoring effect of the main roots and increase of cohesion due to the hair roots in a similar fashion to geofibres(Fatahi 2007; Fatahi et al. 2012). Moreover, tree roots increase matric suction of soil by means of the root water uptake in conjunction with the evapotranspiration of the tree (Cameron 2001, Fatahiet al. 2014,Potter 2006). Therefore the true effect of the vegetation on the soil stability is accountable by the mechanical strengthening, suction improvement as well as the influence of the suction on mechanical strengthening.

Previous research which has been conducted to quantify the effect of mechanical strengthening of tree roots in slope stabilisation are mainly focused on saturated soil conditions, as well as most of this research has been based on empiricism(Docker 2008; Docker 2009). When a mature tree is under the evapo-transpiration process, tree roots are capable of developing 3MPa root suction at wilting point (Fatahi et al. 2009) and this leads to the enhancement and preserving of the vadose zone. Therefore, most of the time, the sub-soil structure is in the unsaturated condition and the parameters calculated for the saturated condition may not represent realistic behaviour. In that case the suction generated on surrounding soil by tree roots is important.

Suction development by a tree directly depends on the tree species, soil condition and other environmental parameters such as temperature, wind speed, humidity since the depth of the root system is determined generally by the above conditions. Therefore a comprehensive understanding about the root system is of utmost importance for in depth study of the effect of suction for soil stabilisation (Cameron 2000)

Because of the complexity and unpredictability of the root system and their subsequent effects on the surrounding soil, engineers were reluctant to use the bio engineering method of strengthening soil using trees in the past. However it has been proven that bioengineering techniques can be effectively used in hill slopes where there are risk of land slides in Australia South East Asia and other tropical regions (Fatahi 2007)

1.1 Root Systems

The functions of roots include anchorage, the absorption of water, minerals and nutrients, synthesis of various essential compounds such as growth regulators and the storage of food in root crops (Weaver 1958). At the same time tree roots give more strength to the adjacent soil by means of mechanical strengthening and also by increasing suction. When soil is mechanically strengthened or strengthened with suction effects, the shape of the root system affects directly. It is a known fact that different tree species have different root systems and Soil profile, climate and water availability also affect the depth and the spatial distribution of the root system. Figure 1(a) and (b) show the two main root systems distinguished in trees.

Many root systems in trees in well-drained soil look like the shape in figure 1(a). There is a combination of lateral and oblique roots and no real tap root. Only a small percentage of tree root systems look like the shape in figure 1(b). (Kramer 1995)

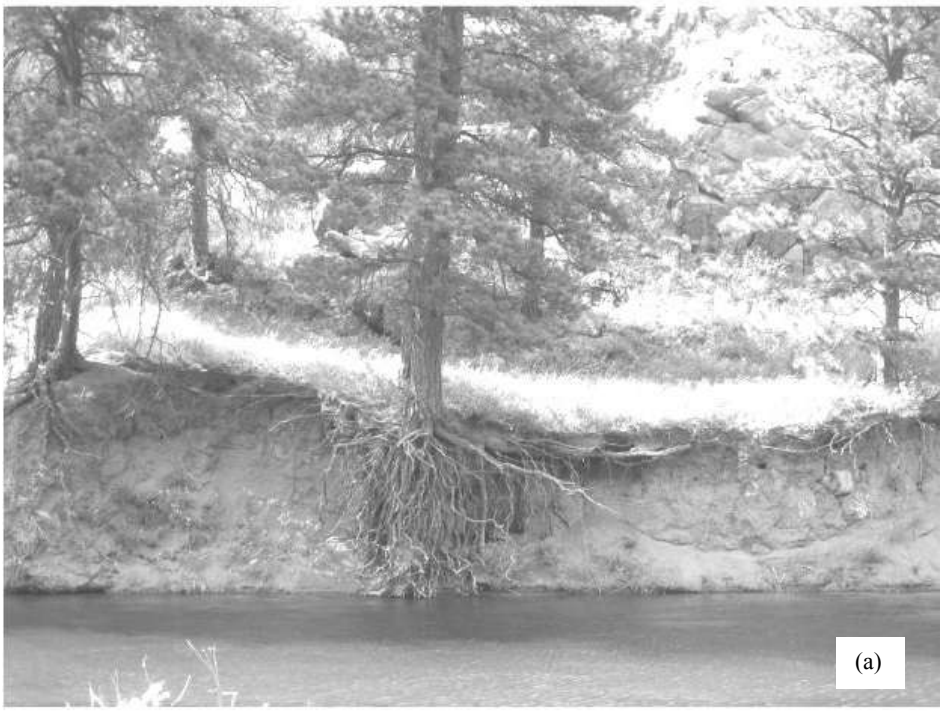

Figure 1 (a) Fibrous root system (b) Tap root system

1.2 Environmental Factors Affecting the Root Growth

Environmental factors which affect the growth of tree roots are soil texture and structure; aeration; moisture; temperature; pH; salinity; the presence of toxic elements such as lead, copper, aluminium; competition with other plants and presence of bacteria, fungi and soil inhabiting animals. (Weaver 1958)

Soil texture and structure

Root growth is affected by properties of the soil, directly due to root penetration restrictions and indirectly due to the aeration and water content. Figure 2 shows the different spatial distribution of roots due to different compaction levels in soils.

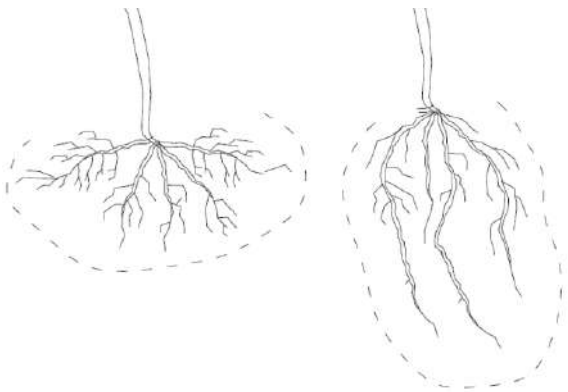

Figure 2. Root system of young barley plants grown in the field in soils with different bulk densities (Left) 1.35 g cm $^{-3}$; (right) 1.50 g cm $^{-3}$. (modified after Gilmen 1980)

Aeration

To have good spatial distribution of root system proper gas exchange in the soil has to be confirmed. Pore structure inside the soil has a great influence on gas exchange inside the soil. Furthermore poor oxygen levels in the soil leads to poor root growth as well as the poor nitrogen level in the soil can limit the nitrogen fixation of roots by legume. Weaver (1958)

Temperature

Optimum temperature which is suitable for vegetation makes maximum spatial distribution of root system. Figure 3 clearly shows the effect of temperature on shape of the root system.

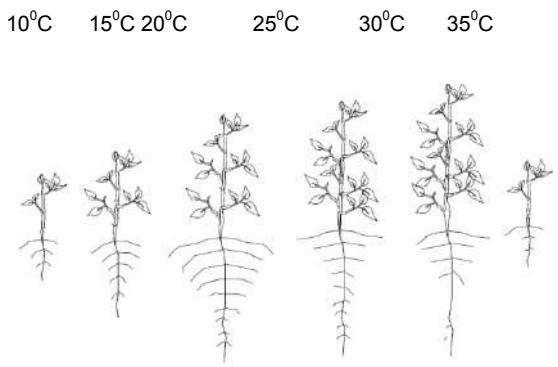

Figure 3. Influence of root zone temperature on root morphology and shoot growth of potato seedlings (modified after Sattelmacher et al. 1990)

Moisture

The Growth of the root system is directly affected by the amount of soil water availability. Excess or deficiency of soil water reduces the growth of root. Excess water limits root growth due to reduction of oxygen level in soil and deficient water levels can cause reduction as well as the cessation of root growth. Moreover the occurrence of the wilting level leads to the permanent death of the root system. Therefore the soil water potential is a dominant factor in root distribution. Figure 4 shows the root depth variation due to the different rail fall precipitations.

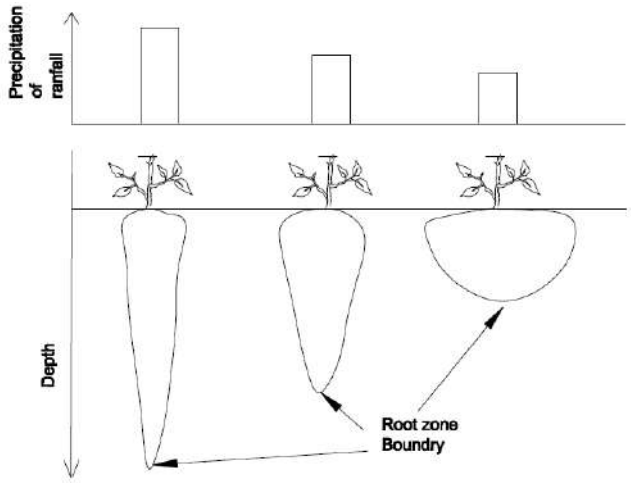

Figure 4. The effect of the amount of rainfall on the depth of rooting of winter wheat (very fine sandy loam - silty loam in the Great Plains)(modified after Weaver 1958)

Root competition

The size of the root system depends on the availability of adjacent plants. The presence of competition in root systems tends to reduce the spatial retribution of roots. Although roots often seem to be intertwined in the soil, there is evidence of a mechanism that prevents root from some kind of plants growing very close to one another. Waisel et al. (2002)

1.3 Measurements of Root Systems

Since there is a high variance of root systems even in the same tree species, measuring of the root system is more important in research projects so that root architecture may be reasonably predicted by practitioners. Most well known methods of measuring root systems are excavation, auger, monolith, profile wall, glass wall and radioactive tracers. Other than radioactive traces, these methods involve tedious excavation process. Some of these methods which are explained in Böhm (1980) and Waisel et al. (2002) are as follows;

Excavation

Excavation is good for trees and shrubs on stiff and dry sandy soils than it is for grass or annual corps. A deep trench is dug with vertical sides in some distance from root and soil is removed applying compressed air parallel to the root since root exerts maximum force parallel to their growth direction. While doing so, figures should be drawn and photographs should be taken to interpret the more reasonable root system.

Monolith

Monoliths of root system are to be taken away through the side of a trench which is 1m long and deepened to the maximum root depth. Metal sheets are driven into the root system through the trench wall are used to extract the monoliths. Then soil is separated from the roots by washing and photographs are taken.

Auger

A hand auger or any other mechanical means is used to obtain the samples with least disturbance to the root system. Samples are broken horizontally and washing is done to separate root from soil.

Profile wall

This method root mapping is done through the trench wall ,which is dug to the required length and depth. No collection of roots is done and if the dry weights of the roots are required, another method has to be incorporated.

Glass wall

A glass wall is placed along the trench wall contacted with the root system and root mapping is done.

Radio active traces

A radio active tracer to be injected to the stem of the plant and soil-root sample is taken to measure the radioactivity.

Trees grown in different areas with different environmental factors display quite different root systems, Nevertheless the root based suction which is able to be applied on the adjacent soil system by a mature tree, is approximately 10 times greater than the practical vacuum for prefabricated vertical drain (Indraratna et al. 2008). Therefore this paper aims to present the model developed to capture the root based suction in conjunction with evapotranspiration and the importance of the combined effect of root reinforcement and suction.

2 SUCTION EFFECT OF TREE ROOTS ON SOIL.

Root water uptake of trees increases the metric suction of adjacent soil due to reduction of the moisture content. Some tree varieties like Pinusradiata can absorb water from soil up to its own weight per day (Teskey, and Sheriff 1995)and some of the mature trees can generate suction in soil- root systems up to 3MPa (Fatahi 2007). The main factor that affects the root water uptake is rate of transpiration of a tree, since the volume of water consumed by plant cells for metabolism is negligible compared to the total root water uptake (Radclife et al 1980). The rate of transpiration mainly depends on environmental parameters and tree physiology.

2.1 Transpiration of a tree

Transpiration of a tree is affected by the environmental factors like humidity, temperature andwind speed, as well as soil moisture condition (soil water potential) and tree physiology.

Humidity is the amount of water vapour in the air and is usually described as vapour density; pressure or relative humidity. Temperature and wind speed also affect the relative humidity. According to Fick's law of diffusion, the rate of transpiration can be stated as directly proportional to the difference in vapour pressure between the leaf and the atmosphere and inversely proportional to the summation of the resistance to water flow encountered in air (Fatahiet al. 2014).

Temperature regulates the transpiration to high extend through its effect on vapour pressure, if there is no any inhabitant acclimatization in the plant species. A leaf exposed to full sunlight may actually reach 50C to 100C higher than ambient air. If stomata remains open transpiration will occur in a leaf even at 100% relative humidity and vapour get condensed once comes out from the leaf. This is a usual phenomenon in tropical jungles called as "steaming jungle" (Hopkins 1999)

Wind speed controls transpiration through the change of resistance and effective length of diffusion path of water vapour (Nobel 1991). In higher wind speeds, the rate of transpiration increases due to the depletion of the diffusion path and vice-versa. Even though the transpiration of tree leaves are affected by wind speed transpiration is also subjected to the inhabitant acclimatization in the plant species.

Soil condition also affects the rate of transpiration of a tree. Soil water potential inversely affects the rate of root water uptake (S). Soil suction relates to the soil moisture content through the soil water characteristic curve. Therefore water uptake reduction factor is a function of moisture content of the soil (Fatahiet al. 2010). A model suggested by Feddes et al. (1974) for root water uptake reduction factor in relation to soil moisture content is shown in Figure 5.

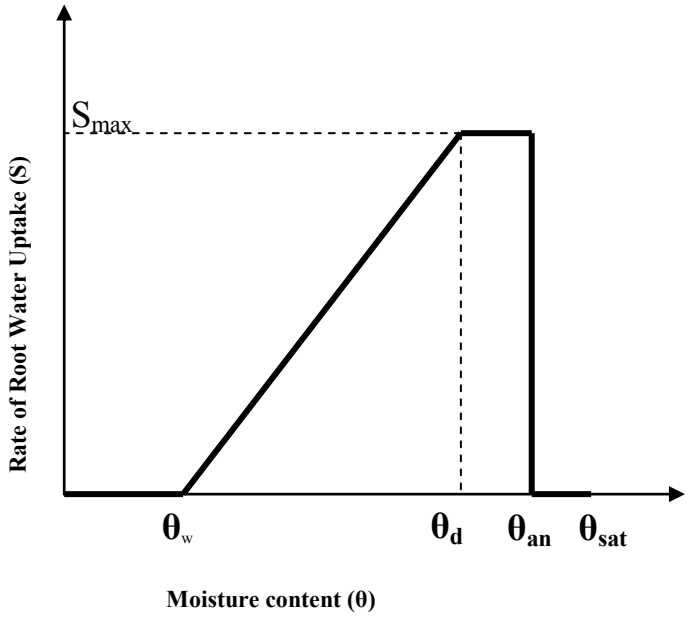

Figure 5.The water uptake – moisture content relationship Feddes et al. (1974)

in this Figure, θ_w is the moisture content at wilting point, θ_d is the minimum moisture content at $S = S_{max}$, θ_{an} is the maximum water content at maximum root water uptake. There are numerous equations to quantify root water uptake reduction factor due to soil suction.

Tree physiology also affects the transpiration. Factors controlling transpiration include leaf area, number of stomata in a leaf and other biological features of the tree,. The total transpiration rate of a plant can be calculated by adding all the transpiration rates of leaves on the plant which means the higher the leaf area, the rate of transpiration is also higher. Based on Green (1993), the transpiration of a whole plant can be calculated using;

$$T_P = \sum_i f_i \left[\frac{sR_{n,i} + 0.93\rho_a C_p D_a / r_{a,i}}{S + 093\gamma(2 + r_{s,i}/r_{a,i})}\right] \quad (1)$$

Where, f_i is the fractional expression of each leaf in terms of the total leaf area of the canopy, $R_{n,i}$ is the net radiation flux density absorbed by each leaf, D_a is the vapour pressure deficit of air, $r_{a,i}$ is the boundary layer resistance of each leaf, $r_{s,i}$ is the stomatal resistance of each leaf, S is the slope of saturation vapour pressure curve at the ambient air temperature, γ is the psychrometric constant, ρ_a is the air density and C_p is the specific heat capacity of air at constant pressure.

2.2 Rate of Root Water Uptake

Rate of root water uptake governs the suction generation on soil by a tree. Root water uptake is done only by active roots of the tree. Tree roots can be broadly classified into two; (a) active roots (b) anchoring roots. Active roots are the smaller roots and absorb water and other nutrients through an osmotic process. Anchoring roots do the main anchoring process of the tree. Rate of root water uptake in a given time varies from a point to point in a root system according to the spatial distribution of the active roots. Therefore a clear interpretation about the active root distribution is essential.

Considering the recent researches by Docker and Hubble (2001), Dabson and Moffat (1995), Fatahi (2007) proposed the following schematic diagram for root shape with a maximum root density is a circle with $r = r_0(t)$ at depth of $z = z_0(t)$ and an exponential reduction in root density in vertical and radial directions

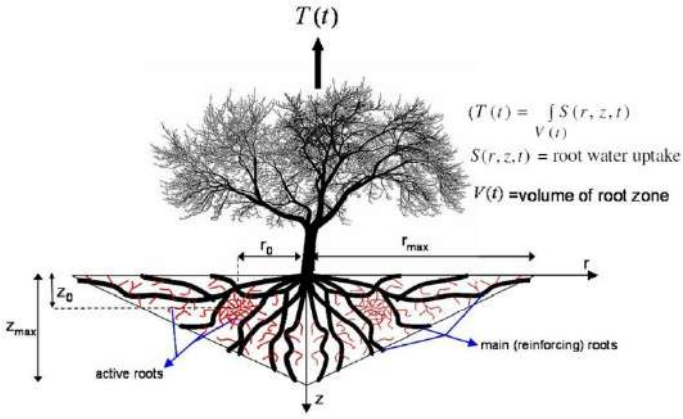

Figure 6. Schematic diagram for soil-plant atmosphere system (Fatahi 2007)

Fatahi et al. (2010) developed an equation for root water uptake at any point of the root zone based on the potential transpiration of the tree and a reduction factor due to suction;

$$S(x, y, z, t) = f(\psi)G(\beta)F(T_P) \quad (2)$$

where, $f(\psi)$ is computed according to figure 6 of Feddeset al. (1974), $F(T_P)$ is factor related to the potential transpiration referred to model developed by Nimah and Hanks (1973) where;

$$F(T_P) = \frac{T_P(1 + k_4 z_{max} + k_4 z)}{\int_{v(t)} G(\beta)\,(1 + k_4 z_{max} + k_4 z)dv} \quad (3)$$

G(β) is root density effect which is directly dependent on tree species and soil condition and k_4 is an experimental coefficient (Fatahi et al. 2014),

$$G(\beta) = \frac{\tanh(k_3\,\beta(t))}{\int \tanh\big(k_3\,\beta(t)\big)\,dv} \tag{4}$$

In equations 2,3, 4 and 5 k_1 ,k_2, k_3 and k_4 are experimental parameters and β(x,y,z,t) is the root density at time in a given point which can be calculated using equation 5

$$\beta(x,y,z,t) = \beta max(t) e^{-k1(t)|z-z0(t)|-k2(t)|r-r0(t)|} \tag{5}$$

Figure 6.shows the initial root water uptake rate developed by Fatahi (2007) using the values for experimental coefficients related to a poplar tree.

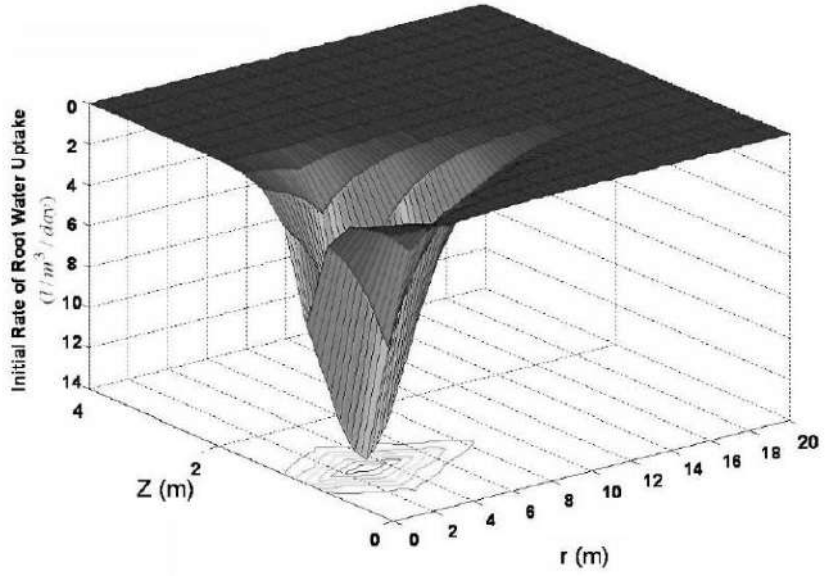

Figure 6. Initial distribution of root water uptake of a poplar tree (Fatahi 2007)

2.3 Suction Development in Soil through Root Water Uptake

Fatahiet al. (2009) developed an unsaturated flow equation using Darcy's Law and Reynold's differential transport theorem with root water uptake as a sink term and it is as follows;

$$\frac{\partial\theta}{\partial t} = \nabla.(k\nabla\psi) - \frac{\partial k}{\partial z} - S(x,y,z,t) \tag{6}$$

where k is hydraulic conductivity ψ is soil suction, z is vertical co-ordinate and t is time. S(x,y,z,t) is root water uptake. Equation 6 can be applied for homogeneous as well as heterogeneous media.

Equation 6 can be used to calculate the instantaneous moisture content according to the root water uptake and the subsequent suction values can be computed by relating to the appropriate soil water characteristic curve which represents the suction variation with respect to the moisture content variation in particular soil

Two dimensional finite element analysis has been conducted by Indraratna et al. (2008) for given soil parameters using governing equations and the developed model verification was done for several case studies. Figures 7,8,9 show the suction values computed using the ABAQUS finite element model for the parameters of Fredlund and Huang's (2001) analysis.

The increasing of suction with time leads to the shear strength improvement of soil and at the same time root water uptake due to transpiration leads to the fast dissipation of pore water.

Above model captures the suction improvement of soil due to transpiration of a tree, but it does not capture the root reinforcement effect which is more significant in shear strength improvement of soil by vegetation.

3 MECHANICAL STRENGTHENING WITH ROOTS.

Tree roots are capable of binding the soil matrix together. Therefore, it gives the fibrous effect to the soil to have good erosion control and to prevent shallow failures within1.5-2.0m (Bache et al. 1989). At the same time large tree roots are capable of providing anchoring effect to the soil. According to the past studies, amount of root materials present in the shear plane is the governing parameter of the reinforcement contribution to the soil. The amount of root material available in the soil is defined as Root Area Ratio (RAR).

$$\text{Root Area Ratio (RAR)} = \frac{Area\ of\ Root\ Along\ the\ Shear\ Plane}{Area\ of\ the\ shear\ Plane}$$

Effect of the tree roots on shear strength increment of soil has been discussed and examined during past few decades by various researchers in different ways and some of them are discussed below

Waldron (1977) defined the increment of shear strength ΔS value and Figure 10 shows the model of flexible elastic root extending vertically thorough a horizontal shear zone.

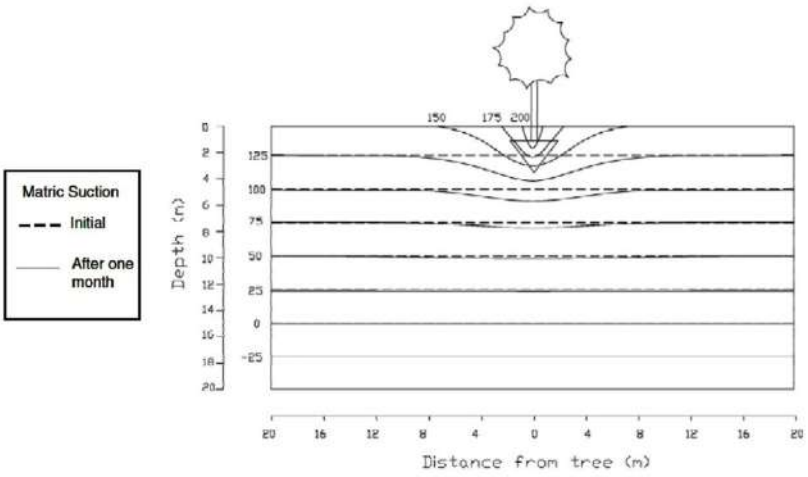

Figure 7.Variation of Matric suction after one month. (Indraratna et al. 2006)

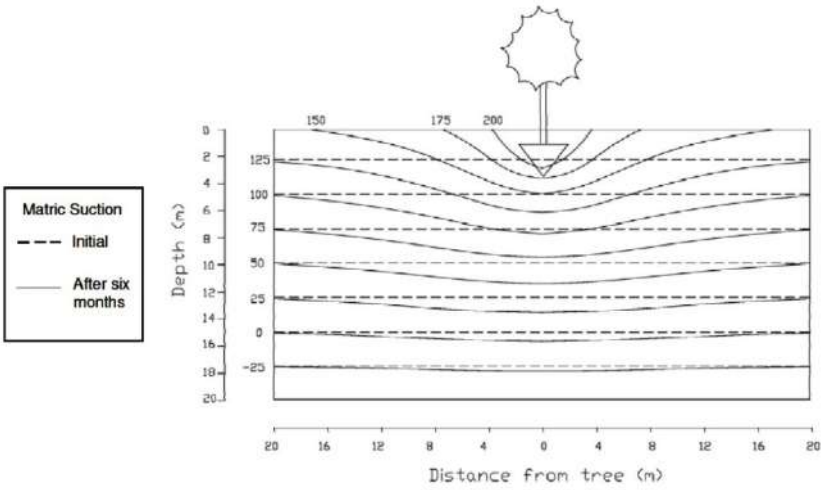

Figure 8.Variation of Matric suction after six month. (Indraratna et al. 2006)

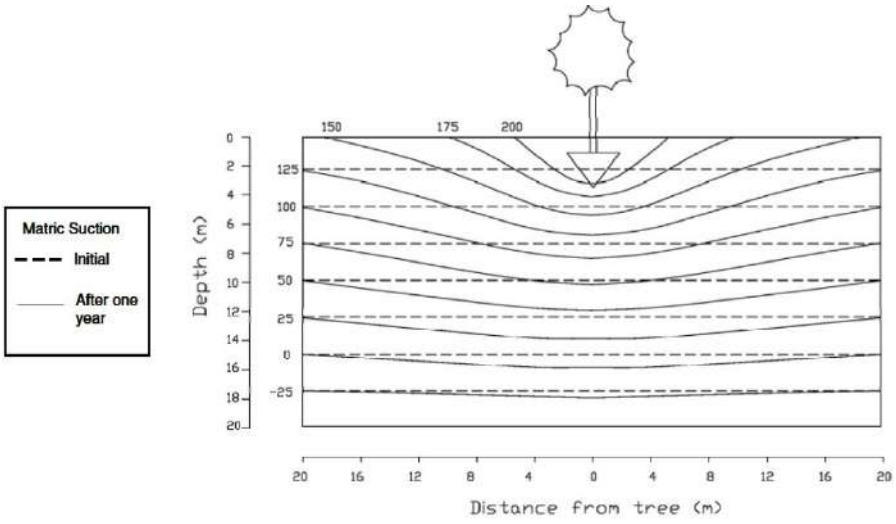

Figure 9.Variation of Matric suction after one year. (Indraratna et al. 2006)

.

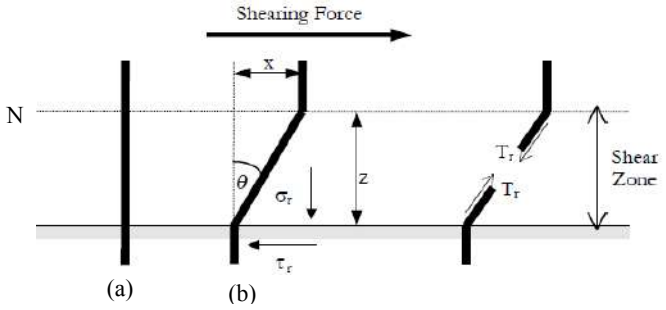

Figure 10. Model of flexible elastic root extending vertically thorough a horizontal shear zone of thickness Z (a) Undisturbed soil (b) Soil above N displaced by x.

According to Waldron (1981),increment of the shear strength (ΔS) can be directly added to the coulomb equation since there is no change in friction angle.

$$\tau = c + \Delta S + \sigma_N \tan\phi \quad (7)$$

In Waldron (1977) model, failure modes of root system were defined as (a) stretching (b) slipping (c) breaking. Three different ΔS values which depend on the tensile strength of roots, bond strength between root and soil and dimensional parameters of roots were introduced for above three different failure modes of roots.

Further, Operstain (2000) obtained and equation for apparent cohesion induced by tree roots

$$\Delta C = k_r T_r(r,z,t) \quad (8)$$

where ΔC is apparent cohesion due to tree roots, Tris the relative root tensile strength contribution and k_r is an experimental constant. The value of the T_r is influenced by root area ratio and the tensile strength of roots and diameter. Further (Operstain and Frydman 2000) described T_r as follows;

$$T_r(r,z,t) = T_i(r,z,t)R_a(r,z,t) \quad (9)$$

whereT_i is the tensile strength of root and $R_a$is the root area ratio, which is the root cross section for the unit area of soil in the failure surface. According to (Operstain and Frydman 2000) T_i can be computed using following equation,

$$T_i(r,z,t) = Ae^{-m1d(r,z,t)}$$

where A and m1 are experimental coefficients and d(r, z, t) is the average root diameter at point (r, z) at time t.

All the above models have been developed for a vertical root. Therefore the practical applications are limited due to the more complex spatial distribution of root systems.

(Docker and Hubble 2008) developed more empirical based equations for four Australian tree species considering progression root failure. Increment of the shear strength of soil due to root system was determined by in-situ field direct shear test of Casuarina glauca, Eucalyptus amplifolia, Eucalyptus elata and Accacia floribunda. Empirical equations for increase in shear strength S_r(KPa) due to root system of each tree species against root area ratio (RAR) are as follows;

Casuarina glauca	$:S_r = 60.61RAR - 1.78.$
Eucalyptus amplifolia	$: S_r = 38.12RAR + 0.85$
Eucalyptus elata	$: S_r = 47.44RAR + 0.07$
Accacia floribunda	$: S_r = 116.43RAR + 8.25$

In the above study it was observed that the amount of shear increment computed by the (Waldron 1981) model was 50% more than the experimental values. Therefore (Docker and Hubble 2008) introduced a model with three stage failure of roots as in Figure 11.

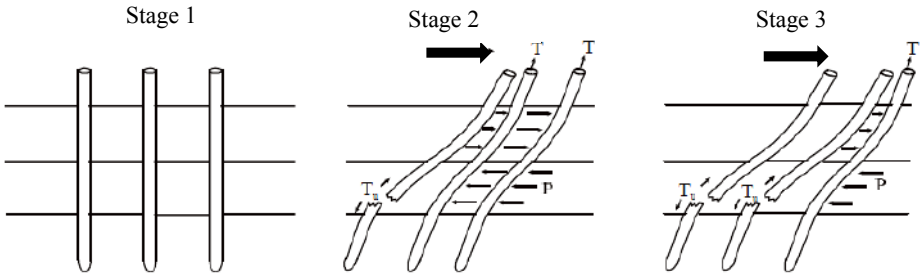

Figure 11.Three stages of failure of root reinforcement for three idealized and identical roots as estimated from the results of direct in-situ shear tests conducted in this investigation. (modified after Docker and Hubble2001)

Three stages of failures are; stage 1: Prior to application of an applied shear force the roots are at rest across the potential shear plane. In the simplest model they are assumed to extend perpendicular to this plane; stage 2: An applied shear force causes deflection of the roots in a wide shear zone. At this stage the majority of roots provide resistance through a tensile force (T) that is mobilised as soil pressure (P) which acts against the root; stage 3: Sufficient displacement of the block has mobilised the full tensile strength (Tu) in a sufficient quantity of roots to cause a reduction in measured shear resistance.

As stated earlier in-situ shear tests have been conducted by Docker & Hubble on blocks of soil containing roots of the four riparian tree species and Figure 13 shows the plots of average shear stress versus displacement for each species. They show that the greatest shear resistance is provided by A. floribunda, followed by E. elata, E. amplifolia, and then C. glauca although there is very little discernible difference between these latter three species. The most likely explanation is the much higher tensile strengths recorded for A. floribunda roots in comparison to the other three species.

With the observation of above test results (Docker and Hubble 2009) described two types of roots systems according to the generated shear resistance against the block displacement. Figure 12 show the sketch of two types of root system and Figure 14 displays main features of variation of the two types.

Type 1;root systems that reached a maximum shear resistance before the conclusion of testing and exhibited a definite decrease in resistance as displacement increased.

Type 2;root systems those that either reached a maximum resistance or recorded no reduction from that level, or blocks where the shear

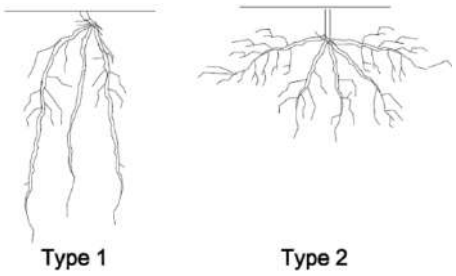

Figure12. The distinct root morphology through an in-situ shear test-block resistance continued to increase for the duration of the test.

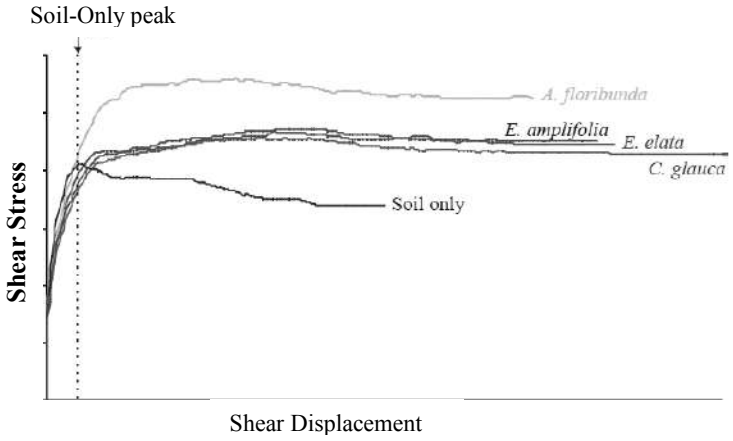

Figure 13.Shear stress versus displacement plots for the four tree species and the soil-only tests (modified after Docker and Hubble 2008)

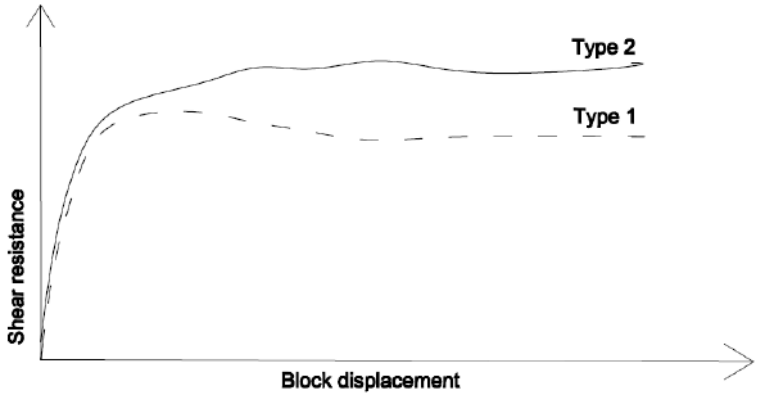

Figure 14.Diagrammatic representation of two generally distinct root system behaviors at direct shearing. (modified after Docker and Hubble 2009).

According to the above facts it is discernible that the spatial distribution of root acts as a major role, despite all the other factors in reinforcing soil. There is no type 1 or type 2 trees which can be distinguished in the environment by the species. The true tree root system depends on the environmental factors described in section 1.2.

4 DISCUSSION

As stated in the introduction most of the time sub soil structure remains as partially saturated state. It is certain that the depth and the degree of saturation of the vadose zone increase in the soil structure which interacts with mature trees. As a result of that, the parameters developed for mechanical strengthening for saturated condition are not realistic. Therefore a combined effect has to be taken into account and parameters should be defined accordingly.

Figure 15 gives a general understanding of improvement in subsoil structure due to combined effect. Soil element A in figure15 is directly under the Railway ballast and Soil element B is in the area of root zone. General unsaturated soil mechanics theories are valid for soil element A and therefore Vanapalliet al. (1996) equation can be sused.

$$\tau = c' + (\sigma_n - u_a)tan\phi' + (u_a - u_w)\,[tan\phi'\left(\frac{\theta-\theta_r}{\theta_s-\theta_r}\right)] \qquad (10)$$

In equation 10 u_a andu_w are pore air and water pressures; θ_s, θ_r, and θ are saturated, residual and instant volumetric water contents and all the other symbols have their usual meaning.

θ value in equation 10, changes with time due to root water uptake and a following equation can be stated considering Fatahi (2007)'s equation and Reynolds differential transport theorem,

$$\frac{\partial \theta}{\partial t} = \nabla.(k\nabla\psi) - \theta\frac{\partial k}{\partial z} - dS(x,y,z,t) + dI(x,y,z,t) \qquad (11)$$

In equation 11 'S' is the Root water uptake sink term and 'I' is the irrigation source term. $\theta$is the volumetric moisture content; k is hydraulic conductivity; ψ is matric suction. At the same time usual soil water characteristic curve can be used for element 'A' .

Element 'B' has great effect from root suction and root reinforcement since it is in the root zone of tree. Therefore usual unsaturated soil mechanics theories cannot be directly used for element 'B'. At the same time stiffness of the root zone results the increasing of shear strength in soil around element A. Therefore it can be defined as a "shear capacity" of the root area zone which acts as an external stiffener with the effect from root reinforcement and suction.

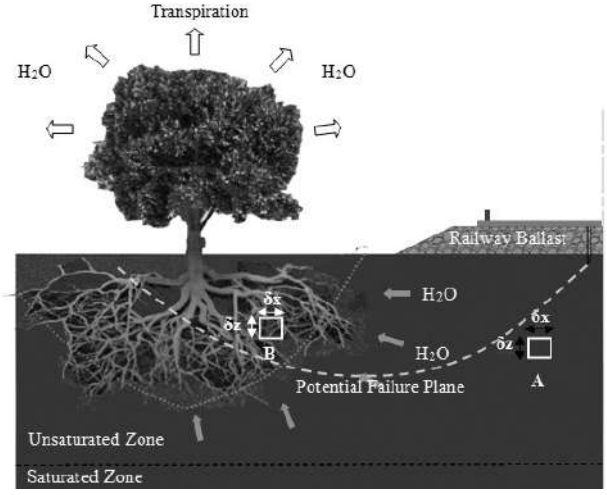

Figure 15 - Schematic diagram of root water uptake process and root reinforcement.

Computing the effects from root reinforcement and suction separately and superimposing them may not give realistic answer since suction has an influence on root reinforcement. Suction changes the bond strength between root and soil as well it alters the material properties of root. In this case the failure of root system due to slipping, stretching, breaking or pulling out with soil annulus are greatly affected by suction induced by tree roots as well as the adjacent soil suction.

5 CONCLUSIONS

Tree roots can be used economically in subgrade improvement after an effective analysis of subsequent effects. Past developed models to compute root based suction and the root reinforcement effect have been contributed considerably for the sub grade improvement, however as described in this paper a comprehensive model which consist of mechanical strengthening as well as root based suction is vital to have more realistic results. Moreover most of the trees are not capable of doing the sub-soil improvement due to their shallow root system and deciduous behaviour. Therefore it is really essential to select the most appropriate plant i.e. good root system and evergreen.

6 ACKNOWLEDGEMENTS

The authors acknowledge funding from the Australian Research Council; industry partners GHD, City of Salisbury and Transport Construction Authority and a number of past PhD students. A substantial component of the technical details presented in this paper can be found in earlier publications by the first author and his co-workers in the Géotechnique, ICE.

7 REFERENCES

Bache, D. H., et al. (1989). " Vegetation In Civil Engineering Construction: Role And Uses." ICE Proceedings 86(1): 247-249.

Böhm, W. (1980)."Methods Of Studying Root Systems." Berlin: Springer (1979), Pp. 200, Dm 69, , Cambridge University Press.

Cameron, D. A. (2000). "Total soil suction regimes near trees in a semi-arid environment " Unsaturated soils for Asia. Proceedings of the Asian Conference on Unsaturated Soils, UNSAT-ASIA 2000, Singapore: 739-744.

Cameron, D. A. (2001)."The extent of soil desiccation near trees in a semi-arid environment." Geotechnical & Geological Engineering 19(3-4): 357-370.

Dobson, M. C. and A. J. Moffat (1995)."A re evaluation of objections to tree planting on containment landfills." Waste management and research 13(6): 579-600.

Docker B. B and Hubble T. T. C. (2001)."Strength And Stability Of Casuarina Glauca Roots In Relation To Slope Stability". 14th Southeast Asian Geotechnical Conference.Lisse: 745-749.

Docker B. B and Hubble T. T. C. (2008). "Quantify Root-Reinforcement Of River Bank Soils By Four Austrailian Tree Species." Science Direct 100 (2008): 401-418.

Docker B. B and Hubble T. T. C. (2009). "Modelling The Distribution Of Enhanced Soil Shaer Strength Beneath Riparian Trees Of South-Eastern Australia." Ecological Engineering 35 (2009): 921-924.

Fatahi, B. (2007). "Modelling Of Influence Of Matric Suction Induced By Native Vegetation On Sub-Soil Improvement", University Of Wollongong.PhD Thesis.

Fatahi, B.,Khabbaz, H. and Indraratna, B. (2009). "Parametric studies on bioengineering effects of tree root-based suction on ground behaviour." Ecological engineering 35(10): 1415-1426.

Fatahi, B., Khabbaz, H. &Indraratna, B. (2010). "Bioengineering ground improvement considering root water uptake model", Ecological Engineering 36(2): 222-229

Fatahi, B., Khabbaz, H. & Fatahi, B. (2012). "Mechanical characteristics of soft clay treated with fibre and cement", Geosynthetics International, 19(2), 252-262.

Fatahi, B., Khabbaz, H. &Indraratna, B. (2014). "Modelling of unsaturated ground behaviour influenced by vegetation transpiration", Geomechanics and Geoengineering: An International Journal, DOI: 10.1080/17486025.2014.880520

Feddes, R. A., Bresler, E. and Neuman, S. P. (1974)."Field test of a modified numerical model for water uptake by root systems". Water Resources Research 10(6): 1199-1206.

Fredlund, D. G. and Hung, V. Q. (2001)."Prediction of volume change in an expansive soil as a result of vegetation and environmental changes." Geotechnical Special Publication 115: 24-43.

Fredlund, D. G.,Rahardjo, H. and Fredlund, M. D. (2012). "Unsaturated soil mechanics in engineering practice" Hoboken, N.J, Wiley-Blackwell.

Gardner, W. R. (1960). "Dynamic Aspects Of Water Availability To Plants." Soil Science 89(2): 63-73.

Gilmen, E. F. (1980) "An Illustrated Guide to Pruning", Environmental Horticulture Department, Ifas, University Of Florida.

Green, S. R. (1992). "Radiation balance, transpiration and photosynthesis of an isolated tree" Agricultural and Forest Meteorology, 64(1993): 201-221.

Hopkins, W. G. (1999). "Introduction To Plant Physiology." JhonWoley& Sons, Usa.

Indraratna, B.,Fatahi, B. and Khabbaz, H. (2006). "Numerical analysis of matric suction effects of tree roots." Proceedings of the Institution of Civil Engineers: Geotechnical Engineering 159(2): 77-90.

Indraratna, B., Khabbaz, H. & Fatahi, B. (2008). "Conceptual Development and Numerical Modelling of Vegetation Induced Suction and implications on Rail Track Stabilisation", Proceedings of the 12th International Conference of International Association for Computer Methods and Advances in Geomechanics (IACMAG), Indian Institute of Technology, Bombay, Mumbai, India, 4335-4344.

Kramer, P.J. (1995) Roots and Root systems, Chapter 5; 115-166

Nimah, M. H. and Hanks, R. J. (1973)."Model for estimating soil water, plant and atmospheric inter relations."Soil Science Society of America Journal.Vol 37(4) : 522-527

Nobel, P. S. (1991). "Physiochemical And Environmental Plant Physiology." Academic Press New York.

Operstain, V. and Frydman, S. (2000). "The Influence Of Vegetation On Soil Strength." Ground Improvement 4: 81-89.

Potter, W. (2006). The Feasibility Of Improving Rail Infrastructure By Using Native Vegetation On Clay Soils. University Of South Australia. MSc. Thesis.

Radcliffe,D., Hayden, T., Watson, K., Crowly, P., and Phillips, R. E. (1980) "Simulation Of Soil Water Within The Root Zone Of A Corn Crop". Agronomy Journal 72: 19-24

Sattelmacher, B.,Marschner, H. and Kuhne, R. (1990). "Effects Of The Temperature Of The Rooting Zone On The Growth And Development Of Roots Of Potato (Solanum-Tuberosum)." Annals Of Botany 65(1): 27-36.

Teskey, R. O. and D. W. Sheriff (1995). "Water use by Pinusradiata trees in a plantation." Tree Physiology 16: 273-279.

Vanapalli, S. K., Fredlund, D. G., Pufahl, D. E., Clifton, A. W. (1996). "Model for the prediction of shear strength with respect to soil suction." Canadian Geotechnical Journal 33(3): 379-392.

Waisel, Y.,Eshel, A. and Kafkafi, U. (2002). Plant roots: the hidden half. New York, Marcel Dekker.

Waldron, L. J. (1977). "The Shear Resistance Of Root-Permeated Homogeneous And Stratified Soil1." Soil Sci. Soc. Am. J. 41(5): 843-849.

Waldren, L. J. and S. Dakessian (1981). "Soil Reinforcement By Roots: Calculation of Increased Soil Shear Resistance From Root Properties." Soil Science 132: 427-435.

Weaver, J.E. (1958), "Classification of Root Systems of Forbs of Grassland and a Consideration of Their Significance"Ecology, Vol. 39(3) (July, 1958). Ecological Society of America.

An Analysis of Compacted Pavement Subgrade Behaviour Due to Climatic Effects

J. Kodikara[1] and T. Islam[1]

1Department of Civil Engineering, Monash University, Victoria, Australia
E-mail: Jayantha.Kodikara@monash.edu

ABSTRACT: The paper presents an analysis of pavement subgrade behaviour subjected to climatic effects. A newly developed framework is used to aid the interpretations. The value of this framework is that it uses the compaction curves as the yield surface while swelling due to wetting and predominantly elastic loading can take place within the surface. The current design approaches are reviewed with some interpretations within this framework. The major wetting of pavements and equilibrium moisture content that develops due to suction equilibration are highlighted as primary changes due to climatic effects. The design needs to take into account these effects and road maintenance needs to sustain design assumptions such as maintaining the integrity of pavement surface seal.

1. INTRODUCTION

Road pavements are valuable infrastructure in a nation's asset base, and influence the living standards of its people. Large sums are spent annually on construction and maintenance of roads. Therefore, improvements in road pavement analysis and design can bring significant savings to communities. Unfortunately, the road pavement area has received less technical advancement than the traditional geotechnical area. One reason may be that the focus of pavement engineers is spread across transport and traffic planning issues, the geometrical design of roads and the geotechnical aspects of road design. For this reason, the behaviour of the road pavement may not have received due attention from a geotechnical point of view. Another reason appears to be that roads are long structures that can spread over tens of kilometres during one construction phase and the control of construction is challenging in comparison to a building site where foundations are constructed. Under these circumstances, top-down empirical approaches are commonly employed for pavement design.

The pavement structure may be considered as a number of geomaterial layers built over the soil subgrade. The stiffnesses of layers above the subgrade are progressively increased so that the strongest layer is at the top of the pavement. The basic concept of this bottom-up construction is that the load is spread quickly on the uppermost stronger and stiffer layers so that only a small stress is finally received at the subgrade, which is normally the weakest layer. The simplest pavement design approach involves the use of the subgrade California bearing ratio (CBR) of the pavement subgrade to assign a pavement layer thickness. Charts or formulae have been developed to estimate a good quality unbound pavement layer required on a subgrade with a given CBR value (Austroads, 2010). Using this technique, it is also possible to design multiple unbound layers with increasing quality over a given subgrade.

The alternative technique is so-called mechanistic modelling, where fatigue relationships are commonly used to design pavement layers. The common fatigue relationships follow the approach given in Equation 1, where the allowable repetitions of traffic loads N_{all} are given:

$$N_{all} = \left(\frac{a}{\varepsilon}\right)^{b} \qquad (1)$$

The constants a and b depend on the material. The strain ε is the vertical strain exerted on the subgrade due to a standard axle load, which is normally a single-axle dual-tyre load configuration with an axle load of 80kN. This means that the actual traffic load spectrum comprising a range of axle configurations with varying axle loads needs to be converted to standard axles, commonly referred to as the design traffic N_d. The design traffic will allow for the design life of the pavement (say 40 years) and the possible growth in traffic during this period. A suitable pavement layer system on a given subgrade is then chosen such that $N_d = N_{all}$. The determination of ε requires the use of a numerical program such as a finite element model to compute the relevant strain. Commonly these layers including the subgrade are assumed to be elastic.

As the subgrade is the weakest link in a pavement system, the preparation of subgrade soil is very important. Normally the subgrade is either compacted or new compacted fill is placed to raise the road surface. Therefore, the compaction specification and process have major influences. Currently, the actual behaviour of a pavement subgrade from the as-compacted state to during pavement operation is not very clear. This behaviour is complex because the clay subgrade will not stay in as-compacted state but will change its properties primarily due to climatic influences. In the current pavement design guides, these behavioural changes are handled in an ad hoc manner without detailed consideration. For instance, although the as-compacted state of the pavement subgrade may be well dry optimum, soaked CBR may be used in pavement design to allow for any future major wetting of the subgrade. This paper presents an analysis of pavement subgrade behaviour due to climatic effects and traffic loading. The MPK framework newly developed by the authors is used to aid the interpretation.

2. INFLUENCE OF COMPACTION STATE

2.1 MPK Framework

Kodikara (2012) presented a novel framework (dubbed the MPK (Monash-Peradeniya-Kodikara) framework) to explain and predict the behaviour of compacted soils. The novel aspect of this framework is that it extends the traditional concept of Proctor's compaction curve to represent the soil volumetric behaviour. In addition, it utilises moisture content (given as moisture ratio $ew = wGs$, where w is the gravimetric moisture content and Gs is the specific gravity of soil) to replace the traditionally used matric suction, which is normally a difficult parameter to quantify, especially in the field. The framework has been used to explain most characteristic behaviours of compacted clays, including volumetric deformation under loading and unloading, swelling behaviour during wetting, collapse behaviour during wetting, swelling pressure development during constrained swelling and cracking during constrained drying.

The typical compaction curve is approximately an inverted parabolic curve with the maximum dry density (γ_s) corresponding to optimum moisture content. However, this curve depends on the applied energy level (or the applied stress) and a family of compaction curves can be obtained corresponding to different energy levels or applied stresses. Figure 1a shows such a family of compaction curves. The maximum density points define a line of optimums, referred to as LOO, which typically falls at 80 to 90% degree of saturation for clayey soils. The

degree of saturation can be defined as $\frac{e_w}{e}$ .It can be considered that soil compacted to the dry side of optimum will have air free to move, therefore maintaining mostly atmospheric air pressure, whereas the soil compacted to the wet side of optimum will have air trapped. In this case, air pressure can develop during fast loading. As shown in Figure 1b, the MPK framework extends the family of compaction curves in the 3-D space using another axis for applied or yield net stress (p) giving a compaction surface. The net stress is defined as the applied stress minus the air pressure. Here, the moisture ratio ew is used in place of gravimetric moisture content. For theoretical analysis, it is convenient to consider this surface in e-e_w - p space, as shown in Figure 1c, which shows the surface depicting the loosest states of soil with stress, referred to as Loading Wetting State Boundary Surface (LWSBS).

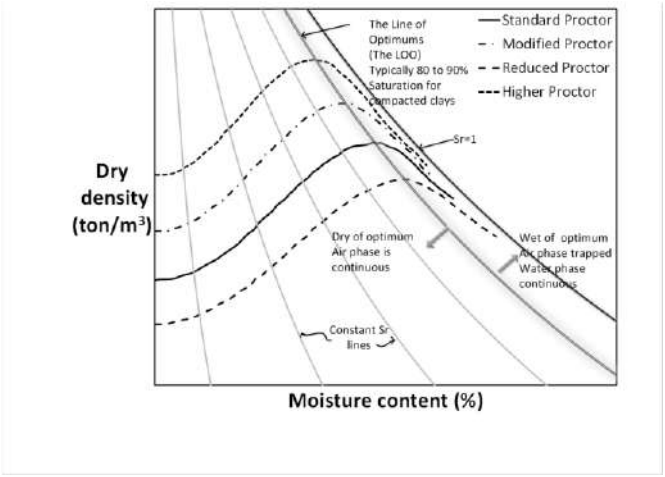

Figure 1a. Family of compaction curves and the line of optimums (Kodikara, 2012)

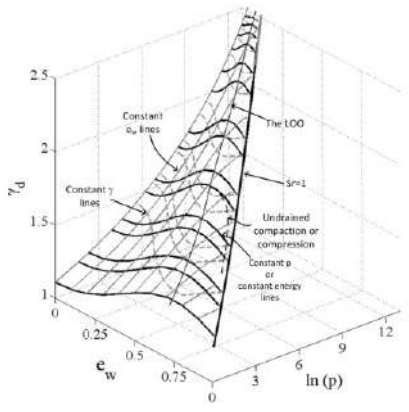

Figure 1b. Compaction surface in 3-dimensional space (Kodikara, 2012)

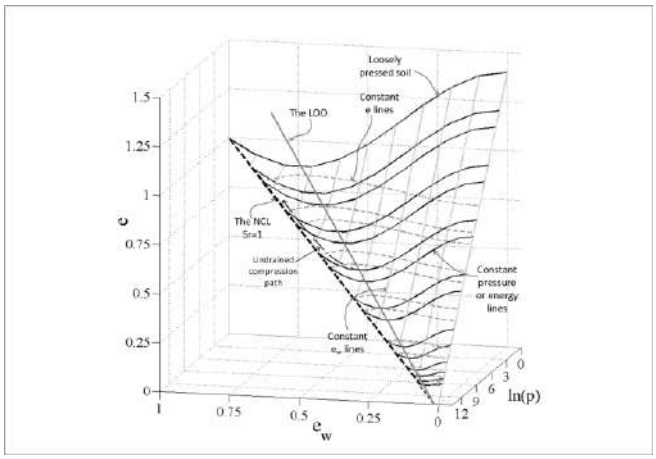

Figure 1c. Compaction surface given as Loading Wetting State Boundary Surface (LWSBS) (Kodikara, 2012)

2.2 Likely Behaviour when Compacted Wet or Dry Side of Optimum

2.2.1 Collapse potential

Collapse in unsaturated compacted soils is referred to as substantial compression that can happen when the soil is wetted. Usually, it is expected that unsaturated compacted soil will swell when wetted. Experimental evidence indicates that collapse can follow swelling under certain stress and initial density (or void ratio) conditions. Collapse is considered to be mostly responsible for the bump that develops at overpass approaches in roads, when the overpass structure remains unsettled while the approach section mainly comprising compacted fill settles with time. This behaviour has been explained within the MPK framework and collapse is likely to occur when soils are compacted dry of LOO only. The reason for this is the collapse of the "cloddy" structure that occurs when soil is compacted dry side of optimum. Figure 2 shows the loading/wetting behaviour of compacted kaolin depicted in this framework. The LWSBS was developed through constant moisture content compression of loosely compacted soils (at 7 kPa, nominal stress) statically in a compaction mould (K_0 conditions) at various moisture ratios. The independent test shown with path ABCD is for a soil compacted at 8.96% (e_w = 0.237) (path A to B) and then wetted to 27.35% moisture content (e_w = 0.725) and then loaded to 2000 kPa stress. It can be seen that when the soil is wetted at 50 kPa stress, it undergoes collapse (compression) along the 50 kPa stress contour to point C. When the soil is loaded further it follows the LWSBS corresponding to new moisture content. While this example shows LWSBS can predict the likely pathway during loading/wetting, in practical compaction, soil is compacted to a higher stress and then unloaded (such as when rollers depart after a number of passes). However, the compacted soil can be further be loaded to some operational stress, which is normally less than 200 kPa or so. In road pavements, only a nominal vertical stress would prevail under operational conditions, except when traffic loading is imposed leading mainly to the momentary rise of vertical stress. This situation is discussed later.

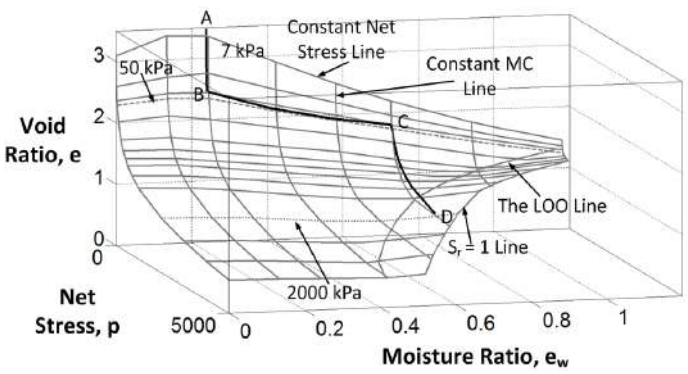

Figure 2. LWSBS for kaolin and loading/wetting pathway of an independent soil specimen.

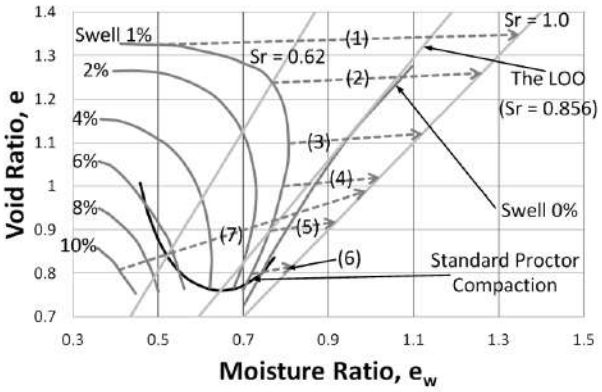

Figure 3. Variation in swelling percentage under nominal vertical stress for first major wetting (based on Holtz and Gibbs, 1956)

2.2.2 Other behaviours

It is well established that the behaviour of compacted clays can differ when compacted wet or dry side of the LOO. Some of these characteristics can be summarised as follows:

- Soil stiffness and shear and tensile strength tend to be higher on the dry side of optimum, but many soils tend to peak at some moisture content drier than optimum, and then even show a reduction in stiffness or strength with decrease of moisture content.
- Soil saturated permeability tends to be orders of magnitude higher dry of optimum and would normally achieve a minimum few percentage points wet of optimum. On the basis of a range of test results, Kodikara and Rahman (2002) indicated that moisture content that will give minimum hydraulic conductivity is about 0.151 x PI wetter than the optimum, where PI is the soil plasticity index. This is why landfill clay liners are normally compacted wet of optimum, targeting the lowest permeability achievable for a certain compaction energy.
- However, when the soil is compacted wet of optimum, the likely shrinkage during initial drying tends to be higher, which can increase the potential for cracking and the severity of cracking during desiccation.
- Soil swelling percentage (or strain given with respect to a soil volume) tends to be higher on the dry side of optimum than on the wet side. Figure 3 shows variation of swelling percentage (with respect to original volume) at nominal stress when subjected to initial major wetting. For this soil, it is evident that percentage of swelling does not vary very much at the same as-compacted void ratio for S_r less than 0.62, meaning that the swelled position on the saturation line (void ratio) would be approximately the same, as shown with the arrow 1. However, as the soil initial compaction state approaches close to the LOO the swelled position (and the amount of swelling given by e_{final}) will drop along the saturation line (as shown by arrows 2, 3, 4, 5 and 6). Arrow 7 shows the swelling that can occur when starting from a high density (lower void ratio) but significantly dry of LOO. However, it should be noted that this amount of swelling is for first swelling and if significant wetting/drying takes place, this final position is considered to move up or e_{final} to increase.
- As a general comment, soils that are compacted significantly dry of optimum appear to compact (or increase in density) with significant wet/dry cycles and soils that are compacted wet side of optimum tend to expand (decompaction or decrease in density) during wet/dry cycles (Kodikara et al., 2014). Decompaction has been a problem in compacted fills, where fills compacted to agreed specifications of dry density have been found during subsequent investigations to have lost compaction and exhibited decrease in dry density after some time. When such fills have experienced some form of failure, numerous cases of litigation have ensued and the evidence of decompaction has been a point of dispute (Burman et al., 2008).

3. MOISTURE VARIATION DURING SERVICE

Once a compacted fill or a pavement subgrade is compacted, its moisture condition can change with time. As shown schematically in Figure 4, it is possible to consider an equilibrium moisture content that soil will eventually achieve in thermodynamic equilibrium with the surrounding layers, water table (if present at the vicinity) and atmospheric interaction. More precisely, it will be the soil suction that will reach equilibrium, since it is the thermodynamic potential that controls the soil moisture energy state. Past research has developed links between climate (characterised by the Thornthwaite Moisture Index or TMI) and equilibrium suction (commonly given in pF or log of water head given in cm (Russam and Coleman, 1961). Then, of course, it is possible to link the equilibrium suction to an equilibrium moisture content (or moisture ratio) referring to a soil water characteristic curve for stabilised soil. This approach is relevant when the water table is well below the ground surface, otherwise its influence may dominate.

As shown in Figure 4, if the soil is compacted at a higher moisture content than the equilibrium moisture content, the soil is likely to undergo drying with intermediate variations in water content (due to climatic events) and then reach the equilibrium state. Over the long term, moisture content may fluctuate around the equilibrium during seasonal variations if they are significant. On the other hand, if the soil is compacted at a lower moisture content than the equilibrium moisture content, the soil is likely to wet up to equilibrium state and undergo cyclic behaviour during seasonal events. Exceptions to such progressive wetting or drying would be events such as flooding that can make the soil wet almost to saturation, regardless of the initial compaction moisture state.

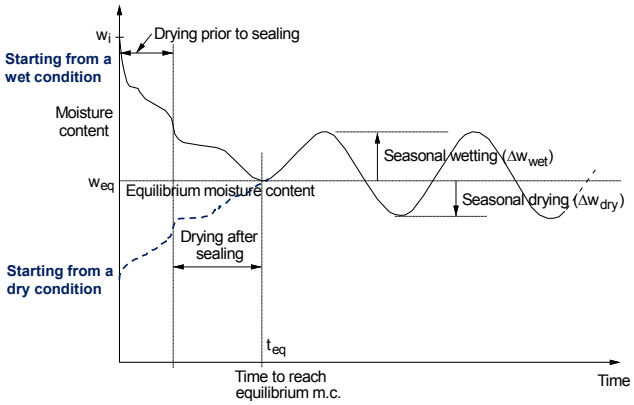

Figure 4. Schematic representation of progressive moisture variation of a subgrade after compaction.

4. BEHAVOURAL CHANGES WITH MOISTURE VARIATION

A major problem with pavements is rutting that can develop when the pavement subgrades become weaker due to moisture ingress. Within MPK framework, an example of a major wetting event is shown Figure 5, where a soil specimen at a moisture content of 4.04% (e_w = 0.107) is compacted to a stress of 1000 kPa, unloaded to 20 kPa stress, then wetted to 23.67% (e_w = 0.627) moisture content at this stress level and finally, compressed to a stress of 2000 kPa at that moisture content. This wetting can be considered a major wetting event that occurred during operation. Figure 2b also shows a subsequent loading which can again intercept the LWSBS, where soil can undergo yielding at a lower stress level, leading to extra deformation. This situation may be likened to rutting in the pavement that may occur after the soil subgrade has been weakened by a significant wetting event or phase. The corresponding pathways in *e-log(p)* plots are shown in Figure 6. The reduction in yield stress due to wetting can be clearly seen associated with excessive deformation. Figure 7 shows this effect in a plot of deformation against traffic load repetitions.

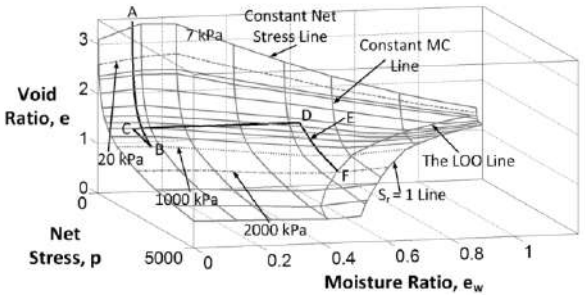

Figure 5. Depiction of a soil specimen compacted and then unloaded to operational stress and then wetted due to a major wetting event and subsequently loaded at wetted state.

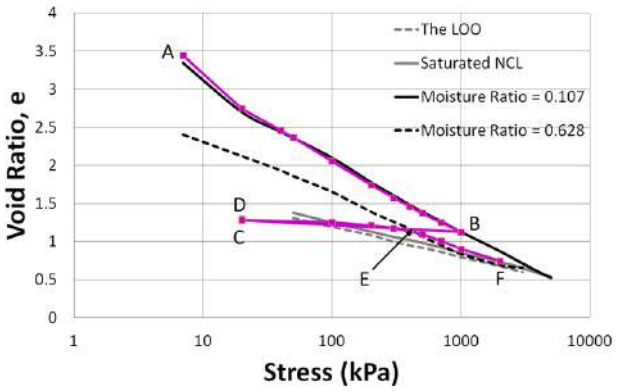

Figure 6. Stress path during loading in *e-log(p)* plane

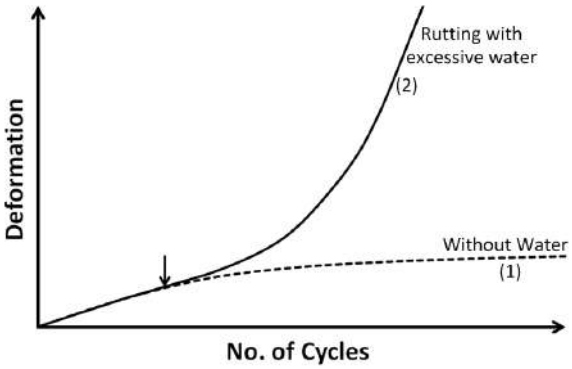

Figure 7. Plastic deformation accumulation with traffic load cycles.

The above analysis within the current MPK framework assumes volumetric deformation of the soil under K_o conditions only. However, significant shear deformation can occur under pavement conditions, since the soil is not laterally confined as in K_o conditions. Under these conditions, further deformation can arise when the shear stress approaches close to the failure stress with wetting. For example, this situation may be depicted as shown in Figure 8, which shows the shear failure envelopes corresponding to normal and excessive moisture conditions. Also shown is the likely stress increase during traffic loading. It can be seen that under normal moisture conditions, the stress state with traffic loading (point B) is well below the failure surface and therefore, soil may behave predominantly in a resilient manner without continual accumulation of plastic deformations (similar to the dashed line shown in Figure 7. When the subgrade is excessively wetted, however, traffic loading will bring the stress state in the subgrade much closer to failure, allowing significant accumulation of plastic deformations, which can lead to rutting deformations on the pavement (similar to the steep line for excessive moisture shown in Figure 7).

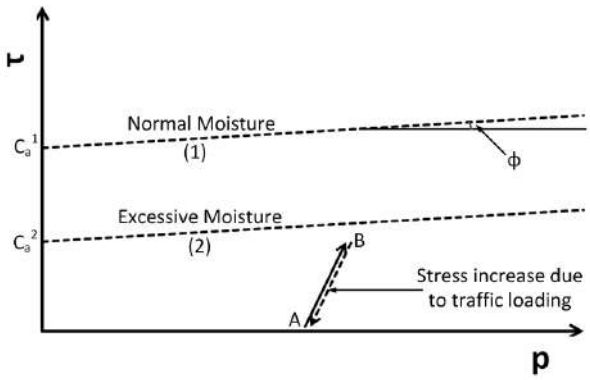

Figure 8. Influence of stress conditions due to excessive wetting as soil shear strength reduces.

5. CURRENT PRACTICE OF MECHANISTIC MODELING

Current practice in pavement design mostly involves the treatment of subgrade as an elastic layer (in some cases infinitely deep). In many design guides, the damage accumulation is treated as in fatigue, where the allowable repetitions of (vertical) stress or strain on the subgrade surface due to traffic loading on the pavement are computed (as in Equation 1). The vertical stress or strain on the subgrade surface is computed using a numerical program (such as finite or boundary element) assuming elastic pavement layers. An inherent assumption is that soil will behave well within the influence of yield limit under repetitive traffic loading, as shown in normal moisture conditions (1) in Figure 8 resulting in deformation behaviour similar to (1) in Figure 7. The elastic modulus is normally the resilient modulus measured in a repetitive loading triaxial apparatus subjected to a certain stress ratio (ratio of applied to failure stress) at a designed moisture content. However, in many situations, the resilient modulus is approximated as a multiple of CBR at that moisture content. In the Austroads Design Guide (2010)), modulus in MPa is assumed to be equal to 10 times the CBR as a percentage value. Because of the lack of certainty of design moisture content allowing field moisture variations, it is also common to use a soaked CBR, where the soil specimen is soaked for a period of time prior to performing the CBR test. Since soaked CBR is generally much smaller than as-compacted CBR, it is generally considered that the "worst case scenario" is used for design to offset uncertainty in field moisture variation, thereby giving a conservative design.

Figure 9 shows the variation of soaked CBR in the unloaded (at nominal stress) compaction plane for basaltic clays in Victoria, Australia. It is apparent that the same CBR can be obtained at lower densities when the compacted moisture content is increased. The reason for this is that along the same CBR contour (say 1% CBR in Figure 9) at a lower void ratio (higher density) and lower moisture content, the percentage swelling would be higher, as can be seen in Figure 3. Therefore, along the same CBR contour (say 1%), the soaked void ratios are brought closer to each other, although their positions are far apart at the compaction states. Therefore, similar CBRs can result for soaked states. In order for that to happen, the soil may have to behave elastically due to the stress increase applied. The stress increase is related to the CBR value, since the CBR gives the force applied. For example, for CBR 1%, the force applied may be given as 1% of the Standard load 19.8 kN (assuming this gives the higher CBR value) applied over a circular area of 49.6 mm diameter. This gives rise to a stress increase of about 100 kPa. Therefore, if the pavements are designed with subgrade properties assumed to be in soaked CBR state and the applied stress on the subgrade remains well below such stress levels (e.g., 100 kPa), the subgrade may not experience significant rutting. However, under soaked conditions, a major influence is also expected from pore pressure generation under traffic loading since the CBR test is normally performed at a faster rate (e.g., 1 mm/minute). However, in the current design approaches, these stress paths and the stress levels are not directly accounted for in deformation accumulation, such as in foundation design, where finite element analysis can be performed to examine the operating settlements, commonly under monotonic loading. A robust three-dimensional model with the capability to undertake cyclic loading is required to do such analysis, but with current models based on suction, this approach has been found to be difficult.

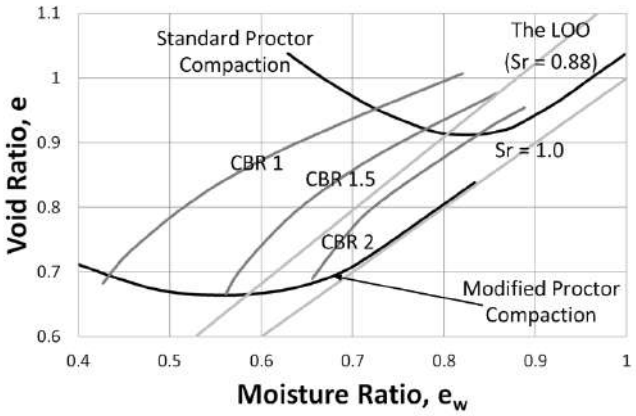

Figure 9. Variation in CBR in unloaded e-e_w plane (adapted from Hillard, 1981).

6. POTENTIAL EFFECTS OF CLIMATE CHANGE

It is commonly accepted that the world's climate is changing based on measurements, although its course remains a matter of debate. The likely influence is considered to vary among countries, but it is predicted that rainfall intensities may increase, despite overall rainfall increasing or decreasing depending on the geographical location. As the world's climate changes, a change in equilibrium moisture content (or suction) with time can be expected. For those areas where rainfall becomes less, a decrease in equilibrium moisture content can be expected, and for those areas where higher rainfall is expected, an increase in equilibrium moisture content can be expected. This overall effect is somewhat subdued since it may happen over a long period (over 50 to 100 years in the medium short term, where climate predictions are normally done). However, it can be argued that the major effect will come from the increase in rainfall intensity and its recurrence. As noted previously, major wetting has the potential to weaken the subgrade significantly. If the wetting conditions prevail for longer periods of time, significant damage could accumulate during traffic passage.

Under such uncertain wetting conditions, maintaining an intact seal on the pavement will be paramount. During flooding, water ingress pathways are through either the road surface or from the shoulders and sides. Even when the road is flooded, if the road has a good intact seal, the water ingress from the road surface will be slow, and the lateral ingress will depend on the permeability of the pavement and subgrade materials. Therefore, if water ingress into the subgrade under the wheel path areas can be minimised during the flooding period by the appropriate design of pavement layers, it may be possible to reduce pavement damage. If the water table is close to the surface, or the water table has risen with the continual increase in rainfall, it is inevitable that pavement subgrades will have high moisture contents. Under such scenarios, elevating the pavement base would be an option.

7. CONCLUDING REMARKS

This paper has presented a brief analysis of the effects of climatic effects on the performance of clayey subgrades of road pavements. The analysis was primarily explained within the MPK framework developed at Monash University. It was highlighted that when clay subgrades are compacted dry of optimum, they have the potential to swell or collapse under load. However, collapse may occur only when the compaction levels are small or when operational stresses are high during wetting. In road pavement scenarios, where the subgrade is only loaded significantly under heavy traffic loading, crucial conditions could occur when the subgrade has swelled during wetting and undergone deformation under subsequent loading. Collapse can become a problem in clay fills in approaches to overpasses.

The current use of CBR in pavement design is an approximate method of ensuring the pavement subgrade does not undergo excessive deformations during repetitive traffic loading. However, the connection of this parameter to the soil constitutive behaviour as needed in advanced mechanistic modelling is only loosely established. Changes in climatic effects have highlighted the need to consider the likely moisture variations in subgrade to be expected in the design life of a pavement. To cater for these conditions, more advanced but robust numerical models and bottom-up simplified analyses are required. The proposed MPK framework may provide a vehicle to achieve this objective.

8. REFERENCES

Austroads (2010). “Guide to Pavement Technology – Pavement Structural Design”, Austroads, Sydney, Australia.

Burman, B.C., Mostyn, G. and Piccolo, P. (2008). “Experiences with post-construction retesting of engineered clay fills”, Australian Geomechanics, 43 (4): 1-30.

Hillard, P. (1981). “Western Freeway – Melton Bypass Section, lime stabilisation of the clay subgrade, Road Construction Authority”, Victoria, Materials Division Report No. 18X429, December, 1981.

Holtz, W. G., and Gibbs, H. J. (1956). "Engineering properties of expansive clays: Transactions." *ASCE*, 121, 641-677.

Kodikara, J., Islam, T., Wijesooriya, S., Bui, H. and Burman, B.C. (2014). “On controlling influence of the line of optimums on the compacted clayey soil behavior”, Unsaturated Soils: Research and Applications, Proceedings of the Sixth International Conference on Unsaturated Soils, UNSAT2014, Sydney, Australia, 2-4 July, Editors: N. Khalili, A.R. Russell and A. Khoshghalb, pp. 219-225.

Kodikara, J. (2012). “New framework for volumetric constitutive behaviour of compacted unsaturated soils”, Canadian Geotechnical Journal, Vol. 49, pp. 1227-1243.

Kodikara, J. and Rahman, F. (2002). Moisture content and hydraulic conductivity relations for compacted clay, Civil Engineering Transactions, IEAUST, Vol. CE43, pp. 13-18.

Russam, K and Coleman, J.D. (1961). “The effect of climatic factors on subgrade moisture conditions, Geotechnique, Vol. XI, No. 1, pp. 22-28.